

**DIGITAL SIGNAL PROCESSING FOR BIOMEDICAL APPLICATIONS
(SYNTHESIS OF SHARP TRANSITION LINEAR PHASE
FIR DIGITAL FILTERS)**

A thesis submitted to Goa University

for the degree of

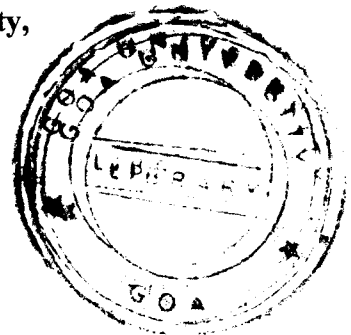
**DOCTOR OF PHILOSOPHY
IN
ELECTRONICS**

**By
Mr. Joseph X. Rodrigues**

621
ROD/D19
T-345

**Faculty of Natural Sciences,
Electronics Programme,
Dept. of Physics, Goa University,
Taleigaon Plateau
Goa-403206**

December 2005



*U.K.C.
(Dr. K.R. Bhat)*

Dr. V.R. Uduppi
(Dr. V.R. Uduppi)

Dedicated to my parents

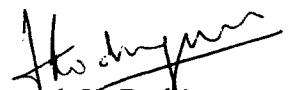
Mrs Magdaline and Late Mr X.B.I.Rodrigues

my first mentors ...

STATEMENT

I hereby state that this thesis for the Ph.D. degree on “Digital Signal Processing for Biomedical Applications (Synthesis of Sharp Transition Linear Phase FIR Digital Filters)” is my original work and that it has not previously formed the basis for the award of any degree, diploma, associateship, fellowship or any other similar title to the best of my knowledge and information.

Date: 20-12-2005


Joseph X. Rodrigues

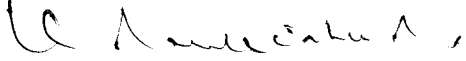
(Candidate)



CERTIFICATE

As required under the Goa University ordinance, I certify that the thesis entitled “Digital Signal Processing for Biomedical Applications (Synthesis of Sharp Transition Linear Phase FIR Digital Filters)” submitted by Mr. Joseph X. Rodrigues for the award of Doctor of Philosophy in Electronics is a research done by the candidate during the period of study under my tutelage and that it has not previously formed the basis for the award to the candidate of any degree, diploma, associateship, fellowship or other similar titles.

Date: 20-12-2005


Research Guide: Dr. K R Pai,
Professor and Head,
Department of Electronics and
Telecommunications,
P. C. College of Engineering,
Verna, Goa.

ABSTRACT

Joseph X. Rodrigues, "Digital Signal Processing for Biomedical Applications (Synthesis of Sharp Transition Linear Phase FIR Digital Filters)", Ph.D. Thesis, Electronics, Goa University, 2005. Guide: Dr K. R. Pai.

A novel technique for the synthesis of linear phase, sharp transition, lowpass, bandpass and multiband FIR filters are proposed in this thesis. The filters designed lay stress on achieving a sharp transition with low passband ripple and good stopband attenuation with least filter order. The filter models are formulated with sinusoidal functions of frequency, making it convenient to evaluate the impulse response coefficients in closed form. Various lowpass filter models formulated are nonmonotonic, monotonic, equiripple, equiripple with linear transition and equiripple with variable density ripple cycles. Transfer function of the filter is evolved in frequency and time domain. Sharp transition FIR filters produce oscillations in the frequency response near the edge of the passband, a trait described as Gibb's phenomenon. The filter models proposed achieve a tradeoff between the transition bandwidth and the Gibb's phenomenon. In the proposed technique, the slopes of the pseudo-magnitude response function, at the edges of the transition region are matched which makes the function of frequency continuous between a pair of adjoining regions defined by the filter model equations. This approach minimizes the effects due to Gibb's phenomenon thereby reducing ripples at the edges of the transition region of the filter and thus decreases peak passband ripple and improves stopband attenuation of the filter. The peak passband ripple in conventional FIR filter designs is about 18% which is reduced to around 2% in the proposed design by using trigonometric functions to model the frequency response and employing slope equalization technique. The synthesized filters prove to be a good alternative to filters in the same class reported in the literature with added advantage of simplicity in design, sharp transition, no filter optimizations, ease of computation of the impulse response and low arithmetic complexity. The accuracy of the filter approximation can be improved by including a larger number of terms in the impulse response sequence.

Linear phase, sharp transition FIR bandpass filter models and design with slope equalization technique are proposed. This approach is a direct one which does not require design of component lowpass and highpass filters to realize bandpass filters as required in many realization schemes in literature. The proposed filter models are also formulated with sinusoidal functions of frequency. The design is adaptable to any change in the center frequency and passband width of the desired bandpass filter. Another bandpass filter model with variable density of ripple cycles in passband and stopband is proposed which reduces Gibb's phenomenon further. This approach can be extended to sharp cutoff bandstop and multiband filters with arbitrary passband width and center frequency.

A Modified Frequency Response Masking (MFRM) technique is proposed for the synthesis of linear phase, sharp transition and low arithmetic complexity FIR filters. This approach employs the proposed lowpass and bandpass filters as subfilters in the MFRM approach and possesses closed form expressions for impulse response coefficients for subfilters and the final MFRM filter unlike the FRM approach.

A speech processing scheme is implemented to reduce the effect of spectral masking in sensorineural hearing impaired and hence to improve speech perception. The proposed linear phase, sharp transition FIR multiband filters are used in speech processing scheme which split the speech spectrum into complementary short time spectral bands based on Zwicker's critical band model. The frequency components that are likely to get masked are separated and presented to different ears for binaural dichotic presentation. The multiband filters possesses large stopband attenuation which aids in better band separation, sharp transition that leads to proper separation of formants to be fed to the ears and low passband loss that prevents deterioration of processed speech quality. All these features when combined lead to improvement in speech recognition for bilateral sensorineural hearing impaired as observed in an experimental study conducted. The proposed multiband filter also reduces arithmetic hardware required for filter realization and hence could be suitable for VLSI implementation of the speech processing scheme in a digital hearing aid.

Acknowledgements

For me, working with the blessings of the almighty, on the reported research has been an enjoyable experience through the amazing world of knowledge and progress. Many have helped me during my research pursuits and it is my sincere desire to acknowledge their invaluable support.

I take this opportunity to express my deep sense of gratitude to my research guide Dr. K. R. Pai, Professor and Head, Electronics and Telecommunications, P.C. College of Engineering, Verna, Goa. Words cannot describe his deep involvement in the work and passion to discuss novel ideas during the course of the work. I am grateful to him for putting me in a position to succeed to greater heights in my career and will continue to cherish his endless help.

My heartfelt thanks to my co-guide, Dr. P. R. Sarode, Dean, Natural Sciences and Head of Department, Physics, Goa University for his encouragement, unflinching support during difficult times and initiating research in the area of Electronics. I also thank him for providing all necessary software MATLAB etc. and other facilities in the VLSI laboratory.

I also thank Dr E. Desa, Reader, for his constant support and valuable suggestions and the faculty and non teaching staff of the Department of Physics for the technical support during the course of my work.

I am grateful to Dr. Rajalakshmi, Department of Audiology, All India Institute of Speech and Hearing, Mysore for her guidance in the area of speech processing and hearing and the authorities at the institute for permitting me to use their testing facilities.

I am also grateful to Prof. A.B. Bhattacharyya, Ex-Professor IIT, Delhi who guided me initially on this research work and Dr. B.S. Sonde, Ex-V.C., Goa University for permitting me to pursue research work in the area of Electronics.

I am also grateful to Rev. Fr. P.M. Rodrigues, Director, Agnel Technical Education Complex, Verna, Goa for the wholehearted support for my research pursuits and also my colleagues for sharing my responsibilities and duties during the course of my research work.

A special thanks to my wife, Mrs. Lucy Gudino, a researcher in Computer Science for her help in the form of technical discussions, programming, editing and moral support both professional and on the domestic front. Words can't convey my feelings towards my son Joel and family members for going through periods of turbulence. I have deprived them many happy moments but they strove to give me joy, support and encouragement at the home front.

Joseph Rodrigues

CONTENTS

Abstract	i	
Acknowledgements	iii	
Contents	v	
List of figures	viii	
List of tables	xi	
List of symbols and abbreviations	xiii	
Chapters		
1	Introduction	1
1.1	Problem overview	1
1.2	Research objectives	4
1.3	Proposed FIR filter design	4
1.4	Organization of the thesis	9
2	Synthesis of Sharp Transition, Linear Phase, Digital Lowpass FIR Filters	11
2.1	Introduction	11
2.2	Review of Gibb's phenomenon	15
2.3	Proposed slope equalization technique	16
2.4	Expressions for impulse response coefficients of a digital filter	18
2.5	Class I FIR lowpass filter with non-monotonic response without slope equalization	19
2.5.1	Filter model and design	19
2.5.2	Expressions for impulse response coefficients	22
2.5.3	Filter synthesis results	24
2.6	Class II FIR lowpass filter with monotonic response without slope equalization	29
2.6.1	Filter model and design	29
2.6.2	Expressions for impulse response coefficients	32
2.6.3	Filter synthesis results	33
2.7	Class III FIR lowpass filter with equiripple response	38
2.7.1	Filter model and design without slope equalization	38
2.7.1.1	Expressions for impulse response coefficients	42
2.7.1.2	Filter synthesis results	44
2.7.2	Filter design with slope equalization	49

2.7.2.1	Filter synthesis results	51
2.8	Class IV FIR lowpass filter with equiripple response and linear transition	56
2.8.1	Filter model and design	56
2.8.2	Slope equalization	58
2.8.3	Expressions for impulse response coefficients	60
2.8.4	Filter synthesis results	62
2.9	Class V FIR lowpass filter with equiripple response, linear transition and variable density ripple cycles	67
2.9.1	Filter model and design	67
2.9.2	Slope equalization	70
2.9.3	Expressions for impulse response coefficients	72
2.9.4	Filter synthesis results	75
2.10	Comparison of various proposed filters with conventional FIR filters	79
2.11	Conclusions	82
3	Synthesis of Sharp Transition, Linear Phase, Digital Bandpass FIR Filters	84
3.1	Introduction	84
3.2	Digital bandpass filter model I and design	86
3.2.1	Slope equalization	89
3.2.2	Expressions for impulse response coefficients	90
3.2.3	Filter synthesis results	93
3.3	Digital bandpass filter model II and design	97
3.3.1	Slope equalization	101
3.3.2	Expressions for impulse response coefficients	105
3.3.3	Filter synthesis results	107
3.4	Lowpass cascade filter model and design	112
3.4.1	Filter synthesis results	117
3.5	Conclusions	118
4	Modified Frequency Response Masking Approach	120
4.1	Introduction	120
4.2	Review of frequency response masking approach	123
4.2.1	Basic frequency response masking approach	123
4.3	Modified frequency response masking approach	127

4.3.1	Filter synthesis results	131
4.4	Proposed filters as subfilters for basic FRM approach	137
4.5	Conclusions	137
5	Multiband FIR Filters in Speech Processing Scheme for Sensorineural Hearing Impaired	139
5.1	Introduction	139
5.1.1	Human auditory system	139
5.1.2	Sensorineural hearing loss	142
5.1.3	Effects of sensorineural loss on speech perception	145
5.2	Binaural dichotic presentation	146
5.2.1	Review of speech processing schemes	148
5.3	Design of novel sharp transition multiband FIR filter	151
5.3.1	Introduction	151
5.3.2	Multiband filter model and design	153
5.3.3	Slope equalization	159
5.3.4	Expressions for impulse response coefficients	160
5.3.5	Filter synthesis results and discussions	162
5.4	Conclusions	168
6	Conclusions and future work	169
6.1	Conclusions	169
6.2	Suggestions for future work	173
Appendices		
A1.1	Review of classical methods for FIR filter design	175
A1.2	An alternative interpretation of impulse response truncation of FIR filter	184
A5.1	Implementation of speech processing scheme and listening tests	188
A6.1	Filter design of proposed FIR Filters	195
A6.2	Listing of programs developed using MATLAB	218
References		221
List of publications		228 231

List of Figures

Fig. No.		Page No.
Fig.2.1	Illustration of novel slope equalization technique: (a) Lowpass FIR filter model with equiripple magnitude response (b) Expanded view of passband (c) Expanded view of stopband.	17
Fig.2.2	Illustration of proposed Class I lowpass filter model with non-monotonic magnitude response	20
Fig.2.3	(a) Magnitude response of the proposed Class I lowpass filter (b) Magnified view of the passband (c) Impulse response sequence (d) Phase response.	28
Fig.2.4	Illustration of proposed Class II lowpass filter model with monotonic magnitude response.	30
Fig.2.5	(a) Magnitude response of the proposed Class II lowpass filter (b) Linear plot (c) magnified view of the passband (d) Impulse response sequence.	37
Fig.2.6	Illustration of proposed Class III lowpass filter model with equiripple magnitude response	39
Fig.2.7	(a) Magnitude response of the proposed Class III lowpass filter without slope equalization (b) magnified view of the passband (c) Impulse response sequence (d) Phase response.	48
Fig.2.8	(a) Magnitude response of proposed Class III for lowpass filter with slope equalization (b) linear plot (c) magnified view of the passband (d) Impulse response sequence.	54
Fig.2.9	Variation of lowpass filter order with passband ripple for constant transition width of 0.01π and passband edge 0.666π with and without slope equalization.	55
Fig.2.10	Variation of lowpass filter order with stopband attenuation for constant transition width of 0.01π and passband edge 0.666π with and without slope equalization.	55
Fig.2.11	Illustration of proposed Class IV lowpass filter model with equiripple magnitude response and linear transition region.	57
Fig.2.12	(a) Magnitude response of the proposed Class IV lowpass filter (b) magnified view of the passband (c) Impulse response sequence (d) Phase response.	65
Fig.2.13	Variation of passband ripple with filter order for constant transition width of 0.011π and passband width of 0.666π for	66

various proposed filters.

Fig.2.14	Variation of stopband attenuation with filter order for constant transition width of 0.011π and passband width of 0.666π for various proposed filters.	66
Fig.2.15	Plot of Filter order Vs Transition width for Class IV filter model with slope equalization for a given passband ripple of 0.1dB, stopband attenuation of 40dB and passband of 0.666π .	66
Fig.2.16	Illustration of proposed Class V lowpass filter model with equiripple magnitude response, linear transition region and variable k_p .	68
Fig.2.17	(a) Magnitude response of the proposed Class V lowpass filter (b) Linear plot (c) magnified view of the passband (d) Impulse response sequence.	78
Fig.2.18	Plot of Filter order Vs peak passband ripple for conventional FIR filter and various proposed FIR filters for a given passband ripple of 0.2dB, stopband attenuation of 40dB, transition bandwidth of 0.01π and passband edge of 0.666π .	81
Fig.2.19	Bar chart showing peak passband ripple for conventional FIR filter and various proposed FIR filters for a transition width of 0.01π and filter order 701.	81
Fig.3.1	Illustration of proposed bandpass filter model I with equiripple magnitude response and linear transition region.	88
Fig.3.2	(a) Magnitude response of the proposed bandpass I filter (b) magnified view of the passband (c) Impulse response sequence (d) Phase response.	96
Fig.3.3	Illustration of proposed bandpass filter model II with equiripple magnitude response, linear transition and variable density ripple cycles.	98
Fig.3.4	Magnitude response of the proposed bandpass II filter (b) Magnified view of the passband (c) Impulse response sequence (d) Phase response.	111
Fig.3.5	Magnitude responses of component filters $H_{pm1}(\omega)$ and $H_{pm2}(\omega)$ of proposed cascade lowpass filter model.	114
Fig.4.1	Block diagram of structure used in basic FRM approach.	125
Fig.4.2	Illustration of basic FRM approach.	126
Fig.4.3	Illustration of the proposed modified frequency response masking	129

approach.

Fig.4.4	Block diagram of structure for low pass Modified FRM filter realization.	131
Fig.4.5	(a) Magnitude response of various subfilters used in proposed MFRM approach with Model filter(light green), Masking filter(red), bandpass filter(green) and final MFRM filter (blue) (b) Linear plot (c) Final MFRM filter magnitude response (d) MFRM impulse response sequence (e) MFRM phase response	135
Fig.4.6	Magnitude response of masking subfilters (using proposed filters) employed in basic FRM approach and the magnitude response of final FRM filter (red colour).	135
Fig.5.1	Major components of the ear.	140
Fig.5.2	Transverse section through the cochlea.	143
Fig.5.3	Illustration of proposed Multiband filter (n^{th} band shown) for speech processing scheme with equiripple magnitude response, linear transition and variable density ripple cycles.	155
Fig.5.4	(a) Magnitude response of the proposed multiband filter used in speech processing scheme (b) Magnified view of the passband (dB) (c) Phase response (d) Impulse response sequence.	165
Fig.5.5	(a) Magnitude response of the proposed complementary multiband filter used in speech processing scheme (b) Magnified view of the passband (c) Phase response (d) Impulse response sequence.	167
Fig.A1.2	Illustration of truncation of the impulse sequence.	185
Fig.A5.1	Block diagram of Multiband filters to used to split speech signal into complementary spectra in the speech processing scheme.	189
Fig.A5.2	(a) Speech spectrogram of syllable 'ada' (b) and (c) Speech spectrogram of syllable 'ada' after splitting into complementary bands based on passbands of multiband filters in Table A5.1.	194

List of Tables

Table No.		Page No.
Table 2.1	Variation of passband ripple and stopband attenuation with filter order for transition band width of 0.01π and passband edge of 0.666π without slope equalization for proposed Class I FIR filter.	26
Table 2.2	Variation of passband ripple and stopband attenuation with filter order for transition bandwidth of 0.01π and passband edge of 0.666π without slope equalization for proposed Class II FIR filter.	35
Table 2.3	Variation of passband ripple and stopband attenuation with filter order for transition bandwidth of 0.01π and passband edge of 0.666π without slope equalization for proposed Class III FIR filter.	46
Table 2.4	Variation of passband ripple and stopband attenuation with filter order for transition bandwidth of 0.01π and passband width of 0.666π with slope equalization for proposed Class III FIR filter.	52
Table 2.5	Variation of passband ripple and stopband attenuation with filter order for transition bandwidth of 0.01π and passband edge of 0.666π with slope equalization for proposed Class IV FIR filter.	63
Table 2.6	Variation of transition width with filter order for passband ripple of 0.2dB and stopband attenuation of 40dB for passband edge of 0.666π with slope equalization for proposed Class IV FIR filter.	63
Table 2.7	Variation of passband ripple and stopband attenuation with filter order for transition width of 0.01π and passband edge of 0.333π with slope equalization for proposed Class IV FIR filter.	63
Table 2.8	Variation of passband ripple and stopband attenuation with filter order for transition bandwidth of 0.01π and passband edge of 0.666π with slope equalization for proposed Class V FIR filter.	76
Table 2.9	Peak passband ripple for conventional FIR filter and proposed FIR filters for various filter orders to illustrate reduction in Gibb's phenomenon.	80
Table 3.1	Proposed bandpass I filter performance for various passband widths, center frequencies and transition bandwidths with	94

required order for filter realization.

Table 3.2	Proposed bandpass II filter performance for various passband widths, center frequencies and transition bandwidths with required order for filter realization.	109
Table 4.1	Filter order required for various proposed subfilters for realization of MFRM filter with transition bandwidths of 0.01π and 0.004π for maximum passband ripple of 0.15dB and minimum stopband attenuation of 40dB.	136
Table 4.2	Filter order required for various proposed subfilters for realization of basic FRM filter with transition bandwidths of 0.01π and 0.005π for maximum passband ripple of 0.15dB and minimum stopband attenuation of 40dB.	136
Table A5.1	Table A5.1 Zwicker's critical band estimate	192

List of symbols and abbreviations

Symbol	Designation
ω	Frequency variable
$H_{pm}(\omega)$	Pseudo-magnitude of the filter response
δ_p	Passband ripple
δ_s	Stopband attenuation
A	Amplitude parameter
$h(n)$	Impulse response coefficients of filter
ω_p	Passband edge /frequency
ω_c	Cut-off edge
ω_s	Stopband edge
$(\omega_s - \omega_c)$	Transition bandwidth of filter
ω_0	Frequency at which $H_{pm}(\omega)$ is unity
ω_z	Frequency at which $H_{pm}(\omega)$ is zero
ω_{p0}	An intermediate frequency in the passband
ω_{s0}	An intermediate frequency in the stopband
ω_b	Center frequency of bandpass filter
$\Delta\omega_m$	Transition bandwidth of model filter in MFRM approach
$\Delta\omega$	Transition bandwidth of MFRM filter
$\omega_{s1, n-1}$	An intermediate stopband edge in multiband filter
$\omega_{s2, n-1}$	An intermediate stopband edge in multiband filter
$\omega_{s2, n+1}$	An intermediate stopband edge in multiband filter

ω_{sn}	Stopband edge of n^{th} band of multiband filter
ω_{pn}	Passband edge of n^{th} band of multiband filter
ω_{bn}	Center frequency of n^{th} band of multiband filter
ω_{zn}	Frequency at which $H_{pm}(\omega) = 0$ of n^{th} band of multiband filter
ω_{n2}	An intermediate passband edge in multiband filter
ω_{cn}	Cutoff frequency of n^{th} band of multiband filter
k_t	Filter design parameter
k_p	Filter design parameter
k_s	Filter design parameter
k_{pb}	Filter design parameter in bandpass filter
k_{p0}	Filter design parameter
$k_{p1}, k_{p2}, k_{p3}, k_{p4}$	Filter design parameters
A_0	Filter gain parameter in bandpass filter
$G(z^M)$	Periodic model filter in FRM approach
$G_c(z^M)$	Periodic complementary model filter in FRM approach
$F_0(z)$	Masking filter in FRM approach
$F_1(z)$	Masking filter in FRM approach
$F_a(z)$	Model filter in MFRM approach
$F_c(z)$	Complementary Model filter in MFRM approach
F_{bp}	Bandpass filter in MFRM approach
$F_{ma}(z)$	Masking filter in MFRM approach
$F_{mc}(z)$	Complementary masking filter in MFRM approach

$F(z)$	Final MFRM filter
θ	Passband edge of model filter $F_a(z)$ in MFRM approach
φ	Stopband edge of model filter $F_a(z)$ in MFRM approach
F_s	Sampling frequency
BP_n	n^{th} bandpass filter

Abbreviation	Explanation
FIR	Finite Impulse Response
IIR	Infinite Impulse Response
FPGA	Field Programmable Gate Array
FRM	Frequency Response Masking
VLSI	Very Large Scale Integration
dB	Decibels
MATLAB	MATrix Laboratory
DSP	Digital Signal Processing
FFT	Fast Fourier Transform
DFT	Discrete Fourier Transform
IDFT	Inverse Discrete Fourier Transform
MFRM	Modified Frequency Response Masking
IFIR	Interpolated Finite Impulse Response
SP	Signal Processing
ASIC	Application Specific Integrated Circuit

Chapter 1

INTRODUCTION

1.1 Problem overview

The signal processing in general and digital signal processing in particular, finds a plethora of applications in the field of biomedical engineering. The application intended in this thesis is related in broader terms, to the field of medical prosthesis, the prosthetic device being a digital hearing aid. The research work reported in this thesis addresses a particular hearing impairment called sensorineural hearing impairment [1], [2] and FIR filters for speech processing scheme in a digital hearing aid.

Sensorineural hearing impairment is characterized by marked distortions or abnormalities in sound perception. Its major causes are the damaged hair cells in the cochlea and/or degeneration of auditory nerve fibers of the ear. The result is increased spectral masking, which in turn causes severe smearing of the spectral envelope of speech signals. The smearing is equivalent to artificially widening of auditory filters. The debilitating effects of this impairment are high frequency hearing loss, increase in the threshold of hearing, compression in the dynamic range, severity of temporal masking and loss of spectral resolution due to spread of masking.

A proven speech processing scheme, that improves the speech perception among the persons suffering from the sensorineural hearing impairment, consists of splitting the speech spectrum into different frequency bands based on a critical band (auditory filter) model proposed by Zwicker [3]. The splitting of speech spectrum is obviously carried out by means of a set of two filter banks generating a pair of complementary spectra. Each of these spectra is

separately presented to left and right ear. This is known as binaural dichotic presentation [1], which helps in reducing the effect of spectral masking and is likely to improve speech perception in cases of bilateral sensorineural hearing impaired persons. Numerous studies were undertaken to verify the concept of critical bands and the concept is extended to other aspects of auditory perception and the frequency resolving capabilities of the human auditory system. The subdivision of the speech signal spectrum into critical bands seems to be correlated very closely to the cochlear mechanics and to frequency discrimination [4]. Zwicker's critical band model was the first comprehensive model of its type and has been used by many researchers. Studebaker et. al. [5] have proposed a model, which shows improvement in intelligibility at lower cutoff frequencies. These critical band models point to the need of synthesizing a multiband filter consisting of several pass and stopbands with near to ideal frequency responses in each constituent band.

Several speech processing schemes for improving speech perception in sensorineural hearing impaired are reported in literature. Lunner et. al. [1] implemented an eight channel signal processing system using TMS320C25 processor for a hearing aid. The filter bank in this scheme consisted of linear phase FIR filters with equal bandwidth of approximately 700 Hz and 40 dB stopband attenuation. For frequency response adjustments, the gain in each filter band is set individually to fit the hearing aid user. In listening tests with subjects having bilateral hearing loss, improvement in recognition score was obtained for dichotic over diotic presentation i.e. without splitting of the speech spectrum.

The hardware realization of the critical-band filter banks reported in the literature [6] uses lowpass, bandpass and highpass filter sections in cascade. However, the passband ripple of these filters is appreciable and band separation is not adequate due to less stopband

attenuation. In addition the filter transition is not sharp. As a result, the ability of the ear to binaurally receive and perceptually combine the dichotically presented speech signal is greatly curtailed. In the case of filters with finite crossovers in magnitude response, i.e. less steeper skirts in the transition region, there is an increased possibility of the spectral components belonging to crossover region being presented to both the ears. This causes an imbalance in loudness perceived at the crossovers between adjacent bands degrading the speech intelligibility.

With sharp transition filters, there is reduced possibility of spectral components presented to both ears at the transition region. Hence imbalance in loudness perceived at the crossovers between adjacent bands will reduce which increases speech intelligibility with sharp transition filters. Several methods have been proposed in the literature for the synthesis of FIR linear phase, sharp transition digital filters. Linear phase FIR digital filters have many advantages in speech processing applications such as guaranteed stability, negligible phase distortion and low coefficient sensitivity. A serious disadvantage of FIR filters is its complexity, which becomes acute in sharp transition filters. One of the most successful techniques for the synthesis of very narrow transition width, linear phase FIR filters is the frequency response masking (FRM) technique [7]. The FRM technique can be used for implementing sharp transition filters with arbitrary bandwidth with the resulting FRM filter has very sparse coefficients.

In the FRM techniques, closed form expressions for impulse response coefficients are not obtained. The subfilters in this technique are optimized to obtain final FRM filter. For a given frequency response specification its effective filter length including both zero and non-zero coefficient and delays required are longer than the infinite word length optimum minimax

filter. Resulting higher group delay is undesirable, particularly in speech processing applications. FRM is a graphical approach and transfer function for subfilters and the FRM filter are not evolved in frequency and time domain.

1.2 Research Objectives

The objective of the research is to synthesize narrow transition bandwidth, linear phase, FIR filters with multiple passbands of arbitrary width in the light of the literature cited above. Further, the synthesized filters were required to possess following desirable features:

- sharp transition with low passband ripple and large stopband attenuation.
- a well behaved function to model filter frequency response.
- closed form expressions for impulse response coefficients.
- impulse response coefficients related to transition width.
- finite transition width and well defined transition region unlike that of the conventional designs.
- a simple design procedure without optimizations involving less complex computations.
- a synthesis procedure without subfilters and their optimizations unlike FRM technique.
- design that is independent of center frequency and passband width for a bandpass/multiband filter.

1.3 Proposed FIR filter design

In pursuant to the stated objective, the method of filter synthesis proposed by us is as follows. The synthesis can be thought of as an extension of the classical methods reviewed in Appendix A1.1. In addition, a line of synthesis that also uses FRM technique is given. Several design procedures, each differing from the other in the formulation of pseudo-magnitude

response, for synthesizing low pass filters are presented. These are followed by the synthesis of band-pass filters with sharp transition, arbitrary passband width and center frequency. Each filter is specified by passband ripple δ_p , stopband attenuation δ_s , passband frequency ω_p (not the same as the cut-off frequency ω_c as defined in classical filter theory), the transition bandwidth $(\omega_s - \omega_c)$ where ω_s is the stopband frequency and ω_c is the cut-off frequency. In the case of bandpass filter, ω_b the center frequency is specified additionally. The specification of the transition bandwidth $(\omega_s - \omega_c)$ and its use in determining pseudo-magnitude in transition region is unique to the synthesis presented here. Hitherto, the transition region was treated as a “don’t care region” and no attention was paid to the shape of its response in the methods of synthesis reported in literature.

The salient points of our synthesis are given below:

- The entire range $[0, \pi]$ of the frequency variable ω is split into three regions, namely pass-band, transition-band and stop-band. Each region of the pseudo-magnitude response is defined in terms of a cosine/sine function of ω , confirming to the filter specifications.
- The pseudo-magnitude response function is assumed to be of the form given by (A 1.6a) and (A 1.6b) for N odd and N even respectively.
- Applying cosine transformation [11] to the pseudo-magnitude function $H_1(\omega)$ in (A 1.6a) and (A 1.6b), we obtain the impulse response sequence as

$$h(n) = \frac{1}{\pi} \left[\int_0^{\pi} H_1(\omega) \cos k\omega \, d\omega \right] \quad (1.1)$$

where $n = 0, 1, \dots, \frac{N-1}{2}$ for N odd ,

$n = 0, 1, \dots, \frac{N}{2} - 1$ for N even and $k = \frac{N-1}{2} - n$.

- The integral in (1.1) is similar to the inverse Fourier transform integral. The impulse-response sequence is extracted from (A1.6a) and (A1.6b) using the orthogonal property of the cosine/sine functions.
- Three parameters k_p, k_t and k_s are used in the sine/cosine functions defining the passband, transition band and stopband respectively. These parameters control the shape of the pseudo-magnitude function $H_1(\omega)$ in the three regions referred to above.
- In our synthesis, the desired response $H_1(\omega)$ is not the ideal lowpass/bandpass response. The ideal (brick-wall) response is convenient to obtain the impulse response using inverse Fourier transform [8]. Instead, we formulate the desired response in terms of sine/cosine functions in pass, transition and stop bands which simplifies the evaluation of impulse-response sequence $h(n)$ greatly. A closed form expression is obtained for $h(n)$ in terms of filter design parameters k_p, k_t, k_s and filters specifications $\omega_p, (\omega_s - \omega_c), \delta_p$ and δ_s .
- Ideal lowpass response with infinite slope at cut-off cannot be synthesized accurately in practice by finite physical functions. In our formulation of $H_1(\omega)$ “well behaved” i.e. sine/cosine functions that are continuous and that possess continuous derivatives of all orders are used.
- The “well behaved” functions used in the formulation also reduce the ripples in $H_1(\omega)$ that result from the “truncation” due to Gibb’s phenomenon as in (A1.2). However

there is a small amount of “discontinuity” present at the boundaries of passband/transition band and transition/stopband regions. This residual discontinuity is removed by “slope-matching” i.e. equalizing slopes of pseudo-magnitude response on either side of the discontinuities. This will reduce the ripples due the Gibb’s phenomenon further.

- Narrow transition band is realized by having a large slope at cut-off or at $\omega = \omega_p$ the passband frequency, either by a large value of parameter k_t , or by having an equiripple passband and an equiripple stopband as in the case of the optimal filter [8]. Additionally, the stopband ripples are allowed to have negative values.
- A lowpass /bandpass filter synthesis is carried out using two values of parameter k_p , one giving a smaller frequency of ripples around the frequencies $\omega=0$ and the other giving a larger ripple frequency around the passband edge ω_p . Similarly two values of the parameter k_s are used the one giving smaller ripple frequency is used closer to $\omega = \pi$ and the other giving larger ripple frequency is used near $\omega = \omega_s$. This technique combined with the “matching of slopes” is found to reduce the ripples due to Gibb’s phenomenon further.
- A linear transition region of constant slope is assumed in the formulation of the pseudo-magnitude response, which greatly simplifies the synthesis.

In summary, the filters proposed by us

- do not possess a flat passband or stopband which is not realizable in practice.
- do not have finite sized discontinuities except in cases without “slope matching”.
- do not have an infinite cut-off slope at band-edges.

- have finite width transition region.
- have considerably reduced band-edge ripple due to Gibb's phenomenon.
- have closed form expression for impulse-response sequence.
- require a considerably simplified synthesis procedure that requires less algebraic computation involving trigonometric functions and also filter of less order (truncated impulse response sequence) to obtain a close degree of matching with the desired response.

An alternative interpretation of the truncation process that yields linear phase FIR filter in the window design is given in Appendix A1.2. With reference to the Appendix A1.2, we can say that the main planks on which our synthesis rests are the following:

- Deriving closed form expression for the impulse response sequence by formulating a pseudo-magnitude response that is practically realizable as in (1.1), unlike the 'brick wall' response.
- Using a large number of these impulse response coefficients obtaining an approximation that approaches the desired response by proposed 'truncation' explained in Appendix A1.2 and
- Design does not involve any optimization steps and the computations are simpler than reported in the literature.

In the window design, the cut-off amplitude is 6 dB, which is fixed independent of filter length N which is a serious disadvantage. This limitation is overcome in the proposed synthesis wherein, the cutoff amplitude is adjusted to within $\pm 0.1\text{dB}$ or 0.2dB . In FRM, the synthesis involves four subfilters. The model and mask filters should be individually synthesized and optimized which requires several cycles of computation. In frequency

sampling techniques, the desired response is the ideal response having the limitations referred to above. The technique also requires a large number of samples for accurate interpolation and does not yield a closed form expression for impulse response sequence. It requires computation of IDFT followed by DFT requiring large number of computations than that of our proposed design method. The optimal filter design requires computation of error function and its maximum in the range $[0, \pi]$. The optimization which minimizes this maximum error i.e. chebyshev criterion require several computations. The response obtained is not unique and depends on the initial response used and number of computations are large. A closed form expression for impulse-response sequence is not obtained. In optimal response, ideal lowpass response is assumed having the limitations enumerated above.

1.4 Organization of the thesis

The thesis is divided into six chapters. In chapter one, problem overview, research objectives and the proposed FIR filter design is given. Chapter two, gives a brief literature survey on sharp transition FIR filters, their features and problems encountered in implementation. Proposed slope equalization technique to reduce Gibb's phenomenon in sharp transition FIR filter is explained. Various lowpass, linear phase, sharp transition, digital filter models are formulated and their designs are proposed. Different lowpass filter models are formulated namely, nonmonotonic, monotonic, equiripple, equiripple with linear transition and finally filter model with equiripple response, linear transition with variable ripple density. Expressions for filter model parameters and impulse response coefficients are derived and coefficients of the filters obtained. Results of the various filter designs are tabulated and comparisons made between various models developed with conventional FIR filter design.

Chapter three, deals with the proposed linear phase, sharp transition FIR bandpass filter with slope equalization technique applied to the design. The bandpass design is a direct approach without need of component highpass and lowpass filters and is adaptable to any change in the center frequency and passband width as verified in this chapter. Another novel bandpass filter technique with variable density of ripple cycles in passband and stopband to further reduce Gibb's phenomenon is proposed.

In chapter four, literature survey for synthesis of very narrow transition width FIR filter using frequency response masking (FRM) technique is given. A modified frequency response masking technique for the synthesis of linear phase, sharp transition FIR filters with low arithmetic complexity is proposed.

In chapter five, functioning of human auditory system is explained and various types of hearing impairments are described. Various speech processing schemes employed in literature, to improve speech perception degraded due to loss of frequency selectivity caused by spectral masking for sensorineural hearing impaired are reviewed. A pair of multiband filters are designed, using the proposed approach to split the speech into various frequency bands, based on Zwicker's model, for binaural dichotic presentation of speech. It is experimentally proved that, this reduces the effect of spectral masking in sensorineural hearing impaired.

Chapter six gives the conclusions of the work done and future work proposed in this research area. The thesis has appendices, where conventional FIR filter design methods are reviewed, an alternative interpretation of impulse response truncation of FIR filter is given along with the implementation of speech processing scheme, listening tests and results of listening tests conducted on sensorineural impaired patients. The filter design steps for various proposed FIR filters developed are worked out and programs developed in MATLAB listed.

Chapter 2

SYNTHESIS OF SHARP TRANSITION LINEAR PHASE DIGITAL LOWPASS FIR FILTERS

2.1 Introduction

For many digital signal processing applications, FIR filters are preferred over their IIR counterparts as the former can be designed with exact linear phase, guaranteed stability, free of phase distortion, absence of limit cycles and low coefficient sensitivity. However, FIR filters require especially in applications demanding narrow transition bandwidth, considerably more arithmetic operations than their IIR equivalents. Since the FIR filter length is inversely proportional to transition bandwidth its complexity becomes prohibitively high for sharp filters, which causes serious implementation problems [12].^[68] First, very large number of multipliers renders real time high speed implementation impractical. Second, the roundoff noise power generated by a filter with large number of nontrivial coefficients will be unacceptable unless the word length of the registers and arithmetic units are sufficiently high. Finally, filters with a large number of nontrivial coefficients have high coefficient sensitivity. As a consequence, very sharp filters will have high hardware complexity, high coefficient sensitivity and high roundoff noise unless the filter coefficient vector is sparse.

Several methods have been proposed in the literature for reducing the arithmetic complexity of sharp transition FIR filters [7], [13]-[15]. One of the techniques employed is the concept of interpolation [14]. One of the computationally efficient realizations for narrow band FIR filters based on this concept is the Interpolated FIR filter or IFIR filter which is a FIR-FIR filter cascade realization. In this realization the first FIR structure called the shaping filter has a very sparse impulse response resulting in a greatly reduced number of arithmetic operations. The second FIR

structure called the interpolator attenuates the undesired spectral images of the desired passband of the shaping filter below the prescribed stopband level and is usually a very simple filter of short length. Interpolating the impulse response of low pass filter has the effect of reducing its passband width by the interpolation ratio. By replacing every delay by M delays, the transition bandwidth is reduced by factor of M but the passband width is also reduced by the same factor. Hence this technique generally is suitable only for narrow passband design.

The total number of multipliers required for the implementation of FIR filters is a widely used performance criterion. Another approach, leading to computationally efficient FIR filters is the multiple use of the same filter. The resulting overall filter requires significantly fewer distinct multipliers than equivalent direct-form designs at the expense of an increased overall filter order. By appropriately cascading these filters large stopband attenuation can be obtained. Subfilter approach for designing efficient FIR filters is described in [16]. There are basically two subfilter approaches, the first one using different subfilters and the second one using identical subfilters. In the first approach, the best results are obtained by forming the subfilters by replacing the basic delay in a conventional prototype filter transfer function by a multiple delay and then by properly designing and combining the subfilters. The subfilters have different basic delays. The transition bandwidths of the prototype filters are very wide compared to that of the overall filter. Hence the required filter orders and correspondingly the number of multipliers required are very low compared to an equivalent direct-form minimax design. The subfilters that result when replacing the basic delays in the prototype filters by multiple delays have sparse impulse responses with the number of non-zero impulse response coefficient values being equal to that of the prototype filter, thus high-order filters are realized using very few multipliers. In the second technique, the overall filter is designed by interconnecting a number of identical subfilters with the aid of a few

additional adders and multipliers. The pass band and stopband edges of the subfilter are the same as those for the overall filter but the passband and the stopband ripples are significantly larger, resulting in a significant reduction in the filter order. Hence, by increasing the number of subfilters, the overall filter order can be reduced to any desired level. However, the realization which employs the minimum number of multipliers may sometimes require a slightly longer word length to achieve a specified noise performance or may result in a slightly longer group delay when compared to another realization which requires a slightly larger number of multipliers. A problem of practical interest is to find the lowest order filter, which satisfies certain maximum ripple requirements.

One of the important problems in digital filtering that has been considered by a number of authors in the past is the design of linear phase FIR filters with a very flat passband response and an equiripple stopband response. The design of linear-phase FIR filters with equiripple stopbands and with a prescribed degree of flatness of passbands is dealt in [17]. The design is based entirely on an appropriate use of well known Remez exchange algorithm for the design of weighted chebyshev FIR filters. Techniques for reduction of passband ripple in FIR filters have been recently investigated in [18] using optimization techniques.

This chapter deals with the formulation of various lowpass FIR digital filter models and their design. Models are proposed for linear phase, sharp transition, lowpass FIR filters with minimum passband ripple, good stopband attenuation with least filter order. The filter models are formulated using sinusoidal functions of frequency to evaluate the impulse response coefficients in closed form. Filter transfer function is evolved in frequency and time domain. The approach is simple, versatile and analytical without extensive computations. Expressions for filter design parameters k_p , k_t , k_s and impulse response coefficients are derived. Magnitude response of the

proposed lowpass filter is obtained. The approach can be extended to design sharp transition arbitrary passband highpass, bandpass and bandstop filters.

Novel slope equalization technique is introduced and the technique is applied to the various lowpass digital filter models formulated. The filter design parameters k_p , k_t and k_s are evaluated by equalizing the slopes of the pseudo-magnitude response function at both the ends of the transition region. This allows the proposed function to be continuous thus reducing the effects due to Gibb's phenomenon and hence decreases passband ripple and increases stopband attenuation.

The filter models proposed in this chapter lay stress on achieving a sharp transition from the passband to the stopband. Sharper this passband, more oscillatory will be the frequency response near the edge of the passband, a trait described as Gibb's phenomenon [8], [12]. The filter models proposed in this chapter achieve a tradeoff between the transition region width and the Gibb's phenomenon. In addition, emphasis is laid upon a good passband i.e. low passband attenuation and good stopband i.e. large stopband attenuation. Thus a three fold compromise for the satisfactory performance of the filter in all the three bands namely passband, transition band and stopband is essential in addition to a trade off between Gibb's phenomenon and sharpness of transition of the filter. The first model namely, Class I FIR filter with nonmonotonic passband has maximum passband attenuation at the extremities of the passband and a negative excursion that is maximum at the extremity of the stopband to obtain a sharp transition. All the three regions of the response are formulated in terms of sinusoidal function to achieve twin objectives of reducing Gibbs phenomenon and evaluating the closed form expression for the impulse response coefficients. The three parameters k_p , k_t and k_s are evaluated with the above stated objectives in mind. The class II filter proposed has a monotonic passband and reduced number of filter design parameters. Its stopband is also monotonic but for these minor differences, its formulation is

similar to class I filter model in many respects. The class III filter model proposed with and without slope equalization has equiripple passband and stopbands. The formulation of the transition region is similar to that of the Class I filter. This filter achieves better filter performance than its predecessors. This model is refined further by applying slope equalization technique which avoids a discontinuity at the edges of the passband and stopband reducing the effects of Gibbs phenomenon and thus further improving the filter performance. The class IV filter model has equiripple passband and stopband and in addition it introduces a linear transition region. In this model the synthesis of the filter is greatly simplified with fewer filter design parameters which reduces the complexity of the design compared to Class III filter. The parameter k_p is uniquely determined from the transition region width. The parameter is independent of passband width ω_p . With the application of slope equalization technique Gibbs phenomenon is found to reduce considerably. The class V filter model has equiripple passband and stopband and has a linear transition region. It has variable density ripples in the passband and stopband. This technique is employed to further reduce the effects of Gibb's phenomenon.

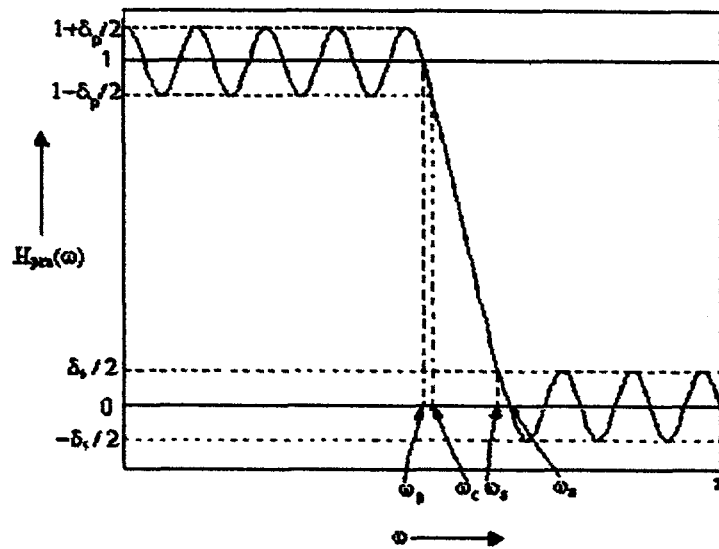
2.2 Review of Gibb's Phenomenon

A causal FIR filter obtained by simply truncating the impulse response of the ideal filter, exhibits an oscillatory behavior in its magnitude response which is more commonly referred to as the Gibb's phenomenon. The oscillatory behavior of the magnitude response is on both sides of cutoff frequency at which the ideal response is discontinuous and the peak ripple moves closer to the discontinuity [12]. As the order of the filter is increased, the number of ripples in both passband and stopband increases and the ripples are squeezed into a narrower interval about the discontinuity. However the overshoots, which occur on both sides of the transition region remain

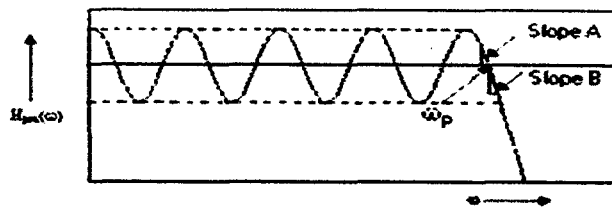
the same independent of the filter order and are approximately 18% of the difference between the passband and stopband magnitudes of the ideal filter [8]. The presence of the oscillatory behavior in the Fourier transform of a truncated Fourier series representation of an ideal filter response is basically due to two reasons. First, the impulse response of an ideal filter is infinitely long and not absolutely summable and as a result the filter is unstable. A stable filter realization needs a finite impulse response obtained by truncation of the impulse response. Second, the rectangular window used for truncation and obtaining an FIR response has an abrupt transition to zero which is the reason behind the appearance of the Gibbs phenomenon in the magnitude response of the windowed or truncated ideal filter impulse response sequence. The Gibbs phenomenon can be reduced by either using a window that tapers smoothly to zero at each end or by providing a smooth transition from the passband to the stopband. Use of a tapered window causes the height of the side lobe to diminish with a corresponding increase in the main lobe width resulting in a wider transition at the discontinuity.

2.3 Proposed Slope Equalization Technique

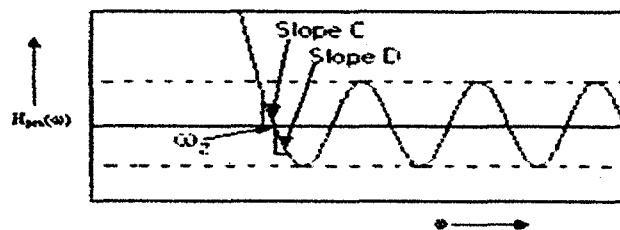
In this section, a novel slope equalization technique is proposed [23]. In the filter design without slope equalization the filter response functions are discontinuous at the passband edge, which leads to ripple at the points of discontinuity. The points of discontinuity are (i) at the end of passband region and start of transition region (ii) at the end of the transition region and start of the stopband region. The slopes of the magnitude response are equalized at these points of discontinuity i.e. ω_p and ω_z shown in Fig.2.1 which makes the function continuous at these points reducing the overshoots due to Gibb's phenomenon. This leads to reduction of the peak ripple at



(a)



(b)



(c)

Fig.2.1. Illustration of novel slope equalization technique: (a) Lowpass FIR filter model with equiripple magnitude response (b) Expanded view of passband (c) Expanded view of stopband.

the points of discontinuities and hence reduces passband ripple and increases stopband attenuation. In Fig.2.1, the slopes are equalized at ω_p i.e., slope A equal to slope B and at ω_z i.e. slope C equal to slope D. The filter is modeled over three regions i.e., passband, transition and stopband regions using trigonometric functions. Filter design parameters of the filter model are evaluated with slope equalization.

2.4 Expressions for Impulse Response Coefficients of a Digital Filter

Let $h(n)$ be the impulse response sequence of an N-point, linear phase FIR digital filter where, $0 \leq n \leq N-1$. The linear phase condition implies that the impulse response satisfies the symmetry condition [8], [19].

$$h(n) = h(N-1-n), \quad \text{where } n = 0, 1, 2, \dots, N-1. \quad (2.1)$$

The frequency response for the linear-phase FIR filters for order N is given by [8].

$$H(e^{j\omega}) = \sum_{n=0}^{N-1} h(n) e^{-j\omega n} \quad (2.2)$$

$$H(e^{j\omega}) = e^{-j\left(\frac{N-1}{2}\right)\omega} H_{pm}(\omega) \quad (2.3)$$

where the pseudo magnitude response $H_{pm}(\omega)$ is

$$H_{pm}(\omega) = h\left(\frac{N-1}{2}\right) + 2 \sum_{n=0}^{\frac{N-1}{2}-1} h(n) \cos\left[\left(\frac{N-1}{2} - n\right)\omega\right] \quad \text{for N odd} \quad \text{and} \quad (2.4)$$

$$H_{pm}(\omega) = 2 \sum_{n=0}^{\frac{N}{2}-1} h(n) \cos\left[\left(\frac{N-1}{2} - n\right)\omega\right] \quad \text{for N even} \quad (2.5)$$

The impulse response sequence (coefficients) $h(n)$ of the filter obtained from this frequency response are,

$$h(n) = \frac{1}{2\pi} \int_{-\pi}^{\pi} H_{pm}(\omega) \cos\left[\left(\frac{N-1}{2} - n\right)\omega\right] d\omega, \quad (2.6)$$

$$n = 0, 1, 2, \dots, \frac{N-1}{2}, \text{ for } N \text{ odd and}$$

$$n = 0, 1, 2, \dots, \frac{N}{2} - 1, \text{ for } N \text{ even} \quad (2.7)$$

2.5 Class I FIR Lowpass Filter with Non-Monotonic Response without Slope Equalization

2.5.1 Filter Model and Design

In this section, the formulation of a linear phase, sharp transition, lowpass FIR filter model with non-monotonic passband response and its design is presented. The filter model magnitude response $H_{pm}(\omega)$ is as shown in Fig.2.2. For the proposed lowpass filter model, the various regions of the filter response are modeled using trigonometric functions of frequency as follows.

In the passband region, the frequency response is

$$H_{pm}(\omega) = 1 + k_p \delta_p \sin(\omega - \omega_0), \quad 0 \leq \omega \leq \omega_p \quad (2.8)$$

where ω is the frequency variable, $H_{pm}(\omega)$ is the pseudo-magnitude of the filter response, δ_p is the passband ripple, k_p is a filter design parameter, ω_p is the passband edge at which $H_{pm}(\omega)$ is maximum and ω_0 is a frequency at which $H_{pm}(\omega)$ is unity.

In the transition region, which also spans part of the passband $[\omega_p, \omega_c]$ as well part of the stopband $[\omega_s, \omega_z]$ the frequency response is given by

$$H_{pm}(\omega) = \left(1 + \frac{\delta_p}{2}\right) \cos[k_t(\omega - \omega_p)], \quad \omega_p \leq \omega \leq \omega_z \quad (2.9)$$

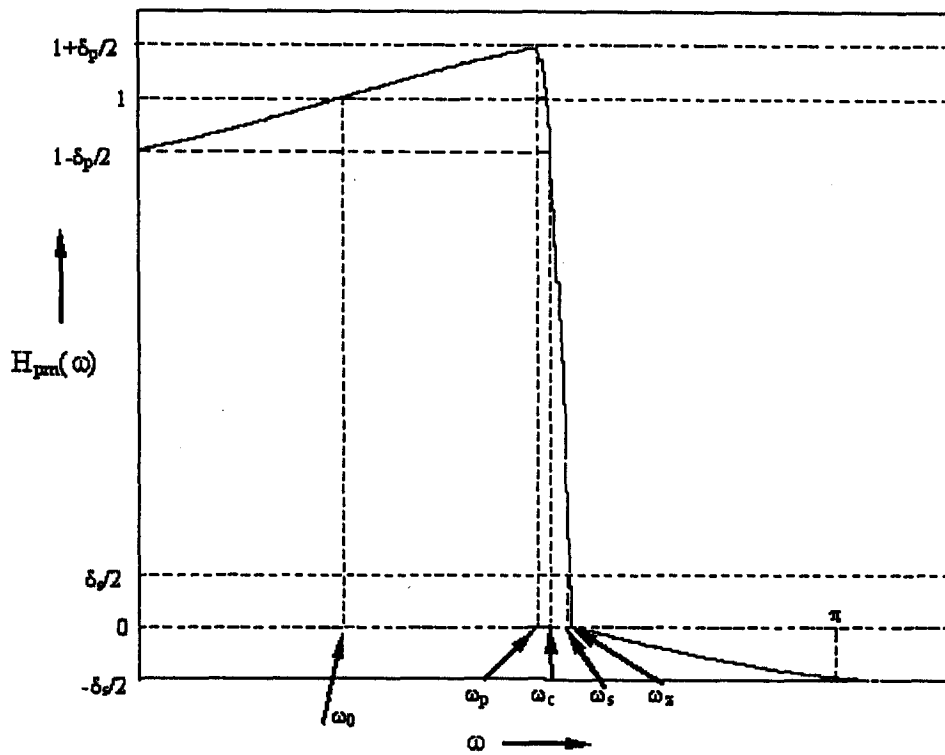


Fig.2.2. Illustration of proposed Class I lowpass filter model with non-monotonic magnitude response

where k_t is a filter design parameter, ω_z is the frequency in the stopband at which $H_{pm}(\omega)$ is zero and ω_s is the stopband-edge.

In the stopband region beyond ω_z , the frequency response is given by,

$$H_{pm}(\omega) = -\frac{k_s \delta_s}{2} \sin(\omega - \omega_z) \quad , \quad \omega_z \leq \omega \leq \pi \quad (2.10)$$

where δ_s is the stopband attenuation and k_s is a filter design parameter.

$$\text{At } \omega = 0, H_{pm}(0) = 1 - \frac{\delta_p}{2} = \left[1 - k_p \delta_p \sin(\omega_0) \right] \quad (2.11)$$

$$\text{Simplifying, we obtain, } k_p = \frac{1}{2 \sin \omega_0} \quad (2.12)$$

$$\text{At } \omega = \omega_p, H_{pm}(\omega_p) = 1 + \frac{\delta_p}{2} = 1 + k_p \delta_p \sin(\omega_p - \omega_0) \quad (2.13)$$

Simplifying we obtain,

$$\omega_p = \omega_0 + \sin^{-1} \left[\frac{1}{2k_p} \right] \quad (2.14)$$

Substituting (2.12) in (2.14) we obtain,

$$\omega_p = 2\omega_0 \quad (2.15)$$

Thus, ω_0 is the mid-band frequency.

$$\text{At } \omega = \omega_z, H_{pm}(\omega_z) = 0 = \left(1 + \frac{\delta_p}{2} \right) \cos k_t (\omega_z - \omega_p) \quad (2.16)$$

$$\text{Simplifying (2.16), } \omega_z = \omega_p + \frac{\pi}{2k_t} = 2\omega_0 + \frac{\pi}{2k_t} \quad (2.17)$$

$$\text{At } \omega = \omega_c, H_{pm}(\omega_c) = \left(1 - \frac{\delta_p}{2} \right) = \left(1 + \frac{\delta_p}{2} \right) \cos k_t (\omega_c - \omega_p) \quad (2.18)$$

$$\text{Simplifying (2.18), } \omega_c = \omega_p + \frac{1}{k_t} \cos^{-1} \left[\frac{1 - \frac{\delta_p}{2}}{1 + \frac{\delta_p}{2}} \right] \quad (2.19)$$

$$\text{At } \omega = \pi, H_{pm}(\pi) = -\frac{\delta_s}{2} = -\frac{k_s \delta_s}{2} \sin(\pi - \omega_z) \quad (2.20)$$

$$\text{Simplifying (2.20), } k_s = \frac{1}{\sin \omega_z} \quad (2.21)$$

$$\text{At } \omega = \omega_s, H_{pm}(\omega_s) = \frac{\delta_s}{2} = \left(1 + \frac{\delta_p}{2}\right) \cos k_t (\omega_s - \omega_p) \quad (2.22)$$

$$\text{Simplifying (2.22), } \omega_s = \omega_p + \frac{1}{k_t} \cos^{-1} \left[\frac{\frac{\delta_s}{2}}{1 + \frac{\delta_p}{2}} \right] \quad (2.23)$$

Using (2.19) and (2.23) we obtain,

$$k_t = \frac{1}{(\omega_s - \omega_c)} \left[\cos^{-1} \left[\frac{\frac{\delta_s}{2}}{1 + \frac{\delta_p}{2}} \right] - \cos^{-1} \left[\frac{1 - \frac{\delta_p}{2}}{1 + \frac{\delta_p}{2}} \right] \right] \quad (2.24)$$

2.5.2 Expressions for Impulse Response Coefficients

Referring to filter design theory of section 2.4, the impulse response coefficients $h(n)$ for the lowpass filter are obtained by evaluating the integral below.

$$h(n) = \frac{1}{\pi} \left[\int_0^{\pi} H_{pm}(\omega) \cos k\omega \, d\omega \right] \quad (2.25)$$

$$h(n) = \frac{1}{\pi} \left[\int_0^{\omega_p} H_{pm}(\omega) \cos k\omega \, d\omega + \int_{\omega_p}^{\omega_z} H_{pm}(\omega) \cos k\omega \, d\omega + \int_{\omega_z}^{\pi} H_{pm}(\omega) \cos k\omega \, d\omega \right] \quad (2.26)$$

$$h(n) = \frac{1}{\pi} \left[\int_0^{\omega_p} [1 + k_p \delta_p \sin(\omega - \omega_0)] \cos k\omega \, d\omega + \int_{\omega_p}^{\omega_z} \left(1 + \frac{\delta_p}{2}\right) \cos[k_t(\omega - \omega_p)] \cos k\omega \, d\omega \right. \\ \left. + \int_{\omega_z}^{\pi} -\frac{k_s \delta_s}{2} \sin(\omega - \omega_z) \cos k\omega \, d\omega \right] \quad (2.27)$$

where $n = 0, 1, \dots, \frac{N-1}{2}$ for N odd,

$$n = 0, 1, \dots, \frac{N}{2} - 1 \text{ for N even and } k = \frac{N-1}{2} - n$$

Evaluating (2.27), the expressions obtained for the impulse response coefficients $h(n)$ for the lowpass filter are

$$h(n) = h\left(\frac{N-1}{2} + k\right) = h\left(\frac{N-1}{2} - k\right) \\ = \frac{\sin(k\omega_p)}{k\pi} + \frac{k_p \delta_p}{\pi(k^2 - 1)} [k \sin(k\omega_p) \sin \omega_0 + \cos(k\omega_p) \cos \omega_0 - \cos \omega_0] \\ + \frac{\left(1 + \frac{\delta_p}{2}\right)}{\pi(k_t^2 - k^2)} [k_t \cos k\omega_z + k \sin k\omega_p] \\ + \frac{k_s \delta_s}{2\pi(k^2 - 1)} [\cos(k\omega_z) + \cos(k\pi) \cos \omega_z - k \sin(k\pi) \sin \omega_z] \quad (2.28)$$

Eq. (2.28) is valid for N even where k is a non-integer. For N odd, (2.28) is valid except for $k=0$, $k=1$ and $k = k_t$.

For N odd, $k=0$ we obtain,

$$h(n) = h\left(\frac{N-1}{2}\right) = \frac{\omega_p}{\pi} + \frac{\left(1 + \frac{\delta_p}{2}\right)}{\pi k_t} - \frac{k_s \delta_s}{2\pi} (1 + \cos \omega_z) \quad (2.29)$$

For N odd, $k=1$ we obtain,

$$\begin{aligned}
 h(n) &= h\left(\frac{N-1}{2}+1\right) = h\left(\frac{N-1}{2}-1\right) = \frac{\sin\omega_p}{\pi} + \frac{k_p\delta_p}{4\pi} [\cos\omega_0 - \cos(3\omega_0)] - \frac{\delta_p\omega_p}{4\pi} \\
 &+ \frac{\left(1 + \frac{\delta_p}{2}\right)}{\pi(k_t^2 - 1)} [k_t \cos\omega_z + \sin\omega_p] + \frac{k_s\delta_s}{4\pi} (\pi - \omega_z) \sin\omega_z
 \end{aligned} \tag{2.30}$$

For N odd, $k= k_t$ we obtain,

$$\begin{aligned}
 h\left(\frac{N-1}{2}+k_t\right) &= h\left(\frac{N-1}{2}-k_t\right) \\
 &= \frac{\sin(k_t\omega_p)}{k_t\pi} + \frac{k_p\delta_p}{\pi(k_t^2 - 1)} [k_t \sin(k_t\omega_p) \sin\omega_0 + \cos(k_t\omega_p) \cos\omega_0 - \cos\omega_0] \\
 &+ \frac{\left(1 + \frac{\delta_p}{2}\right)}{2\pi} \left[(\omega_z - \omega_p) \cos(\omega_p k_t) - \frac{\sin(\omega_p k_t)}{k_t} \right] \\
 &+ \frac{k_s\delta_s}{2\pi(k_t^2 - 1)} [\cos(k_t\omega_z) + \cos(k_t\pi) \cos\omega_z - k_t \sin(k_t\pi) \sin\omega_z]
 \end{aligned} \tag{2.31}$$

2.5.3 Filter Synthesis Results

Design Example: A lowpass linear phase sharp transition FIR filter is designed for the desired filter specifications: Passband edge ω_p is 0.666π , transition bandwidth $(\omega_s - \omega_c)$ is 0.01π , maximum passband ripple δ_p is ± 0.1 dB (0.2 dB) and minimum stopband attenuation δ_s is 40dB using the proposed Class I filter design approach.

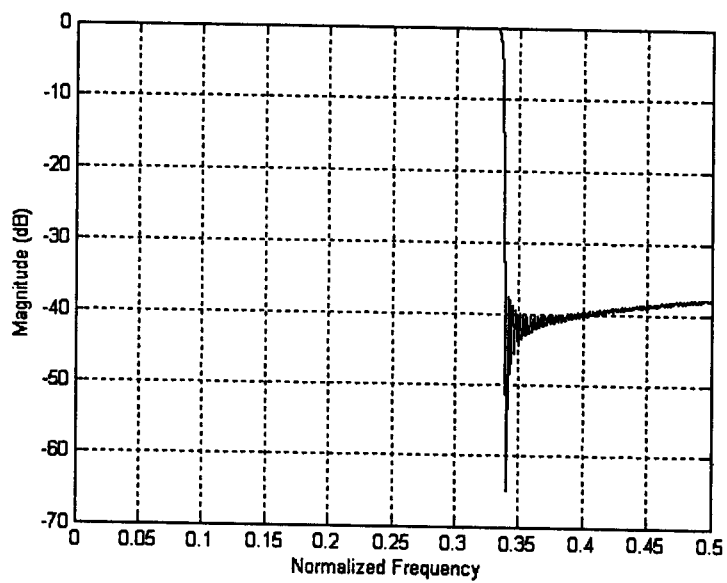
The lowpass filter is designed using MATLAB [20][21] with program MLP-1. The filter specifications obtained by measurement of the magnitude response of the filter using Signal Processing toolbox are passband edge $\omega_p = 0.6667\pi$, cutoff edge $\omega_c = 0.6668\pi$, stopband edge

$\omega_s = 0.6767\pi$, transition bandwidth $(\omega_s - \omega_c) = 0.01\pi$, passband ripple $\delta_p = 0.088\text{dB}$ and stopband attenuation $\delta_s = 32.2\text{dB}$ for a filter order of 701. Results appropriate the desired filter specifications closely but the desired filter specifications of stopband attenuation is not achieved for order 701 and with slight improvement in stopband attenuation for higher filter order. Hence this filter model and design is treated as a developmental one. The magnitude, impulse and phase response of the proposed lowpass filter obtained is shown in Fig.2.3. Also Table 2.1 depicts the performance of the filter. It is observed that for conventional FIR sharp transition filters the peak passband ripple due to Gibb's phenomenon is about 18%. In the proposed Class I filter design the peak passband ripple is 0.99% for the filter order 701 and decreases for higher filter order. Filter synthesis and design steps are shown in Appendix A 6.1.1

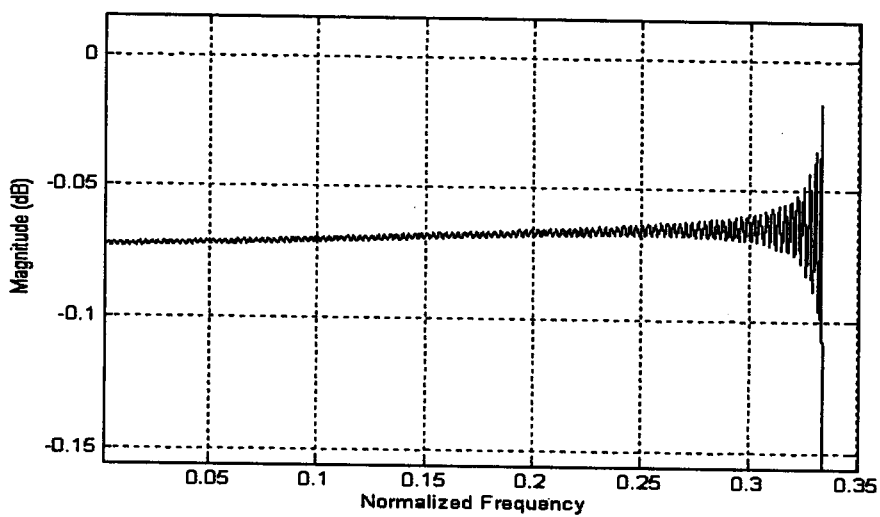
Table 2.1

Variation of passband ripple and stopband attenuation with filter order for transition band width of 0.01π and passband edge of 0.666π without slope equalization for proposed Class I FIR filter.

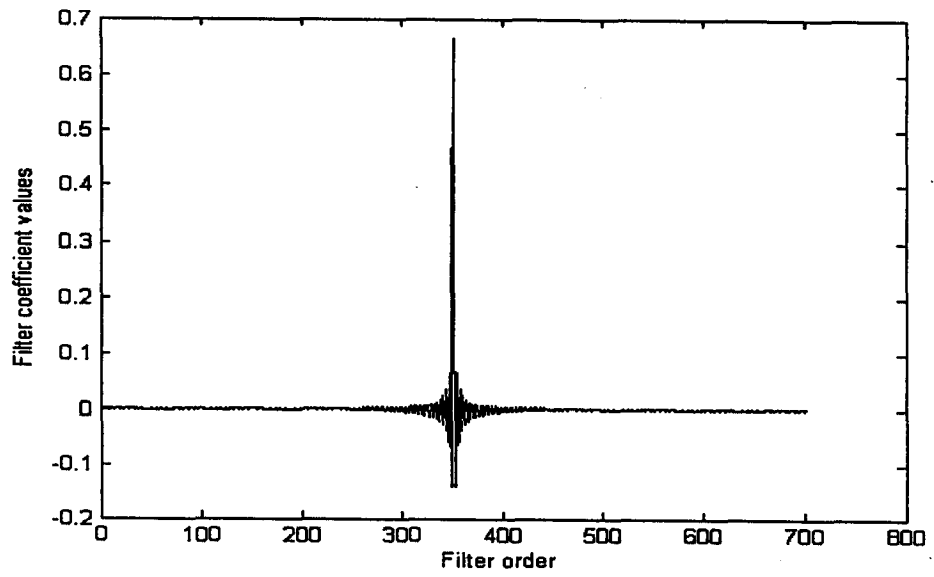
Filter Order	301	401	501	601	701	801
Passband Ripple in dB	0.454	0.129	0.105	0.103	0.088	0.035
Stopband Attenuation in dB	25.72	28.88	30.7	31.57	32.2	33.2



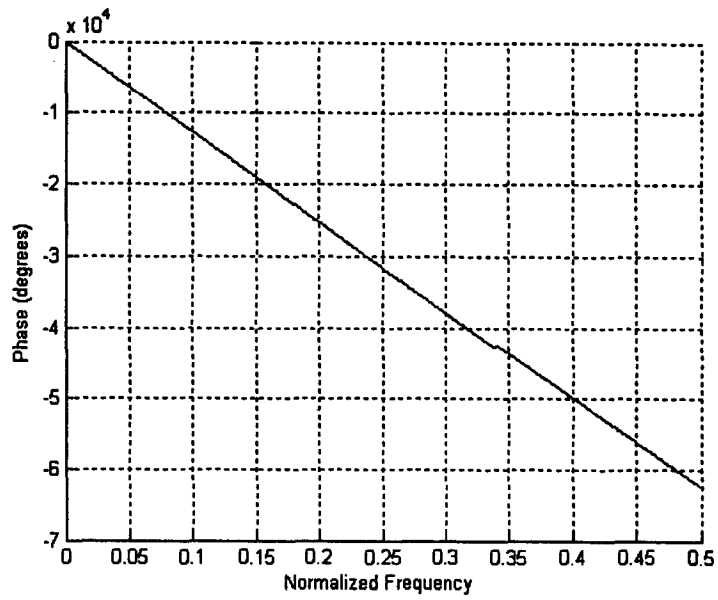
(a)



(b)



(c)



(d)

Fig. 2.3. (a) Magnitude response of the proposed Class I lowpass filter (b) magnified view of the passband (c) Impulse response sequence (d) Phase response.

2.6 Class II FIR Lowpass Filter with Monotonic Response without Slope Equalization

2.6.1 Filter Model and Design

In this section, the formulation of linear phase, sharp transition lowpass FIR filter model with monotonic passband response and its design is presented [22]. The passband and the transition regions are modified in this design. The filter model magnitude response $H_{pm}(\omega)$ is as shown in Fig.2.4. For the proposed lowpass filter model, the various regions of the filter response are modeled using trigonometric functions of frequency as follows.

In the passband region, the frequency response is

$$H_{pm}(\omega) = 1 - k_p \sin \omega, \quad 0 \leq \omega \leq \omega_c \quad (2.32)$$

where as before, ω is the frequency variable, $H_{pm}(\omega)$ is the pseudo-magnitude of the filter response, k_p is a filter design parameter, δ_p is the passband ripple, ω_c is the cut-off edge,

$$H_{pm}(0) = 1 \text{ and } H_{pm}(\omega_c) = 1 - \delta_p.$$

In the transition region and part of the stopband $[\omega_s, \omega_z]$, the frequency response is

$$H_{pm}(\omega) = (1 - \delta_p) [1 - \sin k_t (\omega - \omega_c)] , \quad \omega_c \leq \omega \leq \omega_z \quad (2.33)$$

where $H_{pm}(\omega_z) = 0$ and $H_{pm}(\omega_s) = \frac{\delta_s}{2}$ where δ_s is the stopband attenuation, k_t is a filter design parameter, ω_s is the stopband-edge and ω_z is the frequency in the stopband region at which $H_{pm}(\omega)$ is zero.

In the stopband region, the frequency response is

$$H_{pm}(\omega) = \frac{-k_s \delta_s}{2} \sin (\omega - \omega_z) , \quad \omega_z \leq \omega \leq \pi \quad (2.34)$$

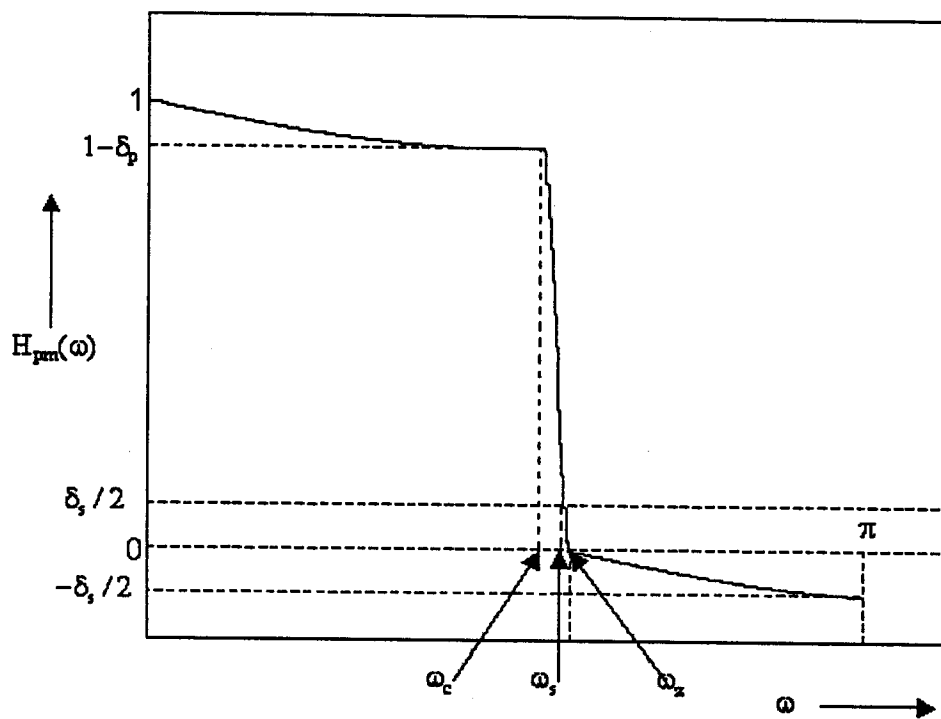


Fig.2.4. Illustration of proposed Class II lowpass filter model with monotonic magnitude response.

where k_s is a filter design parameter.

$$\text{At } \omega = \omega_z, H_{pm}(\omega_z) = 0 = (1 - \delta_p)[1 - \sin k_t(\omega_z - \omega_c)] \quad (2.35)$$

$$\text{Simplifying (2.35), } \omega_z = \omega_c + \frac{\pi}{2k_t} \quad (2.36)$$

$$\text{At } \omega = \omega_c, H_{pm}(\omega_c) = 1 - \delta_p = 1 - k_p \sin \omega_c \quad (2.37)$$

$$\text{Simplifying (2.37), } k_p = \frac{\delta_p}{\sin \omega_c} \quad (2.38)$$

$$\text{At } \omega = \pi, H_{pm}(\pi) = -\frac{\delta_s}{2} = \frac{-k_s \delta_s}{2} \sin(\pi - \omega_z) \quad (2.39)$$

$$\text{Simplifying (2.39), } k_s = \frac{1}{\sin \omega_z} \quad (2.40)$$

$$\text{At } \omega = \omega_s, H_{pm}(\omega_s) = \frac{\delta_s}{2} = (1 - \delta_p)[1 - \sin k_t(\omega_s - \omega_c)] \quad (2.41)$$

Simplifying (2.41),

$$\omega_s = \omega_c + \frac{\sin^{-1} \left[1 - \frac{\delta_s}{2(1 - \delta_p)} \right]}{k_t} \quad (2.42)$$

$$\text{From (2.42), we have, } k_t = \frac{\sin^{-1} \left[1 - \frac{\delta_s}{2(1 - \delta_p)} \right]}{(\omega_s - \omega_c)} \quad (2.43)$$

It is not possible to model the frequency response equalizing the slopes at $\omega = \omega_c$. The slope of the response on the passband side can be shown to be low and equalizing the slope on the transition region side for sharp transition is not possible. Therefore slope equalization technique cannot be applied for this design.

2.6.2 Expressions for Impulse Response Coefficients

Referring to filter design theory of section 2.4, the impulse response coefficients $h(n)$ for the lowpass filter are obtained by evaluating the integrals below.

$$h(n) = \frac{1}{\pi} \left[\int_0^{\pi} H_{pm}(\omega) \cos k\omega \, d\omega \right] \quad (2.44)$$

$$h(n) = \frac{1}{\pi} \left[\int_0^{\omega_c} H_{pm}(\omega) \cos k\omega \, d\omega + \int_{\omega_c}^{\omega_z} H_{pm}(\omega) \cos k\omega \, d\omega + \int_{\omega_z}^{\pi} H_{pm}(\omega) \cos k\omega \, d\omega \right] \quad (2.45)$$

$$h(n) = \frac{1}{\pi} \left[\int_0^{\omega_c} (1 - k_p \sin \omega) \cos k\omega \, d\omega + \int_{\omega_c}^{\omega_z} (1 - \delta_p) [1 - \sin k_t (\omega - \omega_c)] \cos k\omega \, d\omega \right. \\ \left. + \int_{\omega_z}^{\pi} \frac{-k_s \delta_s}{2} \sin(\omega - \omega_z) \cos k\omega \, d\omega \right] \quad (2.46)$$

where $n = 0, 1, \dots, \frac{N-1}{2}$ for N odd

$n = 0, 1, \dots, \frac{N}{2} - 1$ for N even and $k = \frac{N-1}{2} - n$

Evaluating (2.46), the expressions obtained for the impulse response coefficients $h(n)$ for the lowpass filter are

$$h(n) = h\left(\frac{N-1}{2} + k\right) \\ = h\left(\frac{N-1}{2} - k\right) = \frac{\sin(k\omega_c)}{k\pi} + \frac{k_p}{(k^2 - 1)\pi} [1 - k \sin(k\omega_c) \sin \omega_c - \cos(k\omega_c) \cos \omega_c] \\ + \frac{(1 - \delta_p)}{\pi} \left[\frac{\sin(k\omega_z) - \sin(k\omega_c)}{k} + \frac{k \sin(k\omega_z) - k_t \cos(k\omega_c)}{(k_t^2 - k^2)} \right]$$

$$+ \frac{k_s \delta_s}{2(k^2 - 1)\pi} [\cos(k \omega_z) + \cos(k \pi) \cos \omega_z - k \sin(k \pi) \sin \omega_z] \quad (2.47)$$

Eq. (2.47) is valid for N even. For N odd, (2.47) is valid except for $k=0$, $k=1$ and $k=k_t$

For N odd, $k=0$ we obtain

$$h\left(\frac{N-1}{2}\right) = \frac{1}{\pi} \left[(\cos \omega_c - 1)k_p + \omega_c + (1 - \delta_p) \left[(\omega_z - \omega_c) - \frac{1}{k_t} \right] - \frac{k_s \delta_s}{2} (1 + \cos \omega_z) \right] \quad (2.48)$$

For N odd, $k=1$ we obtain

$$\begin{aligned} h\left(\frac{N-1}{2} + 1\right) &= h\left(\frac{N-1}{2} - 1\right) = \frac{k_p}{4\pi} [\cos(2\omega_c) - 1] + \frac{\sin \omega_c}{\pi} \\ &+ \frac{(1 - \delta_p)}{\pi} \left[(\sin \omega_z - \sin \omega_c) + \frac{(\sin \omega_z - k_t \cos \omega_c)}{(k_t^2 - 1)} \right] + \frac{k_s \delta_s}{4\pi} [(\pi - \omega_z) \sin \omega_z] \end{aligned} \quad (2.49)$$

For N odd, $k=k_t$ we obtain

$$\begin{aligned} h\left(\frac{N-1}{2} + k_t\right) &= h\left(\frac{N-1}{2} - k_t\right) \\ &= \frac{\sin(k_t \omega_c)}{\pi} + \frac{k_p}{(k_t^2 - 1)\pi} [1 - k_t \sin(k_t \omega_c) \sin \omega_c - \cos(k_t \omega_c) \cos \omega_c] \\ &+ \frac{(1 - \delta_p)}{\pi} \left[\frac{\sin(k_t \omega_z) - \sin(k_t \omega_c)}{k_t} \right] - \frac{(1 - \delta_p)}{2\pi} \left[\frac{\cos k_t \omega_c}{k_t} + (\omega_z - \omega_c) \sin(k_t \omega_c) \right] \\ &+ \frac{k_s \delta_s}{2(k_t^2 - 1)\pi} [\cos(k_t \omega_z) + \cos(k_t \pi) \cos \omega_z - k_t \sin(k_t \pi) \sin \omega_z] \end{aligned} \quad (2.50)$$

2.6.3 Filter Synthesis Results

Design Example: A lowpass linear phase sharp transition FIR filter is designed for the desired filter specifications: Cutoff edge ω_c is 0.666π , transition bandwidth $(\omega_s - \omega_c)$ is 0.01π , maximum

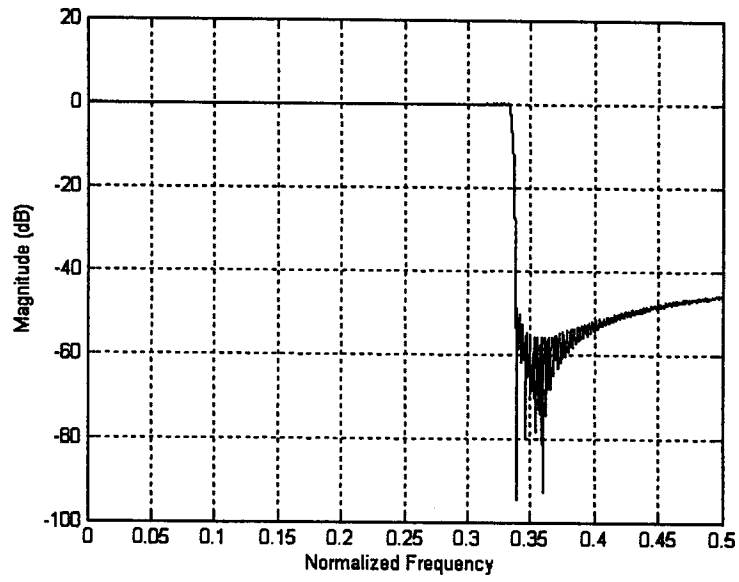
passband ripple δ_p is ± 0.1 dB (0.2 dB) and minimum stopband attenuation δ_s is 40dB using the proposed Class II filter design approach.

The filter is designed using MATLAB with program MLP-2. The filter specifications obtained by measurement of the magnitude response of the filter using Signal Processing toolbox are cutoff edge $\omega_c = 0.6668\pi$, stopband edge $\omega_s = 0.6767\pi$, transition bandwidth $(\omega_s - \omega_c) = 0.01\pi$, passband ripple $\delta_p = 0.204$ dB and stopband attenuation $\delta_s = 46.3$ dB for a filter order of 701. It is observed that the desired filter specifications are obtained as per design example with very good stopband attenuation. It is also observed that passband ripple is higher compared to all proposed filter model designs. The magnitude and impulse response of the proposed lowpass filter obtained is shown in Fig.2.5. Table 2.2 depicts the performance of the filter. In the proposed Class II filter the peak passband ripple is 2.3% for the filter order 701 and decreases for higher filter order as compared to about 18% peak passband ripple in conventional FIR filters. Filter synthesis and design steps are given in Appendix A6.1.2.

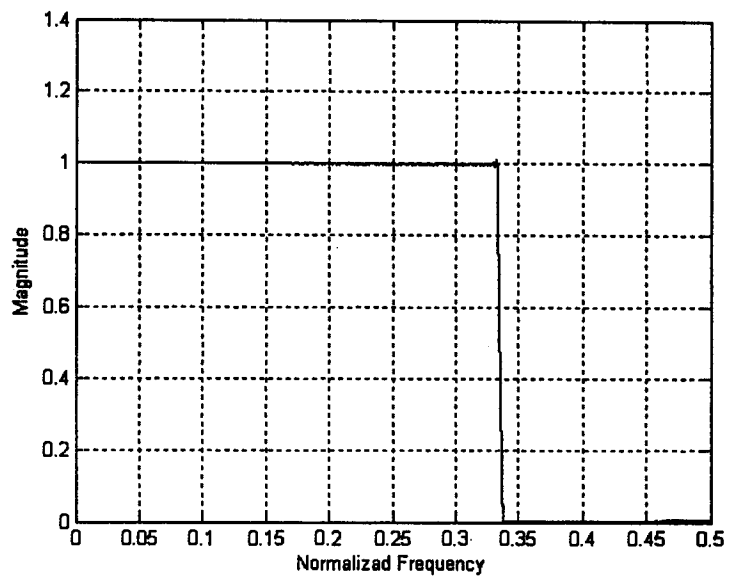
Table 2.2

Variation of passband ripple and stopband attenuation with filter order for transition bandwidth of 0.01π and passband edge of 0.666π without slope equalization for proposed Class II FIR filter.

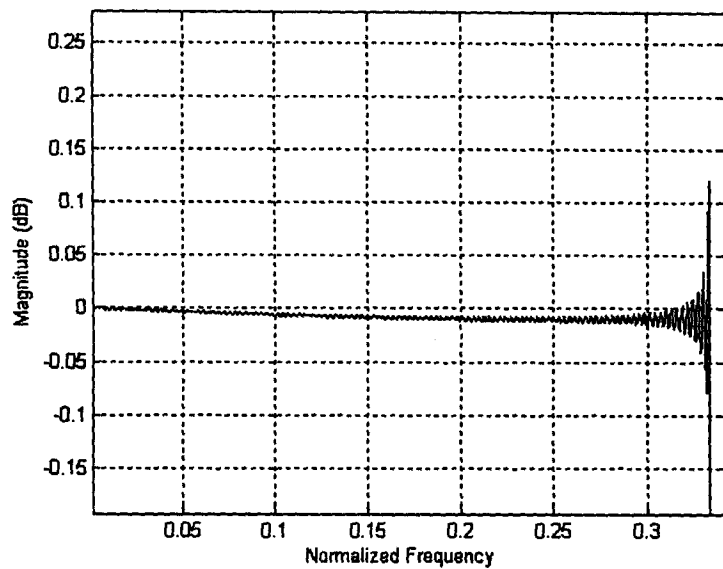
Filter Order	301	401	501	601	701	801
Passband Ripple in dB	0.538	0.34	0.262	0.236	0.204	0.165
Stopband Attenuation in dB	31.95	45.10	45.26	45.79	46.3	46.98



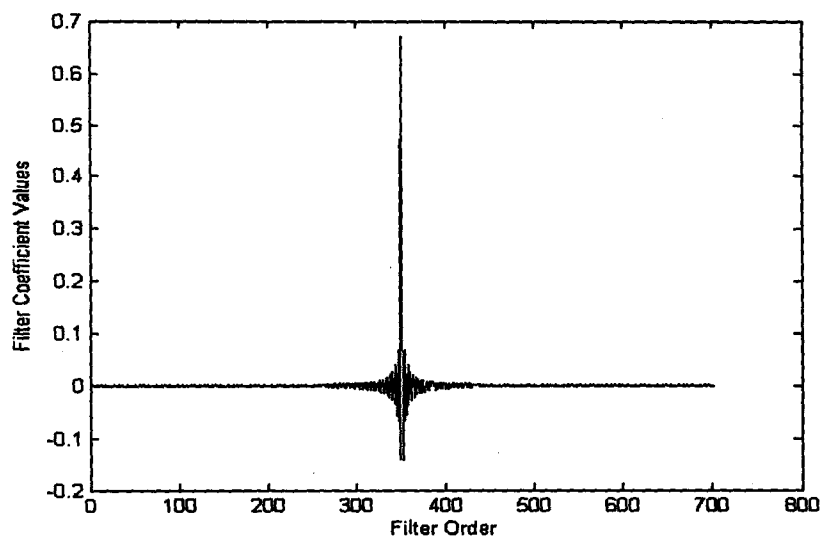
(a)



(b)



(c)



(d)

Fig. 2.5.(a) Magnitude response of the proposed Class II lowpass filter (b) Linear plot (c) magnified view of the passband (d) Impulse response sequence.

2.7 Class III FIR Lowpass Filter with Equiripple Response

2.7.1 Filter Model and Design without slope equalization

In this section, the formulation of a linear phase, sharp transition, lowpass FIR filter model with equiripple passband and stopband with its design is presented [23]. The filter model magnitude response $H_{pm}(\omega)$ is as shown in Fig.2.6. In the proposed lowpass filter model, the various regions of the filter response are modeled using trigonometric functions of frequency as follows.

In the passband region, the frequency response is

$$H_{pm}(\omega) = 1 + \frac{\delta_p}{2} \cos k_p \omega, \quad 0 \leq \omega \leq \omega_p \quad (2.51)$$

where as usual ω is the frequency variable, $H_{pm}(\omega)$ is the pseudo-magnitude of the filter response, δ_p is the passband ripple, k_p is a filter design parameter in the passband and ω_p is the passband edge.

Transition region spans part of the passband $[\omega_p, \omega_c]$ as well as part of the stopband $[\omega_s, \omega_z]$ where ω_c is the cutoff edge and ω_s is the stopband edge and ω_z is the frequency in the stopband region at which $H_{pm}(\omega)$ is zero. In the transition region, the frequency response is given by

$$H_{pm}(\omega) = A \cos k_t (\omega - \omega_0), \quad \omega_p \leq \omega \leq \omega_z \quad \text{and} \quad \omega_0 < \omega_p \quad (2.52)$$

where k_t is a filter design parameter in the transition region, A is amplitude parameter and is chosen greater than 1, ω_0 is the frequency at which $H_{pm}(\omega)$ equals A . It may be noted that, ω_0 is a fictitious frequency parameter used to shape the response in the region $\omega_p \leq \omega \leq \omega_z$ which does not include ω_0 . The formulation according to (2.52) yields some design flexibility later on

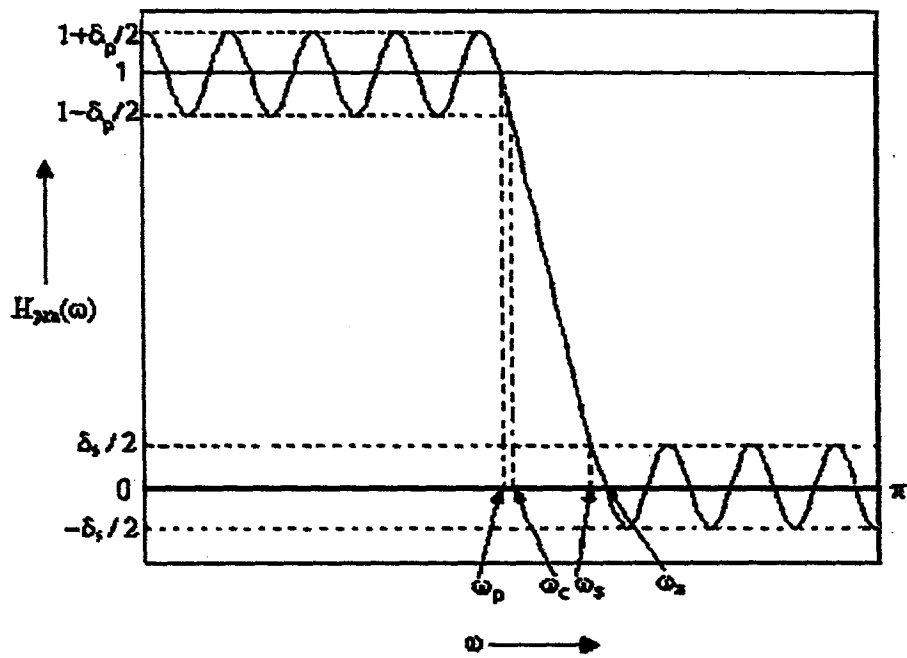


Fig.2.6. Illustration of proposed Class III lowpass filter model with equiripple magnitude response

when slope equalization technique is applied to the design.

In the stopband region, the frequency response is given

$$H_{pm}(\omega) = -\frac{\delta_s}{2} \text{sinc}_s(\omega - \omega_z), \quad \omega_z \leq \omega \leq \pi \quad (2.53)$$

where δ_s is the stopband attenuation, k_s is a filter design parameter in the stopband region.

$$\text{The number of ripple cycles in the passband region } [0, \omega_p] = k_r + \frac{1}{4} \quad (2.54)$$

where $k_r = 0, 1, 2, \dots$ is a non-negative integer.

For the Class III lowpass filter design, the passband region $[0, \omega_p]$ of the filter model possess

$\left(k_r + \frac{1}{4}\right)$ number of ripples cycles and is characterized by filter design parameter k_p

$$\text{Therefore, } k_p \omega_p = 2\pi \left(k_r + \frac{1}{4}\right) \quad (2.55)$$

$$\text{i.e. } k_p = \frac{2\pi \left(k_r + \frac{1}{4}\right)}{\omega_p} \quad (2.56)$$

It may be noted that a large value of k_r lead to a large value of k_p which in turn yields $\omega_c \cong \omega_p$

and $\omega_s \cong \omega_z$ which guarantee a steep transition.

$$\text{At } \omega = 0, H_{pm}(0) = 1 + \frac{\delta_p}{2} \quad (2.57)$$

$$\text{At } \omega = \omega_p, H_{pm}(\omega_p) = 1.0 = A \cos k_t(\omega_p - \omega_0) \quad (2.58)$$

$$\text{From (2.58) we obtain, } A = \frac{1}{\cos k_t(\omega_p - \omega_0)} \quad (2.59)$$

The design strategy envisages the use of a part of the first quarter cycle of a cosine wave to simulate the transition region. To make the transition sharper, only the base of the waveform near zero crossing is used. The amplitude of the cosine wave is A and this wave is shifted in frequency by ω_0 . Accordingly $A > 1$ and/or $\omega_0 \leq \omega_p$ is chosen. To reduce the transition region width a frequency compression factor, $k_t \gg 1$ is used. It is noted that the choice of $\omega_0 < \omega_p$ makes ω_0 fictitious, since only the portion limited by $[\omega_p, \omega_z]$ of the cosine wave is used.

From (2.59) we obtain

$$\omega_0 = \omega_p - \left(\frac{1}{k_t} \right) \cos^{-1} \left(\frac{1}{A} \right) \quad (2.60)$$

$$\text{At } \omega = \omega_0, H_{pm}(\omega_0) = A \quad (2.61)$$

$$\text{At } \omega = \omega_c, H_{pm}(\omega_c) = 1 - \frac{\delta_p}{2} = A \cos k_t (\omega_c - \omega_0) \quad (2.62)$$

$$\text{Simplifying (2.62), } \omega_c = \omega_0 + \frac{1}{k_t} \cos^{-1} \left(\frac{1 - \frac{\delta_p}{2}}{A} \right) \quad (2.63)$$

$$\text{At } \omega = \omega_s, H_{pm}(\omega_s) = \frac{\delta_s}{2} = A \cos k_t (\omega_s - \omega_0) \quad (2.64)$$

Simplifying (2.64),

$$\omega_s = \omega_0 + \frac{1}{k_t} \cos^{-1} \left(\frac{\delta_s}{2A} \right) \quad (2.65)$$

$$\text{Using (2.63) and (2.65), } k_t = \frac{1}{(\omega_s - \omega_c)} \left[\cos^{-1} \left(\frac{\delta_s}{2A} \right) - \cos^{-1} \left(\frac{1 - \frac{\delta_p}{2}}{A} \right) \right] \quad (2.66)$$

$$\text{At } \omega = \omega_z, H_{pm}(\omega_z) = 0 = A \cos k_t (\omega_z - \omega_0) \quad (2.67)$$

$$\text{Simplifying (2.67), } \omega_z = \omega_0 + \frac{\pi}{2k_t} \quad (2.68)$$

$$\text{At } \omega = \pi, H_{pm}(\pi) = -\frac{\delta_s}{2} = -\frac{\delta_s}{2} \text{sinc}_s(\pi - \omega_z) \quad (2.69)$$

$$\text{Simplifying (2.69), } k_s = \frac{\pi(4L+1)}{2(\pi - \omega_z)} \quad (2.70)$$

The lowpass filter design has $(L+1/4)$ number of ripples in the stopband i.e. in the region $[\omega_z, \pi]$ where L is a non-negative integer.

2.7.1.1 Expressions for Impulse Response Coefficients

Referring to filter design theory of section 2.4, the impulse response coefficients $h(n)$ for the lowpass filter are obtained by evaluating the integral below.

$$h(n) = \frac{1}{\pi} \left[\int_0^{\pi} H_{pm}(\omega) \cos k\omega \, d\omega \right] \quad (2.71)$$

$$h(n) = \frac{1}{\pi} \left[\int_0^{\omega_p} H_{pm}(\omega) \cos k\omega \, d\omega + \int_{\omega_p}^{\omega_z} H_{pm}(\omega) \cos k\omega \, d\omega + \int_{\omega_z}^{\pi} H_{pm}(\omega) \cos k\omega \, d\omega \right] \quad (2.72)$$

$$h(n) = \frac{1}{\pi} \left[\int_0^{\omega_p} \left[1 + \frac{\delta_p}{2} \cos k_p \omega \right] \cos k\omega \, d\omega + \int_{\omega_p}^{\omega_z} A \cos k_t (\omega - \omega_0) \cos k\omega \, d\omega + \int_{\omega_z}^{\pi} -\frac{\delta_s}{2} \text{sinc}_s(\omega - \omega_z) \cos k\omega \, d\omega \right] \quad (2.73)$$

where $n = 0, 1, \dots, \frac{N-1}{2}$ for N odd

$n = 0, 1, \dots, \frac{N}{2} - 1$ for N even and $k = \frac{N-1}{2} - n$

Evaluating (2.73), the expressions obtained for the impulse response coefficients $h(n)$ for the lowpass filter are

$$\begin{aligned}
h(n) = h\left(\frac{N-1}{2} + k\right) &= h\left(\frac{N-1}{2} - k\right) = \frac{\sin(k\omega_p)}{k\pi} + \frac{\delta_p k_p \cos(k\omega_p)}{2\pi(k_p^2 - k^2)} \\
&+ \frac{1}{\pi(k_t^2 - k^2)} \left[Ak_t \cos(k\omega_z) - k_t (\sqrt{A^2 - 1}) \cos(k\omega_p) + k \sin(k\omega_p) \right] \\
&+ \frac{\delta_s}{2\pi(k_s^2 - k^2)} \left[k_s \cos k_s (\pi - \omega_z) \cos(k\pi) - k_s \cos(k\omega_z) + k \sin k_s (\pi - \omega_z) \sin(k\pi) \right] \quad (2.74)
\end{aligned}$$

Eq. (2.74) is valid for N even where k is a non-integer. For N odd (2.74) is valid except for $k = 0$, $k = k_p$, $k = k_s$ and $k = k_t$.

For N odd, $k = 0$ we obtain

$$h(n) = h\left(\frac{N-1}{2}\right) = \frac{\omega_p}{\pi} + \frac{\delta_p}{2\pi k_p} + \frac{1}{\pi k_t} (A - \sqrt{A^2 - 1}) + \frac{\delta_s}{2\pi k_s} [\cos k_s (\pi - \omega_z) - 1] \quad (2.75)$$

For N odd, $k = k_s$ we obtain,

$$\begin{aligned}
h\left(\frac{N-1}{2} + k_s\right) &= h\left(\frac{N-1}{2} - k_s\right) = \frac{\sin(k_s \omega_p)}{k_s \pi} + \frac{\delta_p k_p \cos(k_s \omega_p)}{2\pi(k_p^2 - k_s^2)} \\
&+ \frac{1}{\pi(k_t^2 - k_s^2)} \left[Ak_t \cos(k_s \omega_z) - k_t (\sqrt{A^2 - 1}) \cos(k_s \omega_p) + k_s \sin(k_s \omega_p) \right] \\
&+ \frac{\delta_s}{4\pi} (\pi - \omega_z) \sin(k_s \omega_z) + \frac{\delta_s}{4\pi} \frac{[\cos(2k_s \pi - k_s \omega_z) - \cos(k_s \omega_z)]}{2k_s} \quad (2.76)
\end{aligned}$$

For N odd, $k = k_p$ we obtain,

$$h(n) = h\left(\frac{N-1}{2} + k_p\right)$$

$$\begin{aligned}
&= h\left(\frac{N-1}{2} - k_p\right) = \frac{1}{k_p \pi} + \frac{\delta_p \omega_p}{4\pi} + \frac{1}{\pi(k_t^2 - k_p^2)} (A k_t \cos k_p \omega_z + k_p) \\
&\quad + \frac{\delta_s}{2\pi(k_s^2 - k_p^2)} \left[k_s \cos k_s (\pi - \omega_z) \cos(k_p \pi) - k_s \cos(k_p \omega_z) + k_p \sin k_s (\pi - \omega_z) \sin(k_p \pi) \right]
\end{aligned} \tag{2.77}$$

For N odd, $k = k_t$ we obtain,

$$\begin{aligned}
h\left(\frac{N-1}{2} + k_t\right) &= h\left(\frac{N-1}{2} - k_t\right) = \frac{\sin k_t \omega_p}{k_t \pi} + \frac{\delta_p k_p \cos(k_t \omega_p)}{2\pi(k_p^2 - k_t^2)} \\
&\quad + \left(\frac{A}{2\pi}\right) (\omega_z - \omega_p) \cos(k_t \omega_0) - \left(\frac{A}{2\pi}\right) \frac{[\sin(k_t \omega_0) + \sin(2k_t \omega_p - k_t \omega_0)]}{2k_t} \\
&\quad + \frac{\delta_s}{2\pi(k_s^2 - k_t^2)} \left[k_s \cos k_s (\pi - \omega_z) \cos(k_t \pi) - k_s \cos(k_t \omega_z) + k_t \sin k_s (\pi - \omega_z) \sin(k_t \pi) \right]
\end{aligned} \tag{2.78}$$

2.7.1.2 Filter Synthesis Results

Design Example: A lowpass linear phase sharp transition FIR filter is designed for the desired filter specifications: Passband edge ω_p is 0.666π , transition bandwidth ($\omega_s - \omega_c$) is 0.01π , maximum passband ripple δ_p is ± 0.1 dB (0.2 dB) and minimum stopband attenuation δ_s is 40dB using the proposed Class III filter design approach.

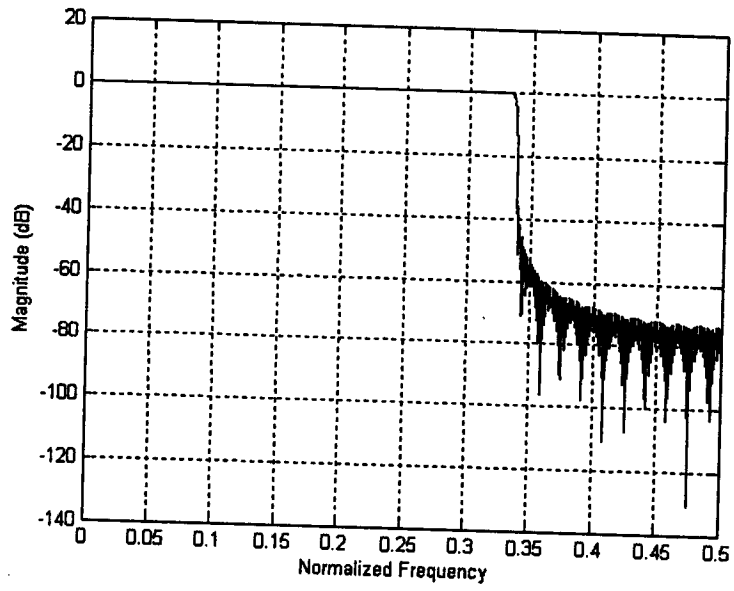
The filter is designed using MATLAB with program MLP-3. The filter specifications obtained by measurement of the magnitude response of the filter using Signal Processing toolbox are passband edge $\omega_p = 0.6667\pi$, cutoff edge $\omega_c = 0.6668\pi$, stopband edge $\omega_s = 0.6767\pi$, transition bandwidth ($\omega_s - \omega_c$) = 0.01π , passband ripple $\delta_p = 0.079$ dB and stopband attenuation

$\delta_s = 35$ dB for a filter order of 701. But it is found that stopband attenuation is less than the desired value of 40 dB, which can be achieved with higher filter order. The magnitude, impulse and phase response of the proposed lowpass filter obtained is shown in Fig.2.7. Also Table 2.3 depicts the performance of the filter. For conventional FIR sharp transition filters the peak passband ripple due to Gibb's phenomenon is about 18%. In the proposed Class III filter design the peak passband ripple is 0.92% for the filter order 701 and decreases for higher filter order. Filter synthesis and design steps are given in Appendix A6.1.3.

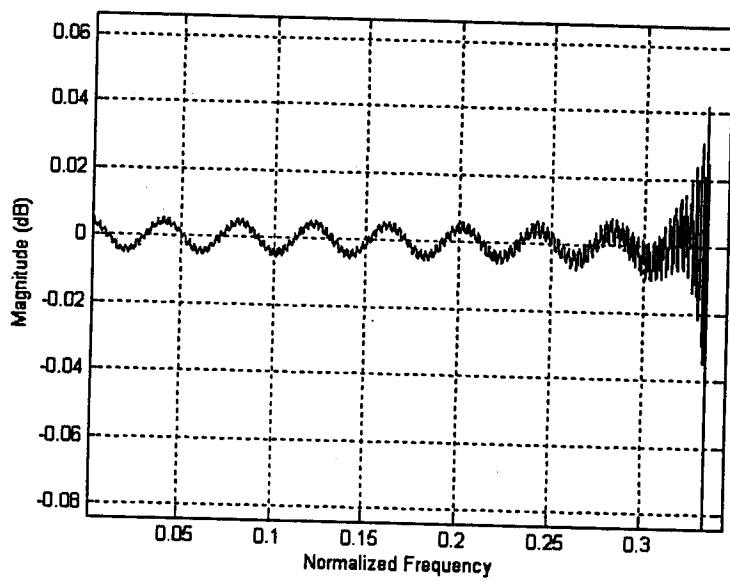
Table 2.3

Variation of passband ripple and stopband attenuation with filter order for transition bandwidth of 0.01π and passband edge of 0.666π without slope equalization for proposed Class III FIR filter.

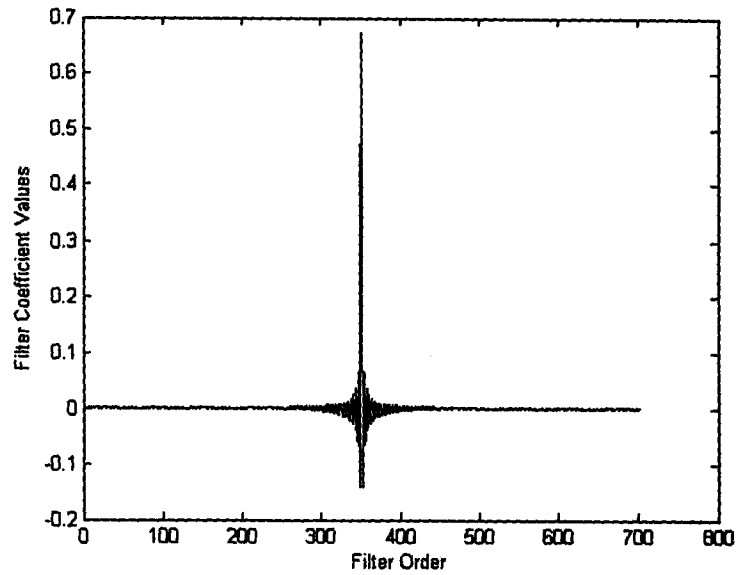
Filter Order	301	401	501	601	701	801
Passband ripple in dB	0.44	0.119	0.1094	0.1056	0.079	0.0351
Stopband Attn. in dB	26.79	31.0	33.22	34.47	35.0	37.0



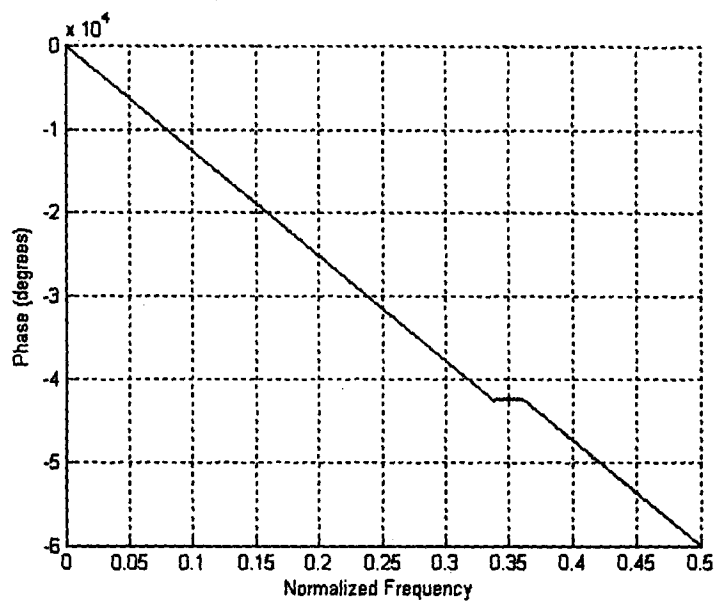
(a)



(b)



(c)



(d)

Fig. 2.7. (a) Magnitude response of the proposed Class III lowpass filter without slope equalization (b) magnified view of the passband (c) Impulse response sequence (d) Phase response.

2.7.2 Filter Design with Slope Equalization

Slope equalization technique is applied to the equiripple filter model of section 2.7.1, which further improves the performance of the filter. The filter design parameters k_p , k_t and k_s are evaluated by equalizing the slopes of the pseudo-magnitude response function at both the ends of the transition region. This allows the proposed function to be continuous thus reducing the effects due to Gibb's phenomenon and hence reduces passband ripple and increases stopband attenuation of the filter.

$$\text{At } \omega = \omega_p, H_{pm}(\omega_p) = 1 = 1 + \frac{\delta_p}{2} \cos k_p \omega_p \quad (2.79)$$

$$\begin{aligned} \text{Slope at } \omega_p &= \frac{d}{d\omega} [H_{pm}(\omega)]_{\omega=\omega_p} \\ &= \frac{d}{d\omega} \left[1 + \frac{\delta_p}{2} \cos k_p \omega_p \right] = -\frac{\delta_p}{2} k_p \sin k_p \omega_p \end{aligned} \quad (2.80)$$

Simplifying (2.79), $\cos k_p \omega_p = 0$ i.e. $\sin k_p \omega_p = \pm 1$

Since the slope of the magnitude response is negative at $\omega = \omega_p$, we choose the positive sign

$$\text{i.e. } \sin k_p \omega_p = 1 \quad (2.81)$$

Substituting (2.81) in (2.80),

$$\text{Slope at } \omega_p = \frac{-k_p \delta_p}{2} \quad (2.82)$$

$$\text{Also at } \omega = \omega_p, H_{pm}(\omega_p) = 1 = A \cos k_t (\omega_p - \omega_0) \quad (2.83)$$

$$\text{Simplifying (2.83), } \omega_0 = \omega_p - \frac{1}{k_t} \cos^{-1} \left(\frac{1}{A} \right) \quad (2.84)$$

$$\text{Slope at } \omega_p = \frac{d}{d\omega} [H_{pm}(\omega)]_{\omega=\omega_p} = \frac{d}{d\omega} [A \cos k_t (\omega - \omega_0)]$$

$$= -A k_t \sin k_t (\omega_p - \omega_0) \quad (2.85)$$

Using (2.83) in (2.85) and simplifying, we obtain,

$$\text{Slope at } \omega_p = -A k_t \sqrt{1 - \frac{1}{A^2}} \quad (2.86)$$

Equalization of slopes at ω_p by equating (2.82) and (2.86) yields,

$$k_p = \frac{2 k_t (\sqrt{A^2 - 1})}{\delta_p} \quad (2.87)$$

The filter design parameter k_t is obtained as before from (2.66) for a given $A > 1$, as

$$k_t = \frac{1}{(\omega_s - \omega_c)} \left[\cos^{-1} \left(\frac{\delta_s}{2A} \right) - \cos^{-1} \left(\frac{1 - \frac{\delta_p}{2}}{A} \right) \right] \quad (2.88)$$

$$\text{At } \omega = \omega_z, H_{pm}(\omega_z) = 0 = A \cos k_t (\omega_z - \omega_0) \quad (2.89)$$

Simplifying (2.89) we obtain, $\sin k_t (\omega_z - \omega_0) = \pm 1$. Since the slope of the response is negative

$$\text{at } \omega = \omega_z, \text{ we choose the positive sign i.e., } \sin k_t (\omega_z - \omega_0) = 1 \quad (2.90)$$

$$\text{Using (2.52), Slope at } \omega_z = \frac{d}{d\omega} [H_{pm}(\omega)]_{\omega=\omega_z}$$

$$= \frac{d}{d\omega} [A \cos k_t (\omega - \omega_0)] = -A k_t \sin k_t (\omega_z - \omega_0) \quad (2.91)$$

$$\text{Substituting (2.90) in (2.91), Slope at } \omega_z = -A k_t \quad (2.92)$$

$$\text{Using (2.53), Slope at } \omega_z = \frac{d}{d\omega} [H_{pm}(\omega)]_{\omega=\omega_z} = \frac{d}{d\omega} \left[-\frac{\delta_s}{2} \sin k_s (\omega - \omega_z) \right]$$

$$= -\frac{\delta_s}{2} k_s \cos k_s (\omega_z - \omega_z) = -\frac{\delta_s}{2} k_s \quad (2.93)$$

Equalizing the slopes at ω_z by equating (2.92) and (2.93),

$$-A k_t = -\frac{\delta_s}{2} k_s \quad (2.94)$$

$$\text{i.e. } k_s = \frac{2A k_t}{\delta_s} \quad (2.95)$$

The expressions for frequency domain parameters ω_z , ω_s and ω_c are identical to those in section 2.7.1. The expressions for impulse response coefficients are same as in section 2.7.1.1.

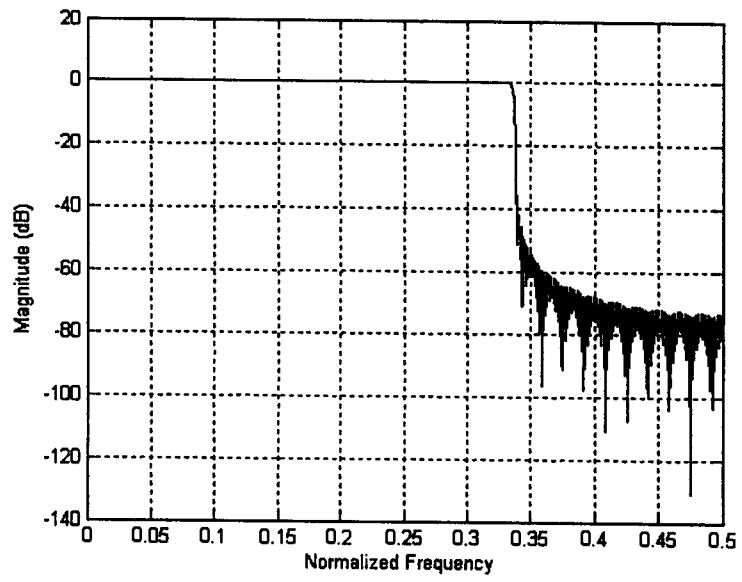
2.7.2.1 Filter Synthesis Results

For the same design example, as in section 2.7.1.2, the filter is designed using MATLAB with program MLP-4. The filter specifications obtained by measurement of the magnitude response of the filter using Signal Processing toolbox. It is found that passband edge, cutoff edge, stopband edge and transition bandwidth are same as in Class III without slope equalization technique but with reduced passband ripple of 0.068 dB and improved stopband attenuation of 35.82 dB for the same filter order of 701. The ripple due to Gibb's phenomenon is reduced with slope equalization technique and hence passband ripple reduces and stopband attenuation of the filter increases. The magnitude and impulse response of the proposed lowpass filter obtained is shown in Fig.2.8. Also Table 2.4, Fig. 2.9 and Fig. 2.10 depict the performance of the filter. For conventional FIR sharp transition filters the peak passband ripple due to Gibb's phenomenon is about 18%. In the proposed Class III filter with slope equalization the passband ripple is 0.7% for the filter order 701 and decreases for higher filter order. Filter synthesis and design steps are given in Appendix A6.1.3.

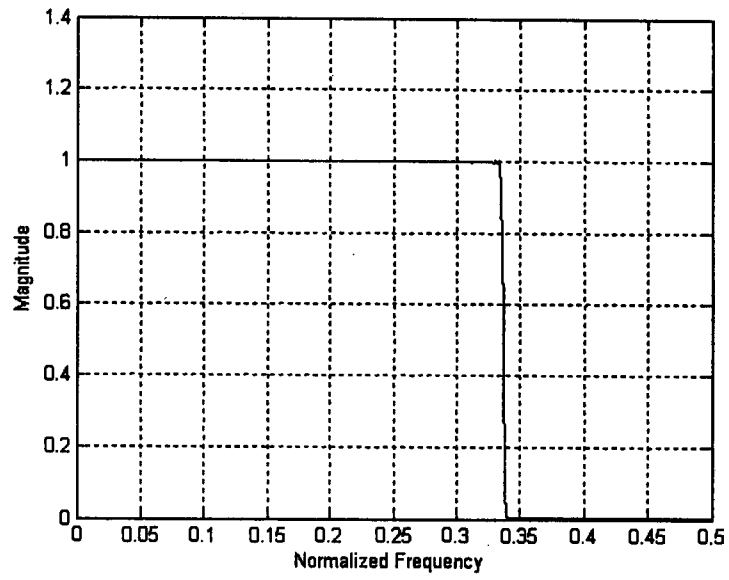
Table 2.4

Variation of passband ripple and stopband attenuation with filter order for transition bandwidth of 0.01π and passband width of 0.666π with slope equalization for proposed Class III FIR filter.

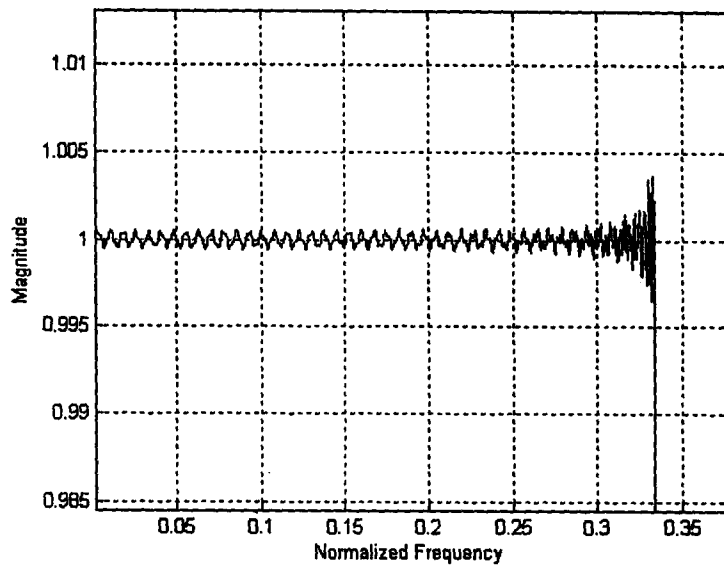
Filter Order	301	401	501	601	701	801
Passband Ripple in dB	0.399	0.092	0.072	0.069	0.068	0.02
Stopband Attenuation in dB	27.2	31.15	33.35	35.09	35.82	37.59



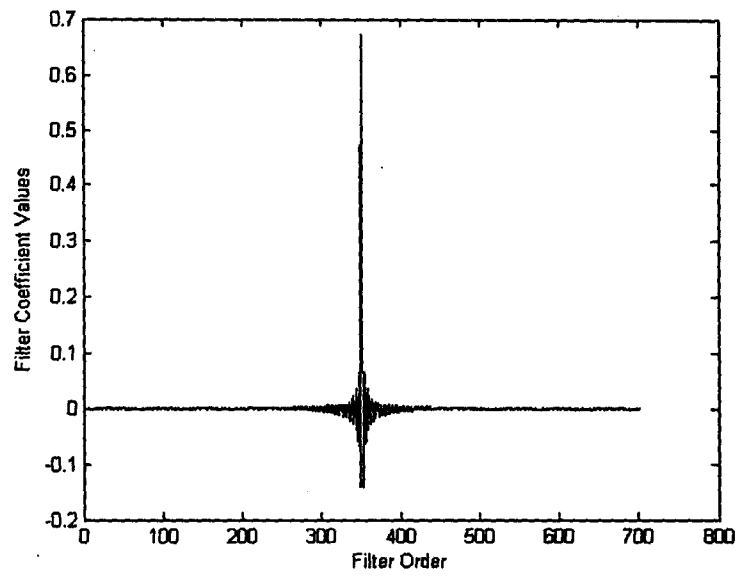
(a)



(b)



(c)



(d)

Fig. 2.8. (a) Magnitude response of proposed Class III for lowpass filter with slope equalization (b) linear plot (c) magnified view of the passband (d) Impulse response sequence.

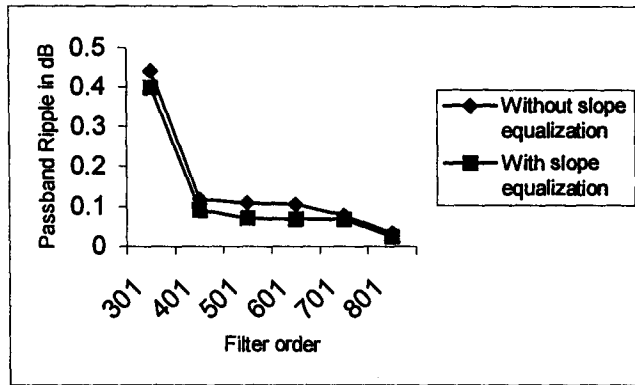


Fig. 2.9. Variation of lowpass filter order with passband ripple for constant transition width of 0.01π and passband edge 0.666π with and without slope equalization.

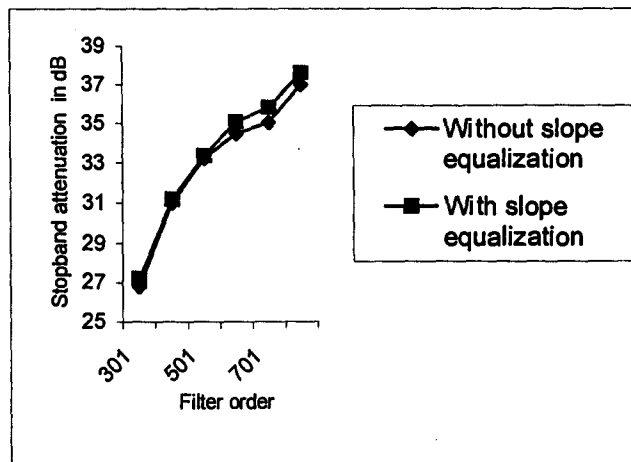


Fig. 2.10. Variation of lowpass filter order with stopband attenuation for constant transition width of 0.01π and passband edge 0.666π with and without slope equalization.

2.8 Class IV FIR Lowpass Filter with Equiripple Response and Linear Transition

2.8.1 Filter Model and Design

In this section, the formulation of a linear phase, sharp transition, lowpass FIR filter model with equiripple passband and stopband response and linear transition region and its design is presented [24]. The filter model magnitude response $H_{pm}(\omega)$ is as shown in Fig.2.11. Synthesis of the filter is greatly simplified with fewer filter design parameters. The filter design parameter k_p is uniquely determined from the transition bandwidth and the parameter is independent of passband edge ω_p . In the proposed lowpass filter model, the various regions of the filter are modeled using trigonometric functions of frequency as follows.

In the passband region, the frequency response is given by

$$H_{pm}(\omega) = 1 + \frac{\delta_p}{2} \cos k_p \omega, \quad 0 \leq \omega \leq \omega_p \quad (2.96)$$

$$\text{where } H_{pm}(0) = 1 + \frac{\delta_p}{2} \text{ and } H_{pm}(\omega_p) = 1$$

where ω is the frequency variable, $H_{pm}(\omega)$ is the pseudo-magnitude of the filter response, δ_p is the passband ripple, k_p is a filter design parameter and ω_p is the passband edge. In the linear transition region $[\omega_p, \omega_z]$ the frequency response is given by

$$H_{pm}(\omega) = 1 - \left[\frac{(\omega - \omega_p)}{(\omega_z - \omega_p)} \right], \quad \omega_p \leq \omega \leq \omega_z \quad (2.97)$$

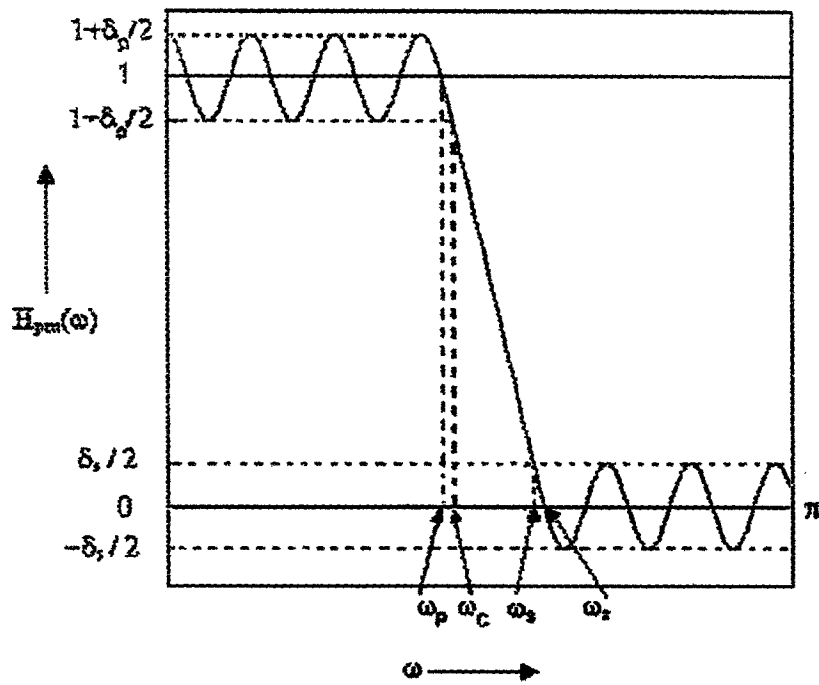


Fig.2.11. Illustration of proposed Class IV lowpass filter model with equiripple magnitude response and linear transition region.

Also, $H_{pm}(\omega_c) = 1 - \frac{\delta_p}{2}$, $H_{pm}(\omega_s) = \frac{\delta_s}{2}$ and $H_{pm}(\omega_z) = 0$

where ω_c is the cutoff edge, ω_s is the stopband edge and ω_z is the frequency at which $H_{pm}(\omega)$ is zero and δ_s is the stopband attenuation.

In the stopband region the frequency response is given by

$$H_{pm}(\omega) = -\frac{\delta_s}{2} \sin k_p(\omega - \omega_z), \quad \omega_z \leq \omega \leq \pi \quad (2.98)$$

2.8.2 Slope equalization

Slope equalization technique is applied to the equiripple filter model with linear transition region, which further improves the performance of the filter. The filter design parameter k_p is evaluated by equalizing the slopes of the pseudo-magnitude response function at both the ends of the transition region as described earlier. This allows the proposed function to be continuous thus reducing the ripples due to Gibb's phenomenon.

$$\begin{aligned} \text{Using (2.96), Slope at } \omega_p &= \frac{d}{d\omega} [H_{pm}(\omega)]_{\omega=\omega_p} \\ &= \frac{d}{d\omega} \left[1 + \frac{\delta_p}{2} \cos k_p \omega \right] \\ &= -\frac{\delta_p}{2} k_p \sin k_p \omega_p \end{aligned} \quad (2.99)$$

$$\text{At } \omega = \omega_p, H_{pm}(\omega_p) = 1.0 = 1 + \frac{\delta_p}{2} \cos k_p \omega_p \quad (2.100)$$

Simplifying, $\cos k_p \omega_p = 0$ and $\sin k_p \omega_p = \pm 1$

Since the slope of the magnitude response at ω_p is negative we choose the positive sign,

$$\text{i.e. } \sin k_p \omega_p = 1 \quad (2.101)$$

Substituting (2.101) in (2.99), we obtain,

$$\text{Slope at } \omega_p = \frac{-k_p \delta_p}{2} \quad (2.102)$$

Since the transition region $[\omega_p, \omega_z]$ is linear, the slopes of the frequency response at ω_p , ω_c , ω_s and ω_z are identical. Thus transition region slope of the magnitude response is given as

$$= -\frac{\frac{\delta_p}{2}}{(\omega_c - \omega_p)} = -\frac{1}{(\omega_z - \omega_p)} = -\frac{\left(1 - \frac{\delta_p}{2}\right)}{(\omega_s - \omega_p)} \quad (2.103)$$

Equalizing the slopes at ω_p and ω_z , from (2.102) and (2.103) we obtain,

$$\frac{-k_p \delta_p}{2} = -\frac{\frac{\delta_p}{2}}{(\omega_c - \omega_p)} \quad (2.104)$$

$$\text{Simplifying (2.104), } \omega_c = \omega_p + \frac{1}{k_p} \quad (2.105)$$

Equalizing the slopes at ω_p and ω_z from (2.102) and (2.103),

$$\frac{-k_p \delta_p}{2} = -\frac{\left(1 - \frac{\delta_p}{2}\right)}{(\omega_s - \omega_p)} \quad (2.106)$$

$$\text{Simplifying (2.106), } \omega_s = \omega_p + \frac{2}{k_p \delta_p} - \frac{1}{k_p} \quad (2.107)$$

Equalizing slopes at ω_p and ω_z from (2.102) and (2.103),

$$\frac{-k_p \delta_p}{2} = -\frac{1}{(\omega_z - \omega_p)} \quad (2.108)$$

Simplifying (2.108),

$$\omega_z = \omega_p + \frac{2}{k_p \delta_p} \quad (2.109)$$

From (2.98), Slope at $\omega_z = \frac{d}{d\omega} [H_{pm}(\omega)]_{\omega=\omega_z}$

$$\begin{aligned} &= \frac{d}{d\omega} \left[-\frac{\delta_s}{2} \sin k_p(\omega - \omega_z) \right] = -\frac{k_p \delta_s}{2} \cos k_p(\omega - \omega_z) \\ &= -\frac{k_p \delta_s}{2} \end{aligned} \quad (2.110)$$

Equalizing the slopes at ω_z from (2.102) and (2.110),

$$\frac{-k_p \delta_p}{2} = -\frac{k_p \delta_s}{2}$$

Thus $\delta_p = \delta_s$ (2.111)

Eq. (2.111) outlines the symmetry of the response.

Using (2.105) and (2.107),

$$k_p = \frac{2(1 - \delta_p)}{\delta_p (\omega_s - \omega_c)} \quad (2.112)$$

2.8.3 Expressions for Impulse Response Coefficients

Referring to filter design theory of section 2.4, the impulse response coefficients $h(n)$ for the lowpass filter are obtained by evaluating the integral below,

$$h(n) = \frac{1}{\pi} \left[\int_0^{\pi} H_{pm}(\omega) \cos k\omega \, d\omega \right] \quad (2.113)$$

$$h(n) = \frac{1}{\pi} \left[\int_0^{\omega_p} H_{pm}(\omega) \cos k\omega \, d\omega + \int_{\omega_p}^{\omega_z} H_{pm}(\omega) \cos k\omega \, d\omega + \int_{\omega_z}^{\pi} H_{pm}(\omega) \cos k\omega \, d\omega \right] \quad (2.114)$$

where $n=0,1,2,\dots,\frac{N-1}{2}$ for N odd.

$$n=0,1,2,\dots,\frac{N}{2}-1 \text{ for N even and } k=\left[\frac{N-1}{2}-n\right]$$

$$h(n)=\frac{1}{\pi}\left[\int_0^{\omega_p}\left(1+\frac{\delta_p}{2}\cos k_p\omega\right)\cos k\omega \, d\omega + \int_{\omega_p}^{\omega_z}\left[1-\frac{(\omega-\omega_p)}{(\omega_z-\omega_p)}\right]\cos k\omega \, d\omega + \int_{\omega_z}^{\pi}\frac{\delta_s}{2}\sin k_p(\omega-\omega_z)\cos k\omega \, d\omega\right] \quad (2.115)$$

Evaluating (2.115), the expressions obtained for the impulse response coefficients $h(n)$ for the lowpass filter are

$$h(n)=\frac{(\delta_p k_p)\cos(k\omega_p)}{2\pi(k_p^2-k^2)}\frac{[\cos(k\omega_z)-\cos(k\omega_p)]}{k^2\pi(\omega_z-\omega_p)} + \frac{\delta_p}{2\pi(k_p^2-k^2)}[k_p\cos k_p(\pi-\omega_z)\cos(k\pi)-k_p\cos(k\omega_z)+k\sin k_p(\pi-\omega_z)\sin(k\pi)] \quad (2.116)$$

Eq. (2.116) is valid for N even where k is a non-integer. For N odd (2.116) is valid except for $k=0$ and $k=k_p$.

For N odd, $k=0$ we obtain

$$h\left(\frac{N-1}{2}\right)=\frac{1}{\pi}\left[\frac{\omega_z+\omega_p}{2}+\frac{\delta_p\cos k_p(\pi-\omega_z)}{2k_p}\right] \quad (2.117)$$

For N odd, $k=k_p$ we obtain

$$h\left(\frac{N-1}{2}-k_p\right)=h\left(\frac{N-1}{2}+k_p\right)=\frac{\delta_p\omega_p}{4\pi}\frac{\cos(k_p\omega_z)}{k_p^2\pi(\omega_z-\omega_p)}$$

$$+ \frac{\delta_p}{4\pi} \left[\frac{\cos(2k_p \pi - k_p \omega_z) - \cos(k_p \omega_z)}{2k_p} + \sin(k_p \omega_z)(\pi - \omega_z) \right] \quad (2.118)$$

2.8.4 Filter Synthesis Results

Design Example: Lowpass linear phase sharp transition FIR filters are designed for the desired filter specifications: Passband edge ω_p is 0.666π , transition bandwidths ($\omega_s - \omega_c$) are 0.005π , 0.01π and 0.02π , maximum passband ripple δ_p is $\pm 0.1\text{dB}$ (0.2dB) and minimum stopband attenuation δ_s is 40dB using the proposed Class IV filter design approach.

The filter is designed using MATLAB with program MLP-5. The filter specifications obtained by measurement of the magnitude response of the filter using Signal Processing toolbox are: passband edge $\omega_p = 0.6667\pi$, cutoff edge $\omega_c = 0.6668\pi$, stopband edge $\omega_s = 0.6767\pi$, transition bandwidth ($\omega_s - \omega_c$) = 0.01π , passband ripple $\delta_p = 0.129\text{dB}$ and stopband attenuation $\delta_s = 40.3\text{dB}$ for a filter order of 701. It is observed that the desired filter specifications are obtained. The magnitude, impulse and phase response of the proposed lowpass filter obtained is shown in Fig.2.12. Also Tables 2.5, 2.6, 2.7 and Figs. 2.13, 2.14 and 2.15 depicts the performance of the filter. No appreciable change in filter performance is observed for narrow and wide passband as seen in Table 2.5 and 2.7. Class IV filter gives the best filter performance compared to Class I, Class II and Class III filter models. From Table 2.6 it is observed that filter order varies almost linearly with a transition bandwidth of the filter for a given passband ripple and stopband attenuation which holds good also with all proposed filter designs. For conventional FIR sharp transition filters the peak passband ripple due to Gibb's phenomenon is about 18%. In proposed Class IV filter the passband ripple is 1.49% for the filter order 701 and decreases for higher filter order. Filter synthesis and design steps are given in Appendix A.6.1.4.

Table 2.5

Variation of passband ripple and stopband attenuation with filter order for transition bandwidth of 0.01π and passband edge of 0.666π with slope equalization for proposed Class IV FIR filter.

Filter Order	301	401	501	601	701	801
Passband Ripple in dB	0.33	0.21	0.2	0.197	0.129	0.088
Stopband Attenuation in dB	32.8	36.46	36.53	36.77	40.3	42.85

Table 2.6

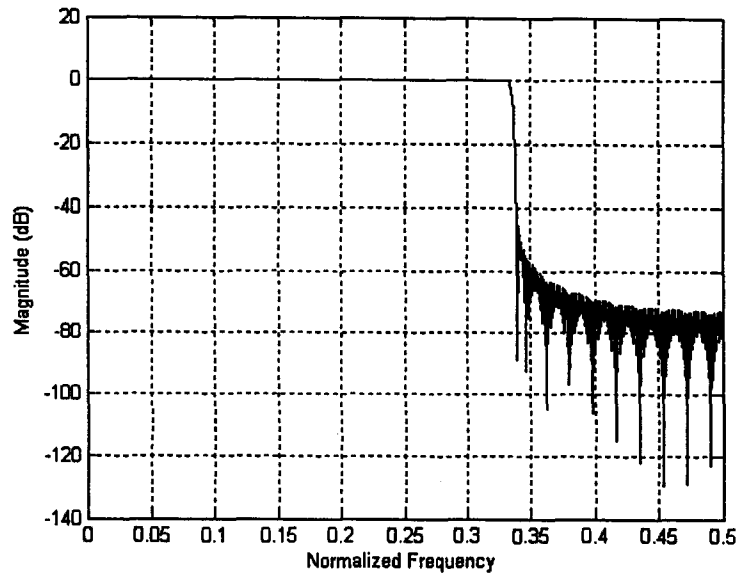
Variation of transition width with filter order for passband ripple of 0.2dB and stopband attenuation of 40dB for passband edge of 0.666π with slope equalization for proposed Class IV FIR filter.

Filter Order	351	701	1401
Transition width	0.022π	0.010π	0.0052π

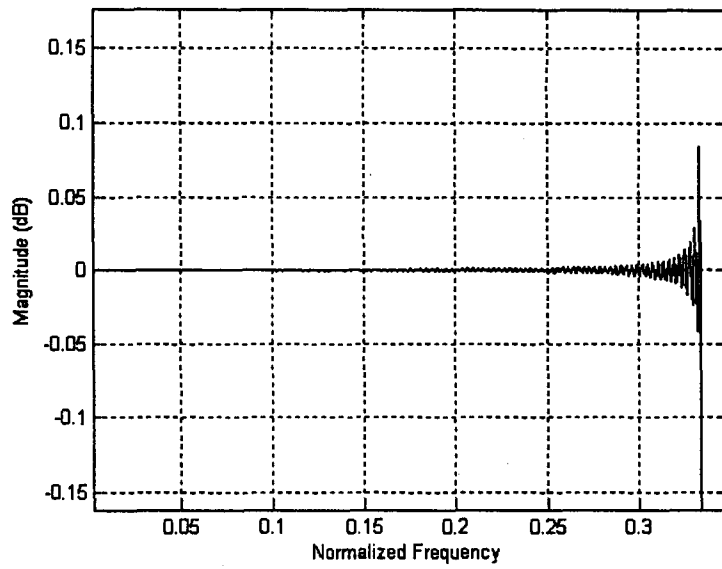
Table 2.7

Variation of passband ripple and stopband attenuation with filter order for transition width of 0.01π and passband edge of 0.333π with slope equalization for proposed Class IV FIR filter.

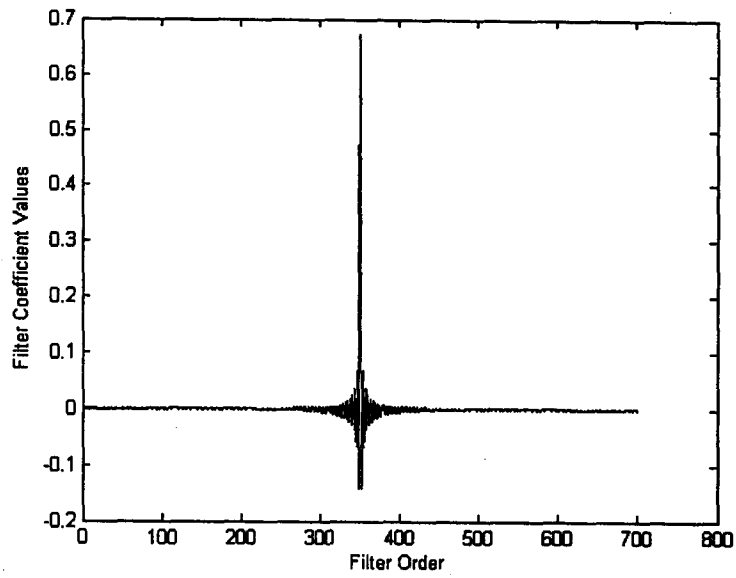
Filter Order	301	401	501	601	701	801
Passband Ripple in dB	0.324	0.21	0.2	0.1965	0.129	0.084
Stopband Attenuation in dB	32.65	35.54	36.04	36.04	40.2	42.05



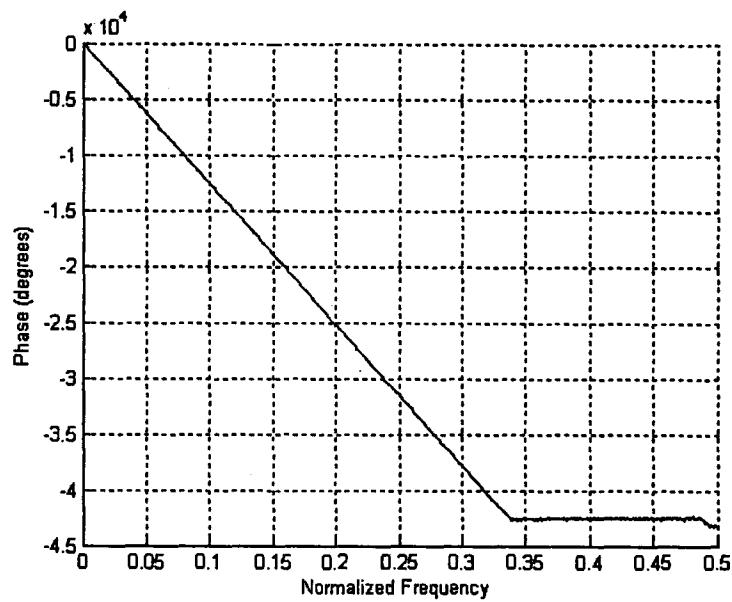
(a)



(b)



(c)



(d)

Fig. 2.12. (a) Magnitude response of the proposed Class IV lowpass filter (b) magnified view of the passband (c) Impulse response sequence (d) Phase response.

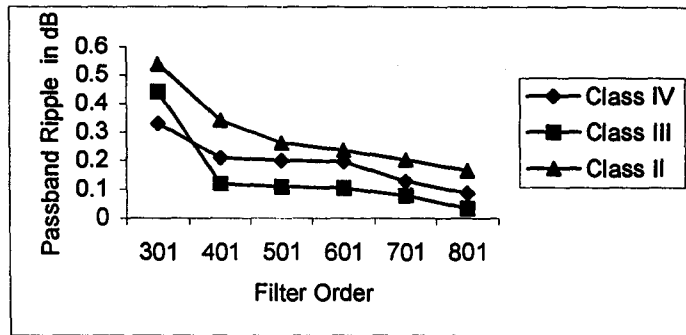


Fig. 2.13. Variation of passband ripple with filter order for constant transition width of 0.011π and passband width of 0.666π for various proposed filters.

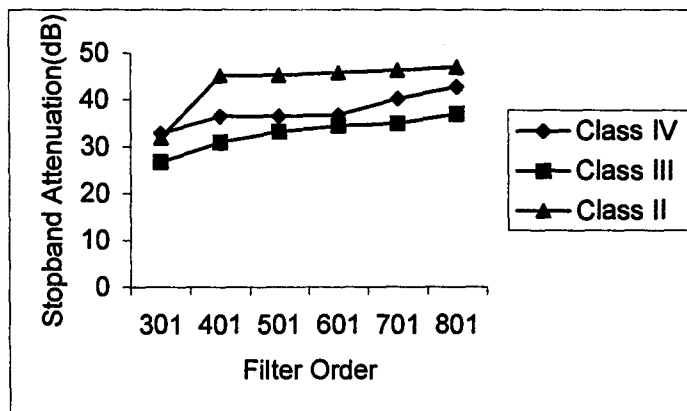


Fig. 2.14. Variation of stopband attenuation with filter order for constant transition width of 0.011π and passband width of 0.666π for various proposed filters.

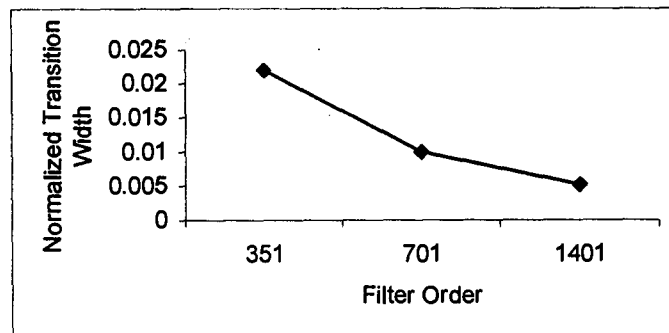


Fig. 2.15. Plot of Filter order Vs Transition width for Class IV filter model with slope equalization for a given passband ripple of 0.1dB, stopband attenuation of 40dB and passband of 0.666π .

2.9 Class V FIR Lowpass Filter with Equiripple Response, Linear Transition and Variable Density Ripple Cycles

2.9.1 Filter model and design

In this section, the formulation of linear phase, sharp transition lowpass FIR filter model with equiripple response and its design is presented. The transition region is linear and the filter design parameter k_p is varied over the passband and stopbands in this design. The filter model magnitude response $H_{pm}(\omega)$ is as shown in Fig.2.16. In the proposed model, the various regions of the filter are modeled using trigonometric functions of frequency as follows.

The passband region, consists of two sub-regions whose frequency responses are given by

$$H_{pm}(\omega) = 1 + \frac{\delta_p}{2} \cos k_{p0}\omega, \quad 0 \leq \omega \leq \omega_{p0} \quad (2.119)$$

$$H_{pm}(\omega) = 1 + \frac{\delta_p}{2} \cos k_p(\omega - \omega_{p0}), \quad \omega_{p0} \leq \omega \leq \omega_p \quad (2.120)$$

where $H_{pm}(0) = 1 + \frac{\delta_p}{2}$ and $H_{pm}(\omega_p) = 1$

where, as usual ω is the frequency variable, $H_{pm}(\omega)$ is the pseudo-magnitude of the filter response, δ_p is passband ripple, k_p and k_{p0} are filter design parameters, ω_p is the passband edge and ω_{p0} is an intermediate frequency in the passband such that $0 < \omega_{p0} < \omega_p$.

In the linear transition region, the frequency response is given by

$$H_{pm}(\omega) = 1 - \left[\frac{(\omega - \omega_p)}{(\omega_z - \omega_p)} \right], \quad \omega_p \leq \omega \leq \omega_z \quad (2.121)$$

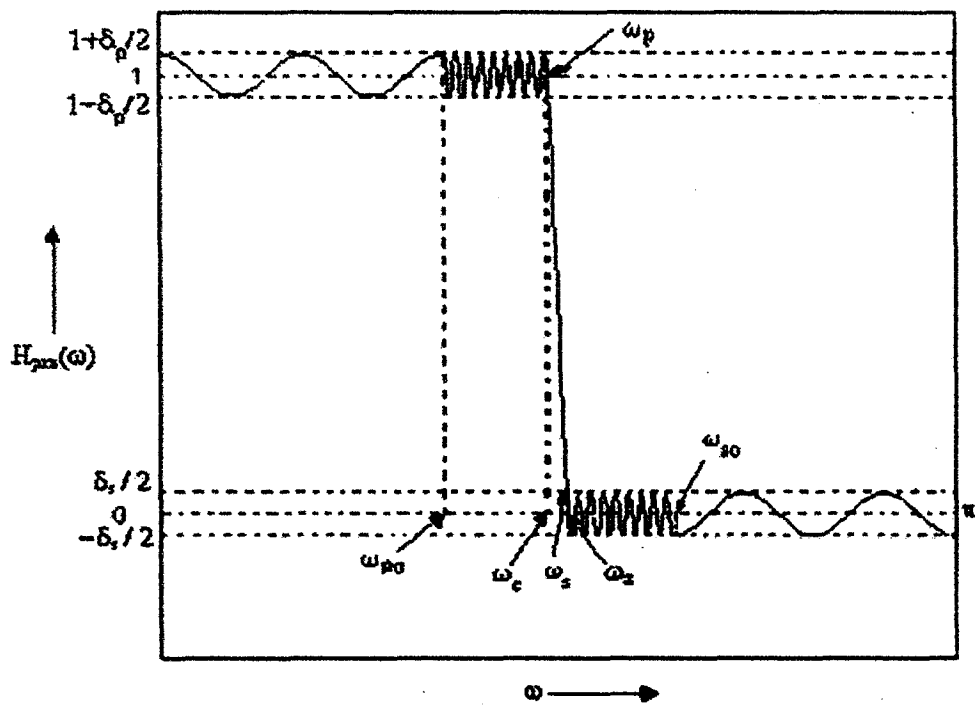


Fig.2.16. Illustration of proposed Class V lowpass filter model with equiripple magnitude response, linear transition region and variable k_p .

where ω_z is the frequency at which $H_{pm}(\omega)$ is zero, i.e. $H_{pm}(\omega_z) = 0$. Also $H_{pm}(\omega_c) = 1 - \frac{\delta_s}{2}$

where ω_c is the cutoff frequency

The stopband region, consists of two sub-regions in which the frequency responses are given by

$$H_{pm}(\omega) = -\frac{\delta_s}{2} \sin k_p(\omega - \omega_z), \quad \omega_z \leq \omega \leq \omega_{s0} \quad (2.122)$$

$$H_{pm}(\omega) = -\frac{\delta_s}{2} \cos k_{p0}(\omega - \omega_{s0}), \quad \omega_{s0} \leq \omega \leq \pi \quad (2.123)$$

where δ_s is the stopband attenuation and ω_{s0} is an intermediate frequency in the stopband such

that $\omega_s < \omega_{s0} < \pi$.

Also $H_{pm}(\omega_s) = \frac{\delta_s}{2}$ and $H_{pm}(\omega_{s0}) = -\frac{\delta_s}{2}$ where ω_s is the stopband edge frequency.

For the Class V lowpass filter design,

The stopband region $[\omega_z, \omega_{s0}]$ of the filter model possesses $\left(m + \frac{1}{4}\right)$ number of ripple cycles and

is characterized by filter design parameter k_p . Therefore,

$$k_p(\omega_{s0} - \omega_z) = 2\pi\left(m + \frac{1}{4}\right) \quad (2.124)$$

where m is a integer.

From (2.124) we get, $\sin k_p(\omega_{s0} - \omega_z) = 1$ (2.125)

The passband region $[\omega_{p0}, \omega_p]$ of the filter model possess $\left(m + \frac{1}{4}\right)$ number of ripple cycles

and is characterized by filter design parameter k_p . Therefore,

$$k_p(\omega_p - \omega_{p0}) = 2\pi\left(m + \frac{1}{4}\right) \quad (2.126)$$

$$\text{From (2.126), } \sin k_p(\omega_p - \omega_{p0}) = 1 \quad (2.127)$$

$$\text{From (2.126), } \omega_{p0} = \omega_p - \left(m + \frac{1}{4}\right) \frac{2\pi}{k_p} \quad (2.128)$$

The passband region $[0, \omega_{p0}]$ of the filter model possesses 'n' number of ripple cycles (n is an integer) and is characterized by filter design parameter k_p . Therefore, $k_{p0}\omega_{p0} = 2\pi n$.

$$\text{The filter design parameter } k_{p0} = \frac{2\pi n}{\omega_{p0}} \quad (2.129)$$

2.9.2 Slope Equalization

Slope equalization technique is applied to the filter model which further improves the performance of the filter. The filter design parameters are evaluated by equalizing the slopes of the pseudo-magnitude response function at both the ends of the transition region. Use of variable filter design parameter k_p further reduces the effects due to Gibb's phenomenon and hence reduces passband ripple and improves stopband attenuation.

$$\begin{aligned} \text{Using (2.120), slope at } \omega_p &= \frac{d}{d\omega} [H_{pm}(\omega)]_{\omega=\omega_p} \\ &= \frac{d}{d\omega} \left[1 + \frac{\delta_p}{2} \cos k_p(\omega - \omega_{p0}) \right] \\ &= -\frac{\delta_p}{2} k_p \sin k_p(\omega_p - \omega_{p0}) \end{aligned} \quad (2.130)$$

Substituting (2.127) in (2.130),

$$\text{Slope at } \omega_p = \frac{-k_p \delta_p}{2} \quad (2.131)$$

Since the transition region $[\omega_p, \omega_z]$ is linear, the slopes of the frequency response at ω_p , ω_c , ω_s and ω_z are identical. Thus transition region slope of the magnitude response $H_{pm}(\omega)$ can be variously given as

$$= \frac{\frac{\delta_p}{2}}{(\omega_c - \omega_p)} = \frac{1}{(\omega_z - \omega_p)} = \frac{\left(1 - \frac{\delta_p}{2}\right)}{(\omega_s - \omega_p)} \quad (2.132)$$

Equalizing the slopes at ω_p and ω_z using (2.131) and (2.132) we obtain,

$$\frac{k_p \delta_p}{2} = \frac{1}{(\omega_z - \omega_p)} \quad (2.133)$$

$$\text{Using (2.133) we have, } \omega_z = \omega_p + \frac{2}{k_p \delta_p} \quad (2.134)$$

$$\begin{aligned} \text{Using (2.122) and simplifying, slope at } \omega_z &= \frac{d}{d\omega} \left[-\frac{\delta_s}{2} \sin k_p(\omega - \omega_z) \right] \\ &= \frac{-k_p \delta_s}{2} \end{aligned} \quad (2.135)$$

Equalization of slopes at ω_z using (2.131) and (2.135),

$$\frac{-k_p \delta_p}{2} = \frac{-k_p \delta_s}{2} \quad (2.136)$$

$$\text{Simplifying (2.136), we obtain, } \delta_s = \delta_p \quad (2.137)$$

Eq. (2.137) outlines the symmetry of the response. Equating the slopes at ω_p and ω_z using

(2.131) and (2.132) we obtain,

$$\frac{-k_p \delta_p}{2} = -\frac{\frac{\delta_p}{2}}{(\omega_c - \omega_p)}$$

$$\omega_c = \omega_p + \frac{1}{k_p} \quad (2.138)$$

$$\omega = \omega_s, H_{pm}(\omega_s) = \frac{\delta_s}{2} = 1 - \frac{(\omega_s - \omega_p)}{(\omega_z - \omega_p)} = \frac{\delta_p}{2} \quad (2.139)$$

Substituting (2.134) in (2.139) and simplifying,

$$\omega_s = \omega_z - \frac{1}{k_p} = \omega_p + \frac{2}{k_p \delta_p} - \frac{1}{k_p} \quad (2.140)$$

Using (2.138) and (2.140), we obtain the filter design parameter

$$k_p = \frac{2 \left[\frac{1}{\delta_p} - 1 \right]}{(\omega_s - \omega_c)} \quad (2.141)$$

2.9.3 Expressions for Impulse Response Coefficients

Referring to filter design theory of section 2.4, the impulse response coefficients $h(n)$ for the lowpass filter are obtained by evaluating the integral below.

$$h(n) = \frac{1}{\pi} \left[\int_0^{\pi} H_{pm}(\omega) \cos k\omega \, d\omega \right] \quad (2.142)$$

$$h(n) = \frac{1}{\pi} \left[\int_0^{\omega_{p0}} H_{pm}(\omega) \cos k\omega \, d\omega + \int_{\omega_{p0}}^{\omega_p} H_{pm}(\omega) \cos k\omega \, d\omega + \int_{\omega_p}^{\omega_z} H_{pm}(\omega) \cos k\omega \, d\omega + \int_{\omega_z}^{\omega_{s0}} H_{pm}(\omega) \cos k\omega \, d\omega + \int_{\omega_{s0}}^{\pi} H_{pm}(\omega) \cos k\omega \, d\omega \right] \quad (2.143)$$

where $n = 0, 1, 2, \dots, \frac{N-1}{2}$ for N odd

$$n = 0, 1, 2, \dots, \frac{N}{2} - 1 \text{ for } N \text{ even} \quad \text{and} \quad k = \left(\frac{N-1}{2} - n \right)$$

$$\begin{aligned} h(n) = & \frac{1}{\pi} \left[\int_0^{\omega_{p0}} \left[1 + \frac{\delta_p}{2} \cos k_{p0} \omega \right] \cos k \omega \, d\omega + \int_{\omega_{p0}}^{\omega_p} \left[1 + \frac{\delta_p}{2} \cos k_p (\omega - \omega_{p0}) \right] \cos k \omega \, d\omega \right. \\ & + \int_{\omega_p}^{\omega_z} \left[1 - \left[\frac{(\omega - \omega_p)}{(\omega_z - \omega_p)} \right] \right] \cos k \omega \, d\omega + \int_{\omega_z}^{\omega_{s0}} \left[-\frac{\delta_s}{2} \sin k_p (\omega - \omega_z) \right] \cos k \omega \, d\omega \\ & \left. + \int_{\omega_{s0}}^{\pi} \left[-\frac{\delta_s}{2} \cos k_{p0} (\omega - \omega_{s0}) \right] \cos k \omega \, d\omega \right] \end{aligned} \quad (2.144)$$

Evaluating (2.144) the expressions obtained for the impulse response coefficients $h(n)$ for the lowpass filter are

$$\begin{aligned} h(n) = & -\frac{[\delta_p k \sin(k \omega_{p0})]}{2\pi(k_{p0}^2 - k^2)} + \frac{\delta_p [k_p \cos(k \omega_p) + k \sin(k \omega_{p0})]}{2\pi(k_p^2 - k^2)} - \frac{[\cos(k \omega_z) - \cos(k \omega_p)]}{k^2 \pi (\omega_z - \omega_p)} \\ & + \frac{\delta_p [k \sin(k \omega_{s0}) - k_p \cos(k \omega_z)]}{2\pi(k_p^2 - k^2)} - \frac{\delta_p [k \sin(k \omega_{s0}) + k_{p0} \sin k_{p0} (\pi - \omega_{s0}) \cos(k\pi)]}{2\pi(k_{p0}^2 - k^2)} \\ & + \frac{\delta_p}{2\pi(k_{p0}^2 - k^2)} [k \cos k_{p0} (\pi - \omega_{s0}) \sin(k\pi)] \end{aligned} \quad (2.145)$$

Eq. (2.145) is valid for N even where k is a non-integer. For N odd (2.145) is valid except for $k = 0$, $k = k_p$ and $k = k_{p0}$.

For N odd, $k = 0$ we obtain,

$$h\left(\frac{N-1}{2}\right) = \frac{1}{\pi} \left[\frac{\omega_z + \omega_p}{2} - \frac{\delta_p}{2k_{p0}} \sin k_{p0} (\pi - \omega_{s0}) \right] \quad (2.146)$$

For N odd, $k = k_p$ we obtain,

$$\begin{aligned} h\left(\frac{N-1}{2} + k_p\right) &= h\left(\frac{N-1}{2} - k_p\right) = -\frac{\left[\frac{\delta_p k_p \sin(k_p \omega_{p0})}{2\pi(k_{p0}^2 - k_p^2)} \right]}{k_p^2 \pi (\omega_z - \omega_p)} - \frac{\left[\cos(k_p \omega_z) - \cos(k_p \omega_p) \right]}{k_p^2 \pi (\omega_z - \omega_p)} \\ &+ \frac{\delta_p}{4\pi} \left[\frac{\left[\sin(2k_p \omega_p - k_p \omega_{p0}) - \sin(k_p \omega_{p0}) \right]}{2k_p} + (\omega_p - \omega_{p0}) \cos(k_p \omega_{p0}) \right] \\ &- \left[\frac{\delta_p}{2\pi(k_{p0}^2 - k^2)} \right] \left[k_p \sin(k_p \omega_{s0}) + k_{p0} \sin k_{p0} (\pi - \omega_{s0}) \cos(k_p \pi) - k_p \cos k_{p0} (\pi - \omega_{s0}) \sin(k_p \pi) \right] \\ &+ \frac{\delta_p}{4\pi} \left[\frac{\left[\cos(2k_p \omega_{s0} - k_p \omega_z) - \cos(k_p \omega_z) \right]}{2k_p} + (\omega_{s0} - \omega_z) \sin(k_p \omega_z) \right] \end{aligned} \quad (2.147)$$

For N odd, $k = k_{p0}$ we obtain,

$$\begin{aligned} h\left(\frac{N-1}{2} + k_{p0}\right) &= h\left(\frac{N-1}{2} - k_{p0}\right) = -\frac{\left(\frac{\delta_p \omega_{p0}}{4\pi} \right) + \frac{\delta_p k_p \cos(k_{p0} \omega_p)}{2\pi(k_p^2 - k_{p0}^2)}}{\left[\cos(k_{p0} \omega_z) - \cos(k_{p0} \omega_p) \right]} - \frac{\delta_p \left[k_{p0} \sin(k_{p0} \omega_{s0}) - k_p \cos(k_{p0} \omega_z) \right]}{2\pi(k_p^2 - k_{p0}^2)} \\ &- \frac{\left[\cos(k_{p0} \omega_z) - \cos(k_{p0} \omega_p) \right]}{k_{p0}^2 \pi (\omega_z - \omega_p)} + \frac{\delta_p \left[k_{p0} \sin(k_{p0} \omega_{s0}) - k_p \cos(k_{p0} \omega_z) \right]}{2\pi(k_p^2 - k_{p0}^2)} \\ &- \frac{\delta_p \left[\sin(2k_{p0} \pi - k_{p0} \omega_{s0}) - \sin(k_{p0} \omega_{s0}) \right]}{4\pi \cdot 2k_{p0}} + \frac{\delta_p \left[(\pi - \omega_{s0}) \cos(k_{p0} \omega_{s0}) \right]}{4\pi} \end{aligned} \quad (2.148)$$

2.9.4 Filter Synthesis Results

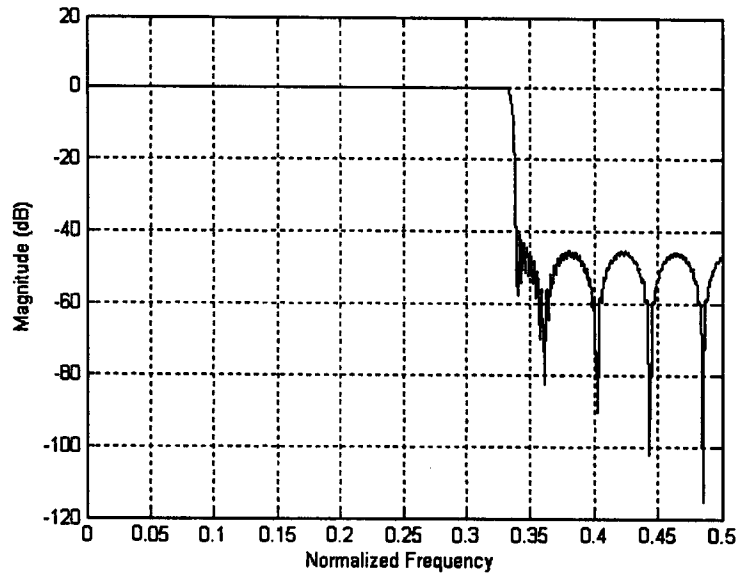
Design Example: A lowpass linear phase sharp transition FIR filter is designed for the desired filter specifications: Passband edge ω_p is 0.666π , transition bandwidth $(\omega_s - \omega_c)$ is 0.01π , maximum passband ripple δ_p is ± 0.1 dB (0.2 dB) and minimum stopband attenuation δ_s is 40dB using the proposed Class V filter design approach.

The filter is designed using MATLAB with program MLP-6. The filter specifications obtained by measurement of the magnitude response of the filter using Signal Processing toolbox are passband edge $\omega_p = 0.6667\pi$, cutoff edge $\omega_c = 0.6668\pi$, stopband edge $\omega_s = 0.6767\pi$, transition bandwidth $(\omega_s - \omega_c) = 0.01\pi$, passband ripple $\delta_p = 0.13$ dB and stopband attenuation $\delta_s = 40.19$ dB are obtained for a filter order of 701. It is observed that the desired filter specifications are obtained. The magnitude and impulse response of the proposed lowpass filter obtained is shown in Fig.2.17. Table 2.8 depicts the performance of the filter. Class V also gives the best filter performance for a given filter order compared to all filter models developed i.e. Class I, Class II and Class III filters with no appreciable change in filter performance compared to Class IV. But peak passband ripple is reduced compared to Class IV filter indicating the further reduction of Gibb's phenomenon with this filter design. For conventional FIR sharp transition filters the peak passband ripple due to Gibb's phenomenon is about 18%. In proposed Class V filter the passband ripple is 1.47% for the filter order 701 and decreases for higher filter order. Filter synthesis and design steps are given in Appendix A6.1.5.

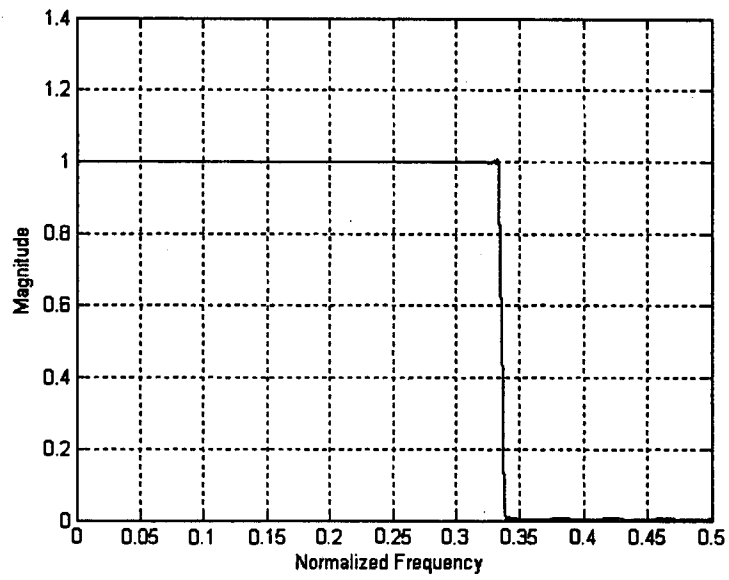
Table 2.8

Variation of passband ripple and stopband attenuation with filter order for transition bandwidth of 0.01π and passband edge of 0.666π with slope equalization for proposed Class V FIR filter.

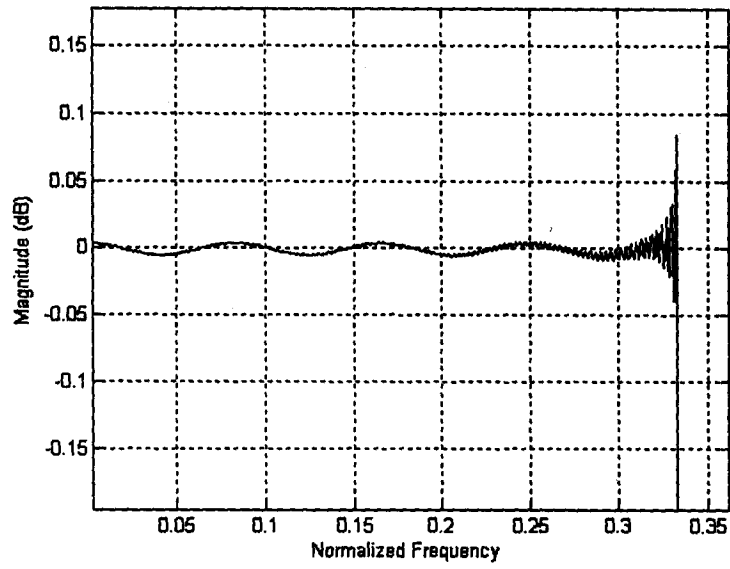
Filter Order	301	401	501	601	701	801
Passband Ripple in dB	0.337	0.192	0.19	0.189	0.13	0.085
Stopband Attenuation in dB	31.96	35.2	35.71	36.46	40.19	43.01



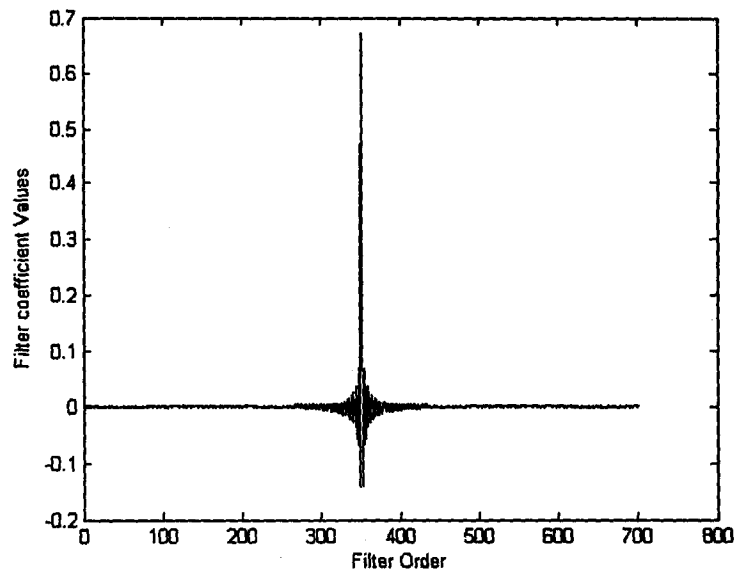
(a)



(b)



(c)



(d)

Fig. 2.17. (a) Magnitude response of the proposed Class V lowpass filter (b) Linear plot (c) magnified view of the passband (d) Impulse response sequence.

2.10 Comparison of Various Proposed FIR Filters with Conventional FIR filters

For comparison of proposed FIR filter design with filters designed using conventional techniques, consider the design example of the proposed FIR filter. Using our proposed approach, the desired filter specifications are obtained for a low filter order of 701 without any optimization technique being used. In window method, the cutoff is at 6 dB. Such a large passband ripple is undesirable and does not meet the desired passband ripple specifications. In frequency sampling method, it is found that for obtaining the desired filter specifications the minimum FIR filter order required is 1025 which is large compared to proposed approach. In Remez approach, which employs optimization techniques, to obtain the desired filter specifications the filter order required is 401. But in this case closed form expressions for impulse response coefficients cannot be obtained because optimization techniques are used. Our proposed filter can be also used as an initial filter for optimization which may then match the filter order obtained in Remez approach. Also, if the filter is suitably truncated it will reduce the filter complexity appreciably with minimum deterioration in passband ripple and stopband attenuation. As seen in Table 2.9 and Fig. 2.19, peak passband ripple due to Gibb's phenomenon is drastically reduced for the proposed lowpass filters with class V filter having the least peak passband ripple of 1.47% for a filter order of 701 and decreases for higher filter order. In conventional filter design peak passband ripple is fixed at about 18% and does not decrease with filter order. In the proposed approach as seen in Table 2.9 peak passband ripple reduces with increase in filter order.

Table 2.9

Peak passband ripple for conventional FIR filter and proposed FIR filters for various filter orders to illustrate reduction in Gibb's phenomenon.

Filter Order	% Peak Passband Ripple						
	Conventional Filter	Class I	Class II	Class III*	Class III**	Class IV	Class V
301	18	5.332	6.376	4.950	4.600	3.80	3.796
401	18	1.485	3.939	1.370	1.088	1.66	1.655
501	18	0.683	2.727	0.722	0.840	2.29	2.260
601	18	1.241	2.729	1.249	1.230	2.28	2.220
701	18	0.991	2.310	0.920	0.700	1.49	1.473
801	18	0.401	1.897	0.351	0.342	1.03	0.970
901	18	0.220	1.733	0.296	0.350	1.24	1.210
1001	18	0.465	1.598	0.510	0.450	1.28	1.260

* Without slope equalization

** With slope equalization

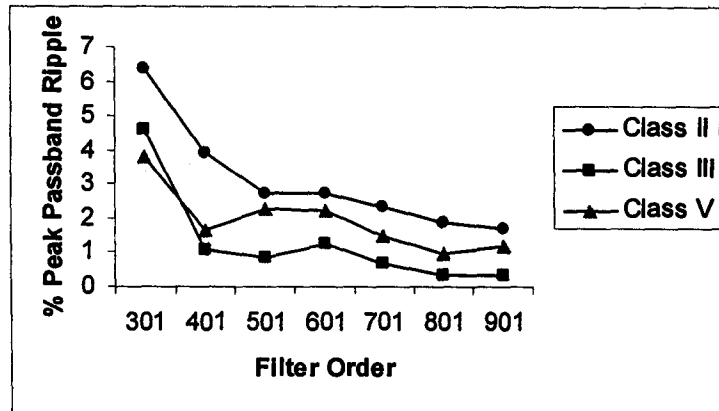


Fig.2.18. Plot of Filter order Vs peak passband ripple for conventional FIR filter and various proposed FIR filters for a given passband ripple of 0.2dB, stopband attenuation of 40dB, transition bandwidth of 0.01π and passband edge of 0.666π .

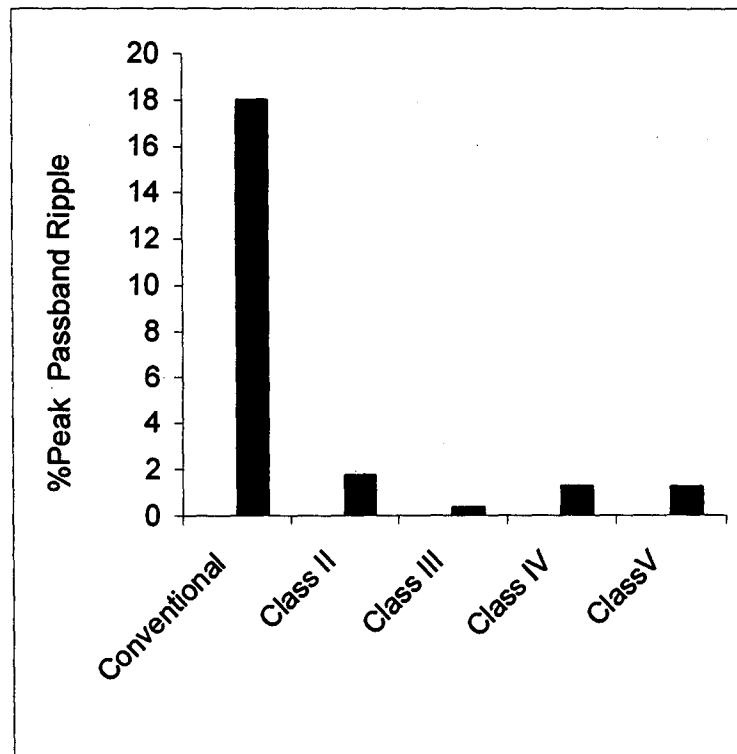


Fig. 2.19. Bar chart showing peak passband ripple for conventional FIR filter and various proposed FIR filters for a transition width of 0.01π and filter order 701.

2.11 Conclusions

Various proposed sharp transition, linear phase, lowpass FIR filters are designed. Various regions of the filter are approximated with trigonometric functions of frequency. The design possesses closed form expressions for impulse response coefficients of the filter and its transfer function is evolved in frequency and time domain.

A novel technique is devised to reduce Gibb's phenomenon. Equations are derived for slopes of the frequency response of the filter, at the edges of the transition region and the slopes are matched. The filter design parameters of the model are evaluated by equalizing the slopes of the pseudo-magnitude response function at both the ends of the transition region. It is proved in the proposed approach that equalizing the slopes at the edges of the transition region makes the proposed function of frequency continuous between a pair of adjoining regions defined by the model equations and hence reduces the effects due to Gibb's phenomenon thereby reducing ripples at the edges of the transition region of the filter. Comparison is made with filters designed with the same set of specifications without slope equalization and it was found that the ripple at the transition edges has reduced with slope equalization. This reduces passband ripple and improves stopband attenuation of the filter as observed in Class III filter without and with slope equalization.

This proposed design approach is without optimizations and hence computation is reduced unlike filter designs based on optimization techniques. In the proposed filters, if the impulse response sequence is suitably truncated subjected to a finite word length there is a appreciable reduction in filter order with marginal deterioration in filter performance i.e. increase in passband ripple and decrease in stopband attenuation. The proposed filters performance is better compared to window and frequency sampling techniques and simpler than optimum filter design without

the need for optimization and complex computational procedures. Peak passband ripple due to Gibb's phenomenon is drastically reduced for the proposed lowpass filters and decreases for higher filter order. In conventional filter design peak passband ripple is about 18% and does not decrease with filter order.

The proposed design approach is found to compare favorably with frequency response masking techniques [7] in terms of sharp transition, least passband ripple and good stopband attenuation with least filter order. The proposed filter design approach is a direct one without subfilters and filter optimizations and closed form expressions for impulse response coefficients are obtained unlike FRM approach where four subfilters are to be synthesized and are to be optimized. With the proposed approach sharp transition filters for any narrow transition bandwidth can be synthesized. The actual filter length (including zero and nonzero coefficients) and delays in FRM approach is higher than our approach to meet a given filter specification. Lesser group delay which is very much desired particularly in speech processing applications.

Chapter 3

SYNTHESIS OF SHARP TRANSITION LINEAR PHASE DIGITAL BANDPASS FIR FILTERS

3.1 Introduction

Various approaches for the design of sharp transition FIR bandpass filters have been dealt in literature. In many of these bandpass realization schemes, the location of the passband as well as the passband width are critical factors affecting the design procedure and the resulting filter implementations [69]. Sharp transition bandpass filters reported in literature generally involve design of component lowpass and highpass filters to realize them. An approximate analytical characterization for a wide band sharp transition bandpass filter realization using FRM approach is dealt in [25]. The component narrow band lowpass and highpass filters of the bandpass filter are implemented using the Interpolated FIR technique. In this case, the frequency specifications for the two component filters depend on the edge frequencies of the desired band pass filter. The two component filters are approximately of the same length as they have the same transition bandwidths. But they have to be designed separately because their passband bandwidths are different depending upon the location and bandwidth of the desired passband of the bandpass filter. The two component filters may have to be redesigned if the center frequency of the bandpass filter is changed. Approximate expressions for the value of interpolating factor and filter hardware required are derived which minimizes the total arithmetic hardware used in the overall bandpass realization. Two branch structure realization [15] is used which is computationally more efficient than the conventional direct form realization with a moderate increase in the number of delays. The value of interpolation factor depends on the center frequency of the bandpass filters. As the

interpolating factor is increased, the computational complexity of the shaping filter decreases and that of the interpolator increases. Theory and approximate design is developed in [26] along with formulas that enables to design the overall bandpass filter with minimal computational complexity. The filter structure utilizes the symmetry of the coefficients to reduce the number of multipliers in the linear phase case and shares the same set of delays between the two branches in a two branch structure. As each of the two branches is essentially an IFIR filter, the overall filter has good roundoff noise and coefficient sensitivity properties. The two branch method can be used for the design of symmetrical and nonsymmetrical bandpass filters.

Another approach for the design and implementation of computationally efficient symmetric bandpass FIR filters is described in [26]. The implementation takes the form of two parallel, real, quadrature filter branches with each branch derived from a complex modulation of a lowpass Interpolated FIR filter prototype by complex exponentials. The input data stream is explicitly modulated with a sine /cosine sequence in order to achieve the desired frequency shift in the frequency response. Practical design rules for design of optimal FIR digital bandpass filters using a program is dealt in [26]. A problem of practical interest is to find the lowest order filter, which satisfies certain maximum ripple requirements in pass and stopbands. To study the effect of the center frequency on the bandpass filter order, a large number of filters were designed to meet different ripple requirements. The filter order was observed to be nearly independent of passband width but is largely dependent on the transition bandwidth.

A new direct technique is proposed for synthesis of a sharp transition, equiripple passband, and linear phase bandpass FIR filter with low arithmetic complexity from a model of pseudo-magnitude bandpass response with equiripple passband, equiripple stopband and linear

transition region. Sharp transition bandpass filters reported in literature generally involve design of component lowpass and highpass filters to realize bandpass filters. Also specifications of component filters i.e. lowpass and highpass filters are to be redesigned for any change in center frequency and passband width of the desired bandpass filter. The proposed technique radically departs from this approach. The frequency response of the proposed filter with narrow transition width is modeled using trigonometric functions of frequency. Slopes of the response are matched at the edges of the transition region, which makes the proposed function continuous and hence reduces the effects due to Gibb's phenomenon thereby reducing passband ripple of the filter. Expressions for impulse response coefficients are derived, coefficients obtained and simulation of the bandpass filter is carried out. The bandpass design is adaptable to any change in the center frequency and passband width.

3.2 Digital Bandpass Filter Model I and Design

In this section, the formulation and design of a linear phase, sharp transition bandpass FIR filter model with equiripple passband, stopband and linear transition region is presented [27]. The filter is designed for arbitrary center frequency and passband width. In the proposed bandpass I filter model the various regions of the filter are modeled using trigonometric functions of frequency as follows. The filter model magnitude response $H_{pm}(\omega)$ is as shown in Fig. 3.1.

In the passband region the frequency response is given by,

$$H_{pm}(\omega) = A_0 \left(1 + \frac{\delta_p}{2} \cos k_{pb} (\omega - \omega_b) \right), \quad (\omega_b - \omega_p) \leq \omega \leq (\omega_b + \omega_p) \quad (3.1)$$

where ω is the frequency variable, $H_{pm}(\omega)$ is the pseudo-magnitude of the bandpass filter response, A_0 is the filter gain parameter, δ_p is the passband ripple, k_{pb} is a filter design parameter, ω_b is the center frequency and ω_p is half passband width of the bandpass filter, $H_{pm}(\omega_b \pm \omega_p) = A_0$, and $(\omega_b \pm \omega_p)$ are the passband edges of the bandpass filter.

In the transition region the frequency response is given by,

$$H_{pm}(\omega) = A_0 \left[1 - \frac{\omega - (\omega_b + \omega_p)}{(\omega_z - \omega_p)} \right], \quad (\omega_b + \omega_p) \leq \omega \leq (\omega_b + \omega_z) \quad (3.2)$$

$$\text{and } H_{pm}(\omega) = A_0 \left[1 - \frac{(\omega_b - \omega_p) - \omega}{(\omega_z - \omega_p)} \right], \quad (\omega_b - \omega_z) \leq \omega \leq (\omega_b - \omega_p) \quad (3.3)$$

In the stopband regions the frequency response is given by,

$$H_{pm}(\omega) = -\frac{\delta_s}{2} A_0 \sin k_{pb} (\omega - (\omega_b + \omega_z)) \quad , \quad (\omega_b + \omega_z) \leq \omega \leq \pi \quad (3.4)$$

$$H_{pm}(\omega) = -\frac{\delta_s}{2} A_0 \sin k_{pb} ((\omega_b - \omega_z) - \omega) \quad , \quad 0 \leq \omega \leq (\omega_b - \omega_z) \quad (3.5)$$

where δ_s is the stopband attenuation and $(\omega_b \pm \omega_z)$ are the frequencies at which $H_{pm}(\omega)$ is zero which lie close to but beyond the edge of the stopband. Similarly $(\omega_b \pm \omega_c)$ are cut-off edges at which $H_{pm}(\omega) = A_0 \left(1 - \frac{\delta_p}{2} \right)$.

$$\text{At cut-off edge } (\omega_b - \omega_c), \quad H_{pm}(\omega) = A_0 \left[1 - \frac{\delta_p}{2} \right] \quad (3.6)$$

$$\text{Using (3.3), } H_{pm}(\omega_b - \omega_c) = A_0 \left[1 - \frac{((\omega_b - \omega_p) - (\omega_b - \omega_c))}{(\omega_z - \omega_p)} \right] \quad (3.6a)$$

Equating (3.6) and (3.6a) and simplifying we get,

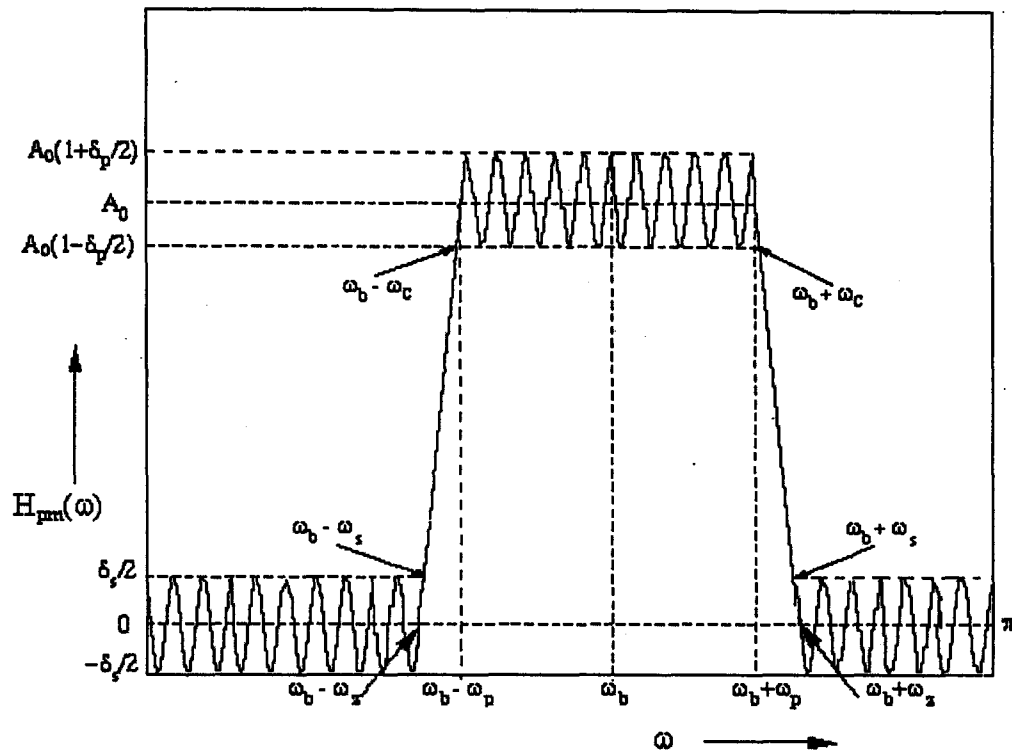


Fig.3.1. Illustration of proposed bandpass filter model I with equiripple magnitude response and linear transition region.

$$\omega_c = \omega_z - \left(1 - \frac{\delta_p}{2}\right)(\omega_z - \omega_p) \quad (3.7)$$

$$\text{Using (3.3), } H_{pm}(\omega_b - \omega_s) = \frac{\delta_s}{2} = A_0 \left[1 - \frac{((\omega_b - \omega_p) - (\omega_b - \omega_s))}{(\omega_z - \omega_p)} \right] \quad (3.8)$$

$$\text{Simplifying, } \omega_s = \omega_z - \frac{\left(\frac{\delta_s}{2}\right)(\omega_z - \omega_p)}{A_0} \quad (3.9)$$

$(\omega_b \pm \omega_s)$ are the stopband edges at which $H_{pm}(\omega) = \frac{\delta_s}{2}$

Using (3.7) and (3.9), we obtain the transition region width

$$(\omega_s - \omega_c) = (\omega_z - \omega_p) \left[\left(1 - \frac{\delta_p}{2}\right) - \frac{(\delta_s/2)}{A_0} \right] \quad (3.10)$$

3.2.1 Slope Equalization

The parameters of the model are evaluated by equalizing the slopes of the pseudo-magnitude response function at $(\omega_b \pm \omega_p)$ and $(\omega_b \pm \omega_z)$. This allows the proposed function to be continuous at the extremes of the transition region thus reducing the effects due to Gibb's phenomenon.

Using (3.1), we obtain,

$$\begin{aligned} \text{Slope at } (\omega_b + \omega_p) &= \frac{d}{d\omega} [H_{pm}(\omega)]_{\omega=(\omega_b + \omega_p)} \\ &= \frac{d}{d\omega} \left[A_0 \left(1 + \frac{\delta_p}{2} \cos k_{pb} (\omega - \omega_b) \right) \right] \\ &= -\frac{A_0 \delta_p}{2} k_{pb} \sin k_{pb} \omega_p \end{aligned} \quad (3.11)$$

Using (3.1) and also from the filter model we have,

$$H_{pm}(\omega_b + \omega_p) = A_0 \left[1 + \frac{\delta_p}{2} \cos k_{pb} \omega_p \right] = A_0$$

Simplifying, $\cos k_{pb} \omega_p = 0$ and $\sin k_{pb} \omega_p = \pm 1$. Positive sign is used to yield the negative slope, i.e., $\sin k_{pb} \omega_p = 1$ (3.12)

Substituting (3.12) in (3.11) we have,

$$\text{Slope at } (\omega_b + \omega_p) = \frac{-k_{pb} \delta_p A_0}{2} \quad (3.13)$$

Since the transition region $[(\omega_b + \omega_p), (\omega_b + \omega_z)]$ is linear, the slope of the frequency

$$\text{response at } (\omega_b + \omega_z) = -\frac{A_0}{(\omega_z - \omega_p)} \quad (3.14)$$

Equating the slopes at $(\omega_b + \omega_p)$ and $(\omega_b + \omega_z)$ we obtain from (3.13) and (3.14) we obtain,

$$k_{pb} = \frac{2}{\delta_p} \left[\frac{1}{\omega_z - \omega_p} \right] \quad (3.15)$$

Substituting (3.10) in (3.15) we obtain

$$k_{pb} = \frac{2}{\delta_p (\omega_s - \omega_c)} \left[\left(1 - \frac{\delta_p}{2} \right) - \frac{(\delta_s / 2)}{A_0} \right] \quad (3.16)$$

From (3.15) we obtain,

$$\omega_z = \omega_p + \frac{2}{\delta_p k_{pb}} \quad (3.17)$$

3.2.2 Expressions for Impulse Response Coefficients

Referring to filter design theory of section 2.4, the impulse response coefficients $h(n)$ for the bandpass filter are obtained by evaluating the integral below.

$$h(n) = \frac{1}{\pi} \left[\int_0^{\pi} H_{pm}(\omega) \cos k\omega \, d\omega \right] \quad (3.18)$$

$$h(n) = \frac{1}{\pi} \left[\int_0^{\omega_b - \omega_z} H_{pm}(\omega) \cos k\omega \, d\omega + \int_{\omega_b - \omega_z}^{\omega_b - \omega_p} H_{pm}(\omega) \cos k\omega \, d\omega \right. \\ \left. + \int_{\omega_b - \omega_p}^{\omega_b + \omega_p} H_{pm}(\omega) \cos k\omega \, d\omega + \int_{\omega_b + \omega_p}^{\omega_b + \omega_z} H_{pm}(\omega) \cos k\omega \, d\omega + \int_{\omega_b + \omega_z}^{\pi} H_{pm}(\omega) \cos k\omega \, d\omega \right] \quad (3.19)$$

$$h(n) = \frac{1}{\pi} \left[\int_0^{\omega_b - \omega_z} -\frac{\delta_s A_0}{2} \sin k_{pb} ((\omega_b - \omega_z) - \omega) \cos k\omega \, d\omega \right. \\ \left. + \int_{\omega_b - \omega_z}^{\omega_b - \omega_p} A_0 \left[1 - \frac{((\omega_b - \omega_p) - \omega)}{(\omega_z - \omega_p)} \right] \cos k\omega \, d\omega + \int_{\omega_b - \omega_p}^{\omega_b + \omega_p} A_0 \left[1 + \frac{\delta_p}{2} \cos k_{pb} (\omega - \omega_b) \right] \cos k\omega \, d\omega \right. \\ \left. + \int_{\omega_b + \omega_p}^{\omega_b + \omega_z} A_0 \left[1 - \frac{(\omega - (\omega_b + \omega_p))}{(\omega_z - \omega_p)} \right] \cos k\omega \, d\omega + \int_{\omega_b + \omega_z}^{\pi} -\frac{\delta_s A_0}{2} \sin k_{pb} [\omega - (\omega_b + \omega_z)] \cos k\omega \, d\omega \right] \quad (3.20)$$

where $n=0,1,\dots,\frac{N-1}{2}$ for N odd

$$n=0,1,2,\dots,\frac{N}{2}-1 \text{ for N even} \quad \text{and} \quad k = \frac{(N-1)}{2} - n$$

Evaluating (3.20), the expressions obtained for the impulse response coefficients $h(n)$ for the bandpass filter are,

$$h(n) = \frac{A_0 \delta_p \cos k \omega_b}{\pi(k_{pb}^2 - k^2)} \left[k_{pb} \sin k_{pb} \omega_p \cos k \omega_p - k \cos k_{pb} \omega_p \sin k \omega_p \right]$$

$$\begin{aligned}
& + \frac{A_0 \delta_s k_{pb}}{2\pi(k_{pb}^2 - k^2)} \left[\cos k_{pb}(\omega_b - \omega_z) - \cos k(\omega_b - \omega_z) \right] \\
& + \frac{A_0}{k^2 \pi(\omega_z - \omega_p)} \left[\cos k(\omega_b - \omega_p) - \cos k(\omega_b - \omega_z) + k(\omega_z - \omega_p) \operatorname{sinc}(\omega_b - \omega_p) \right] \\
& + \frac{A_0}{k^2 \pi(\omega_z - \omega_p)} \left[\cos k(\omega_b + \omega_p) - \cos k(\omega_b + \omega_z) - k(\omega_z - \omega_p) \operatorname{sinc}(\omega_b + \omega_p) \right] \\
& + \frac{A_0 \delta_s}{2\pi(k_{pb}^2 - k^2)} \left[\left[k_{pb} \cos k_{pb}(\pi - (\omega_b + \omega_z)) \cos k\pi - k_{pb} \cos k(\omega_b + \omega_z) \right] \right. \\
& \left. + k \sin k_{pb}(\pi - (\omega_b + \omega_z)) \sin k\pi \right] + \frac{2A_0}{k\pi} \cos k\omega_b \operatorname{sinc}\omega_p
\end{aligned} \tag{3.21}$$

Eq. (3.21) is valid for N even where k is a non-integer, for N odd (3.21) is valid except for $k = 0$ and $k = k_{pb}$.

For N odd, $k = 0$,

$$\begin{aligned}
h\left(\frac{N-1}{2}\right) &= \frac{A_0 \delta_s}{2\pi k_{pb}} \left[\cos k_{pb}(\pi - (\omega_b + \omega_z)) + \cos k_{pb}(\omega_b - \omega_z) - 2 \right] \\
&+ \frac{A_0(\omega_p + \omega_z)}{\pi} + \frac{A_0 \delta_p \sin k_{pb} \omega_p}{\pi k_{pb}}
\end{aligned} \tag{3.22}$$

For N odd, $k = k_{pb}$

$$\begin{aligned}
h(n) &= h\left(\frac{N-1}{2} - k_{pb}\right) = h\left(\frac{N-1}{2} + k_{pb}\right) = -\frac{A_0 \delta_s}{4\pi} \left[(\omega_b - \omega_z) \operatorname{sinc}_{pb}(\omega_b - \omega_z) \right] \\
&+ \frac{A_0}{k_{pb}^2 \pi(\omega_z - \omega_p)} \left[\cos k_{pb}(\omega_b - \omega_p) - \cos k_{pb}(\omega_b - \omega_z) + k_{pb}(\omega_z - \omega_p) \operatorname{sinc}_{pb}(\omega_b - \omega_p) \right] \\
&+ \frac{A_0 \delta_p}{4\pi} \left[\frac{\sin 2k_{pb} \omega_p \cos k_{pb} \omega_b}{k_{pb}} + 2\omega_p \cos k_{pb} \omega_b \right] + \frac{2A_0}{k_{pb} \pi} \cos k_{pb} \omega_b \operatorname{sinc}_{pb} \omega_p
\end{aligned}$$

$$\begin{aligned}
& + \frac{A_0}{k_{pb}^2 \pi(\omega_z - \omega_p)} \left[\cos k_{pb}(\omega_b + \omega_p) - \cos k_{pb}(\omega_b + \omega_z) - k_{pb}(\omega_z - \omega_p) \text{sinc}_{pb}(\omega_b + \omega_p) \right] \\
& + \frac{A_0 \delta_s}{4\pi} \left[\frac{\cos 2k_{pb}\pi - k_{pb}(\omega_b + \omega_z) - \cos k_{pb}(\omega_b + \omega_z)}{2k_{pb}} \right] + [\pi - (\omega_b + \omega_z)] \text{sinc}_{pb}(\omega_b + \omega_z)
\end{aligned} \tag{3.23}$$

3.2.3 Filter Synthesis Results

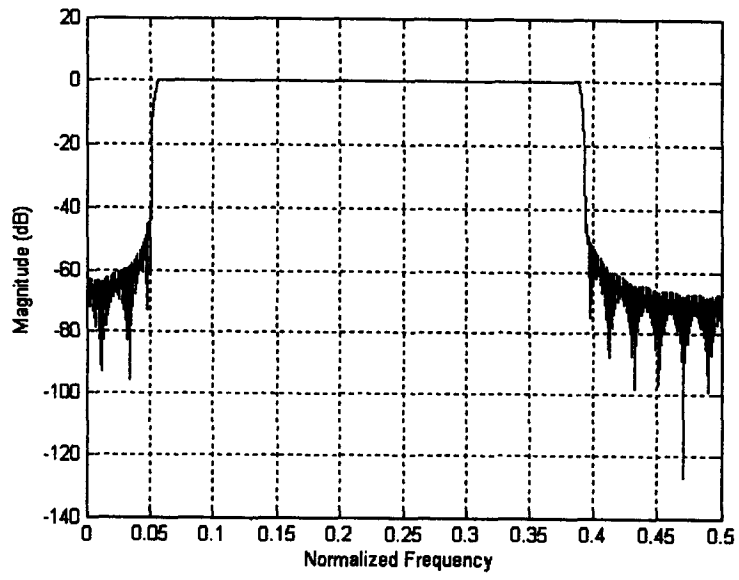
Design Example: A bandpass linear phase sharp transition FIR filter is designed for the desired specifications of center frequencies, passband widths and transition bandwidths as specified in Table 3.1. The maximum passband ripple is $\pm 0.1\text{dB}$ (0.2 dB) and the minimum stopband attenuation is 40dB.

The filter is designed using MATLAB with program MBP-1 and measurement of various filter specifications is done using MATLAB's Signal Processing toolbox. Results approximate the desired filter specifications closely with low filter order with the desired passband widths, center frequencies, passband ripple and stopband attenuation obtained as shown in Table 3.1. The magnitude, impulse and phase response of the proposed bandpass filter with center frequency $\omega_b = 0.444\pi$, passband width $\omega_p = 0.6667\pi$, transition bandwidth $(\omega_s - \omega_c) = 0.011\pi$, passband ripple $\delta_p = 0.144\text{dB}$ and stopband attenuation $\delta_s = 39.4\text{dB}$ obtained for a filter order of 701 as shown in Fig.3.2. Table 3.1 depicts the performance of the bandpass filter. From Table 3.1, it is observed that the bandpass filter design is adaptable to any change in passband width (wideband to narrowband) and arbitrary center frequencies. Filter synthesis and design steps are given in Appendix A6.1.6.

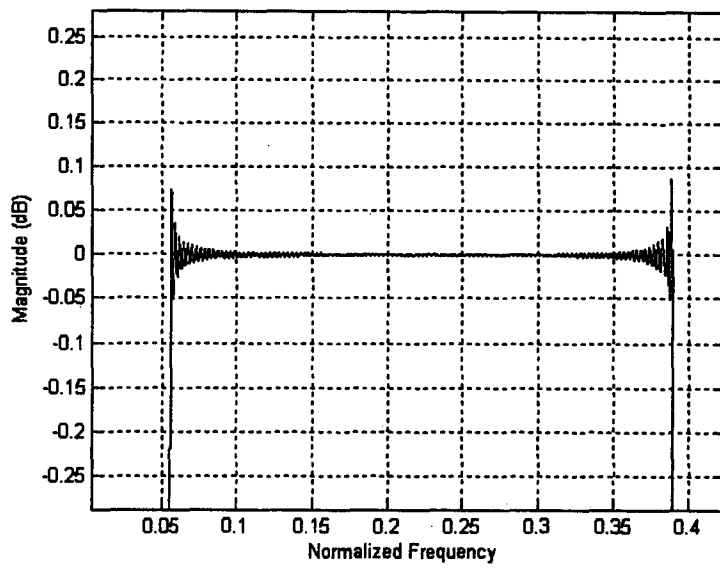
Table 3.1

Proposed bandpass I filter performance for various passband widths, center frequencies and transition bandwidths with required order for filter realization.

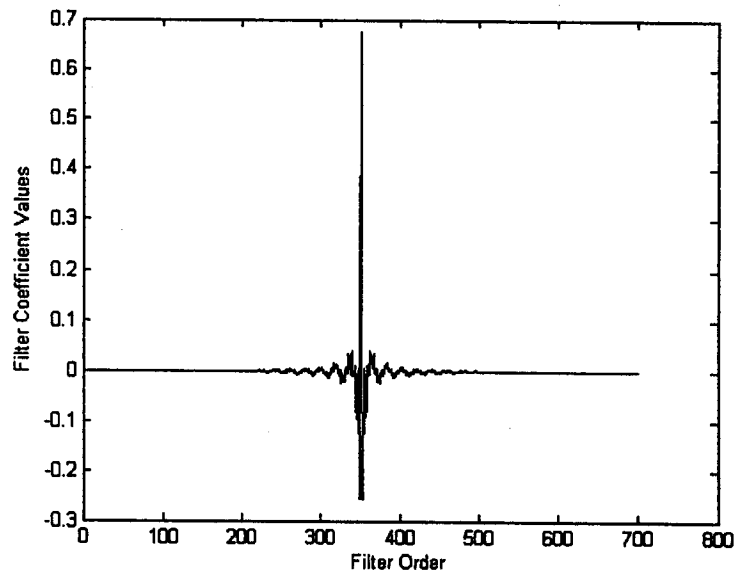
Filter Order	Transition bandwidth	Center Frequency	Passband width	Passband ripple in dB	Stopband attenuation in dB
451	0.0215π	0.6667π	0.5556π	0.113	41.40
225	0.0418π	0.6667π	0.5556π	0.114	41.57
701	0.0110π	0.4444π	0.6666π	0.144	39.40
451	0.0209π	0.3333π	0.2778π	0.108	41.59



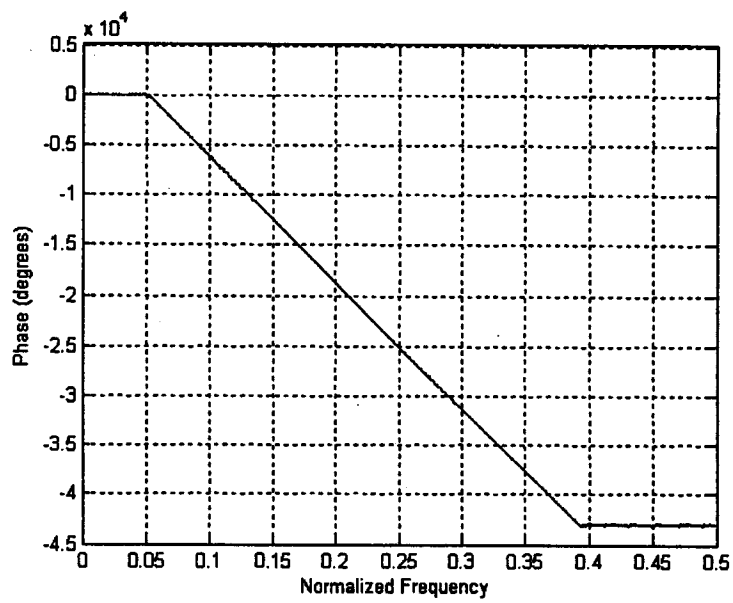
(a)



(b)



(c)



(d)

Fig. 3.2 (a) Magnitude response of the proposed bandpass I filter (b) Magnified view of the passband (c) Impulse response sequence (d) Phase response.

3.3 Digital Bandpass Filter Model II and Design

In this section, the formulation and design of a linear phase, sharp transition bandpass FIR filter model with equiripple passband, equiripple stopband and variable density of ripple cycles in passband and stopband regions of the filter is presented. Filter model is such that large density of ripples are introduced in the regions where discontinuities are present to increase the sharpness of the transition and a non-ideal frequency response modeled without any abrupt discontinuities is used to reduce Gibb's phenomenon. The filter model magnitude response $H_{pm}(\omega)$ is as shown in Fig. 3.3. The filter is designed for arbitrary center frequency and passband width. In the proposed filter model, the various regions of the filter are modeled using trigonometric functions of frequency as follows.

In the stopband region, $0 \leq \omega \leq (\omega_b - \omega_{s0})$ the frequency response is given by

$$H_{pm}(\omega) = \frac{\delta_s}{2} \cos \left[k_{p0} \left((\omega_b - \omega_{s0}) - \omega \right) \right], \quad 0 \leq \omega \leq (\omega_b - \omega_{s0}) \quad (3.24)$$

where ω the frequency variable, $H_{pm}(\omega)$ is the pseudo-magnitude of the bandpass filter response, δ_s is stopband attenuation, ω_b is the band center frequency, $(\omega_b - \omega_{s0})$ is an intermediate frequency of the stopband such that $0 < (\omega_b - \omega_{s0}) < (\omega_b - \omega_z)$ and k_{p0} is the filter design parameter in this region. At frequencies $(\omega_b \pm \omega_{s0})$, the filter design parameter k_p

changes and $H_{pm}(\omega) = \frac{\delta_s}{2}$.

In the stopband region, preceding the passband i.e. $(\omega_b - \omega_{s0}) \leq \omega \leq (\omega_b - \omega_z)$ the frequency response is,

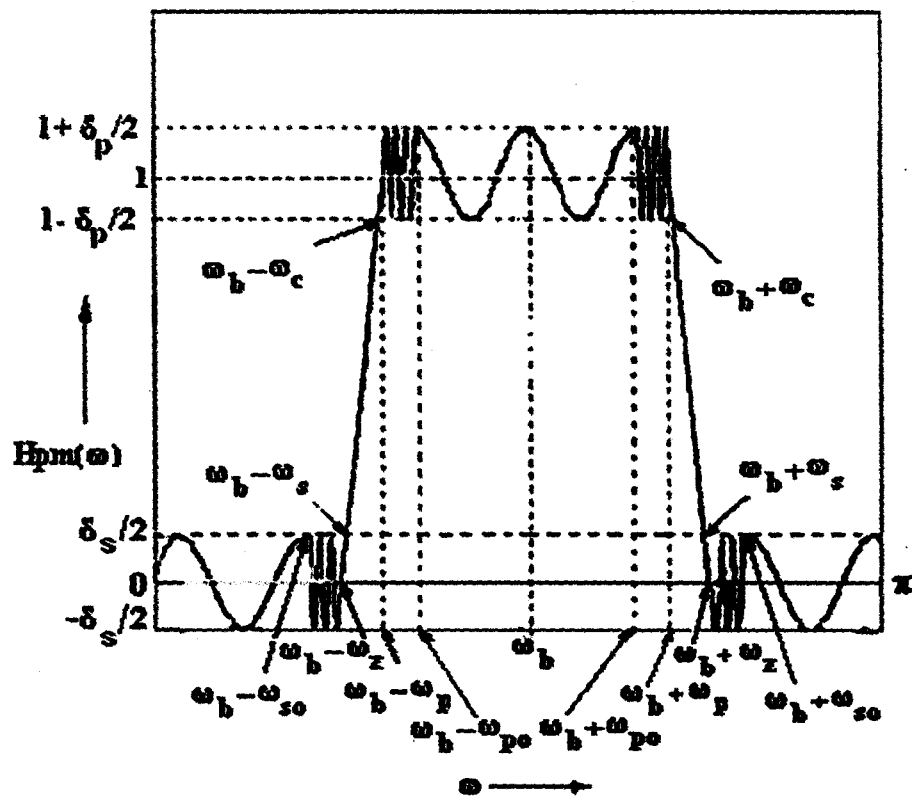


Fig. 3.3 Illustration of proposed bandpass filter model II with equiripple magnitude response, linear transition and variable density ripple cycles.

$$H_{pm}(\omega) = \frac{\delta_s}{2} \cos \left[k_p \left(\omega - (\omega_b - \omega_{s0}) \right) \right], \quad (\omega_b - \omega_{s0}) \leq \omega \leq (\omega_b - \omega_z) \quad (3.25)$$

In the transition region, $(\omega_b - \omega_z) \leq \omega \leq (\omega_b - \omega_p)$ the frequency response is,

$$H_{pm}(\omega) = \left[\frac{\omega - (\omega_b - \omega_z)}{(\omega_z - \omega_p)} \right], \quad (\omega_b - \omega_z) \leq \omega \leq (\omega_b - \omega_p) \quad (3.26)$$

ω_p is half passband width of bandpass filter, $(\omega_b \pm \omega_z)$ are the frequencies at which $H_{pm}(\omega)$ is zero which lie close to but beyond the edge of the stopband and $(\omega_b \pm \omega_p)$ are the passband edges at which $H_{pm}(\omega) = 1$.

In the passband region, $(\omega_b - \omega_p) \leq \omega \leq (\omega_b - \omega_{p0})$ the frequency response is,

$$H_{pm}(\omega) = 1 + \frac{\delta_p}{2} \sin \left[k_p \left(\omega - (\omega_b - \omega_p) \right) \right], \quad (\omega_b - \omega_p) \leq \omega \leq (\omega_b - \omega_{p0}) \quad (3.27)$$

δ_p is passband ripple, k_p is the filter design parameter and $(\omega_b \pm \omega_{p0})$ are intermediate frequencies in the passband at which filter design parameter k_p changes.

In the passband region, $(\omega_b - \omega_{p0}) \leq \omega \leq \omega_b$ the frequency response is

$$H_{pm}(\omega) = 1 + \frac{\delta_p}{2} \cos \left[k_{p0} \left(\omega - (\omega_b - \omega_{p0}) \right) \right], \quad (\omega_b - \omega_{p0}) \leq \omega \leq \omega_b \quad (3.28)$$

In the passband region, $\omega_b \leq \omega \leq (\omega_b + \omega_{p0})$ the frequency response is

$$H_{pm}(\omega) = 1 + \frac{\delta_p}{2} \cos \left[k_{p0} (\omega - \omega_b) \right], \quad \omega_b \leq \omega \leq (\omega_b + \omega_{p0}) \quad (3.29)$$

In the passband region, $(\omega_b + \omega_{p0}) \leq \omega \leq (\omega_b + \omega_p)$ the frequency response is

$$H_{pm}(\omega) = 1 + \frac{\delta_p}{2} \cos \left[k_p \left(\omega - (\omega_b + \omega_{p0}) \right) \right], \quad (\omega_b + \omega_{p0}) \leq \omega \leq (\omega_b + \omega_p) \quad (3.30)$$

In the transition region, $(\omega_b + \omega_p) \leq \omega \leq (\omega_b + \omega_z)$ from the frequency response is

$$H_{pm}(\omega) = 1 - \frac{[\omega - (\omega_b + \omega_p)]}{(\omega_z - \omega_p)}, \quad (\omega_b + \omega_p) \leq \omega \leq (\omega_b + \omega_z) \quad (3.31)$$

In the stopband region, $(\omega_b + \omega_z) \leq \omega \leq (\omega_b + \omega_{s0})$ the frequency response is

$$H_{pm}(\omega) = -\frac{\delta_s}{2} \sin \left[k_p (\omega - (\omega_b + \omega_z)) \right], \quad (\omega_b + \omega_z) \leq \omega \leq (\omega_b + \omega_{s0}) \quad (3.32)$$

In the stopband region, $(\omega_b + \omega_{s0}) \leq \omega \leq \pi$ the frequency response is

$$H_{pm}(\omega) = \frac{\delta_s}{2} \cos \left[k_{p0} (\omega - (\omega_b + \omega_{s0})) \right], \quad (\omega_b + \omega_{s0}) \leq \omega \leq \pi \quad (3.33)$$

$(\omega_b + \omega_{s0})$ is an intermediate frequency of the stopband succeeding the passband such that

$$(\omega_b + \omega_z) \leq \omega_{s0} \leq \pi.$$

The bandpass filter design, has three regions in the passband and possesses a total of $(n+1/2)$ cycles of ripple in the entire passband. In the proposed model, the first region possesses $(m+1/4)$ cycles of ripple where m is an integer and ranges from $(\omega_b - \omega_p)$ to $(\omega_b - \omega_{p0})$. It is characterized by filter design parameter k_p . The second region possesses $(n-2m)$ cycles of ripple where n is an even integer and this region spans the frequency range from $(\omega_b - \omega_{p0})$ to $(\omega_b + \omega_{p0})$. It is characterized by filter design parameter k_{p0} . The third region possesses $(m+1/4)$ cycles of ripple where m is an integer and ranges from $(\omega_b + \omega_{p0})$ to $(\omega_b + \omega_p)$. It is characterized by filter design parameter k_p .

For the bandpass design we have,

$$k_p(\omega_{s0} - \omega_z) = 2\pi(p + 3/4) \quad \text{where } p \text{ is a positive integer} \quad (3.34)$$

$$\text{From (3.34), } \omega_{s0} = \omega_z + \frac{2\pi(p + 3/4)}{k_p}$$

$$\text{Also, } k_p(\omega_p - \omega_{p0}) = 2\pi(m + 1/4) \quad (3.35)$$

$$\text{From (3.35), } \omega_{p0} = \omega_p - \frac{2\pi}{k_p}(m + 1/4) \quad (3.36)$$

$$\text{Also, } k_{p0} \omega_{p0} = 2\pi(n/2 - m) \quad (3.37)$$

$$\text{From (3.37), } k_{p0} = \frac{2\pi(n/2 - m)}{\omega_{p0}} \quad (3.38)$$

From (3.34), (3.35) and (3.37)

$$\text{cosh } k_p(\omega_{s0} - \omega_z) = 0 \quad \text{i.e. } \sinh k_p(\omega_{s0} - \omega_z) = -1$$

$$\text{cosh } k_p(\omega_p - \omega_{p0}) = 0 \quad \text{i.e. } \sinh k_p(\omega_p - \omega_{p0}) = 1$$

$$\text{cosh } k_{p0} \omega_{p0} = 1 \quad \text{i.e. } \sinh k_{p0} \omega_{p0} = 0 \quad (3.38a)$$

where p, n, m are integers and assumed where n must be even.

In the bandpass filter model we have,

$$H_{pm}(\omega_b) = \left(1 + \frac{\delta_p}{2}\right), \quad H_{pm}(\omega_b \pm \omega_p) = 1,$$

$$H_{pm}(\omega_b \pm \omega_{p0}) = \left(1 + \frac{\delta_p}{2}\right), \quad H_{pm}(\omega_b \pm \omega_z) = 0, \quad H_{pm}(\omega_b \pm \omega_{s0}) = \frac{\delta_s}{2}, \quad H_{pm}(\omega_b \pm \omega_c) = 1 - \frac{\delta_p}{2} \quad \text{and}$$

$$H_{pm}(\omega_b \pm \omega_s) = \frac{\delta_s}{2} \quad (3.38b)$$

3.3.1 Slope Equalization

The parameters of the model are evaluated by equalizing the slopes of the pseudo-magnitude response function at $(\omega_b \pm \omega_p)$ and $(\omega_b \pm \omega_z)$. This allows the proposed function to be continuous at the extremes of the transition region thus reducing the effects due to Gibb's phenomenon.

$$\begin{aligned} \text{Slope at } (\omega_b + \omega_p) &= \frac{d}{d\omega} [H_{pm}(\omega)]_{\omega=(\omega_b + \omega_p)} = \frac{d}{d\omega} \left[1 + \frac{\delta_p}{2} \cos k_p [\omega - (\omega_b + \omega_{p0})] \right]_{\omega=(\omega_b + \omega_p)} \\ &= \frac{-k_p \delta_p}{2} \sin k_p (\omega_p - \omega_{p0}) \end{aligned}$$

$$\text{Using (3.38a) we get, slope at } (\omega_b + \omega_p) = \left(\frac{-k_p \delta_p}{2} \right) \quad (3.39)$$

Since the transition region $[(\omega_b + \omega_p), (\omega_b + \omega_z)]$ is linear,

$$\text{slope at } (\omega_b + \omega_z) = -\frac{1}{(\omega_z - \omega_p)} \quad (3.40)$$

Equating the above slopes at $(\omega_b + \omega_p)$ and $(\omega_b + \omega_z)$, using (3.39) and (3.40),

$$\left(\frac{-k_p \delta_p}{2} \right) = \left(-\frac{1}{(\omega_z - \omega_p)} \right) \quad (3.41)$$

$$\text{Simplifying (3.41), } \omega_z = \omega_p + \frac{2}{k_p \delta_p} \quad (3.42)$$

$$\begin{aligned} \text{Slope at } (\omega_b - \omega_p) &= \frac{d}{d\omega} [H_{pm}(\omega)]_{\omega=(\omega_b - \omega_p)} = \frac{d}{d\omega} \left[1 + \frac{\delta_p}{2} \sin k_p [\omega - (\omega_b - \omega_p)] \right]_{\omega=(\omega_b - \omega_p)} \\ &= \frac{k_p \delta_p}{2} \cos k_p [\omega - (\omega_b - \omega_p)]_{\omega=(\omega_b - \omega_p)} \end{aligned}$$

$$= \left(\frac{k_p \delta_p}{2} \right) \quad (3.43)$$

In the linear region, $(\omega_b - \omega_z) \leq \omega \leq (\omega_b - \omega_p)$,

$$\text{Slope at } (\omega_b - \omega_z) = \frac{1}{(\omega_z - \omega_p)} \quad (3.44)$$

Equating the slopes at $(\omega_b - \omega_p)$ and $(\omega_b - \omega_z)$ we obtain,

$$\left(\frac{k_p \delta_p}{2} \right) = \frac{1}{(\omega_z - \omega_p)} \quad (3.45)$$

Using (3.32) slope at $(\omega_b + \omega_z)$,

$$\begin{aligned} &= \frac{d}{d\omega} [H_{pm}(\omega)]_{\omega=(\omega_b + \omega_z)} = \frac{d}{d\omega} \left[-\frac{\delta_s}{2} \text{sinc}_p [\omega - (\omega_b + \omega_z)] \right]_{\omega=(\omega_b + \omega_z)} \\ &= -\frac{k_p \delta_s}{2} \text{cosk}_p [\omega - (\omega_b + \omega_z)] \\ &= -\left(\frac{k_p \delta_s}{2} \right) \end{aligned} \quad (3.46)$$

Using (3.25) slope at $(\omega_b - \omega_z)$

$$\begin{aligned} &= \frac{d}{d\omega} [H_{pm}(\omega)]_{\omega=(\omega_b - \omega_z)} = \frac{d}{d\omega} \left[\frac{\delta_s}{2} \text{cosk}_p (\omega - (\omega_b - \omega_{s0})) \right]_{\omega=(\omega_b - \omega_z)} \\ &= -\frac{k_p \delta_s}{2} \text{sinc}_p (\omega_{s0} - \omega_z) \\ &= \left(\frac{k_p \delta_s}{2} \right) \end{aligned} \quad (3.47)$$

The magnitudes of the slopes at $(\omega_b \pm \omega_z)$ are equal as seen in (3.46) and (3.47).

$$\text{Also, } H_{pm}(\omega_b + \omega_c) = 1 - \frac{\delta_p}{2} \quad (3.48)$$

From the linear region relation, using (3.31)

$$H_{pm}(\omega_b + \omega_c) = 1 - \frac{[(\omega_b + \omega_c) - (\omega_b + \omega_p)]}{(\omega_z - \omega_p)} = 1 - \frac{\omega_c - \omega_p}{(\omega_z - \omega_p)} \quad (3.49)$$

Equating (3.48) and (3.49) and using (3.41) we get,

$$\omega_c = \omega_p + \frac{1}{k_p} \quad (3.50)$$

$$\text{Also, as stated earlier, } H_{pm}(\omega_b + \omega_s) = \frac{\delta_p}{2} \quad (3.50a)$$

Using the linear region (falling edge), we obtain from (3.31) and (3.50a),

$$H_{pm}(\omega_b + \omega_s) = 1 - \frac{[(\omega_b + \omega_s) - (\omega_b + \omega_p)]}{(\omega_z - \omega_p)} = \frac{\delta_p}{2} \quad (3.51)$$

Simplifying (3.51) and using (3.42) we get,

$$\omega_z = \omega_s + \frac{1}{k_p} = \omega_p + \frac{2}{k_p \delta_p} \quad (3.52)$$

$$\text{From (3.52), } \omega_s = \omega_p - \frac{1}{k_p} + \frac{2}{k_p \delta_p} \quad (3.53)$$

From (3.50) and (3.53) we get,

$$(\omega_s - \omega_c) = \frac{2}{k_p} \left(\frac{1}{\delta_p} - 1 \right) \quad (3.54)$$

In the bandpass filter model, $(\omega_s - \omega_c)$ is the transition region width.

$$\text{From (3.54), } k_p = \frac{2 \left(\frac{1}{\delta_p} - 1 \right)}{(\omega_s - \omega_c)} \quad (3.55)$$

3.3.2 Expressions for Impulse Response Coefficients

Referring to filter design theory of section 2.4, the impulse response coefficients $h(n)$ for the bandpass filter are obtained by evaluating the integral below.

$$h(n) = \frac{1}{\pi} \left[\int_0^{\pi} H_{pm}(\omega) \cos k\omega \, d\omega \right] \quad (3.56)$$

$$\begin{aligned} h(n) = \frac{1}{\pi} \left[\int_0^{\omega_b - \omega_{s0}} H_{pm}(\omega) \cos k\omega \, d\omega + \int_{\omega_b - \omega_{s0}}^{\omega_b - \omega_z} H_{pm}(\omega) \cos k\omega \, d\omega + \int_{\omega_b - \omega_z}^{\omega_b - \omega_p} H_{pm}(\omega) \cos k\omega \, d\omega \right. \\ \left. + \int_{\omega_b - \omega_p}^{\omega_b - \omega_{p0}} H_{pm}(\omega) \cos k\omega \, d\omega + \int_{\omega_b - \omega_{p0}}^{\omega_b} H_{pm}(\omega) \cos k\omega \, d\omega + \int_{\omega_b}^{\omega_b + \omega_{p0}} H_{pm}(\omega) \cos k\omega \, d\omega \right. \\ \left. + \int_{\omega_b + \omega_{p0}}^{\omega_b + \omega_p} H_{pm}(\omega) \cos k\omega \, d\omega + \int_{\omega_b + \omega_p}^{\omega_b + \omega_z} H_{pm}(\omega) \cos k\omega \, d\omega \right. \\ \left. + \int_{\omega_b + \omega_z}^{\omega_b + \omega_{s0}} H_{pm}(\omega) \cos k\omega \, d\omega + \int_{\omega_b + \omega_{s0}}^{\pi} H_{pm}(\omega) \cos k\omega \, d\omega \right] \quad (3.57) \end{aligned}$$

$$\begin{aligned} h(n) = \frac{1}{\pi} \left[\int_0^{\omega_b - \omega_{s0}} \frac{\delta_s}{2} \cos k_{p0} [(\omega_b - \omega_{s0}) - \omega] \cos k\omega \, d\omega + \int_{\omega_b - \omega_{s0}}^{\omega_b - \omega_z} \frac{\delta_s}{2} \cos k_p [\omega - (\omega_b - \omega_{s0})] \cos k\omega \, d\omega \right. \\ \left. + \int_{\omega_b - \omega_z}^{\omega_b - \omega_p} \frac{[\omega - (\omega_b - \omega_z)]}{[\omega_z - \omega_p]} \cos k\omega \, d\omega + \int_{\omega_b - \omega_p}^{\omega_b - \omega_{p0}} \left[1 + \frac{\delta_p}{2} \sin k_p [\omega - (\omega_b - \omega_p)] \right] \cos k\omega \, d\omega \right. \\ \left. + \int_{\omega_b - \omega_{p0}}^{\omega_b} 1 + \frac{\delta_p}{2} \cos k_{p0} [\omega - (\omega_b - \omega_{p0})] \cos k\omega \, d\omega + \int_{\omega_b}^{\omega_b + \omega_{p0}} 1 + \frac{\delta_p}{2} \cos k_{p0} (\omega - \omega_b) \cos k\omega \, d\omega \right. \\ \left. + \int_{\omega_b + \omega_{p0}}^{\omega_b + \omega_p} 1 + \frac{\delta_p}{2} \cos k_p [\omega - (\omega_b + \omega_{p0})] \cos k\omega \, d\omega + \int_{\omega_b + \omega_p}^{\omega_b + \omega_z} 1 - \frac{[\omega - (\omega_b + \omega_p)]}{[\omega_z - \omega_p]} \cos k\omega \, d\omega \right] \end{aligned}$$

$$+ \int_{\omega_b + \omega_z}^{\omega_b + \omega_{p0}} -\frac{\delta_s}{2} \text{sinc}_p \left[\omega - (\omega_b + \omega_z) \right] \cos k\omega \, d\omega + \int_{\omega_b + \omega_{s0}}^{\pi} \frac{\delta_s}{2} \text{cosk}_{p0} \left[\omega - (\omega_b + \omega_{s0}) \right] \cos k\omega \, d\omega \quad (3.58)$$

where $n = 0, 1, \dots, \frac{N-1}{2}$ for N odd

$$n = 0, 1, 2, \dots, \frac{N}{2} - 1 \text{ for N even} \quad \text{and} \quad k = \frac{(N-1)}{2} - n$$

Evaluating (3.58), the expressions obtained for the impulse response coefficients $h(n)$ for the lowpass filter

$$\begin{aligned} h(n) = & \frac{k \cos(k\omega_b)}{\pi} \left[\frac{1}{(k_p^2 - k^2)} - \frac{1}{(k_{p0}^2 - k^2)} \right] \left[\delta_p \sin(k\omega_{p0}) - \delta_s \sin(k\omega_{s0}) \right] \\ & + \frac{\cos(k\omega_b) [\cos(k\omega_p) - \cos(k\omega_z)]}{\pi} \left[\frac{2}{k^2 (\omega_z - \omega_b)} \right] + \frac{k_p \cos(k\omega_b) [\delta_p \cos(k\omega_p) - \delta_s \cos(k\omega_z)]}{\pi (k_p^2 - k^2)} \\ & + \frac{\delta_s k_{p0}}{2\pi (k_{p0}^2 - k^2)} \left[\text{sinc}_{p0}(\omega_b - \omega_{s0}) + \cos(k\pi) \text{sinc}_{p0}[\pi - (\omega_b + \omega_{s0})] \right] \end{aligned} \quad (3.59)$$

(3.59) is valid for N even where k is a non-integer. For N odd (3.59) is valid except for $k=0$ and $k = k_{p0}$.

For N odd, $k=0$ we obtain,

$$h\left(\frac{N-1}{2}\right) = \frac{(\omega_z + \omega_p)}{\pi} + \frac{\delta_s}{\pi k_{p0}} \sin k_{p0} \left(\frac{\pi}{2} - \omega_{s0} \right) \cos k_{p0} \left(\frac{\pi}{2} - \omega_b \right) + \frac{(\delta_p - \delta_s)}{\pi^2} \quad (3.60)$$

For N odd, $k = k_{p0}$ we obtain,

$$\begin{aligned}
h\left(\frac{N-1}{2}-k_{p0}\right) &= h\left(\frac{N-1}{2}+k_{p0}\right) = -\frac{\delta_s \cos(k\omega_b) \left[k \sin(k\omega_{s0}) + k_p \cos(k\omega_z) \right]}{\pi(k_p^2 - k^2)} \\
&\quad - \frac{\delta_s}{2k_{p0}\pi} \left[\cos(k_{p0}\omega_b) \sin(k_{p0}\omega_{s0}) \right] + \frac{\delta_p \cos(k\omega_b) \left[k_p \cos(k\omega_p) + k \sin(k\omega_{p0}) \right]}{\pi(k_p^2 - k^2)} \\
&\quad + \frac{\delta_s}{4\pi} \left[(\omega_b - \omega_{s0}) \cos k_{p0}(\omega_b - \omega_{s0}) + (\pi - (\omega_b + \omega_{s0})) \sin k_{p0}(\omega_b + \omega_{s0}) \right] \\
&\quad - \frac{2}{k\pi} \left[\cos(k\omega_b) \sin(k\omega_{p0}) \right] + \frac{2 \cos(k\omega_b) \left[\cos(k\omega_p) - \cos(k\omega_z) \right]}{\pi k^2 (\omega_z - \omega_p)} \tag{3.61}
\end{aligned}$$

3.3.3 Filter Synthesis Results

Design Example: A bandpass linear phase sharp transition FIR filter is designed for the desired specifications of center frequencies, passband widths and transition bandwidths as specified in Table 3.2. The maximum passband ripple is ± 0.1 dB (0.2 dB) and the minimum stopband attenuation is 40dB.

The filter is designed using MATLAB with program MBP-2 and measurement of various filter specifications is done using MATLAB's Signal Processing toolbox. Results approximate the desired filter specifications closely with low filter order with the desired passband widths, center frequencies, passband ripple and stopband attenuation obtained as shown in Table 3.2. The magnitude, impulse and phase response of the proposed bandpass filter with center frequency $\omega_b = 0.6667\pi$, passband width $\omega_p = 0.5556\pi$, transition bandwidth $(\omega_s - \omega_c) = 0.011\pi$, passband ripple $\delta_p = 0.14$ dB and stopband attenuation $\delta_s = 40.2$ dB obtained for a filter order of 701 as shown in Fig.3.4. Table 3.2 depicts the performance of the bandpass filter. From Table 3.2, it is observed that the bandpass filter

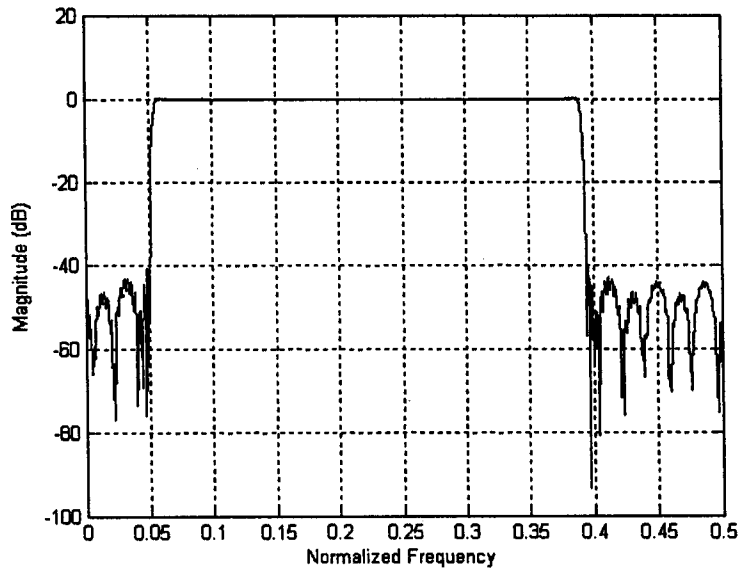
design is adaptable to any change in passband width (wideband to narrowband) and arbitrary center frequencies.

It is observed that there is a marginal improvement in filter performance in terms of decrease in passband ripple and increase in stopband attenuation because of further reduction in Gibb's phenomenon by employing variable ripple cycles density technique compared to previous bandpass model. The bandpass filter design is adaptable to any change in passband width and arbitrary center frequencies. Filter synthesis and design steps are given in Appendix A6.1.7.

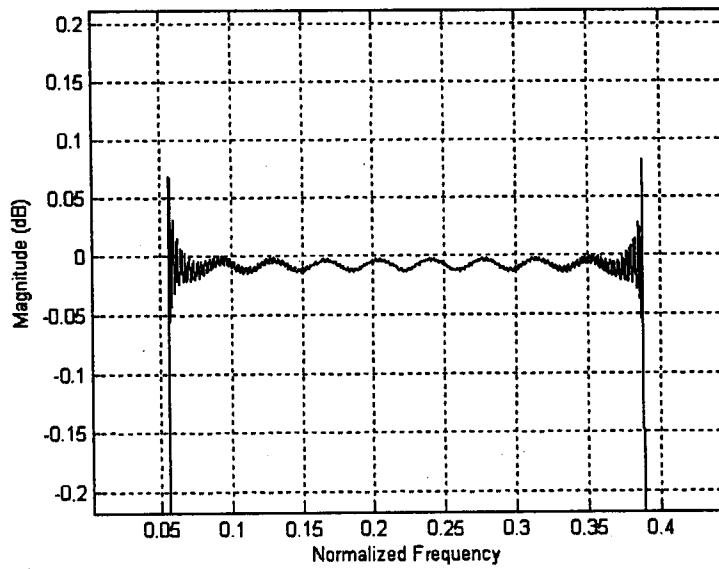
Table 3.2

Proposed bandpass II filter performance for various passband widths, center frequencies and transition bandwidths with required order for filter realization.

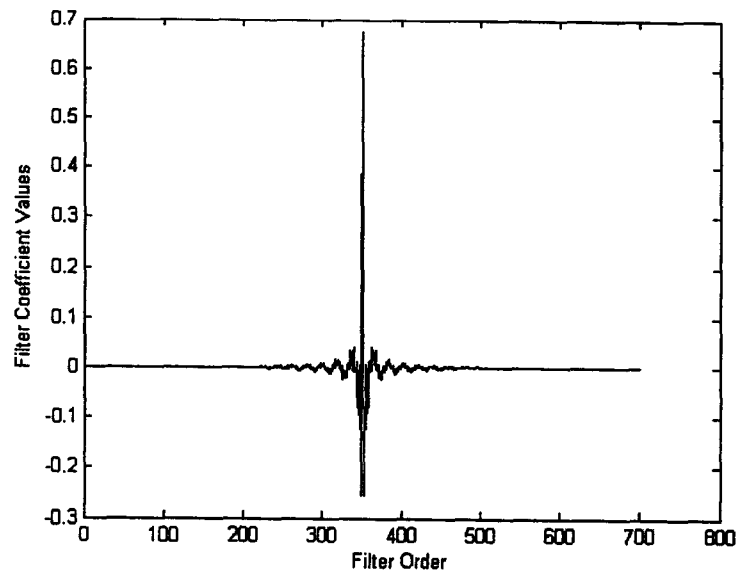
Filter Order	Transition bandwidth	Center Frequency	Passband width	Passband ripple in dB	Stopband attenuation in dB
451	0.021π	0.6667π	0.5556π	0.11	42.15
225	0.010π	0.6667π	0.5556π	0.11	41.69
701	0.011π	0.6667π	0.5556π	0.14	40.20
451	0.021π	0.3333π	0.2778π	0.10	40.10



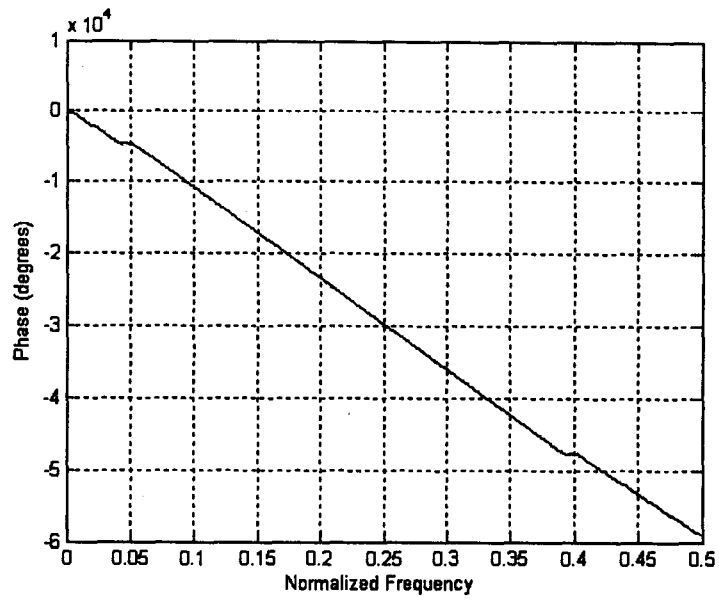
(a)



(b)



(c)



(d)

Fig. 3.4 (a) Magnitude response of the proposed bandpass II filter (b) Magnified view of the passband (c) Impulse response sequence (d) Phase response.

3.4 Lowpass Cascade Filter Model and Design

In this section, a cascade of two lowpass linear phase FIR filters is modeled with out of phase passband ripples, parallel skirts in the transition regions and equiripple stopband ripples [28]. The magnitude responses $H_{pm1}(\omega)$ and $H_{pm2}(\omega)$ of the filters are as shown in Fig. 3.5. The pseudo-magnitude responses of the two filters sections of the proposed filters to be cascaded are formulated as follows.

In the passband region, the frequency responses of component filters are given by

$$H_{pm1}(\omega) = 1 + \frac{\delta_p}{2} \sin k_p \omega \quad 0 \leq \omega \leq \omega_{p1} \quad (3.62)$$

$$\text{and } H_{pm2}(\omega) = 1 - \frac{\delta_p}{2} \sin k_p \omega \quad 0 \leq \omega \leq \omega_{p2} \quad (3.63)$$

where ω the frequency variable, $H_{pm1}(\omega)$, $H_{pm2}(\omega)$ are the pseudo-magnitudes of the individual filter responses of the component filters constituting the cascade, δ_p is passband ripple, k_p is a filter design parameter in the passband, ω_{p1}, ω_{p2} are the passband edges.

We have, $H_{pm1}(\omega_{p1}) = H_{pm2}(\omega_{p2}) = 1.0$

In this design for a specified ω_{p1} ,

$$\omega_{p2} = \omega_{p1} + \frac{\pi}{k_p} \quad (3.64)$$

Since the component filter responses are shifted by $\frac{\pi}{k_p}$ along the frequency axis, this leads to parallel skirts in the transition region of the two responses.

In the transition region, frequency responses of component filters are given by

$$H_{pm1}(\omega) = A \cos k_t (\omega - \omega_0) \quad \omega_{p1} \leq \omega \leq \omega_{z1} \quad (3.65)$$

$$\text{and } H_{pm2}(\omega) = A \cos k_t \left(\omega - \left(\omega_0 + \frac{\pi}{k_p} \right) \right) \quad \omega_{p2} \leq \omega \leq \omega_{z2} \quad (3.66)$$

where k_t is a filter design parameter in the transition region, A is amplitude parameter and is chosen greater than 1, ω_0 is the frequency at which $H_{pm1}(\omega)$ equals A and $\left(\omega_0 + \frac{\pi}{k_p} \right)$ is the frequency at which $H_{pm2}(\omega)$ equals A . Note that ω_0 is a fictitious frequency used to shape the transition regions as was done in proposed Class III filter. Also,

$$H_{pm1}(\omega_{c1}) = H_{pm2}(\omega_{c2}) = 1 - \frac{\delta_p}{2} \quad \text{and} \quad H_{pm1}(\omega_{z1}) = H_{pm2}(\omega_{z2}) = 0.$$

Finally, the stopband region of the component frequency responses are given by

$$H_{pm1}(\omega) = -\frac{\delta_s}{2} \sin k_s (\omega - \omega_{z1}) \quad \omega_{z1} \leq \omega \leq \pi \quad (3.67)$$

$$H_{pm2}(\omega) = -\frac{\delta_s}{2} \sin k_s (\omega - \omega_{z2}) \quad \omega_{z2} \leq \omega \leq \pi, \text{ respectively} \quad (3.68)$$

where δ_s is the stopband attenuation, k_s is the filter design parameter in the stopband region

$$\text{and } H_{pm1}(\omega_{s1}) = H_{pm2}(\omega_{s2}) = \frac{\delta_s}{2}.$$

In the stopband region, we have

$$\omega_{z2} = \left(\omega_{z1} + \frac{\pi}{k_p} \right) \quad (3.69)$$

$$\text{Also, } H_{pm1}(\omega_{p1}) = 1.0 = 1 + \frac{\delta_p}{2} \sin k_p \omega_{p1} \quad (3.70)$$

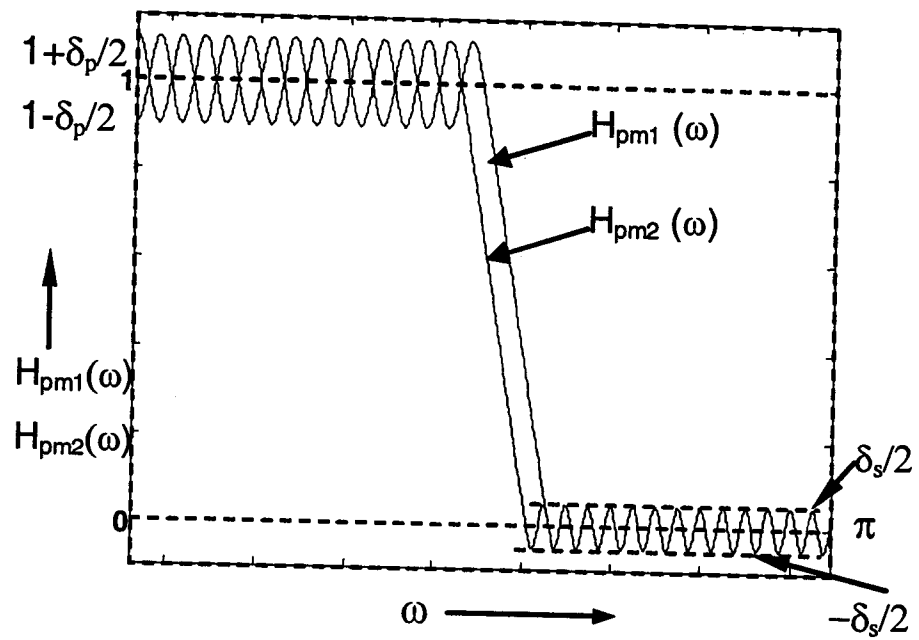


Fig.3.5 Magnitude responses of component filters $H_{pm1}(\omega)$ and $H_{pm2}(\omega)$ of proposed cascade lowpass filter model.

Simplifying (3.70) $\sin k_p \omega_{p1} = 0$ i.e. $\cos k_p \omega_{p1} = \pm 1$. Since the slope shall be negative, we

$$\text{have } \cos k_p \omega_{p1} = -1 \quad (3.71)$$

$$\text{From (3.65), } H_{pm1}(\omega_{p1}) = 1.0 = A \cos k_t (\omega_{p1} - \omega_0) \quad (3.72)$$

$$\text{yielding, } \cos k_t (\omega_{p1} - \omega_0) = \frac{1}{A} \quad \text{and } \sin k_t (\omega_{p1} - \omega_0) = \sqrt{1 - \frac{1}{A^2}} \quad (3.73)$$

Positive sign is chosen for $\sin k_t (\omega_{p1} - \omega_0)$ from the consideration of the slope of the response at $\omega = \omega_{p1}$.

$$\text{From (3.65), } H_{pm1}(\omega_{z1}) = 0 = A \cos k_t (\omega_{z1} - \omega_0) \quad (3.74)$$

$$\text{yielding, } \cos k_t (\omega_{z1} - \omega_0) = 0 \quad \text{or} \quad \sin k_t (\omega_{z1} - \omega_0) = \pm 1 \quad (3.75)$$

where ω_{s2} and ω_{s1} are respective stopband edges and ω_{c2}, ω_{c1} are the respective cutoff edges. Positive sign is chosen for $\sin k_t (\omega_{z1} - \omega_0)$ from the consideration of the slope of the response at $\omega = \omega_{z1}$.

$$\text{From (3.65), } H_{pm1}(\omega_{c1}) = 1 - \frac{\delta_p}{2} = A \cos k_t (\omega_{c1} - \omega_0)$$

$$\text{Simplifying, } \omega_{c1} = \frac{1}{k_t} \cos^{-1} \left(\frac{1 - \frac{\delta_p}{2}}{A} \right) + \omega_0 \quad (3.76)$$

$$\text{From (3.65), } H_{pm1}(\omega_{s1}) = \frac{\delta_s}{2} = A \cos k_t (\omega_{s1} - \omega_0)$$

$$\text{Simplifying, we obtain, } \omega_{s1} = \frac{1}{k_t} \cos^{-1} \left(\frac{\frac{\delta_s}{2}}{A} \right) + \omega_0 \quad (3.77)$$

Using (3.76) and (3.77) we have,

$$k_t = \left(\frac{1}{(\omega_{s1} - \omega_{c1})} \right) \left[\cos^{-1} \left(\frac{\frac{\delta_s}{2}}{A} \right) - \cos^{-1} \left(\frac{1 - \frac{\delta_p}{2}}{A} \right) \right] \quad (3.78)$$

Slope Equalization

The various filter design parameters of the cascade model are evaluated by equalizing the slopes of the pseudo-magnitude response function at ω_{p1}, ω_{p2} and ω_{z1}, ω_{z2} . This allows the proposed function to be continuous thus reducing the effects due to Gibb's phenomenon.

The slope of the response given by (3.62) at $\omega = \omega_{p1}$ is

$$\text{Slope at } \omega_{p1} = \frac{d}{d\omega} [H_{pm1}(\omega)]_{\omega=\omega_{p1}} = \frac{k_p \delta_p}{2} \cos(k_p \omega_{p1}) \quad (3.79)$$

$$\text{Substituting (3.71) in (3.79),} \quad \text{Slope at } \omega_{p1} = -\frac{k_p \delta_p}{2} \quad (3.80)$$

$$\begin{aligned} \text{Using (3.65) and (3.73) we obtain the slope at } \omega_{p1} &= -A k_t \sin k_t (\omega_{p1} - \omega_0) \\ &= -k_t (\sqrt{A^2 - 1}) \end{aligned} \quad (3.81)$$

Equalization of slopes at ω_{p1} , using (3.80) and (3.81) we obtain,

$$k_t = \frac{k_p \delta_p}{2(\sqrt{A^2 - 1})} \quad (3.82)$$

Equalization of slope at ω_{p2} also gives identical expression for k_t as above.

Using (3.67) we obtain,

$$\text{Slope at } \omega_{z1} = \frac{d}{d\omega} [H_{pm1}(\omega)]_{\omega=\omega_{z1}} = -\frac{k_s \delta_s}{2} \cos k_s (\omega_{z1} - \omega_{z1})$$

$$= -\frac{k_s \delta_s}{2} \quad (3.83)$$

Using (3.65) and (3.75), we obtain,

$$\text{Slope at } \omega_{z1} = -Ak_t \sin k_t (\omega_{z1} - \omega_0) = -Ak_t \quad (3.84)$$

From (3.83) and (3.84), equalization of slopes at ω_{z1} yields

$$k_s = \frac{2A k_t}{\delta_s} \quad (3.85)$$

Equalization of slope at ω_{z2} also gives an identical expression for k_s .

The expressions for impulse response coefficients $h(n)$ for the cascade filter are obtained by evaluating the integrals below.

$$\begin{aligned} h(n) = \frac{1}{\pi} & \left[\int_0^{\omega_{p1}} H_{pm1}(\omega) H_{pm2}(\omega) \cos k\omega \, d\omega + \int_{\omega_{p1}}^{\omega_{p2}} H_{pm1}(\omega) H_{pm2}(\omega) \cos k\omega \, d\omega \right. \\ & + \int_{\omega_{p2}}^{\omega_{z1}} H_{pm1}(\omega) H_{pm2}(\omega) \cos k\omega \, d\omega + \int_{\omega_{z1}}^{\omega_{z2}} H_{pm1}(\omega) H_{pm2}(\omega) \cos k\omega \, d\omega \\ & \left. + \int_{\omega_{z2}}^{\pi} H_{pm1}(\omega) H_{pm2}(\omega) \cos k\omega \, d\omega \right] \quad (3.86) \end{aligned}$$

where $n = 0, 1, 2, \dots, \frac{N-1}{2}$ for N odd

$$n = 0, 1, 2, \dots, \frac{N}{2} - 1 \text{ for } N \text{ even} \quad \text{and} \quad k = \left(\frac{N-1}{2} - n \right)$$

3.4.1 Filter Synthesis Results

Design Example: Consider the design of a proposed cascade lowpass FIR filter, where a pair of Class III lowpass linear phase FIR filters are cascaded, one component lowpass filter with

passband edge specified at 0.558π and stopband edge at 0.572π and another component filter shifted with passband and stopband edge to $\left(0.558\pi + \frac{\pi}{k_p}\right)$ and $\left(0.572\pi + \frac{\pi}{k_p}\right)$ respectively, each with passband ripple of $\pm 0.1\text{dB}$ and stopband attenuation of 35dB .

The filter is designed using MATLAB with program MCS. The integrals in (3.86) is evaluated to obtain the coefficients of the resultant filter. The filter obtained after cascading the two component filters has specifications of cutoff edge $\omega_c = 0.5587\pi$, stopband edge $\omega_s = 0.5724\pi$, passband ripple of 0.14dB , stopband attenuation of 38dB and transition bandwidth of 0.01π was obtained for filter order of 701. Stopband attenuation of the resultant filter improves however there is imperceptible change in transition region width. Passband ripple of the resultant filter increases slightly from those of the component filters. Hence it is found that there is no much improvement in filter specifications by cascading proposed lowpass sharp transition filters.

3.5 Conclusions

Linear phase, sharp transition, equiripple response, low arithmetic complexity, bandpass FIR filter designs are proposed. Various regions of the filter are approximated with trigonometric functions of frequency, making it convenient to evaluate the impulse response coefficients in closed form and thus its transfer function is evolved in frequency and time domain. The novel slope equalizing technique is applied to bandpass filter design which makes the proposed function continuous across transition band and hence reduces the effects due to Gibb's phenomenon thereby reducing ripples at the edges of the transition region of the filter. The synthesized filter proves to be a good alternative to filters of the same class reported

in the literature with added advantage of ease of computation of the impulse response and simplicity of design since the filter is without any subfilters i.e. direct design compared to sharp transition bandpass filters realized using highpass and lowpass filters in literature. Also the proposed filters are designed for arbitrary center frequency and passband width with no separate design required. In another proposed bandpass approach, the filter model is such that large density of ripple cycles are introduced in the regions where discontinuities are present in the filter magnitude response, to increase the sharpness of the transition and remove any abrupt discontinuities, which further reduces Gibb's phenomenon. In the proposed approximation technique impulse response coefficients are obtained for facilitating the direct synthesis of the filter. The approach can be extended to design of sharp cutoff bandstop and multiband filters with arbitrary passband and center frequencies.

Chapter 4

MODIFIED FREQUENCY RESPONSE MASKING APPROACH

4.1 Introduction

One of the most difficult problems in filter synthesis is the design of narrow transition band FIR filters, which require high order for their implementation using conventional methods. Linear phase FIR digital filters require in applications demanding narrow transition bands considerably more arithmetic computations and hardware than their IIR equivalents [29]. The search of design and synthesis techniques which will produce efficient filters for the implementation of narrow transition width FIR filters has attracted much research efforts in the past few years.

Several methods have been proposed in the literature for reducing the complexity of very sharp FIR filters. One of the most successful techniques for synthesis of very narrow transition width filter is the Frequency Response Masking (FRM) technique because of reduced arithmetic complexity involved [7], [30]-[35]. FRM approach can be used to implement both linear phase and approximately linear phase high-speed recursive digital filters. When the frequency response masking technique is used to synthesis an FIR filter, resulting filter will ^{consists} ~~comprise~~ of a sparse coefficient filter and a pair of masking filters. The major advantages of FRM approach is that the filter has a very sparse coefficient vector so its arithmetic complexity is very low, though its length and delays are slightly longer than those in the conventional implementations. For a given frequency response specification its effective filter length including both zero and non-zero coefficients is only slightly longer than the infinite word length optimum minimax filter. These filters are suitable for VLSI implementations since hardware complexity is reduced. In addition to low pass designs the FRM approach can be extended to the design of highpass and bandpass filters [35].

Optimization techniques are being developed for superior filter performance with minimum filter hardware complexity and recently optimization techniques have been developed for reduction in passband ripple and increasing stopband attenuation for IIR filters using FRM approach which is dealt in [36].

Basic FRM technique [7] for implementing sharp linear phase FIR filters with arbitrary bandwidth was generalized in [30]. Very sharp transition filters are implemented using several simple subfilters with significant saving in arithmetic operations as high as 4:1 compared to conventional implementations was achieved. The overall FRM filter is designed by separately optimizing the model and masking filters in which case the filters can be designed easily and fast. The FRM filters obtained in the approach of separate subfilter optimization serve as good initial filters for further optimizations. A drawback is that the resulting overall filter is not optimal. It can therefore be beneficial to consider simultaneous optimization of the model and masking filters.

Design methods are presented for reducing the complexity of the masking filters by capitalizing on the fact that the frequency responses of the masking filters are similar. They are able to produce savings in terms of number of multipliers having different group delay and round off noise performances. Synthesis of very sharp half-band filter using frequency response masking technique is dealt in [37]. An important property of a half band filter is that half of its coefficient values are trivial. This yields significant advantages in terms of reduction in computational complexity.

The frequency response masking approach for high speed recursive infinite impulse response (IIR) digital filters is introduced in [33]. In this approach, the overall filter consists of a periodic IIR filter, its power complementary periodic filter and two linear phase FIR masking filters. High speed narrow band recursive filters are realized using an IIR filter for the model filter and an FIR filter for the masking filter. An advantage of using

techniques based on periodic and nonperiodic filters is that there is a large freedom to choose structures for the model and masking filters that are well suited for the specification and problem at hand. IIR model filters are realizable as a parallel connection of two all-pass filters, with a large freedom to choose structures with good properties since all pass filters can be realized in many different ways like lattice wave digital filters etc. In addition, the all pass filters can always be realized by cascading low order sections, which is attractive from an implementation point of view.

The maximal sample frequency for the overall filter is M times that of the corresponding conventional IIR filter. The maximal sample frequency can be increased to an arbitrary level for arbitrary bandwidths. The overall FRM filter can be designed by separately optimizing the model and masking filters with the aid of conventional approximation techniques. The obtained overall filter also serves as a good initial filter for further optimization. Further, robust filters under finite arithmetic conditions can always be obtained by using wave digital all pass filters and non-recursive FIR filters. Recursive infinite impulse response (IIR) digital filters have a drawback in that they restrict the sample frequency at which an implementation of the filters can operate. This may affect not only the speed but also the power consumption, since excess speed can be traded for low power consumption through the use of power supply voltage scaling techniques.

As an application of the FRM techniques, the design of a linear phase digital filter bank for audio system frequency response equalization is dealt in [38]. This filter bank uses frequency response masking and complementary filtering principles to achieve very sharp frequency response for each band, unity gain at all frequencies and extremely low hardware complexity. Several structures are discussed for implementing the overall FRM filter the two-branch structure being commonly used [7]. These structures are compared with each other and with equivalent direct-form minimax designs in terms of the number of distinct

multipliers, overall filter order, overall multiplication rate, number of delay elements, coefficient sensitivity and output noise variance.

In the FRM techniques [7], closed form expressions for impulse response coefficients were not obtained. We propose an analytical approach to the design of sharp transition filters with least arithmetic complexity. The approach for the design of subfilters is simple, analytical, without extensive computations and can be extended to design sharp cutoff, highpass, bandpass and multiband filters with arbitrary passband. This chapter deals with a modified Frequency Response Masking (MFRM) technique for the synthesis of linear phase, sharp transition and low arithmetic complexity FIR filter. The structure is composed of proposed linear phase, sharp transition FIR lowpass and bandpass filters used as subfilters to obtain the MFRM filter. The frequency response of the subfilters are modeled using trigonometric functions of frequency and the design yields closed form expressions for the impulse response coefficients of the subfilters and the final MFRM. The bandpass filter eliminates one masking filter and a model filter from the basic FRM approach thereby simplifying the synthesis of the proposed MFRM filter. Expressions for impulse response coefficients are derived, coefficients obtained and simulation of the lowpass and bandpass filters required for realization of MFRM filter is carried out.

4.2 Review of Frequency Response Masking Approach

4.2.1 Basic Frequency Response Masking Approach

The basic idea behind the frequency response masking technique [7] is to compose the FRM filter using several sub-filters. The first sub-filter is known as model filter or edge shaping filter is upsampled to form the sharp edge needed in the FRM filter. The second sub-filter is the complement of the model filter, which helps to form the arbitrary bandwidth of the FRM filter response. The other two subfilters are masking filters, which

extract one or several passbands of the periodic model filter and periodic complementary model filter and remove unwanted frequency components to form the stop band of the FRM filter response [39], [40].

In the FRM approach, the transfer function of the FRM filter is expressed as

$$H(Z) = G(Z^M)F_0(Z) + G_c(Z^M)F_1(Z) \quad (4.1)$$

The filters $G(z)$ and $G_c(z)$ are prototype linear phase model and a complementary model filter respectively. The filters $F_0(z)$ and $F_1(z)$ are masking filters which extract one or several pass bands of the periodic model filter $G(z^M)$ and periodic complementary model filter $G_c(z^M)$ respectively. The frequency responses of $G(z^M)$ and $G_c(z^M)$ are those of $G(z)$ and $G_c(z)$ compressed in frequency scale by a factor M , that is replacing every delay in $G(z)$ and $G_c(z)$ by M delays each. In particular, the transition band of the filters $G(z^M)$ and $G_c(z^M)$ is M times as sharp as that of $G(z)$ and $G_c(z)$.

$$\text{Also } G_c(Z^M) = Z^{-M\left(\frac{N-1}{2}\right)} - G(Z^M) \quad (4.2)$$

where N is the model filter length and M is some positive integer. The corresponding structure is as shown in Fig. 4.1. Typical magnitude responses for the model, masking and overall FRM filter $H(z)$ is as shown in Fig. 4.2 where k is some positive integer. The transition band of overall FRM filter $H(z)$ can be selected to be equal to one of the transition region of one of the periodic filters $G(z^M)$ or $G_c(z^M)$. In order that the two branches should be added in phase at the output the delays along with the two parallel paths must be same in Fig. 4.1.

The transitions of the frequency masking filter $F_0(z)$ and $F_1(z)$ shown in the Fig. 4.2 are governed by the width of the individual tooth in $G(z^M)$ and by the separation between neighboring teeth. When the desired transition is very sharp, M can be quite large, making

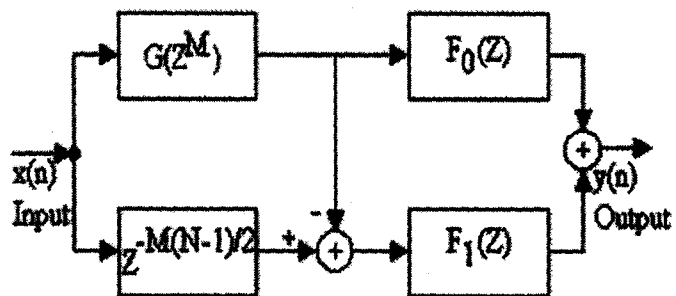


Fig.4.1. Block diagram of structure used in basic FRM approach.

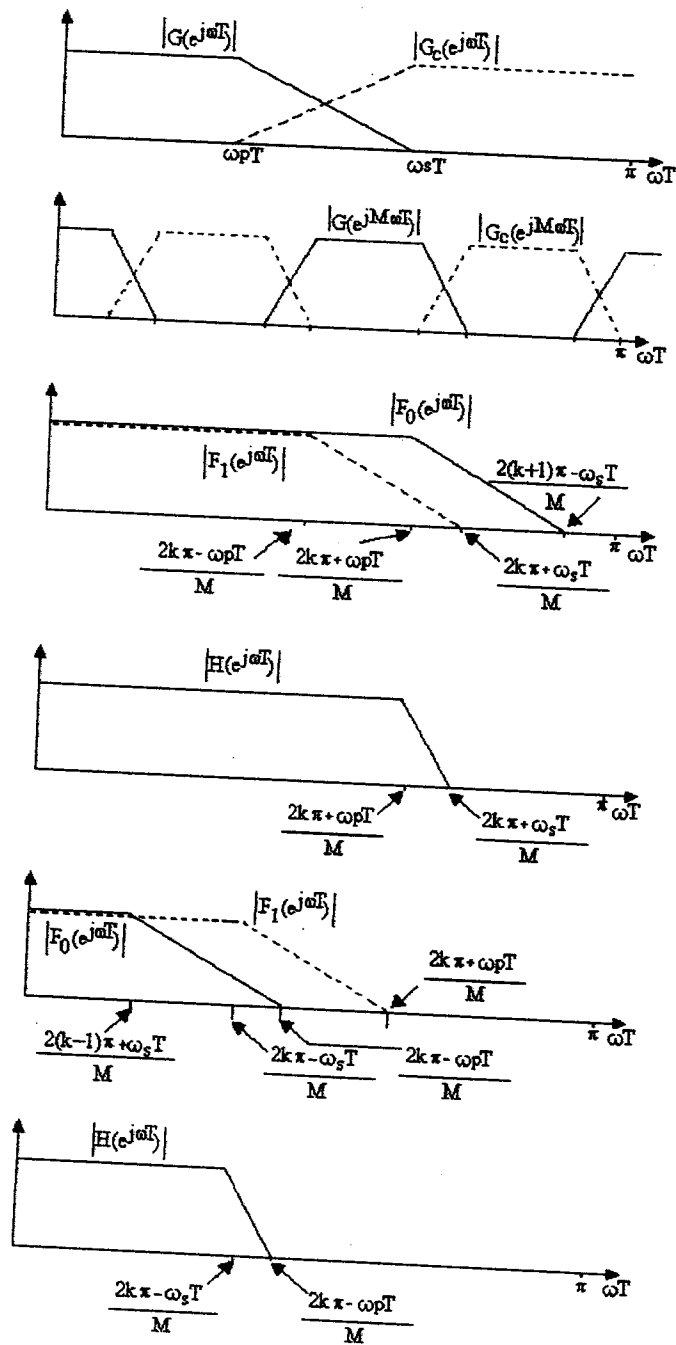


Fig. 4.2. Illustration of basic FRM approach

the tooth width very narrow. In this case, the transition width of the two masking $F_0(z)$ and $F_1(z)$ is also very narrow, leading to high order masking filters. To overcome this difficulty, the idea of frequency compression is applied to the design of these masking filters [30]. Two prototype masking filters $F_0(z)$ and $F_1(z)$ are designed and then by applying frequency compression to these filters i.e. $F_0'(z) = F_0(z^N)$ and $F_1'(z) = F_1(z^N)$ for some integer N . The transition band of $F_0'(z)$ and $F_1'(z)$ are now N times as sharp as those of $F_0(z)$ and $F_1(z)$ respectively. However this frequency compression introduces spurious teeth in $F_0'(z)$ and $F_1'(z)$ at high frequencies. These teeth can be removed by a low pass filter $E(z)$ which has a rather gentle transition hence will not be of high order. The basic frequency response masking approach can be regarded as a special case where N is one and $E(z)$ is not needed in this case. Also a two stage FRM structure is used when the desired transition band is extremely narrow [30]. Therefore in this design, M can be very large making the transition width of the model filter very narrow. Hence transition width of masking filters will also be sharp and hence require a high order. Therefore, in this case, a second stage of frequency masking can be added with masking filters also compressed in suitable frequency scale.

4.3 Modified Frequency Response Masking Approach

Linear phase, equiripple passband and stopband, sharp transition lowpass and bandpass FIR filters designed using our proposed approach are used as various subfilters for the realization of the sharp transition modified FRM (MFRM) lowpass FIR filter [27]. Let φ , θ be the stopband and passband edges of model filter $F_a(z)$ respectively and ω_s , ω_c be the stopband and passband edges of modified FRM filter $F(z)$. The transition bandwidth $\Delta\omega_m$ of model filter of length N_m is

$$\Delta\omega_m = \varphi - \theta = M(\omega_s - \omega_c) = M \Delta\omega \quad (4.3)$$

where $\Delta\omega$ is the transition bandwidth of the MFRM filter.

The complementary model filter $F_c(z)$ has a transfer function

$$F_c(z) = z^{\frac{-(N_m-1)}{2}} - F_a(z) \quad (4.4)$$

In our approach, the model and complementary model filters need not be symmetrical around $\omega = \frac{\pi}{2}$ as in the conventional FRM filter. This makes the design more flexible and universal such that a wide range of narrow and wide passbands can be achieved. Fig. 4.3 illustrates the proposed MFRM approach with band edges and slopes of various subfilters shown. The frequency domain responses of the periodic model and periodic complementary model filters are related as

$$F_a(e^{jM\omega}) + F_c(e^{jM\omega}) = 1 \quad (4.5)$$

Masking filters $F_{ma}(z)$ and $F_{mc}(z)$ used to mask $F_a(z)$ and $F_c(z)$ respectively have frequency responses with equal transition bandwidth and are parallel in the respective transition region. The transition bandwidth of the masking filters depends on the values of θ and φ which are functions of M and k which are positive integers. The frequency domain synthesis of this scheme with typical magnitude responses of model, masking and bandpass filters is as shown in Fig.4.3. The frequency response of the two masking filters are related by

$$F_{ma}(e^{j\omega}) = F_{mc}(e^{j\omega}) + F_{bp}(e^{j\omega}) \quad (4.6)$$

where $F_{bp}(e^{j\omega})$ is a bandpass filter designed with center frequency, passband edges and passband width as shown in Fig.4.3.

Referring to Fig.4.3, Gain of bandpass filter, $A = \frac{2(\pi-\varphi)}{M} * \frac{M}{2\pi-(\varphi+\theta)}$ (4.7)

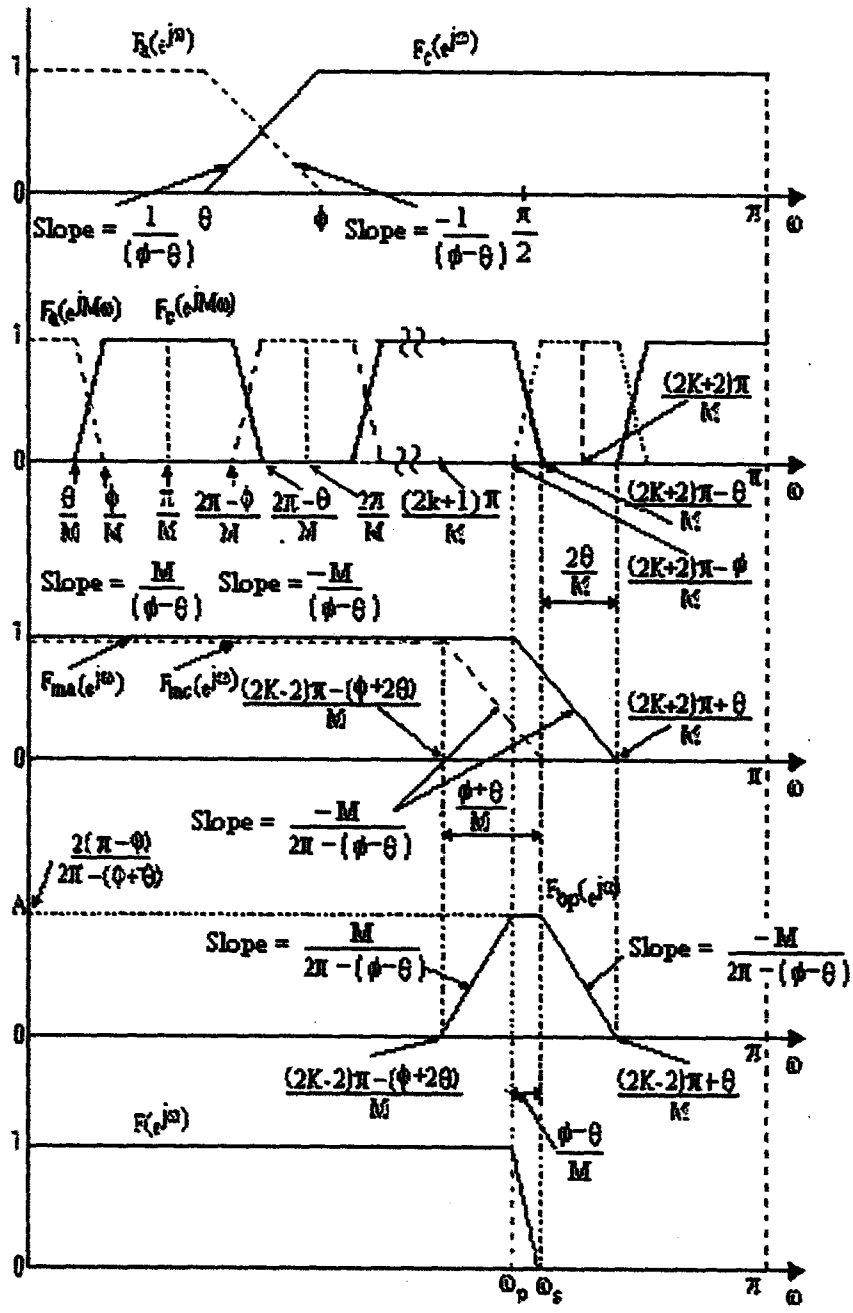


Fig. 4.3 Illustration of the proposed modified frequency response masking approach

$$\text{Simplifying, } A = \frac{2(\pi - \varphi)}{2\pi - (\varphi + \theta)} \quad (4.8)$$

A is chosen to give a passband gain of unity for the MFRM filter. We have for the basic FRM approach,

$$F(e^{j\omega}) = F_a(e^{jM\omega})F_{ma}(e^{j\omega}) + F_c(e^{jM\omega})F_{mc}(e^{j\omega}) \quad (4.9)$$

Substituting (4.5) and (4.6) in (4.9), we obtain,

$$F(e^{j\omega}) = F_{mc}(e^{j\omega}) + F_a(e^{jM\omega})F_{bp}(e^{j\omega}) \quad (4.10)$$

Hence the proposed transfer function for the sharp transition lowpass MFRM filter realization derived from the basic FRM approach is

$$F(z) = F_{mc}(z) + F_a(z^M)F_{bp}(z) \quad (4.11)$$

The proposed structure shown in Fig.4.4 is a two branch realization where the delays of the two parallel paths must be same in order to be added in phase at the output. In Fig 4.4, it is assumed that the delay in the two parallel branches are equalized. In our approach the bandpass filter eliminates one of the masking filter and one periodic model filter greatly simplifying the synthesis of FRM filter. The slopes of the various sub-filters and their filter edges have been designed for the MFRM approach as shown in Fig.4.3. Our proposed lowpass and bandpass filters designed in earlier sections have been used as subfilters in the MFRM approach. The expressions for the impulse response coefficients $h(n)$ of the proposed linear phase lowpass and bandpass FIR filter are as in Section (2.8.3) and (3.2.2) respectively.

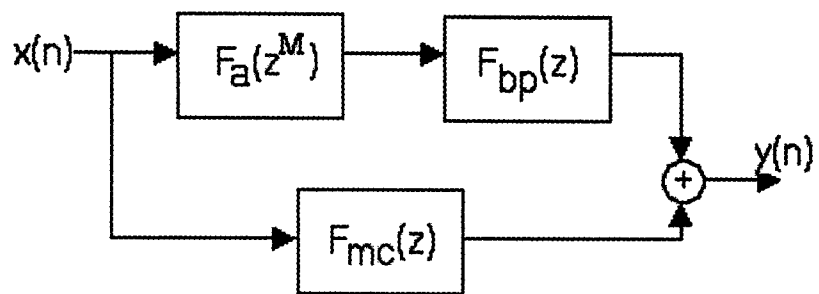
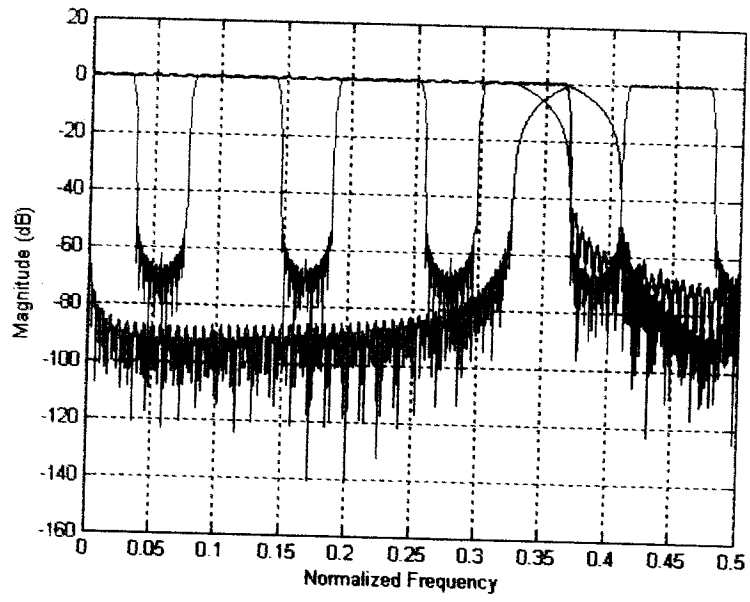


Fig.4.4. Block diagram of structure for low pass Modified FRM filter realization.

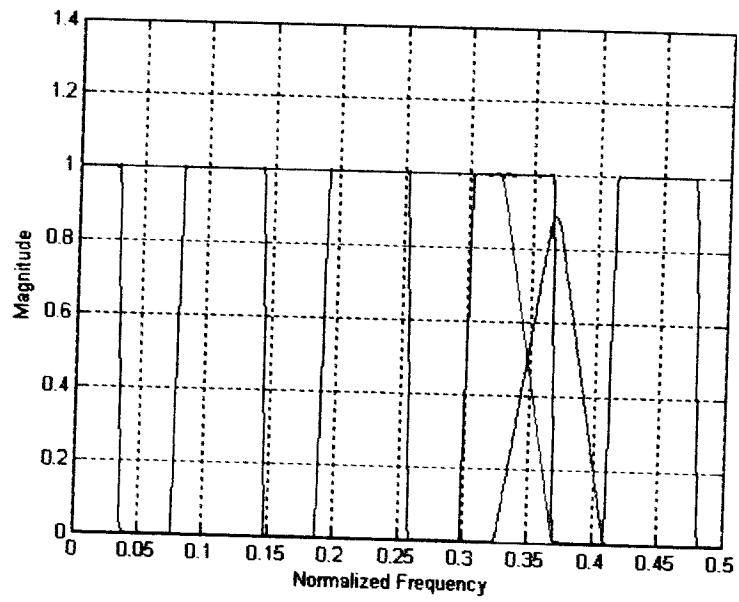
4.3.1 Filter Synthesis Results

Design Example: Lowpass linear phase sharp transition FIR filters are designed for the desired filter specifications: cutoff edge ω_c is 0.7332π , stopband edge ω_s is 0.7432π , maximum passband ripple δ_p is $\pm 0.1\text{dB}$ (0.2 dB) and minimum stopband attenuation δ_s is 40dB using the proposed Modified FRM approach.

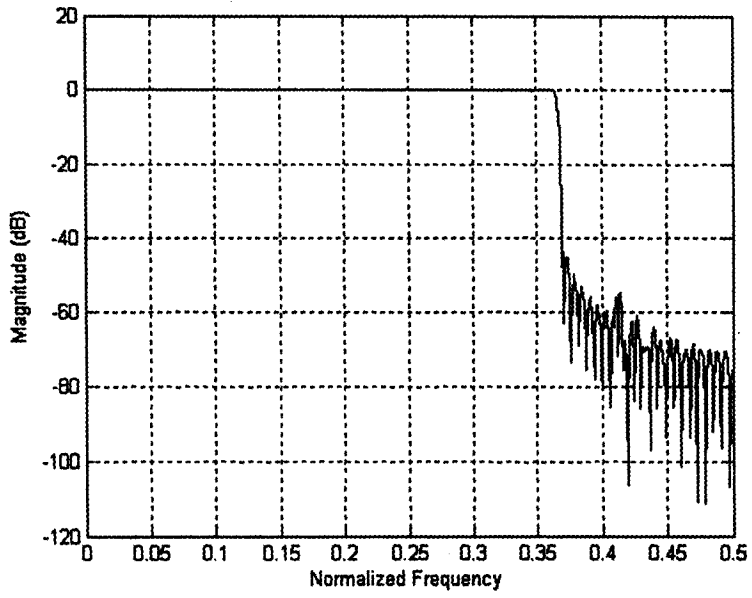
The filter is designed using MATLAB with program MMF and measurement of various filter specifications is done using MATLAB's SP toolbox. Results are tabulated in Table 4.1. The Modified FRM approach, composed of proposed lowpass and bandpass filters as subfilters (refer Sections 2.8 and 3.2). The MFRM filter is synthesized with various band edges for the lowpass and bandpass subfilters obtained using equations in Fig.4.3. The specifications of subfilters band edges measured using SP toolbox meet the design specifications and the final MFRM filter passband edge is 0.7332π and stopband edge is 0.7432π with a transition width of 0.01π with passband ripple δ_p of 0.13dB and stopband attenuation δ_s of 42.2dB are obtained for a 'sum of subfilter order' of 273. The magnitude response of various subfilters, final MFRM filter, impulse response sequence and phase response is as shown in Fig. 4.5. The actual MFRM filter order is higher than 'sum of subfilter order' but it does not contribute to filter complexity because it has zero value coefficients which only increases delays in the MFRM filter. Table 4.1 gives filter order of various subfilters and final MFRM filter for a transition bandwidths of 0.01π and 0.004π .



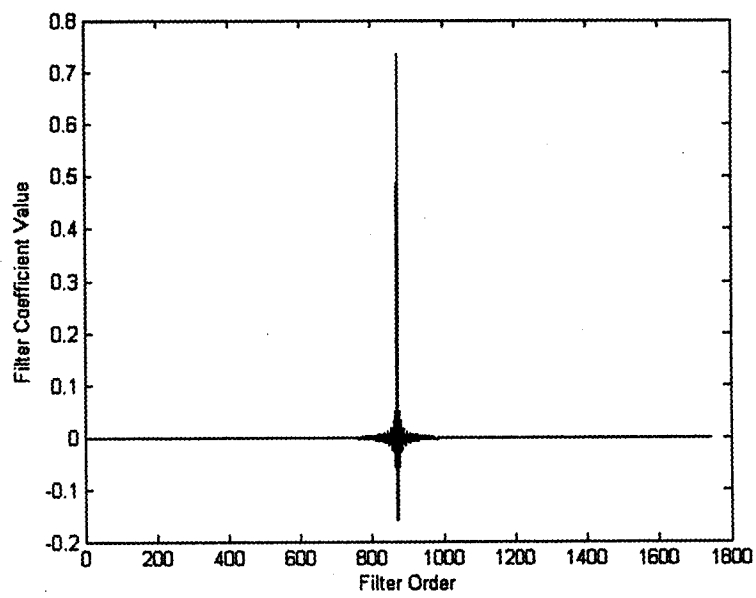
(a)



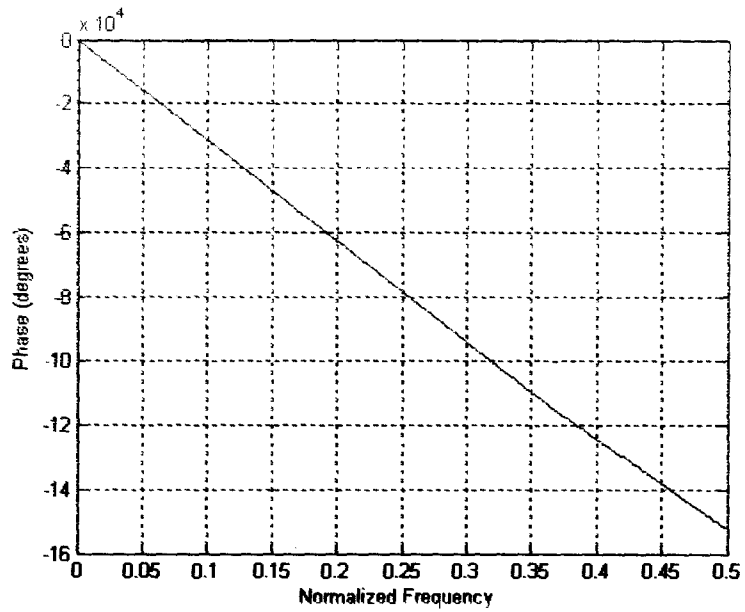
(b)



(c)



(d)



(e)

Fig. 4.5 (a) Magnitude response of various subfilters used in proposed MFRM approach with Model filter(light green) , Masking filter(red), bandpass filter(green) and final MFRM filter (blue) (b) Linear plot (c) Final MFRM filter magnitude response (d) MFRM impulse response sequence (e) MFRM phase response .

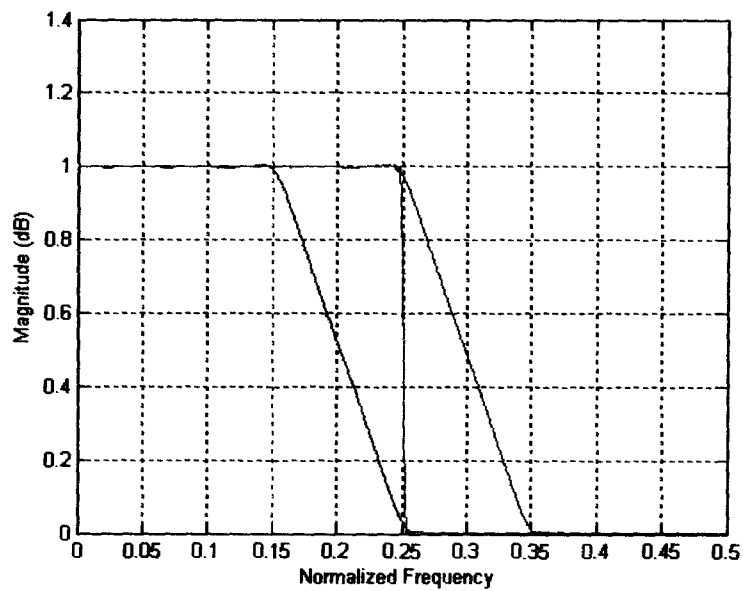


Fig. 4.6. Magnitude response of masking subfilters (using proposed filters) employed in basic FRM approach and the magnitude response of final FRM filter (red colour).

Table 4.1

Filter order required for various proposed subfilters for realization of MFRM filter with transition bandwidths of 0.01π and 0.004π for maximum passband ripple of 0.15dB and minimum stopband attenuation of 40dB.

M	k	Model filter order	Masking filter order	Bandpass filter order	Sum of Subfilter order	Passband Ripple in dB	Stopband Attn. in dB	Transition bandwidth
9	3	71	161	101	333	0.076	36.8	0.004π
9	3	66	86	121	273	0.13	42.2	0.01π

Table 4.2

Filter order required for various proposed subfilters for realization of basic FRM filter with transition bandwidths of 0.01π and 0.005π for maximum passband ripple of 0.15dB and minimum stopband attenuation of 40dB.

M	k	Model filter order	Masking filter1 order	Masking filter2 order	Sum of Subfilter order	Passband ripple in dB	Stopband Attn. in dB	Transition width
5	3	67	67	67	201	0.14	40.4	0.01π
9	3	40	120	150	310	0.15	42.1	0.005π

4.4 Proposed filters as subfilters in FRM approach

Using our proposed lowpass filters as subfilters for the basic FRM approach [7] in Fig.4.2 the impulse response coefficients can be obtained for the component subfilters as well as the overall FRM filter. The filter is designed using MATLAB with program MFRM. The FRM filter order is higher in our case since the subfilters i.e. proposed lowpass filters are not optimized to obtain the desired filter specifications with least filter order as done for subfilters designed by Lim [7]. Magnitude response of masking subfilters and final FRM filter using proposed filters is shown in Fig. 4.6.

4.5 Conclusions

We have proposed a novel technique for a sharp transition, linear phase ,lowpass FIR filter with low arithmetic complexity obtained by modifying the basic frequency response masking approach. The subfilters required i.e. lowpass and bandpass filters are designed using our approach which is a simple direct design and possesses closed form expressions for impulse response coefficients. In our approach, only one masking filter need to be synthesized instead of the two masking filters required in [7]. The bandpass filter has wider transition response which decreases arithmetic complexity of the subfilter. Unlike in frequency response masking approach, the transfer function for subfilters and final MFRM filter in our approach is evolved both in frequency and time domain. The accuracy of the filter approximation can be improved by including a larger number of terms in the impulse response sequence. The lowpass realization can be extended to the realization highpass, bandstop, bandpass and multiband filters.

Basic FRM approach is a graphical approach. In the proposed approach, the same philosophy is adopted as in basic FRM approach, while greatly simplifying the design of subfilters majority of which do not have a steep transition. Lim's filter [7] uses subfilter optimization hence FRM filter is of lower order. Our subfilters are without optimizations

and of higher order. Hence the resulting final MFRM filter possesses higher order for the same filter specifications of passband ripple and stopband attenuation compared to FRM approach [7]. With MFRM approach sharp to very sharp transition filters can be synthesized.

Chapter 5

MULTIBAND FIR FILTERS IN SPEECH PROCESSING SCHEME FOR SENSORINEURAL HEARING IMPAIRED

5.1 Introduction

This chapter provides an overview of the human auditory system, various types of hearing impairment and effects of sensorineural impairment on speech perception. Speech processing schemes for improving speech perception for sensorineural hearing impaired subjects are reviewed. FIR filters designed for speech processing schemes in literature are studied. Novel multiband filters are designed and implemented in a speech processing scheme to improve speech perception in sensorineural hearing impaired.

5.1.1 Human Auditory System

Fig. 5.1 shows the major components of the human ear. The sound waves received by external ear pass through ear canal and cause vibrations of the tympanic membrane or eardrum. The middle ear consists of a cavity with a delicate chain of three tiny bones, the malleus, the incus and the stapes. These bones couple the vibration of the tympanic membrane to the inner ear. The inner ear consists of a fluid filled bony spiral of two and a half turn called cochlea [41]. Fig. 5.2 shows the structure of the inner ear that is transverse section of the cochlea with its three chambers, scala vestibuli, scala media and scala tympani. At upper side, the scala media is separated from scala vestibuli by Reissner's membrane. In turn, it is separated from scala tympani by basilar membrane and a bony shelf at lower side. The organ of corti sits on the basilar membrane and it is covered by tectorial membrane. The organ of corti contains about 30,000 hair cells. In our auditory system, there is one single row of inner hair cells and three rows of outer hair cells. The inner and outer hair cells play different roles in sound reception. Incidence of sound waves

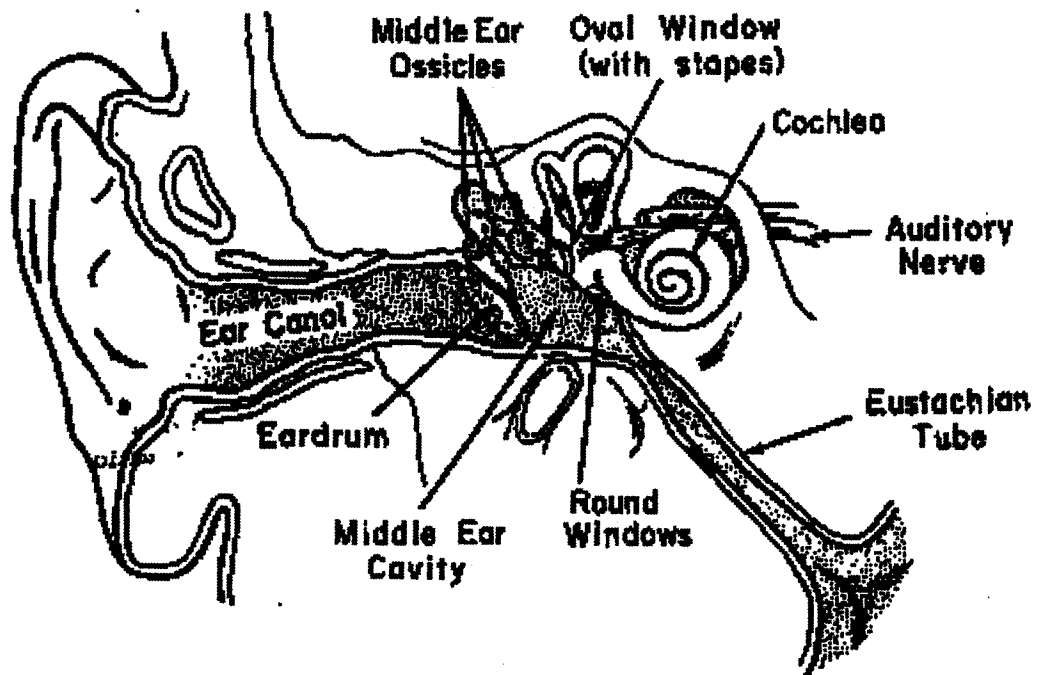


Fig.5.1. Major components of the ear.

on tympanic membrane causes it to vibrate. This energy reaches the oval window and gets transmitted to the fluid in the cochlear chambers i.e. perilymph and endolymph setting up traveling waves and causing basilar membrane to vibrate. The basilar membrane with stiffness highest near the oval window and progressively reducing along the length behaves like a dispersive transmission medium in which the traveling waves lose the high frequency energy while propagating towards apical end. Differential spatial activity takes place in response to these traveling waves of different frequencies. The highest frequency in audible range affects the region near the oval window whereas the lowest frequencies affect the far end, the helicotrema [42]. The low frequency sounds set relatively higher length of basilar membrane into vibration as compared to high frequency sounds. This might be the reason for high sensitivity of the ear to low frequency sounds. The upward and downward movement of basilar membrane results in upward-inward and downward-outward movement of reticular lamina respectively. The inward and outward bending of hair cell cause generation of electric potential difference, which stimulates the cochlear nerve endings resulting in nerve impulses. These impulses are transmitted over the cochlear nerve, a part of vestibulo-cochlear nerve to the higher processes of the brain. The information travels through the cochlear nucleus, the superior olivary complex, the inferior colliculus and the medial geniculate body ending at left and right hemisphere of the auditory cortex. The fibers in the pathways undergo considerable amount of convergence and divergence at many stages.

Hearing losses are classified as conductive loss, central loss, functional loss and sensorineural loss [2]. Conductive loss results due to defects of the ear canal, ear drum or middle ear cavity which results in less acoustic energy reaching the cochlea. It may be due to wax in the external auditory meatus, fluid, pus or infection in the middle ear. In conductive hearing loss the hearing threshold and discomfort levels get increased but

frequency selectivity does not degrade and losses are greater for frequencies below 1 KHz. Central impairment is usually caused by damage to auditory cortex, inflammation of the membrane covering the brain and spinal cord, skull trauma or congenital defect. It may result in decreased speech comprehension ability even though hearing thresholds may not increase. In central masking, the threshold of signal presented to one ear is raised due to a masking sound presented to another ear. The causes for the functional loss are psychological factors rather than physiological disorder. On the basis of hearing thresholds, the impairment can be graded into several categories like mild, moderate, severe and profound. In audiological clinics, the hearing threshold level as a function of pure tone frequency is routinely measured and plotted as audiogram. Frequency selective amplification is primary aim of most hearing aids for overcoming the problem of elevated hearing threshold.

5.1.2 Sensorineural Hearing Loss

Sensorineural loss is caused by defects in cochlea i.e. sensory and/or auditory nerve i.e. neural and is associated with decrease in frequency resolving capacity of the auditory system due to spread of spectral masking along the cochlear partition [43]. It is characterized by increase in threshold of hearing, reduction in dynamic range of hearing, degradation of temporal resolution, increase in temporal masking, degradation of frequency resolution or selectivity due to increase in spectral masking and an abnormal increase in perceived loudness with increase in sound level. The loss of frequency selectivity due to broadening of critical bands results in poor speech perception[65]. Sensorineural loss causes include congenital or hereditary factors, destruction of organ of corti, basilar membrane discontinuity, degeneration of neurons in the auditory nerve in ascending pathway, tumors, long term exposure to industrial noise, acoustic trauma, action

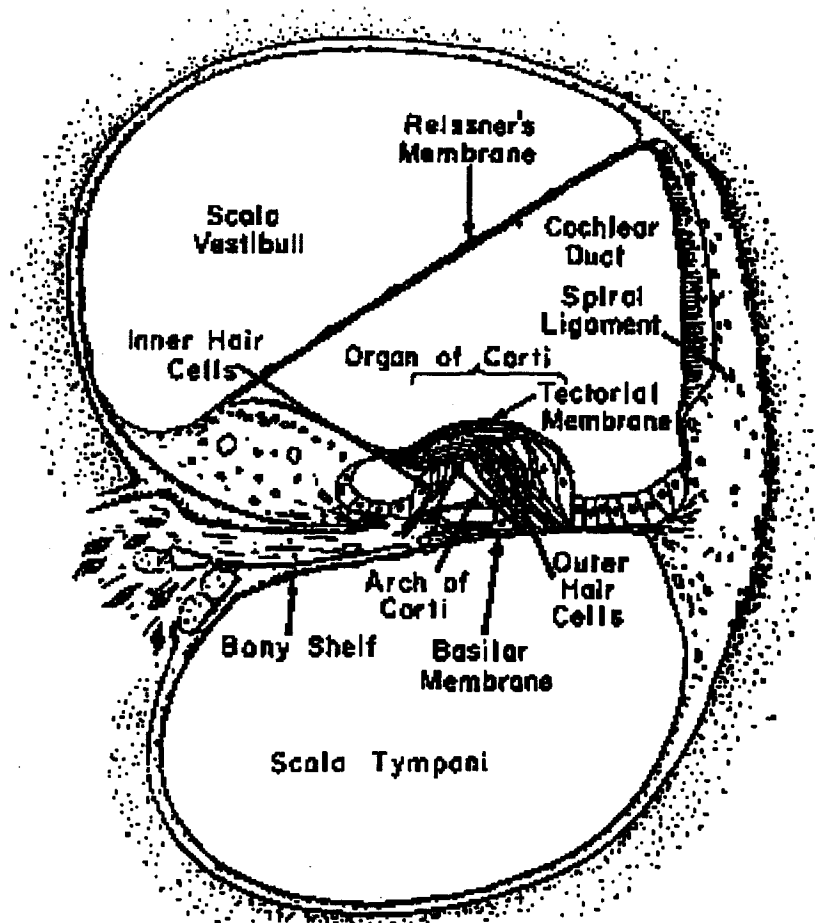


Fig: 5.2. Transverse section through the cochlea.

of the toxic agents, and degeneration of hair cells due to aging, interruption of blood supply to inner ear, viral infection spread from middle ear etc. In general, this loss is not medically curable and it becomes progressively worse with time. Two other phenomena associated with sensorineural loss are diplacusis and tinnitus. In case of diplacusis, a pure tone is perceived as sound with more than one pitch or as a harsh or buzzing sound. Also different pitches may be heard at the two ears for the same tone. Its causes may include mild injury to organ of corti or long term exposure to very intense sound. Tinnitus or ringing in ear is a commonly occurring auditory disorder. It may be caused by spontaneous discharge of hair cells or auditory nerves and may also be induced by exposure to intense sound. It occurs with many types of sensorineural impairment and can contribute significantly to the disruption of speech comprehension in severe cases. The cochlear loss could result due to a number of factors and typically deviated audiogram configurations indicate the various pathologies [44]. Flat audiogram is noticed due to salicylate poisoning. Damage in the organ of corti by ototoxic drug, stiffening of basilar membrane and damage to hair cells and supporting deiters cell manifest as audiogram with hearing threshold increasing with frequency. In sensorineural loss, it is quite common to find some hearing in low frequency up to 1 or 2 KHz. A very high threshold at a particular frequency between 3-6 KHz usually suggest an acoustic trauma i.e. loss of hair cell due to exposure to loud sound. The hearing threshold are relatively elevated for the frequencies in the 1-4 KHz range in the congenital sensorineural damage [45]. Various diseases like typhoid, meningitis, mumps etc indicate a peculiar pattern in audiogram e.g., moderate to severe [70], [71], [72]. bilateral sensorineural loss is seen in typhoid. Retro-cochlear impairment results due to damage of auditory nerve fibers. Its causes may include tumor and hemorrhage. Viral infection may results in primary degeneration of auditory neurons which is relatively

uncommon. Secondary degeneration involves the peripheral processes of auditory neurons constituting loss of hair cells mostly in the first half of basal turn.

5.1.3 Effects of Sensorineural Loss on Speech Perception

Speech signal generally can be described as having a dynamically varying broadband spectrum. The important acoustic characteristics include the amplitude, frequency, bandwidth of formants i.e. spectral resonances specific to the vocal tract configuration, nature of excitation i.e. voiced /unvoiced and pitch [46]. The degradation in temporal resolution and increase in temporal masking also severely affect speech perception. Proper perception of consonants requires adequate temporal resolution of subphonic segments like noise bursts and formant frequency transition. Further, in speech signals, vowels are generally more intense while the consonants carrying much of the information have lower intensities [47]. Therefore, there is a possibility of masking of consonantal segment by vowels. The loudness discomfort level is the level at which a tone becomes uncomfortably loud. The dynamic range is the difference between the loudness discomfort and hearing threshold levels. In case of sensorineural loss, the hearing threshold increases with no corresponding change in the discomfort levels and thus the dynamic range may get drastically reduced. This abnormal increase in perceived loudness with increase in sound level is known as recruitment. Increase in hearing threshold of one sound in the presence of another sound is known as 'masking'. Intense sound has a masking effect on preceding and following weak sound known as backward and forward masking respectively and this phenomena gets very severe in case of sensorineural impairment. Most forward and backward masking occurs within 100ms either at onset or ending of masking sound. The backward masking at most extends over 20ms before the masker. Both the masking effect exists due to temporal overlap of cochlear responses. Sensorineural loss is associated with widening of the auditory filter bandwidth and the

filter slope becomes shallower. Researchers have tried to understand the characteristics of sensorineural hearing loss in terms of the role of the hair cells in the transduction mechanism and role of auditory filters for presenting the information to the higher brain processes [48]. It has been reported that basilar membrane does exhibit sharp tuning curves for tone stimuli of different frequencies. The basilar membrane vibrations at a particular location produce synchronized activity in the auditory nerve fibers innervating the corresponding hair cells. Inner hair cells act as the transducer for vibrations. The outer hair cells control the sensitivity of the inner hair cells in such a way that it is high at low levels of vibrations and progressively decreases for higher levels of vibrations. They also play a role in sharpening the tuning curves of the basilar membrane. Damage to inner hair cells reduces their transduction sensitivity for basilar membrane vibrations [49]. Hearing thresholds get increased, but the loudness growth curve and the dynamic range do not get much affected. Frequency selectivity does not get very much degraded. Damage to the outer hair cells drastically impairs the active control role played by them. The sensitivity at low sound levels get reduced resulting in recruitment i.e. loudness growth curve becomes more linear and consequently dynamic range get very much reduced. Further, the tuning curves become much broader resulting in severe spectral masking and reduces frequency selectivity. Damage to the auditory nerve fiber alters the loudness growth curve depending on the damage pattern.

5.2 Binaural Dichotic Presentation

As stated earlier, sensorineural loss is associated with widening of the auditory filter bandwidths and reduced frequency selectivity at the peripheral auditory system. The peripheral auditory system behaves like a bank of bandpass filters called auditory filters or critical bands with overlapping passbands. A tuning curve resembles the magnitude response of a band pass filter with a rounded top and sloping edges [50]. The effective

bandwidth of these tuning curves are known as critical bands. The tuning curve shapes and critical band estimates are obtained by various researchers using different type of masker and experimental technique. The shapes of auditory filters are nearly symmetric at moderate sound level and they become asymmetric at high level with shallower slope on the low frequency side.

Most of the speech processing techniques for hearing aids involve monaural listening which refers to sound presentation to one ear only whereas binaural listening involves both the ears. Binaural listening offers overall sound quality, clear speech intelligibility and more relaxed listening and it helps in source localization. Binaural listening could be “diotic” with same signals presented to both the ears or it could be “dichotic” with different signals presented to the two ears. One of the possible ways of improving speech perception degraded due to loss of frequency selectivity caused by masking at the peripheral level would be to split the speech signal on the basis of its short time spectrum into two complimentary spectra for presentation to the two ears dichotically. The main objective of spectral splitting for dichotic presentation should be to enhance the perception of spectral contrast of resonance peaks without adversely affecting the perception of features cued by amplitude and duration. Considering the perception of formants to be really important, a speech processing system can be devised such that the alternate formants are presented to different ears and therefore do not contribute to masking of each other. The splitting of speech should be done in such a way that the two adjacent strong spectral components that are likely to mask each other get presented to different ears. Several schemes are employed for splitting speech for binaural dichotic presentation. Listening tests using synthesized vowels in which first formant is presented to one ear and the second to the other was carried out by [50]. Research on binaural dichotic presentation

has also been carried out earlier by [1], [6] and [51]. Binaural hearing aids which can split the speech signal on the basis of critical bands can be helpful to hearing impaired persons.

5.2.1 Review of Speech Processing Schemes

Many investigations of the frequency resolving capabilities of the auditory system have evolved out of the concept of the critical band that originated with the auditory masking studies conducted. The subdivision into critical bands seems to be correlated very closely to the cochlear mechanics and to frequency discrimination. Studies of critical bands in hearing impaired with direct measurements provide evidence of an enlarged critical band. Zwicker's critical band model [3] has been used by many researchers.

One of the earliest reported studies of splitting speech on the basis of frequency, a scheme for dichotic presentation to improve speech intelligibility in noise due to reduced frequency selectivity was evaluated by Lunner et. al. [1]. They tested the use of an 8-channel digital filter bank in monaural, diotic and dichotic modes. The filter bank was designed to give eight parallel filtered outputs, which are added together with individually adjustable weighting factors in order to obtain a proper fit of the gain frequency response of the hearing aid as per the need of the individual hearing aid user. The scheme used comb filters with constant bandwidth of 700Hz and 40dB stopband attenuation so as to present signal containing different frequency components to the two ears. By combining alternate bands together, the filter bank was used for dichotic presentation. The filter bank was realized using complementary interpolated linear phase FIR filters so that most of the coefficients were zero valued in order to minimize the number of arithmetic computations. The scheme was implemented in real time using a digital signal processor and a computer. The signal-sampling rate was 11.6k samples/s and signal processing delay was about 4 ms. The test material consisted of a list of ten five word sentences. The processing system was later rebuilt using a digital signal processor and incorporated as part of a pocket type

hearing aid. The listening tests were conducted under three conditions i.e. dichotic presentation of odd numbered bands to the one ear and even numbered bands to the other ear and diotic presentation in which all the bands are presented to both the ears. Three subjects in age group of 39 to 69 years with bilateral and moderate sensorineural hearing loss participated. The gain of the filters was adjusted depending on the hearing loss of individual subject. The scheme achieved spectral splitting but the filters did not have the sharp transition bands. The results indicated an overall improvement in speech perception for dichotic conditions. Although use of constant bandwidth filters can be exploited for very efficient realization, a single bandwidth value may not be optimal for reducing the effect of spectral masking over the entire frequency range of speech signal. Too wide a band will not resolve the lower formants for presentation to different ears. If the bandwidth is too narrow, the pitch harmonics under the same formant peak are likely to be presented to different ears resulting in reduced perception of spectral contrast. Narrow bandwidths are also likely to smear timing related cues.

Lyregaard [50] conducted experiments with three values of comb filter bandwidths of 200 Hz, 500 Hz and 800 Hz. However improvements in the speech recognition scores for the dichotic over the diotic presentation were not statistically significant. No improvement was found in speech intelligibility indicating that the lack of improvement was possibly due to unsuitable filtering, lack of subject's listening experience and lack of the binaural fusion of dichotic signals.

Chaudhari et. al. [6], [54] investigated a scheme for splitting the speech into two complementary spectra each with nine bands on the basis of critical bands for binaural dichotic presentation to lessen the effect of reduced auditory frequency selectivity and hence improve speech intelligibility. The reported scheme was aimed at reducing the effect of spectral masking due to loss of spectral resolution. This scheme used critical bands

corresponding to auditory filters based on psychophysical tuning curves as described by Zwicker [3]. Eighteen critical bands over 5 KHz frequency range were used. The critical bands formed the passbands of the FIR filters with linear phase response in order to maintain the timing related cues desirable to preserve the relative phases of the frequency components in speech signal. Initially, the scheme was implemented for off-line processing of digitized speech signals. The signal sampling rate was 10k samples/sec. For offline processing, the efficiency of filter realization is not critical. The listening tests were conducted under two conditions i.e. diotic presentation in which all the bands are presented to both the ears and dichotic presentation where alternate bands were presented to the left and right ear. The gains of the filter bands are adjustable as a way of partial matching of the filter response to the frequency characteristics of individual subject's hearing loss. The listening test were carried out on five normal hearing subjects with hearing loss simulated by mixing broadband noise as a masker. The listening tests in another experiment was conducted on ten subjects with bilateral sensorineural hearing loss. In offline processing, a cascade combination of nine FIR band reject filters each were used for the speech processing scheme. The scheme was implemented for real-time processing for use in a binaural hearing aid. Efficient realization for real time implementation is obtained by using two comb FIR filter with arbitrary frequency response for approximating the overall magnitude response coupled with linear phase for each channel. The filters used for real time speech processing were designed using frequency sampling method of FIR filter design. For analysis of speech signals, a spectrographic analysis package which can display the time-varying spectrum of speech was used. For ascertaining the improvement in the speech quality due to processing, a compilation of qualitative assessment by the subjects about the test stimuli under various listening conditions was carried out. The stimulus-response data was analyzed for obtaining recognition scores. The test stimuli consisted of

nonsense syllables formed with twelve English consonants /p, b, t, d, k, g, m, n, s, z, f, v/ with vowel /a/ in vowel consonant vowel VCV and consonant vowel CV contexts. These were used for studying the reception of consonantal features of duration, frication, nasality, manner, place and voicing. A computer based setup was developed for off-line processing, real-time processing, signal acquisition, analysis and automated administration of listening tests. The scheme was able to improve speech quality, response time, recognition scores and transmission of consonantal features particularly the place feature, indicating the usefulness of the scheme for better reception of the spectral characteristics. The scheme does not adversely affect the reception of other consonantal features.

5.3 Design of Novel Sharp Transition Multiband FIR Filter

5.3.1 Introduction

This section deals with the review of filters used for the speech processing schemes. For the speech processing schemes for critical band filtering in literature [1], [6], [55] linear phase FIR filters with symmetric impulse response were used. Thus degradation in speech quality due to non-linear phase response is avoided and hence the relative phases of the frequency components in speech signal are preserved so that the timing related cues are not affected [52]. One of the widely used method for designing FIR filters is the windowing technique in which impulse response of an ideal filter is truncated to a finite duration sequence using a suitable window function. The window function should reduce the filter transition overshoot and reduce the side lobes in the stopband. Another approach for design of FIR filter is the frequency sampling technique. In this technique the desired magnitude and phase responses are specified at uniformly spaced N frequency samples for filter order N and the finite impulse response is obtained by taking the IDFT of the

nonsense syllables formed with twelve English consonants /p, b, t, d, k, g, m, n, s, z, f, v/ with vowel /a/ in vowel consonant vowel VCV and consonant vowel CV contexts. These were used for studying the reception of consonantal features of duration, frication, nasality, manner, place and voicing. A computer based setup was developed for off-line processing, real-time processing, signal acquisition, analysis and automated administration of listening tests. The scheme was able to improve speech quality, response time, recognition scores and transmission of consonantal features particularly the place feature, indicating the usefulness of the scheme for better reception of the spectral characteristics. The scheme does not adversely affect the reception of other consonantal features.

5.3 Design of Novel Sharp Transition Multiband FIR Filter

5.3.1 Introduction

This section deals with the review of filters used for the speech processing schemes. For the speech processing schemes for critical band filtering in literature [1], [6], [55] linear phase FIR filters with symmetric impulse response were used. Thus degradation in speech quality due to non-linear phase response is avoided and hence the relative phases of the frequency components in speech signal are preserved so that the timing related cues are not affected [52]. One of the widely used method for designing FIR filters is the windowing technique in which impulse response of an ideal filter is truncated to a finite duration sequence using a suitable window function. The window function should reduce the filter transition overshoot and reduce the side lobes in the stopband. Another approach for design of FIR filter is the frequency sampling technique. In this technique the desired magnitude and phase responses are specified at uniformly spaced N frequency samples for filter order N and the finite impulse response is obtained by taking the IDFT of the

frequency response. The frequency response is recalculated with a finer resolution and is compared with the desired response.

Chaudhari [54] for off-line processing of speech signals used two filter banks each with parallel combination of nine band pass filters with different gains. In this approach, there is a possibility of notches in the magnitude at crossover frequencies due to phase shifts in the adjacent filters, hence cascade combination of band reject filters were used. All the filters are linear phase FIR filters with 255 coefficients. The filter coefficients were obtained from the sampled magnitude response using rectangular window [53]. The FIR filters had transition bandwidths of 55 Hz with pass-band ripple of 2dB and stopband attenuation of 40 dB with each filter of 256 coefficients [54]. Rectangular window and filters of such a high order was selected in order to obtain sharp cut-off so that there is no significant overlap from the neighboring bands. For real time processing comb filter are used with passbands based on critical bands using frequency sampling FIR design method which laid emphasis on flat magnitude response in the passbands, sharp transition and linear phase response [55],[54].

In another similar binaural dichotic scheme with FIR comb filter designed using frequency sampling design method with linear optimization techniques [55], the filter transitions were kept the sharpest possible at 78 to 117 Hz for various bands which resulted in maximum pass-band ripple of 1dB and stopband attenuation of 38 dB with filters each of 256 coefficients. The signal sampling rate was 10k samples/sec.

Recently, a novel analytical method for the design of equiripple optimal comb FIR filters is presented [18]. The design algorithm provides a simple and robust tool for the evaluation of highly selective optimal equiripple comb FIR filters. Independent control is possible over number of notch bands, width of notch bands and passband attenuation. A digital cochlear filter [56],[57]^[54], which is an electronic model of cochlea was implemented

frequency response. The frequency response is recalculated with a finer resolution and is compared with the desired response.

Chaudhari [54] for off-line processing of speech signals used two filter banks each with parallel combination of nine band pass filters with different gains. In this approach, there is a possibility of notches in the magnitude at crossover frequencies due to phase shifts in the adjacent filters, hence cascade combination of band reject filters were used. All the filters are linear phase FIR filters with 255 coefficients. The filter coefficients were obtained from the sampled magnitude response using rectangular window [53]. The FIR filters had transition bandwidths of 55 Hz with pass-band ripple of 2dB and stopband attenuation of 40 dB with each filter of 256 coefficients [54]. Rectangular window and filters of such a high order was selected in order to obtain sharp cut-off so that there is no significant overlap from the neighboring bands. For real time processing comb filter are used with passbands based on critical bands using frequency sampling FIR design method which laid emphasis on flat magnitude response in the passbands, sharp transition and linear phase response [55],[54].

In another similar binaural dichotic scheme with FIR comb filter designed using frequency sampling design method with linear optimization techniques [55], the filter transitions were kept the sharpest possible at 78 to 117 Hz for various bands which resulted in maximum pass-band ripple of 1dB and stopband attenuation of 38 dB with filters each of 256 coefficients. The signal sampling rate was 10k samples/sec.

Recently, a novel analytical method for the design of equiripple optimal comb FIR filters is presented [18]. The design algorithm provides a simple and robust tool for the evaluation of highly selective optimal equiripple comb FIR filters. Independent control is possible over number of notch bands, width of notch bands and passband attenuation. A digital cochlear filter [56],[57],^[64] which is an electronic model of cochlea was implemented

and tested using IIR filters with a field programmable gate array. It gives a good fit to the cochlear data with efficiency of filter hardware usage.

For implementing the speech processing scheme as part of a binaural hearing aid, the factors like power consumption, FIR filter circuit complexity etc. are to be taken into consideration. Also a need was felt for better FIR filter design techniques to develop FIR filters with less passband ripple, good stopband attenuation and sharp transition and to vary the filter specification without the need of separate design [51]. The present work deals with the design of two FIR multiband filters with linear phase response to be employed in a speech processing scheme for splitting speech into two complementary short-time spectra signals. The filter passbands correspond to auditory filters as per Zwicker model to reduce the effect of spectral masking in sensorineural hearing impaired and hence increase speech intelligibility.

Filters having finite crossovers in magnitude response, the spectral components lying in the transition region are presented to both ears. With sharp transition band of filters, there is reduced possibility of spectral components presented to both ears at the transition region. Hence imbalance in loudness perceived at the crossovers between adjacent bands will reduce which increases speech intelligibility [55].

5.3.2 Multiband Filter Model and Design

In this section, the formulation of a linear phase, sharp transition, multiband FIR filter model with equiripple response, linear transition and variable density of ripple cycles in different regions of the filter is proposed. This design allows arbitrary center frequency and passband width without need of separate design. Filter model is such that large density of ripples is introduced in the regions where discontinuities are present to increase the sharpness of the transition and a non-ideal frequency response modeled without any abrupt discontinuities is used to reduce Gibb's phenomenon.

The magnitude response $H_{pm}(\omega)$ of the multiband filter model is as shown in Fig.5.3. Index n refers to various bands which are nine in our application i.e. $n=1, 2, \dots, 9$ where BP_n is the n^{th} band pass component of the multiband filter. In the proposed multiband filter model, the various regions of the filter response are modeled using simple trigonometric functions of frequency as before.

In the stopband region BR_{n-1} preceding the bandpass section BP_n from $\omega_{s, n-1} \leq \omega \leq \omega_{s2, n-1}$

$$H_{pm}(\omega) = \frac{\delta_s}{2} \cos k_{p2}(\omega - \omega_{s, n-1}), \quad \omega_{s, n-1} \leq \omega \leq \omega_{s2, n-1} \quad (5.1)$$

where ω is the frequency variable, $H_{pm}(\omega)$ is the pseudo-magnitude of the bandpass filter response, δ_p is passband ripple, $\omega_{s, n-1}$ is the center frequency of the stopband preceding passband of bandpass response BP_n , k_{p2} is the filter design parameter and $\omega_{s2, n-1}$ the frequency at which second stopband region (preceding the passband) starts, ω_{bn} is the center frequency of the bandpass section BP_n and ω_{pn} is half passband width of BP_n and $H_{pm}(\omega_{bn} \pm \omega_{pn}) = 1$.

In the stopband region from $\omega_{s2, n-1} \leq \omega \leq (\omega_{bn} - \omega_{zn})$ the frequency response is

$$H_{pm}(\omega) = \frac{\delta_s}{2} \cos k_p(\omega - \omega_{s2, n-1}), \quad \omega_{s2, n-1} \leq \omega \leq (\omega_{bn} - \omega_{zn}) \quad (5.2)$$

where, $(\omega_{bn} \pm \omega_{zn})$ is the frequency at which magnitude response is zero, ω_{bn} is the center frequency of passband BP_n and k_p is the filter design parameter.

In the transition region from $(\omega_{bn} - \omega_{zn}) \leq \omega \leq (\omega_{bn} - \omega_{pn})$ the frequency response is

$$H_{pm}(\omega) = \frac{1}{(\omega_{zn} - \omega_{pn})} \left[\omega - (\omega_{bn} - \omega_{zn}) \right], \quad (\omega_{bn} - \omega_{zn}) \leq \omega \leq (\omega_{bn} - \omega_{pn}) \quad (5.3)$$

where $(\omega_{bn} \pm \omega_{pn})$ are passband edge frequencies.

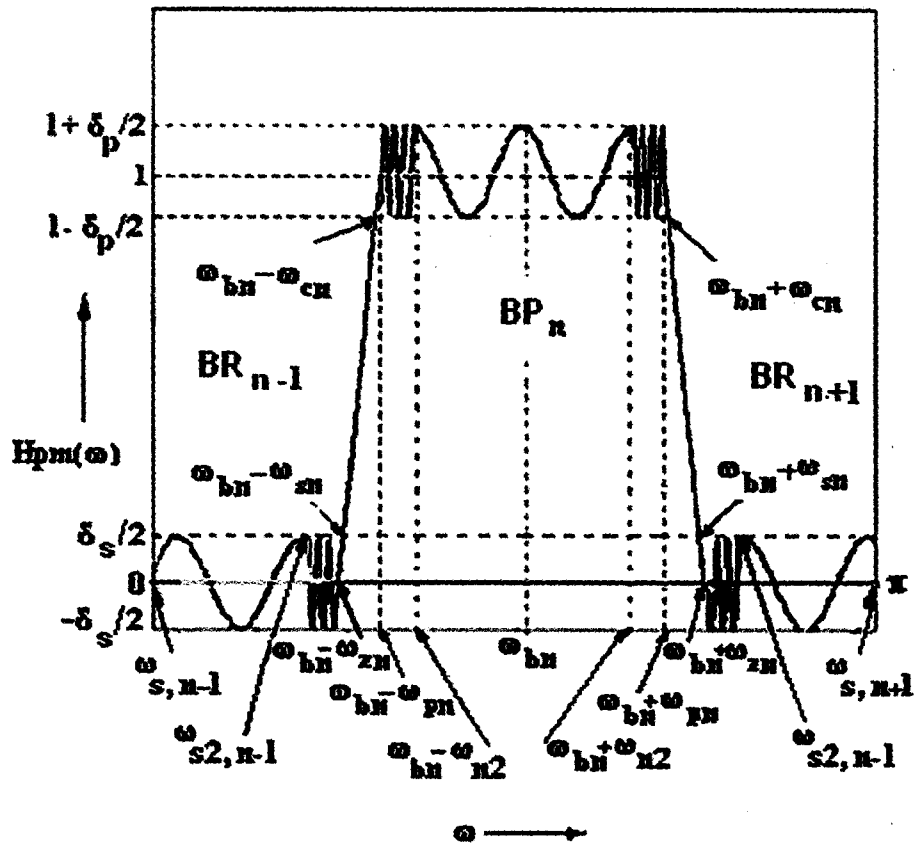


Fig. 5.3. Illustration of proposed Multiband filter (n^{th} band shown) for speech processing scheme with equiripple magnitude response, linear transition and variable density ripple cycles.

In the passband region $(\omega_{bn} - \omega_{pn}) \leq \omega \leq (\omega_{bn} - \omega_{n2})$ the frequency response is

$$H_{pm}(\omega) = 1 + \frac{\delta_p}{2} \text{sinc}_p \left[\omega - (\omega_{bn} - \omega_{pn}) \right], \quad (\omega_{bn} - \omega_{pn}) \leq \omega \leq (\omega_{bn} - \omega_{n2}) \quad (5.4)$$

where $(\omega_{bn} - \omega_{n2})$ is the frequency at which second passband region starts.

In the passband region from $(\omega_{bn} - \omega_{n2}) \leq \omega \leq (\omega_{bn} + \omega_{n2})$ the frequency response is

$$H_{pm}(\omega) = 1 + \frac{\delta_p}{2} \text{cosk}_{p1} \left[\omega - (\omega_{bn} - \omega_{n2}) \right], \quad (\omega_{bn} - \omega_{n2}) \leq \omega \leq (\omega_{bn} + \omega_{n2}) \quad (5.5)$$

where $(\omega_{bn} + \omega_{n2})$ is the frequency at which third passband region starts and k_{p1} is the filter design parameter.

In the passband region from $(\omega_{bn} + \omega_{n2}) \leq \omega \leq (\omega_{bn} + \omega_{pn})$ the frequency response is

$$H_{pm}(\omega) = 1 + \frac{\delta_p}{2} \text{cosk}_p \left[\omega - (\omega_{bn} + \omega_{n2}) \right], \quad (\omega_{bn} + \omega_{n2}) \leq \omega \leq (\omega_{bn} + \omega_{pn}) \quad (5.6)$$

In the transition region $(\omega_{bn} + \omega_{pn}) \leq \omega \leq (\omega_{bn} + \omega_{zn})$ from the frequency response is

$$H_{pm}(\omega) = 1 - \frac{1}{(\omega_{zn} - \omega_{pn})} \left[\omega - (\omega_{bn} + \omega_{pn}) \right], \quad (\omega_{bn} + \omega_{pn}) \leq \omega \leq (\omega_{bn} + \omega_{zn}) \quad (5.7)$$

In the stopband region from $(\omega_{bn} + \omega_{zn}) \leq \omega \leq \omega_{s2, n+1}$ the frequency response is

$$H_{pm}(\omega) = -\frac{\delta_s}{2} \text{sinc}_p \left[\omega - (\omega_{bn} + \omega_{zn}) \right], \quad (\omega_{bn} + \omega_{zn}) \leq \omega \leq \omega_{s2, n+1} \quad (5.8)$$

where δ_s is the stopband attenuation, $\omega_{s2, n+1}$ the frequency at which third region of the stopband starts (succeeding the passband).

In the stopband region from $\omega_{s2, n+1} \leq \omega \leq \omega_{s, n+1}$ the frequency response is

$$H_{pm}(\omega) = \frac{\delta_s}{2} \text{sinc}_{p3} (\omega - \omega_{s2, n+1}), \quad \omega_{s2, n+1} \leq \omega \leq \omega_{s, n+1} \quad (5.9)$$

$\omega_{s,n+1}$ is the center frequency of the stopband succeeding the band BP_n and k_{p3} is a filter design parameter.

In the multiband filter design, in the formulation and design of n^{th} component bandpass filter section the magnitude response has three regions in the passband BP_n and possesses a total of $(n+1/2)$ cycles of ripple in the entire passband. In the proposed model, the first region possesses $(m+1/4)$ cycles of ripple where m is an integer and ranges from $(\omega_{bn} - \omega_{pn})$ to $(\omega_{bn} - \omega_{n2})$. It is characterized by the filter design parameter k_p . The third region possesses $(m+1/4)$ cycles of ripple and this region is in the frequency range from $(\omega_{bn} + \omega_{n2})$ to $(\omega_{bn} + \omega_{pn})$. It is characterized also by filter design parameter k_p . The second region possess $(n-2m)$ cycles of ripples (n is even for symmetry) and spans the frequency range from $(\omega_{bn} - \omega_{n2})$ to $(\omega_{bn} + \omega_{n2})$. This region is characterized by the filter design parameter k_{p1} .

$$\text{Therefore, for multiband design we have, } \omega_{n2} = \left(\frac{n}{2} - m\right) \frac{2\pi}{k_{p1}}, \quad (5.10)$$

$$\text{From (5.10), } k_{p1} = \left(\frac{n}{2} - m\right) \frac{2\pi}{\omega_{n2}} \quad (5.11)$$

$$\text{Also, } \omega_{n2} = \omega_{pn} - \left(m + \frac{1}{4}\right) \frac{2\pi}{k_p} \quad (5.12)$$

The stopband regions BR_{n-1} preceding BP_n and possesses a total of $(n0+3/4)$ cycles of ripple in the frequency range of $\omega_{s,n-1}$ to $(\omega_{bn} - \omega_{zn})$. The first region possesses $(n0-p)$ cycles of ripple where m is an integer, in the frequency range from $\omega_{s,n-1}$ to $\omega_{s2,n-1}$ characterized by k_{p2} . The second region possesses $(p+3/4)$ cycles of ripple in the frequency range from $\omega_{s2,n-1}$ to $(\omega_{bn} - \omega_{zn})$ characterized by k_p .

Therefore, $(\omega_{bn} - \omega_{zn}) - \omega_{s, n-1} = \left(p + \frac{3}{4}\right) \frac{2\pi}{k_p} + (n_0 - p) \frac{2\pi}{k_{p2}}$ (5.13)

Also, $\omega_{s2, n-1} = \omega_{s, n-1} + (n_0 - p) \frac{2\pi}{k_{p2}}$ (5.14)

using (5.13) in (5.14) we obtain,

$$\omega_{s2, n-1} = (\omega_{bn} - \omega_{zn}) - \left(p + \frac{3}{4}\right) \frac{2\pi}{k_p} \quad (5.15)$$

The parameter k_{p2} can be computed from (5.13) for any specified value of p and n_0 . The bandpass filter has stopband region BR_{n+1} succeeding BP_n and possesses a total of $(n_2 + 3/4)$ cycles of ripple in the frequency range of $(\omega_{bn} + \omega_{zn})$ to $\omega_{s, n+1}$ which is split up into two regions characterized by parameters k_p and k_{p3} respectively.

The first region possesses $(q + 3/4)$ cycles of ripple from $(\omega_{on} + \omega_{zn})$ to $\omega_{s2, n+1}$ characterized by k_p and q is any integer. The second region possesses $(n_2 - q)$ cycles of ripple where m is an integer from $\omega_{s2, n+1}$ to $\omega_{s, n+1}$ characterized by k_{p3} .

$$\omega_{s, n+1} - (\omega_{on} + \omega_{zn}) = \left(q + \frac{3}{4}\right) \frac{2\pi}{k_p} + (n_2 - q) \frac{2\pi}{k_{p3}} \quad (5.16)$$

k_{p3} can be computed from (5.16) for specified values of q and k_p .

Using k_{p3} we obtain,

$$\omega_{s2, n+1} = (\omega_{on} + \omega_{zn}) + \left(q + \frac{3}{4}\right) \frac{2\pi}{k_p} \quad (5.17)$$

For the multiband filter model we have from (5.3),

$$\text{at } \omega = (\omega_{bn} - \omega_{cn}), H_{pm}(\omega) = \left[1 - \frac{\delta_p}{2} \right] = \left[\frac{(\omega_{zn} - \omega_{cn})}{(\omega_{zn} - \omega_{pn})} \right] \quad (5.18)$$

$$\text{Simplifying, } \omega_{cn} = \frac{\delta_p}{2}(\omega_{zn} - \omega_{pn}) + \omega_{pn} \quad (5.19)$$

From (5.3) we also have,

$$\text{At } \omega = (\omega_{bn} - \omega_{sn}), H_{pm}(\omega) = \frac{\delta_s}{2} = \frac{(\omega_{zn} - \omega_{sn})}{(\omega_{zn} - \omega_{pn})} \quad (5.20)$$

$$\text{Simplifying, } \omega_{sn} = \omega_{zn} - (\delta_s / 2)(\omega_{zn} - \omega_{pn}) \quad (5.21)$$

Using (5.19) and (5.21) we obtain

$$(\omega_{sn} - \omega_{cn}) = (\omega_{zn} - \omega_{pn}) \left(1 - \frac{\delta_s + \delta_p}{2} \right) \quad (5.22)$$

5.3.3 Slope Equalization

For the multiband design, the slope equalization technique applied to bandpass filters of section 3.3.1 holds good because each bandpass section of the multiband filter is designed using the same technique. It can be shown using (3.39) that slope of the frequency response at $\omega_{bn} \pm \omega_{pn}$ all the bands of the multiband filter is

$$-\frac{k_p \delta_p}{2} \quad (5.23)$$

Similarly, slope in the transition regions of all component bands of the multiband filter

$$\text{obtained using (3.40), i.e. slope at } \omega_{bn} \pm \omega_{zn} = \pm \left(-\frac{1}{(\omega_{zn} - \omega_{pn})} \right) \quad (5.24)$$

Equating the slopes at $(\omega_{bn} + \omega_{pn})$ and $(\omega_{bn} + \omega_{zn})$ using (5.23) and (5.24) we obtain,

$$k_p = \frac{2}{\delta_p(\omega_{zn} - \omega_{pn})} \quad (5.25)$$

Also, substituting (5.22) in (5.25) we get,

$$k_p = \frac{2 \left[1 - \left(\frac{\delta_s + \delta_p}{2} \right) \right]}{\delta_p (\omega_{sn} - \omega_{cn})} \quad (5.26)$$

Note that equalization of slopes leads to $\delta_s = \delta_p$.

5.3.4 Expressions for Impulse Response Coefficients

Referring to filter design theory of section 2.4, the impulse response coefficients $h(n)$ for the lowpass filter are obtained by evaluating the integrals below to obtain the expressions for the impulse response coefficients $h(n)$ for the multiband filter. Thus,

$$h(n) = \frac{1}{\pi} \left[\int_0^{\pi} H_{pm}(\omega) \cos k\omega \, d\omega \right] \quad (5.27)$$

$$\begin{aligned} h(n) = \frac{1}{\pi} & \left[\int_{\omega_{s,n-1}}^{\omega_{s2,n-1}} H_{pm}(\omega) \cos k\omega \, d\omega + \int_{\omega_{s2,n-1}}^{\omega_{on}-\omega_{zn}} H_{pm}(\omega) \cos k\omega \, d\omega + \int_{\omega_{on}-\omega_{zn}}^{\omega_{on}-\omega_{pn}} H_{pm}(\omega) \cos k\omega \, d\omega \right. \\ & + \int_{\omega_{on}-\omega_{pn}}^{\omega_{on}-\omega_{n2}} H_{pm}(\omega) \cos k\omega \, d\omega + \int_{\omega_{on}-\omega_{n2}}^{\omega_{on}+\omega_{n2}} H_{pm}(\omega) \cos k\omega \, d\omega + \int_{\omega_{on}+\omega_{n2}}^{\omega_{on}+\omega_{pn}} H_{pm}(\omega) \cos k\omega \, d\omega \\ & \left. + \int_{\omega_{on}+\omega_{pn}}^{\omega_{on}+\omega_{zn}} H_{pm}(\omega) \cos k\omega \, d\omega + \int_{\omega_{on}+\omega_{zn}}^{\omega_{s2,n+1}} H_{pm}(\omega) \cos k\omega \, d\omega + \int_{\omega_{s2,n+1}}^{\omega_{s,n+1}} H_{pm}(\omega) \cos k\omega \, d\omega \right] \quad (5.28) \end{aligned}$$

$$\begin{aligned} h(n) = \frac{1}{\pi} & \left[\int_{\omega_{s,n-1}}^{\omega_{s2,n-1}} \frac{\delta_s}{2} \cos k_{p2}(\omega - \omega_{s,n-1}) \cos k\omega \, d\omega + \int_{\omega_{s2,n-1}}^{(\omega_{bn}-\omega_{zn})} \frac{\delta_s}{2} \cos k_p(\omega - \omega_{s2,n-1}) \cos k\omega \, d\omega \right. \\ & + \int_{\omega_{bn}-\omega_{zn}}^{\omega_{bn}-\omega_{pn}} \left[\frac{1}{\Delta\omega} \left[\omega - (\omega_{bn} - \omega_{zn}) \right] \right] \cos k\omega \, d\omega \\ & + \int_{\omega_{bn}-\omega_{pn}}^{\omega_{bn}-\omega_{n2}} \left[1 + \frac{\delta_p}{2} \sin \left[k_p \left(\omega - (\omega_{bn} - \omega_{pn}) \right) \right] \right] \cos k\omega \, d\omega \\ & + \int_{\omega_{bn}-\omega_{n2}}^{\omega_{bn}+\omega_{n2}} \left[1 + \frac{\delta_p}{2} \cos \left[k_{p1} \left(\omega - (\omega_{bn} - \omega_{n2}) \right) \right] \right] \cos k\omega \, d\omega \\ & \left. + \int_{\omega_{bn}+\omega_{n2}}^{\omega_{bn}+\omega_{pn}} \left[1 + \frac{\delta_p}{2} \cos \left[k_p \left(\omega - (\omega_{bn} + \omega_{n2}) \right) \right] \right] \cos k\omega \, d\omega \right] \end{aligned}$$

$$\begin{aligned}
& + \int_{\omega_{bn} + \omega_{pn}}^{\omega_{bn} + \omega_{zn}} 1 - \left[\frac{1}{\Delta\omega} (\omega - (\omega_{bn} + \omega_{pn})) \right] \cos k\omega \, d\omega \\
& + \int_{\omega_{bn} + \omega_{zn}}^{\omega_{s2,n+1}} \left[-\frac{\delta_s}{2} \text{sinc}_p (\omega - (\omega_{bn} + \omega_{zn})) \right] \cos k\omega \, d\omega \\
& + \int_{\omega_{s2,n+1}}^{\omega_{s,n+1}} \left[\frac{\delta_s}{2} \text{sinc}_{p3} (\omega - \omega_{s2,n+1}) \right] \cos k\omega \, d\omega \quad (5.29)
\end{aligned}$$

where

$$\Delta\omega = (\omega_{zn} - \omega_{pn}) \text{ and } \delta_s = \delta_p$$

$$n=0,1,\dots,\frac{N-1}{2} \text{ for } N \text{ odd,}$$

$$n=0,1,2,\dots,\frac{N}{2}-1 \text{ for } N \text{ even and } k = \frac{(N-1)}{2} - n.$$

Evaluating (5.29), the expressions obtained for the impulse response coefficients $h(n)$ for the bandpass filter are

$$\begin{aligned}
h(n) = & \frac{k\delta_s [\text{sinc}\omega_{s,n-1} - \text{sinc}\omega_{s2,n-1}]}{2\pi(k_{p2}^2 - k^2)} + \frac{k\delta_s [\text{sinc}\omega_{s2,n+1} - \text{sinc}\omega_{s,n+1}]}{2\pi(k_{p3}^2 - k^2)} - \frac{k\delta_p [2\cos k\omega_{bn} \text{sinc}\omega_{n2}]}{2\pi(k_{p1}^2 - k^2)} \\
& + \frac{2\cos k\omega_{bn} (\cos k\omega_{pn} - \cos k\omega_{zn})}{\pi k^2 (\omega_{zn} - \omega_{pn})} + \frac{\delta_p \text{sinc}\omega_{bn} (k\cos k\omega_{n2} - k_p \text{sinc}\omega_{pn})}{\pi(k_p^2 - k^2)} \\
& + \frac{\delta_s (k\text{sinc}\omega_{s2,n-1} - 2k_p \cos k\omega_{bn} \cos k\omega_{zn} - k\text{sinc}\omega_{s2,n+1})}{2\pi(k_p^2 - k^2)} \quad (5.30)
\end{aligned}$$

Eq. (5.30) is valid for N even where k is a non-integer, for N odd (5.30) is valid except for $k = 0$.

For N odd, $k = 0$,

$$h\left(\frac{N-1}{2}\right) = \left(\frac{\omega_{zn} + \omega_{pn}}{\pi}\right) \quad (5.31)$$

5.3.5 Filter Synthesis Results and Discussions

Design Example: Two multiband linear phase, sharp transition FIR filters are designed each for the following desired specifications using the proposed multiband filter design approach.

Number of passbands: Nine

Passband-width: As per Zwicker's model in Table A5.1.

Transition bandwidth (constant for all bands) is 35Hz

$$\text{i.e. } 2 \times 35 / 11025 = 0.0063 \text{ (normalized).}$$

Maximum passband ripple (for all bands) is ± 0.15 dB

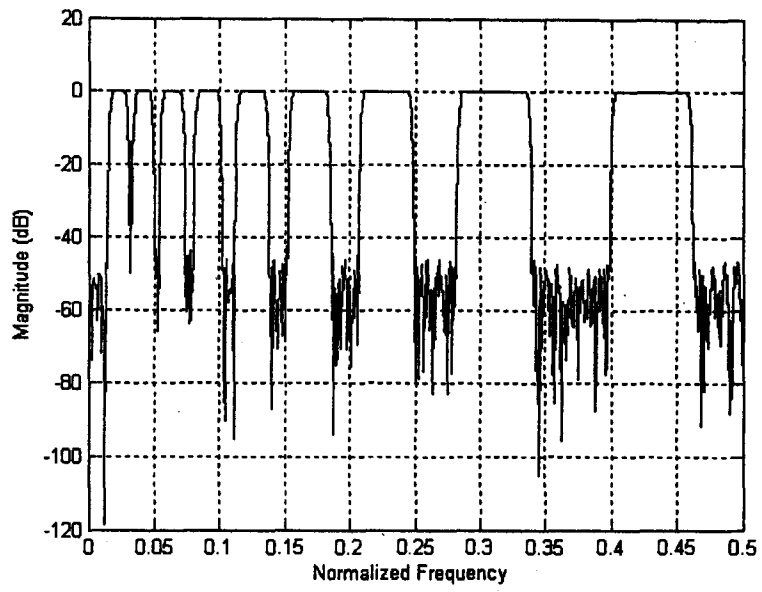
Minimum stopband attenuation (for all bands) is 40dB

Sampling Frequency is 11025 Hz

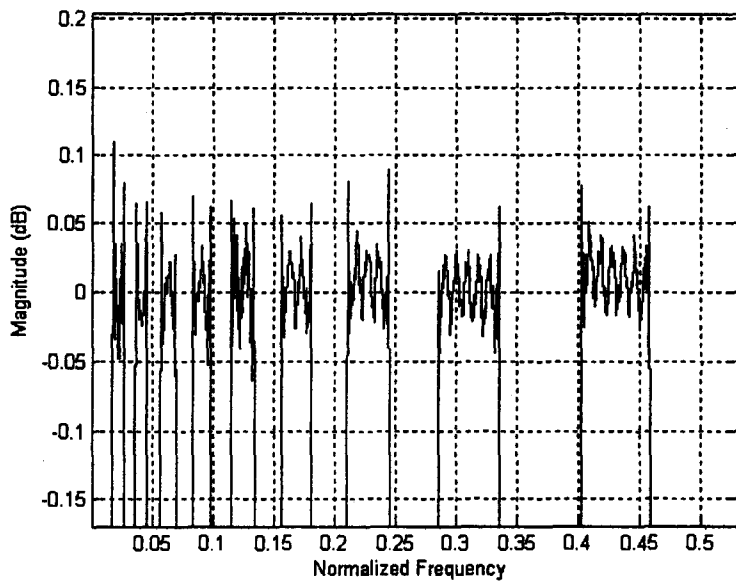
The filter was designed using MATLAB with program MML and measurements of various performance specifications of the designed filter done using MATLAB's Signal Processing Toolbox. Results approximate the desired multiband filter specifications closely. For the two multiband filters, the eighteen desired passbands are obtained as per specifications. The passband ripple for each band does not exceed 0.15dB, stopband attenuation for each band is more than 40dB and the transition bandwidth of each band is 35 Hz (normalized 0.0063) for a sampling frequency is 11025 Hz obtained with a low filter order of 1025. For the multiband filters designed for the speech processing scheme the magnitude, phase and impulse response are shown in Fig.5.4 and Fig.5.5. Filter synthesis and design steps are given in Appendix A 6.1.8.

Multiband filters designed using our approach have linear phase, sharp transition, least passband ripple and good stopband attenuation with low arithmetic complexity to avoid distortion of processed speech fed to the impaired ears. The performance of our proposed multiband filters are superior compared to the most efficient filters used for the

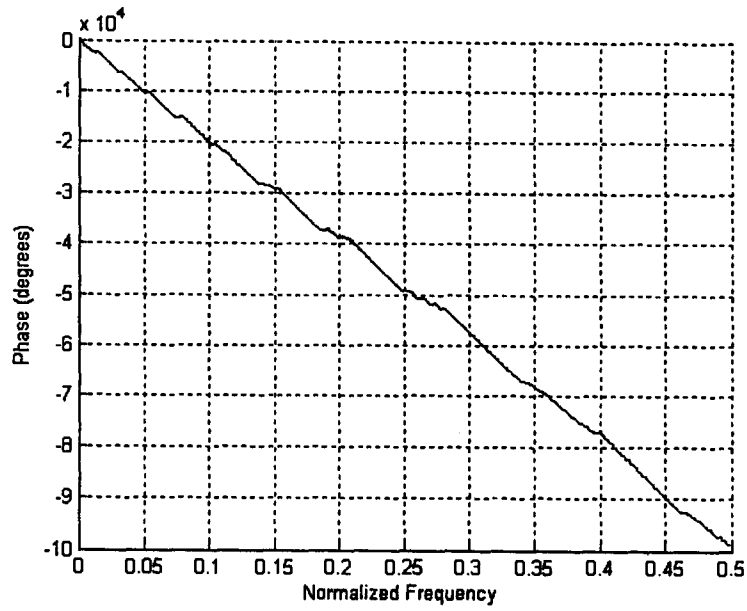
same speech processing scheme. These filters [55] are comb filters with transition bandwidth of 70 Hz to 120 Hz, stopband attenuation of 38 dB and passband ripple of 1 dB with a sampling frequency is 10 KHz. The transition width, passband ripple, stopband attenuation, center frequency and passband width can be easily varied in our multiband filter design. The proposed multiband filter design yields closed form expression for impulse response coefficients.



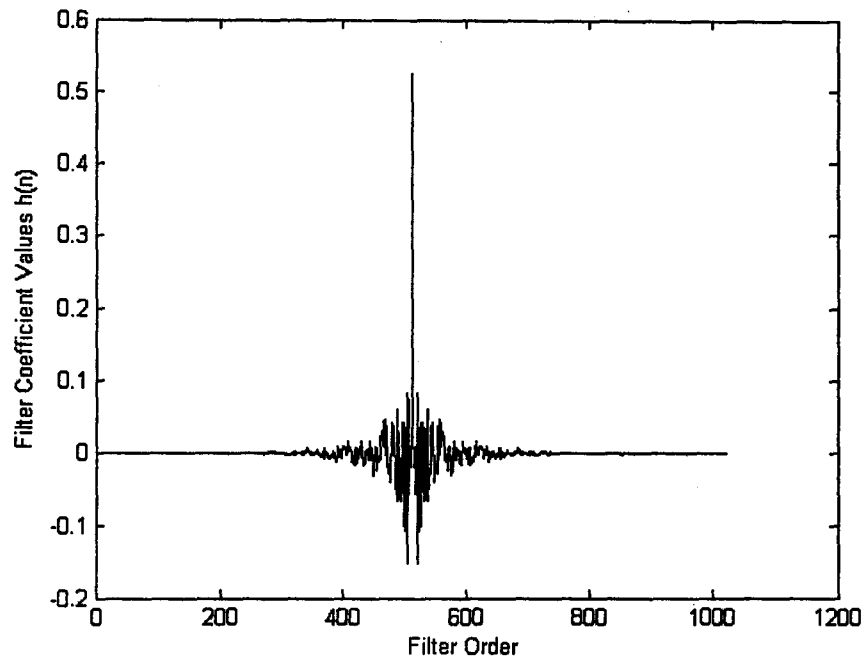
(a)



(b)

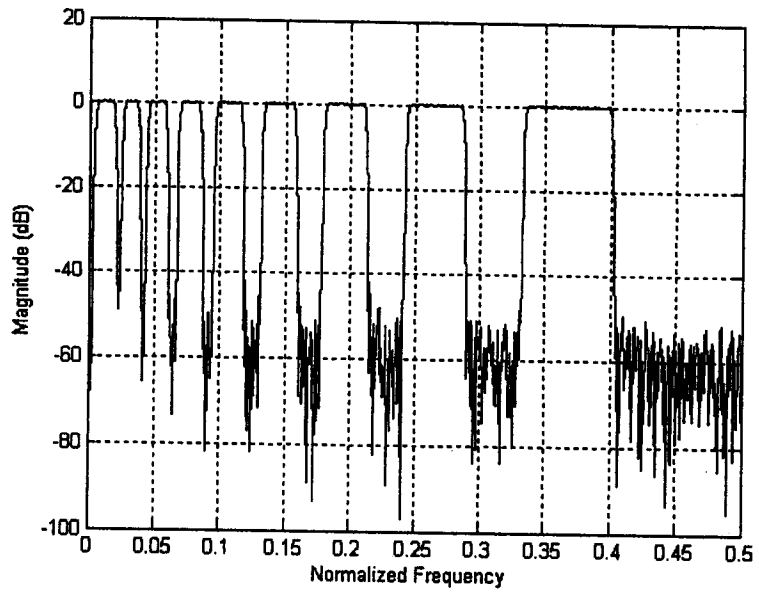


(c)

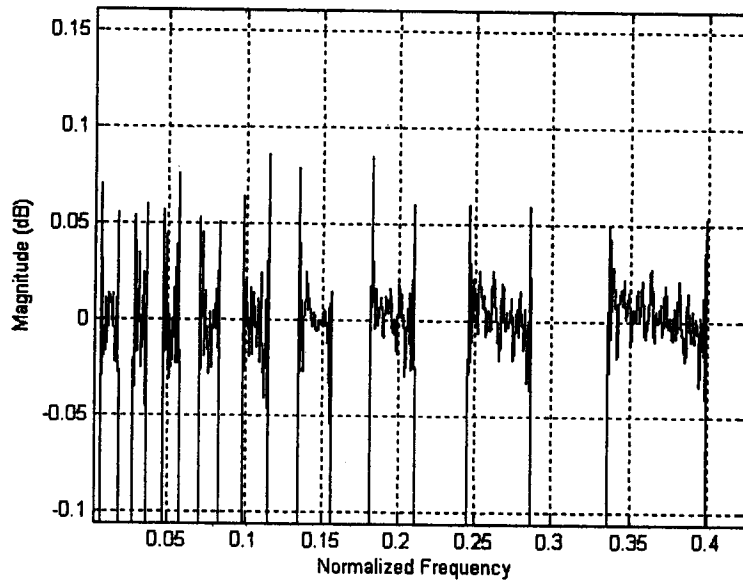


(d)

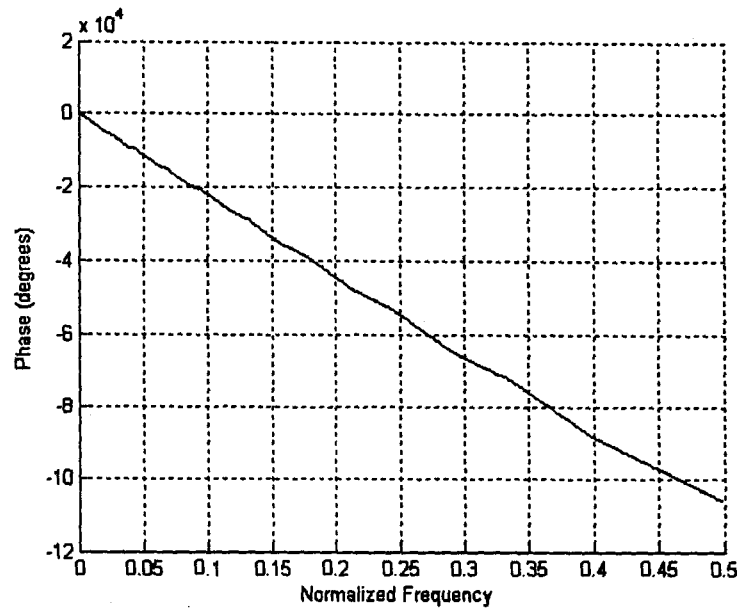
Fig. 5.4. (a) Magnitude response of the proposed multiband filter used in speech processing scheme (b) Magnified view of the passband (dB) (c) Phase response (d) Impulse response sequence.



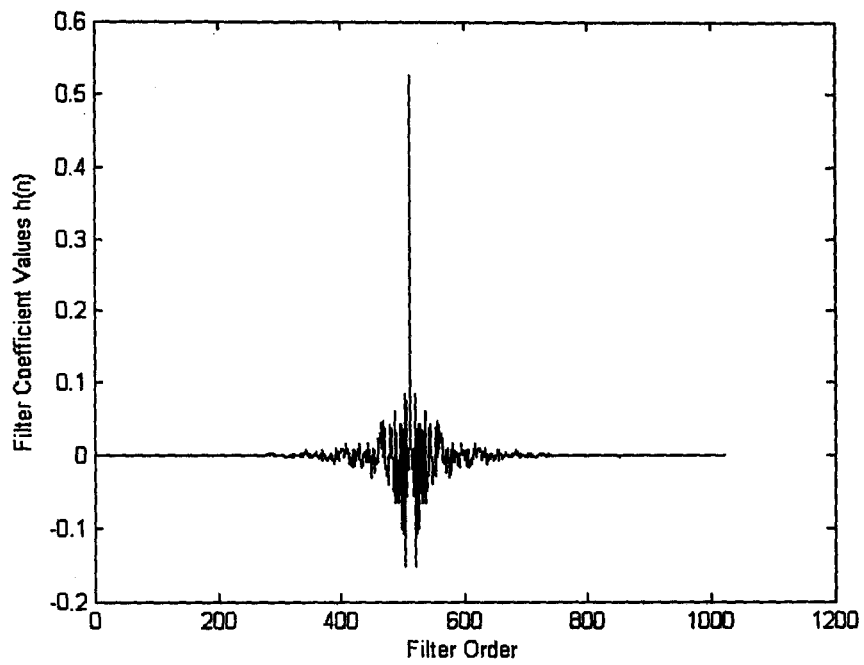
(a)



(b)



(c)



(d)

Fig. 5.5. (a) Magnitude response of the proposed complementary multiband filter used in speech processing scheme (b) Magnified view of the passband (c) Phase response (d) Impulse response sequence.

5.4 Conclusions

The proposed multiband filters possess large stopband attenuation which aids in better band separation, sharp transition that leads to proper separation of formants to be fed to the ears and low passband ripple that prevents deterioration of processed speech quality. All these features when combined lead to improvement in speech recognition for bilateral hearing impaired as observed in an experimental study conducted. It indicates that the processing scheme reduces the effect of spectral masking at the cochlear level.

Earlier schemes used conventional methods for design of FIR filters with filters in parallel, cascade and comb filters [55] were used. The use of the proposed multiband filters in the speech processing scheme leads to large savings in arithmetic hardware over conventional FIR filters and hence suitable for VLSI implementation in a digital hearing aid. The processed speech sample spectrographic analysis showed that the formants of most of the syllables were presented dichotically thus aided in higher speech intelligibility and verifies the usefulness of the scheme [58]. Listening tests were carried out on five sensorineural hearing impaired subjects and statements made by the subjects are recorded[59]. Subjects reported that there is an improvement in quality of speech after processing and they preferred the processed binaural dichotic presentation to unprocessed diotic presentation. For all the subjects the recognition scores for processed speech were higher than those for unprocessed speech.

Chapter 6

CONCLUSIONS AND FUTURE WORK

6.1 Conclusions

Various lowpass, linear phase, sharp transition FIR digital filter models are formulated and their designs implemented with least passband ripple, good stopband attenuation with least filter order. Various regions of the filter response in frequency domain are approximated using trigonometric functions of frequency making it convenient to evaluate the impulse response coefficients in closed form.

The filter models proposed lay stress on achieving a sharp transition. Sharper the transition more oscillatory will be the frequency response near the edge of the passband, a trait described as Gibb's phenomenon. The filter models proposed achieve a tradeoff between the transition bandwidth and the Gibb's phenomenon. In addition, emphasis is laid upon a low passband ripple and large stopband attenuation. Thus a three fold compromise for the satisfactory performance in all the three bands namely passband, transition and stopband is essential in addition to a trade off between Gibb's phenomenon and sharpness of transition of the filter.

A novel technique is devised to reduce Gibb's phenomenon in FIR filters. Equations are derived for slopes of the frequency response of the filters at the edges of the transition region and these slopes are matched. The filter design parameters of the model are evaluated by equalizing the slopes of the pseudo-magnitude response function at both the ends of the transition region. It is found that equalizing the slopes at the edges of the transition region makes the proposed pseudo-magnitude of frequency response continuous between a pair of adjoining regions that bridge the transition region defined by the model equations. This reduces the effects due to Gibb's phenomenon, thereby reducing ripples at

the edges of the transition region of the filter and hence reduces passband ripple and improves stopband attenuation of the filter.

The first model namely, Class I FIR filter with nonmonotonic passband has maximum passband attenuation at the extremities of the passband and a negative excursion that is maximum at the extremity of the stopband to obtain a sharp transition. All the three regions of the response are formulated in terms of sinusoidal function to achieve twin objectives of reducing Gibbs phenomenon and evaluating the closed form expression for the impulse response coefficients. The three filter design parameters k_p , k_t and k_s are evaluated with the above stated objectives in mind. The class II filter proposed has a monotonic passband and reduced number of parameters and its stopband is also monotonic. The class III filter model proposed next with and without slope equalization has equiripple passband and stopbands. Two additional parameters A and ω_0 are also incorporated in the model so as to enable the bridging of passband and stopband by the sinusoidal function proposed for the transition region. This filter achieves a better filter performance than its predecessors. This model is refined further by applying slope equalization technique which avoids a discontinuity at the edges of the passband and stopband thus reducing the effects of Gibbs phenomenon and improving the filter performance. The class IV filter model has equiripple passband and stopband and in addition it introduces a linear transition region. The synthesis of this filter is greatly simplified with fewer parameters and reduces the complexity of the design compared to Class III filter. Slope equalization technique is applied to reduce Gibbs phenomenon. The response has identical ripple in the passbands and stopbands. The parameter k_p is uniquely determined from the transition region width and the parameter is independent of passband width ω_p . The class V filter model has equiripple passband and stopband. A linear

transition region with variable density of ripple cycles is introduced in the passband and stopband of this filter to reduce Gibb's phenomenon and hence further improve performance of the filter.

In the proposed technique, filter transfer function is evolved both in frequency and time domain. The approach is simple, versatile and analytical without extensive computations. The accuracy of the approximation can be improved by including a larger number of terms in the impulse response sequence. This design approach is without optimizations and hence number of computations is reduced unlike filters using optimization methods. Results show that the proposed filters have sharp transition, good stopband attenuation and less passband ripple with least filter order. This approach is better than the conventional FIR design methods of window and frequency sampling techniques. The peak passband ripple in conventional FIR filter designs is about 18% which is reduced to around 2% with the use of trigonometric functions in the proposed filter model combined with slope equalization technique.

A novel direct approach is proposed for synthesis of a sharp transition, linear phase, equiripple passband, low arithmetic complexity, bandpass FIR filter. Sharp transition bandpass filters in literature generally involves design of component filters i.e. lowpass and highpass filters to realize bandpass filters. Component filters synthesis is not required in our proposed approach. Also in conventional designs, the component filters are to be redesigned for any change in center frequency and passband width of the desired bandpass filter. The proposed bandpass filter design is adaptable to any change in the center frequency and passband width of the desired bandpass filter with no separate design required. In this design also, slopes of the pseudo-magnitude response function are matched at the edges of the transition region, which makes the proposed function continuous and hence reduces the effects due to Gibb's phenomenon thereby reducing

passband ripple of the filter. Another novel bandpass filter model with equiripple, linear transition and variable density of ripple cycles in passband and stopband to further reduce Gibb's phenomenon is introduced. This technique further reduces passband ripple and improves stopband attenuation of the filter.

A modified Frequency Response Masking (MFRM) technique for the synthesis of linear phase, sharp transition and low arithmetic complexity FIR filter is proposed. The structure is composed of our proposed linear phase, sharp transition, low arithmetic complexity lowpass and bandpass FIR filters as subfilters in the proposed MFRM approach. The design yields closed form expressions for the impulse response coefficients for the subfilters and final MFRM filter. The synthesis of the proposed modified FRM filter is simplified because it eliminates one masking filter and a model filter from the basic FRM approach. The bandpass filter has wider transition bandwidth, which simplifies its synthesis and decreases arithmetic complexity of subfilter.

In the FRM techniques [7], closed form expressions for impulse response coefficients were not obtained. The proposed approach is simple, without extensive computations and can be extended to design sharp cutoff highpass, bandpass, bandstop and multiband filters with arbitrary passband and center frequency. FRM approach is a graphical approach with masking filters designed to possess parallel skirts in the transition region which mask the periodic model filters that are compressed in frequency domain to achieve the sharp transition edges for the FRM filter. A high degree of parallelism can be obtained for the skirts of the masking filters in the transition region through our approach as is evident from the synthesis of proposed cascade filter design. Thus proposed filter design approach is found to compare favorably with Frequency Response Masking techniques [7] in terms of sharp transition and good filter performance without use of optimization techniques.

In the present study, a speech processing scheme is implemented for sensorineural hearing impaired. It involves binaural dichotic presentation of speech signal to the ears splitting it into two complementary short-time spectra using two proposed multiband filters having linear phase, sharp transition and passbands based on Zwicker's critical band model. Earlier speech processing schemes [51], [55] used conventional methods for design of FIR filters. Proposed multiband filters have good stopband attenuation so that proper band separation is possible. Also processed speech is not distorted because of less passband ripple of the proposed filters. In the case of practical filters with finite crossovers in magnitude response, the spectral components lying in the transition region are presented to both ears. Hence there is an imbalance in loudness perceived at the crossovers between adjacent bands, which reduces speech intelligibility and recognition score. In the case of the proposed filters with sharp transition band, there is reduced possibility of spectral components presented to both ears and hence increases speech recognition. All these features when combined lead to improvement in the recognition of speech for hearing impaired subjects as observed in an experimental study conducted. Also use of proposed multiband filters leads to large savings in arithmetic hardware over conventional FIR filters and hence suitable for VLSI implementation in a digital hearing aid. The processed speech sample spectrographic analysis showed that the formants of most of the syllables were presented dichotically thus aided in higher speech intelligibility and verifies the usefulness of the proposed filters and the speech processing scheme.

6.2 Suggestions for future work

For the various proposed FIR filters, a suitable filter structure can be developed and investigation of finite wordlength effects, coefficient sensitivity analysis and roundoff noise analysis can be carried out. Detail comparative study with other FIR filters in literature as regards to filter performance can be done. The proposed filters can be taken up

as initial filters for optimization to obtain better filter performance with reduced filter order. For a suitable filter structure, the hardware details like number of multipliers and delays etc. required to realize the filter can be worked out. The proposed filters can be implemented on a FPGA/ASIC/DSP processor and performance studied. Using the proposed approach, filter models with any desired magnitude response can be developed for any specific signal processing application. The proposed filter coefficients can be truncated and some feedback method can be devised to obtain desired filter specifications with reduced filter order without decline in filter performance. Speech processing scheme can be implemented in real time on a digital hearing aid. Gain of the individual bands in the multiband filter can be adjusted depending on subject's hearing loss, in accordance with individual subject's audiogram for additional improvements in speech perception. Proposed filters could be used in applications such as cochlear modeling, speech , image processing etc.

Appendix A1.1

Review of Classical Methods for FIR Filter Design

In the following we briefly review the classical methods of FIR filter synthesis that are relevant to the filters proposed in the thesis.

Window method:

Window method is one of the three well known design methods for FIR filters with linear phase. The desired frequency response $H_d(e^{j\omega})$ of a filter is represented by a Fourier series [8].

$$H_d(e^{j\omega}) = \sum_{n=-\infty}^{\infty} h_d(n) e^{-j\omega n} \quad (\text{A1.1})$$

The impulse response sequence $h_d(n)$ has infinite length. In order to obtain a realizable filter, the impulse response sequence is truncated to obtain a new sequence having length N with defining relation

$$\begin{aligned} h(n) &= h_d(n) & 0 \leq n \leq N-1 \\ &= 0 & \text{otherwise} \end{aligned} \quad (\text{A1.2})$$

The frequency response now becomes

$$H_d(e^{j\omega}) = \sum_{n=0}^{N-1} h_d(n) e^{-j\omega n} \quad (\text{A1.3})$$

which is an approximation to the desired response. To reduce the error in the approximation, the sequence $h_d(n)$ is multiplied by another sequence $\omega_R(n)$ defined by

$$\begin{aligned} \omega_R(n) &= \omega_{RS}(n) & 0 \leq n \leq N-1 \\ &= 0 & \text{otherwise} \end{aligned} \quad (\text{A 1.4})$$

The truncated series in (A1.3) now becomes

$$\begin{aligned}
 H_d(e^{j\omega}) &= \sum_{n=0}^{N-1} h_d(n) \omega_{RS}(n) e^{-j\omega n} \\
 &= \sum_{n=0}^{N-1} h(n) e^{-j\omega n}
 \end{aligned} \tag{A 1.5}$$

where $h(n) = h_d(n) \omega_{RS}(n)$

To obtain the linear phase response (or piecewise linear), the impulse response of the causal FIR filter must be either symmetric i.e. $h(n) = h(N-1-n)$ or be anti-symmetric i.e. $h(n) = -h(N-1-n)$ in (A1.5). With the symmetry condition applied we can rewrite the frequency response expression as

$$\begin{aligned}
 H(e^{j\omega}) &= \sum_{n=0}^{N-1} h(n) e^{-j\omega n} \\
 &= e^{-j\omega \left(\frac{N-1}{2}\right)} \left[h\left(\frac{N-1}{2}\right) + 2 \sum_{n=0}^{\frac{(N-3)}{2}} h(n) \cos\left(\frac{N-1}{2} - n\right) \omega \right] \text{ for } N \text{ odd}
 \end{aligned} \tag{A1.6a}$$

$$= e^{-j\omega \left(\frac{N-1}{2}\right)} \left[2 \sum_{n=0}^{\frac{N-1}{2}} h(n) \cos\left(\frac{N-1}{2} - n\right) \omega \right] \text{ for } N \text{ even} \tag{A1.6b}$$

In both the cases, the frequency response can be written compactly as

$$H(e^{j\omega}) = H_1(\omega) e^{-j\varphi(\omega)} \tag{A1.7}$$

where $H_1(\omega)$ is the pseudo magnitude function (which may assume negative values in the stopband and hence the ‘‘pseudo’’ label) and $\varphi(\omega)$ is the phase response function.

$$\varphi(\omega) = -\omega \left(\frac{N-1}{2}\right) \tag{A 1.8}$$

The desired frequency response of an ideal low-pass filter has a finite discontinuity at the boundary between the passband and the stopband of the ideal lowpass filter. The truncation of the infinite impulse sequence, i.e. fitting the finite discontinuity by using a finite number terms of the series given by (A1.5) leads to the Gibb's phenomenon. This phenomenon gives rise to overshoot and ripple before and after the discontinuity i.e. in the pass as well as stopband of the frequency response. This phenomenon occurs because it is impossible to obtain an infinite slope at the discontinuity using only a finite number of terms.

The ideal frequency response of a digital filter, which is a Fourier transform, is periodic in frequency domain and has a few finite discontinuities at band edges. It satisfies dirichlet conditions [9], which guarantee the representation of the ideal lowpass filter response by a Fourier series, such as (A1.1). The dirichlet conditions also guarantee that the infinite series (A1.1) equals the ideal frequency response i.e. brick-wall characteristics except at isolated values of frequency ω , for which the response is discontinuous. At the discontinuities the infinite series (A1.1) converges to the average of the values on either side of the discontinuity. If a finite series such as (A1.5) is used to represent the frequency response, the Gibb's phenomenon manifests itself. As the number of terms N increases, the ripples do not decrease, but are squeezed into a narrower interval about the discontinuity.

In the window design, various window profiles are used [8]. The simplest among these is the rectangular window, which uses uniform weighting of the Fourier coefficients i.e. $\omega_{RS} = 1.0$ for all n in (A1.4), which is not desirable because of the resulting Gibb's phenomenon. Better results are achieved with other windows, the popular ones being Hann, Hamming and Kaiser windows, which use a more severe weighting of the coefficients that are kept in the truncation process.

Frequency sampling technique:

The second method namely, frequency sampling technique uses a set of samples, determined from the desired frequency response of the filter, which are identified as Discrete Fourier Transform (DFT) coefficients. The filter coefficients (impulse response sequence) are then determined from the Inverse Discrete Fourier Transform (IDFT) of this set of samples. There are two variants of the design namely Type I and Type II design. In type I design, the desired frequency response $H_d(e^{j\omega})$ is sampled at N points ω_k , $k = 0, 1, \dots, N-1$, uniformly spaced around the unit circle and are chosen to be

$$\omega_k = \left(\frac{2k\pi}{N} \right), \quad k = 0, 1, \dots, N-1 \tag{A1.9}$$

The set of samples are

$$\begin{aligned} \bar{H}(k) &= H_d(e^{j\omega})_{\omega=\omega_k} \\ &= H_d \left(e^{j \frac{2k\pi}{N}} \right), \quad k = 0, 1, \dots, N-1 \end{aligned} \tag{A1.10}$$

This set of sampling points are considered as DFT samples and using IDFT the coefficients $h(n)$ can be computed from

$$h(n) = \frac{1}{N} \sum_{k=0}^{N-1} \bar{H}(k) e^{j \frac{2k\pi}{N} n}, \quad n = 0, 1, 2, \dots, N-1. \tag{A1.11}$$

The coefficients $h(n)$ must all be real. This requires that the complex terms should appear in complex conjugate pairs. In other words, the term $\bar{H}(k)$ shall match with the term $\bar{H}(N-k)$ which have exponential terms that are conjugate. The required conditions can be summed up as follows.

(i) $\bar{H}(0)$ should be real

(ii) $\bar{H}(N-k) = \bar{H}^*(k)$, for N odd $k = 1, 2, \dots, \frac{N-1}{2}$ and

(iii) $\bar{H}(N-k) = \bar{H}^*(k)$, $k = 1, 2, \dots, \frac{N}{2}-1$ and (A1.12)

$$\bar{H}\left(\frac{N}{2}\right) = 0, \quad \text{for N even}$$

Once the filter coefficients $h(n)$ have been determined, the frequency response can be determined from (A1.5)

In type II design, the frequency $\omega=0$ is excluded by choosing the sampling points

$$\omega_k = 2\pi\left(\frac{2k+1}{2N}\right), \quad k = 0, 1, \dots, N-1 \quad (\text{A1.13})$$

In this case the DFT coefficients are defined by

$$\bar{H}(k) = H_d \left(e^{j2\pi\frac{(k+1)}{N}} \right), \quad k = 0, 1, \dots, N-1 \quad (\text{A1.14})$$

The conditions for $h(n)$ to be real in this case are,

$$\bar{H}(N-k-1) = \bar{H}^*(k), \quad k = 0, 1, \dots, \frac{N-1}{2}-1 \quad \text{and}$$

$$\bar{H}\left(\frac{N-1}{2}\right) = 0 \quad \text{for N odd} \quad \text{and} \quad (\text{A1.15a})$$

$$\bar{H}(N-k-1) = \bar{H}^*(k), \quad k = 0, 1, \dots, \frac{N}{2}-1 \quad \text{for N even.} \quad (\text{A1.15b})$$

From the DFT samples in (A1.14) and using IDFT, the coefficient $h(n)$ can be computed from (A1.11). From the filter coefficients $h(n)$, the frequency response can be determined from (A1.5) as before.

Optimal FIR filter design:

In the third method namely, optimal FIR filter design, a mini-max or chebyshev type of approximation is employed. The technique involves the determination of a weighted error function and the general form of the response function. The coefficients in the general form of the response function are then determined so as to minimize the maximum error that occurs.

The general form of the response function can be written using (A1.6) as [8]

$$H(e^{j\omega}) = e^{-j\omega\left(\frac{N-1}{2}\right)} H_1(\omega) \quad (\text{A1.16})$$

where, N is the filter length as in (A1.5) and $H_1(\omega)$ is the pseudo-magnitude given by

$$H_1(\omega) = Q(\omega)P(\omega) \quad (\text{A1.17})$$

The expressions for $Q(\omega)$ and $P(\omega)$ for the cases N even and N odd are

$$\text{For N odd, } Q(\omega) = 1 \text{ and } P(\omega) = \sum_{n=0}^{\frac{N-1}{2}} a(n)\cos(n\omega)$$

$$\text{For N even, } Q(\omega) = \cos\left(\frac{\omega}{2}\right) \text{ and } P(\omega) = \sum_{n=0}^{\frac{N-1}{2}} b(n)\cos(n\omega) \quad (\text{A.1.17a})$$

For N odd, starting with (A1.6a) substituting, $\left(\frac{N-1}{2} - n\right) = k$, then affecting the change of

variable from k back to n once again relation for $P(\omega)$ is obtained. For N even, starting with

(A1.6b) making the substitution $\left(\frac{N}{2} - n\right) = k$, then affecting the change of variable from k to

n once again and then using the trigonometric identity

$$2 \cos\left(\frac{\omega}{2}\right) \cos(n\omega) = \cos\left(n + \frac{1}{2}\right)\omega + \cos\left(n - \frac{1}{2}\right)\omega$$

the relation for $P(\omega)$ is obtained.

In the case of a lowpass filter, the desired function that is to be approximated by $H_1(\omega)$ is given by

$$\begin{aligned} \overline{H_1}(\omega) &= 1, & 0 \leq \omega \leq \omega_p \\ &= 0, & \omega_s \leq \omega \leq \pi \end{aligned} \tag{A1.18}$$

where $0 \leq \omega \leq \omega_p$ is the passband and $\omega_s \leq \omega \leq \pi$ is the stopband. The weighted error function is defined by

$$E(\omega) = W(\omega) \left(\overline{H_1}(\omega) - H_1(\omega) \right) \tag{A1.19}$$

where $W(\omega)$ is the weighting function given as

$$\begin{aligned} W(\omega) &= \frac{1}{k}, & 0 \leq \omega \leq \omega_p \\ &= 1, & \omega_s \leq \omega \leq \pi \end{aligned} \tag{A1.20}$$

According to the theory of chebyshev approximation, E_{\max} , the maximum absolute error over the stopband and passband can be minimized (yielding optimum approximation) when the value of $E(\omega)$ exhibits at least $(N_0 + 2)$ alternations in sign. The value of N_0 is $\frac{N+1}{2}$ for odd N and $\frac{N}{2} - 1$ for even N , i.e., the upper limit on the summation describing $P(\omega)$ in (A1.17a).

A set of $(N_0 + 2)$ frequencies termed 'extrema frequencies' at which $|E(\omega)|$ exhibits maxima are defined over passbands and stopbands i.e. the frequency range from 0 to π excluding $\omega_p \leq \omega \leq \omega_s$, the transition region such that

$$E(\omega_i) = -E(\omega_{i-1}) = \pm E_{\max}, \quad i = 1, 2, \dots, N_0 + 1$$

where $\omega_0 < \omega_1 < \dots < \omega_{N_0 + 1}$

Assuming $E_{\max} = \delta_2$ and for convenience taking $k = \frac{\delta_1}{\delta_2}$ we obtain a variation between

$(1 + \delta_1)$ and $(1 - \delta_1)$ in the passband and a variation between δ_2 and $-\delta_2$ in the stopband.

The chebyshev approximation procedure results in an equiripple approximation for $H_1(\omega)$ in the optimal case. This response is similar to that of the elliptic analog filter, which is optimum for analog filter.

The number of relative extrema, N_p of $H_1(\omega)$ in the passband and relative extrema, N_s of $H_1(\omega)$ in the stopband add up to N_e i.e., $N_p + N_s = N_e$. These extrema correspond to the values of ω for which $H_1(\omega)$ is either $(1 + \delta_1)$, $(1 - \delta_1)$, δ_2 or $-\delta_2$. The two parameters N_s and N_p are arbitrary except that their sum is fixed by the value of N_e . For N odd, $N_0 = \frac{N-1}{2}$ from

(A1.17a). For this case we obtain $N_e \leq \frac{N+1}{2} = N_0 + 1$.

Similarly, for N even, $N_0 = \frac{N}{2} - 1$ from (A1.17a). For this case we obtain

$N_e \leq \frac{N}{2} = N_0 + 1$, as before.

As stated above, there must be at least $N_0 + 2$ alternations for the optimal filter.

Possible alternations can occur at $N_e = (N_0 + 1)$ relative extrema of $H_1(\omega)$. There are always two alternations at ω_p and ω_s so that the total number of alternations can be $N_0 + 3$ if alternations occurs both at $\omega = 0$ and $\omega = \pi$. If there is an alternation at only one of these frequencies there are $(N_0 + 2)$ alternations in all. The filters having $(N_0 + 3)$ alternations are

referred to as 'extraripple filters' and those having $(N_0 + 2)$ alternations are called 'equiripple filters.'

From the above, we note that the parameters that can be used to describe $H_1(\omega)$ are $N_0, N, N_p, N_s, \omega_p, \omega_s, \delta_1, k$ and δ_2 . There are various procedures for designing the optimal filters, but the most widely used method is that of Mc Clellan, Parks and Rabiner [10]. In input parameters for their program are the filter length N , the band edges in hertz and the weight in each band. The program uses the Remez exchange algorithm to obtain the correct extrema frequencies. The output data provided by the program are the impulse response coefficients $h(n)$, the extremal frequencies of $H_1(\omega)$ in hertz and the deviations.

Appendix A1.2

An alternative interpretation of Impulse Response Truncation of FIR Filter

An alternative interpretation of the 'truncation' process is given in the following. If the impulse response is assumed to be a real and even function of time (discrete), frequency response given by (A1.1), with condition of symmetry $h(n) = h(-n)$, reduces to $H_1(\omega)$ and phase function $\varphi(\omega)$ becomes zero.

$$\text{Thus, } H_d(e^{j\omega}) = \sum_{n=-\infty}^{+\infty} h_d(n) e^{-j\omega n} = H_1(\omega)$$

$$H_1(\omega) = \begin{cases} h_d(0) + 2[h_d(1)\cos(\omega) + \dots + h_d(M)\cos(M\omega) + \dots] \\ h_d(0) + 2\sum_{n=1}^{+\infty} h_d(n) \cos n\omega \end{cases} \quad (\text{A1.21})$$

But the FIR filter corresponding to (A1.21) is non casual and hence not realizable. The function $H_1(\omega)$ can be also referred to as 'zero-phase' frequency response for obvious reasons. If we carve out a causal part, we are left with only $h(0)$, a trivial case. The resulting filter is an all pass filter.

In Fig.A1.2 truncating the classical Fourier series is equivalent to making truncated part causal and symmetric to yield a realizable linear phase filter. As filter order N increases more terms are included in the truncated sequence and performance of the filter improves. In Fig. A 1.2 (a) the sinc function representing the impulse response coefficients is non-causal and delay is zero. Further, in Fig. A 1.2(b) the sinc function is shifted one step to the right i.e. one delay is introduced i.e. $e^{-j\omega}$. The truncated impulse response is symmetric i.e.

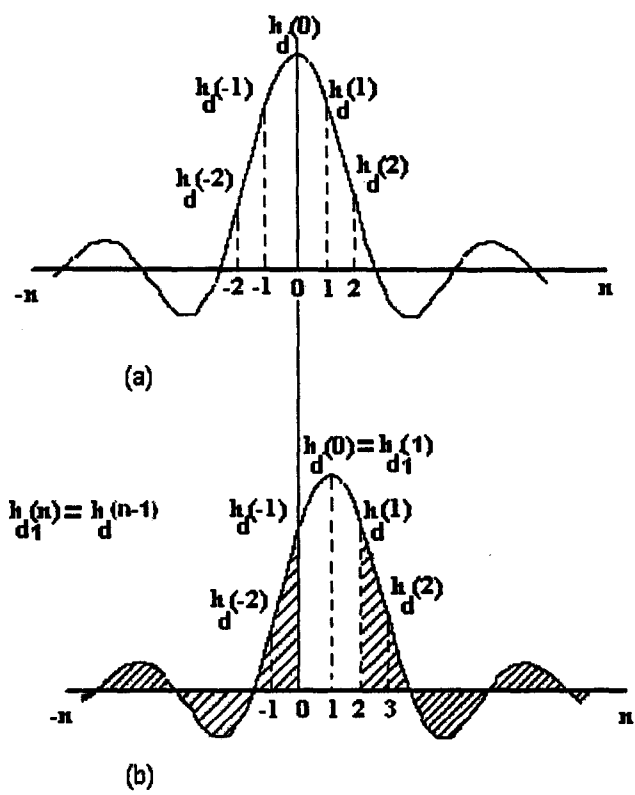


Fig. A1.2 Illustration of truncation of the impulse sequence.

$h_d(n) = h_d(N-1-n)$, where $n = 0, 1, 2$ and $N=3$ (truncation). This makes it causal and linear phase with $h(0)$, $h(1)$, $h(2)$ only present. The hatched portion consists of deleted coefficients in the interior continuing this way, if entire sequence is shifted to right by M units and only causal symmetric part is retained by truncation then, we obtain the modified linear phase frequency response.

$$\begin{aligned}
 H_{dM}(e^{j\omega}) &= h_d(-M) + h_d(-M+1)e^{-j\omega} + \dots + h_d(0)e^{-jM\omega} + \dots + h_d(M)e^{-j2M\omega} \\
 &= \sum_{n=0}^{2M} h_d(n-M)e^{-jn\omega}, \quad N = 2M+1, \text{ odd integer} \\
 &= \sum_{n=0}^{2M} h_{dM}(n)e^{-jn\omega} \\
 &= e^{-jM\omega} \left\{ h_d(0) + 2 \sum_{n=1}^M h_d(n) \cos n\omega \right\} \tag{A1.22}
 \end{aligned}$$

In the above the coefficients correspond to those of Fig. A1.2 (a). Thus $h_d(-M)$ at $n=-M$, when shifted to right by M places occupies the position corresponding to $n=0$. Accordingly the symmetry condition becomes $h_d(n) = h_d(-n)$ i.e. $h_d(M) = h_d(-M)$ and so on.

If we name the shifted sequence by $h_{dM}(n)$ then $h_{dM}(n) = h_d(n-M)$ and symmetry condition becomes $h_{dM}(n) = h_{dM}(2M-n)$.

If the desired response in (A1.21) corresponds to an ideal lowpass frequency response then [8]

$$h_d(n) = \frac{1}{2\pi} \left[\int_{-\pi}^{\pi} H_d(e^{j\omega}) e^{jn\omega} d\omega \right] = \frac{1}{2\pi} \left[\int_{-\omega_c}^{\omega_c} (e^{jn\omega}) d\omega \right]$$

$$= \frac{\sin \omega_c n}{\pi n}, \text{ for } n \neq 0 \quad (\text{A1.23})$$

with $H_d(e^{j\omega}) = 1, \quad \omega \leq \omega_c \leq \pi$

$$= 0, \text{ otherwise} \quad (\text{A1.24})$$

where, ω_c is the cut-off frequency of the ideal response. For $n=0$, we have

$$h_d(0) = \frac{\omega_c}{\pi} \quad (\text{A1.25})$$

The plot of $h_d(n)$ versus n will have an envelope that is a 'sinc' function given by [8]

i.e. $\frac{\omega_c}{\pi} \text{sinc}\left(\frac{\omega_c n}{\pi}\right)$. The zeros of this function occur at integer values of n . As we shift each of

the members of impulse sequence as envisaged in (A1.22) and truncate and retain only the symmetrical part we obtain a causal, linear-phase FIR filter, which is an approximation to the ideal filter response. As M increases, the associated delay also increases and the approximation improves, as is evident from (A1.22). As M tends to ∞ , the approximation converges to the ideal and associated delay also tends to ∞ , which is not realizable in practice.

In conclusion, we can say that, the 'truncation' process is a process by which, the members of impulse-response sequence are shifted to the right in steps and after each shift, if we retain only the 'causal' symmetric part we obtain an approximation to the ideal low-pass response. For N even, impulse response sequence is given by $h(n+1/2)$, where n is an integer. For a filter of length N , the number of delays and terms in the impulse response sequence to be computed are $(N-1)/2$ for N odd and $(N/2)-1$ for N even.

Appendix A 5.1

Speech Processing Scheme and Listening Tests

Implementation of Speech Processing Scheme

In this section, the implementation of speech processing scheme for sensorineural hearing impaired subjects is presented. The recording and processing of speech is 'offline' using multimedia PC, which means voice is pre-recorded and speech after passing through multiband filters i.e. split speech is stored in memory and then presented to the subjects for identification. The recording of a male voice at normal speech levels is done in a sound proof room using nonsense syllables in Vowel Consonant Vowel (VCV) context. The speech acquisition is done using multimedia PC. Time domain speech signals are converted to frequency domain signals for speech processing. Speech signal is band-limited to 60Hz-5.2 KHz and the speech is digitized with 16 bit, pulse code modulation at a sampling frequency of 11025 Hz and stored in wav format. A MATLAB program MSP is developed for speech acquisition and band limiting, conversion of speech from time to frequency domain and vice versa, to split the speech into critical bands using two proposed multiband FIR filters and to present the processed speech samples to the subject ears. The speech samples are split into complementary frequency bands based on Zwicker's critical band model. The outputs of the two filters are fed to the left and right ear as shown in Fig.A5.1. The filtered speech signal is converted from frequency domain to time domain for recognition by the ears. During the test, processed and unprocessed sound clips are fed to the left and right ears of the subject using headphones and subjects are asked to identify the sound clip [59].

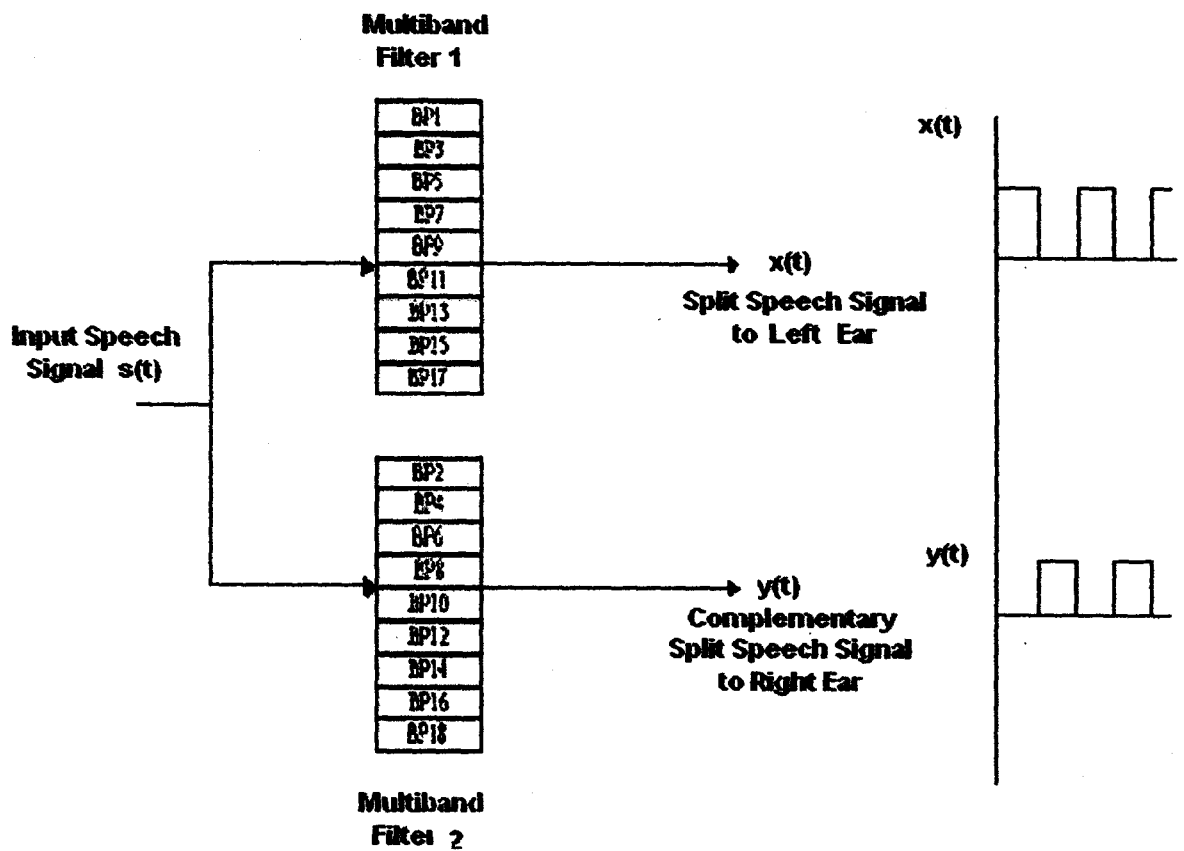


Fig.A5.1. Block diagram of Multiband filters to used to split speech signal into complementary spectra in the speech processing scheme.

The details of multiband FIR filters designed for speech processing scheme are given below.

Filter Type: Two multiband, linear phase, FIR filters using proposed approach with a fixed gain and variable bandwidths based on Zwicker's critical band model (Table A5.1).

Number of passbands: Nine (for each multiband filter).

Sampling frequency: 11025 Hz.

Maximum passband ripple for individual bands: ± 0.15 dB.

Minimum stop band attenuation for individual bands: 40 dB.

Transition bandwidth for all bands: 35Hz.

Multiband filter order: 1025.

Listening Tests

In the listening tests, five subjects with bilateral moderate sensorineural hearing impairment participated. Male and female subjects of different age groups with experience in listening tests are participated in the listening tests. The test stimulus had ten syllables in VCV context which were obtained with vowel /a/ and consonants /d, m, n, s, v, b, g, z, f, p/ like 'aba, 'ada' etc. The listening tests were conducted on sensorineural hearing-impaired subjects with moderate and severe hearing loss at All India Institute of Speech and Hearing, Mysore. Listening tests were done in a noise free environment using headphones and multimedia PC. The test stimulus was administered for unprocessed speech and processed speech dichotically presented using multimedia PC and subjects were asked to identify each sound clip (stimulus) and their responses were recorded. A compilation of subject's qualitative assessments about the test stimulus for assessing any improvement in speech perception was done [59].

Observations

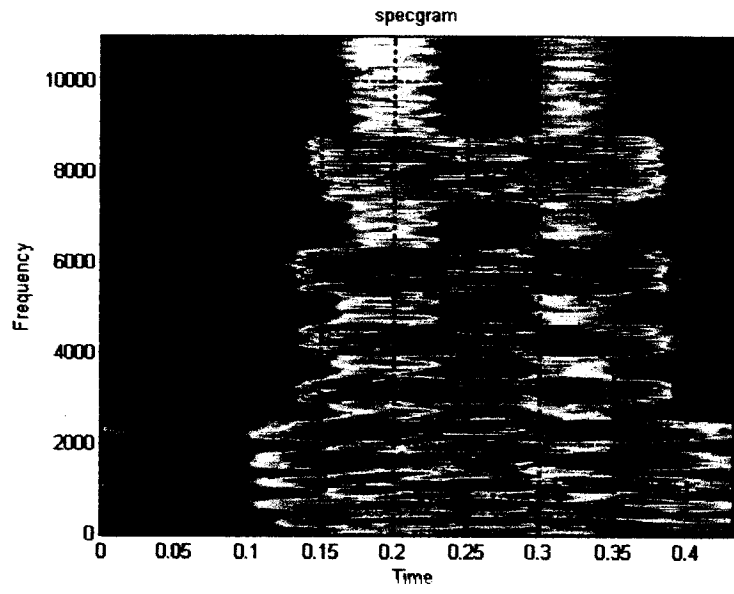
- Five subjects with bilateral moderate sensorineural hearing impairment were tested.
- Out of the ten syllables presented in VCV context on an average five syllables could be identified by them.
- Subjects preferred processed dichotic presentation to unprocessed dichotic presentation.
- Subjects showed an improvement in recognition of the speech syllables presented to the ear.
- For all the subjects the recognition scores for processed speech were higher than those for unprocessed speech.
- Response time to respond to speech syllables presented to the ears is reduced which is an indication of effective speech processing.
- Spectrographic analysis to verify adjacent formants being presented to different ears is carried out.

Spectrographic Analysis

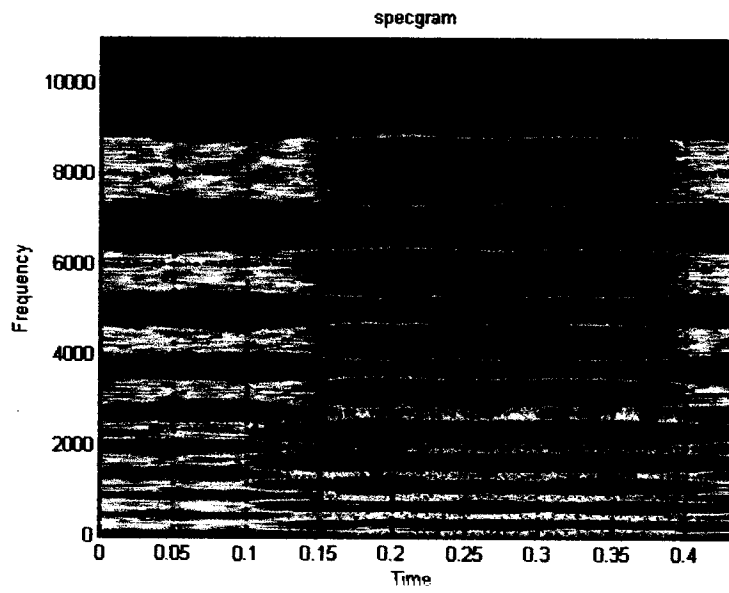
The processed speech has been spectrographically analyzed to verify splitting of speech into various frequency bands. Fig. A5.2 shows the bands have been split as per multiband filter passbands. The formants of the speech syllables are analyzed and it is found that the adjacent formant frequencies are presented to alternate ears thus aided in better recognition of speech presented to the ears.

Table A5.1 Zwicker's critical band estimate

No.	Bands	Freq. (KHz)	No.	Bands	Freq.(KHz)
1	BP1	0.07-0.2	2	BP2	0.2-0.3
3	BP3	0.30-0.40	4	BP4	0.40-0.51
5	BP5	0.51-0.63	6	BP6	0.63-0.77
7	BP7	0.77-0.92	8	BP8	0.92-1.08
9	BP9	1.08-1.27	10	BP10	1.27-1.48
11	BP11	1.48-1.72	12	BP12	1.72-2.00
13	BP13	2.00-2.32	14	BP14	2.32-2.70
15	BP15	2.70-3.15	16	BP16	3.15-3.70
17	BP17	3.70-4.40	18	BP18	4.40-5.012



(a)



(b)

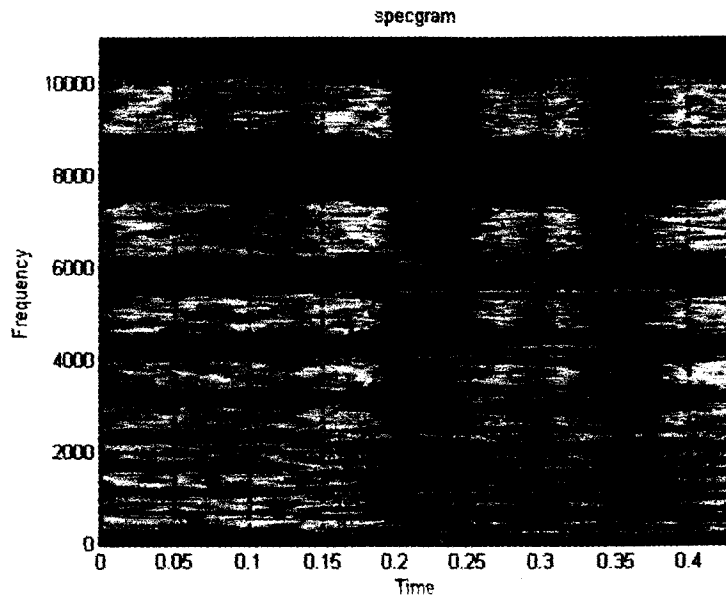


Fig. A5.2. (a) Speech spectrogram of syllable 'ada' (b) and (c) Speech spectrogram of syllable 'ada' after splitting into complementary bands based on passbands of multiband filters in Table A5.1. (Note: In the above figures, frequency is in Hz and time is in m sec).

Appendix A 6.1

Filter Design of Proposed FIR Filters

This appendix gives the filter synthesis and design methodology illustrated by means of a design example for the proposed lowpass, bandpass, multiband and modified FRM linear phase, sharp transition FIR filters. For the desired FIR filter specifications namely passband width ω_p , passband ripple δ_p , stopband attenuation δ_s and transition width $(\omega_s - \omega_c)$ the design parameters of the proposed filter $k_p, k_t, k_s, \omega_0, \omega_z$ cutoff frequency ω_c , stopband edge frequency ω_s and the filter impulse response coefficients are computed. The design is carried out using MATLAB [60], [61] and measurement of filter specifications done using Signal Processing Toolbox. The design example is same for all designs for comparison of filter performance of all the proposed filter designs.

A 6.1.1 Filter Synthesis and Design of Class I FIR Lowpass Filter with Non-Monotonic Response without Slope Equalization

Design Example: Consider the design of a proposed Class I lowpass, linear phase, sharp transition FIR filter to meet the following specifications: passband edge ω_p is 0.6667π , transition bandwidth $(\omega_s - \omega_c)$ is 0.01π , maximum passband ripple δ_p is $\pm 0.1\text{dB}$ (0.2dB) and minimum stopband attenuation δ_s is 40dB .

Step 1: The desired filter specifications namely, ω_p , $(\omega_s - \omega_c)$, δ_p and δ_s are given as in design example.

Step 2: The frequency response of the proposed FIR filter is reproduced below for convenience.

$$H_{pm}(\omega) = 1 + k_p \delta_p \sin(\omega - \omega_0) \quad 0 \leq \omega \leq \omega_p \quad (2.8)$$

$$H_{pm}(\omega) = \left(1 + \frac{\delta_p}{2}\right) \cos[k_t(\omega - \omega_p)] \quad \omega_p \leq \omega \leq \omega_z \quad (2.9)$$

$$H_{pm}(\omega) = -\frac{k_s \delta_s}{2} \sin(\omega - \omega_z) \quad \omega_z \leq \omega \leq \pi \quad (2.10)$$

$$H_{pm}(0) = 1 - \frac{\delta_p}{2} = \left[1 - k_p \delta_p \sin(\omega_0)\right] \quad (2.11)$$

$$H_{pm}(\omega_p) = 1 + \frac{\delta_p}{2} \quad (2.13)$$

$$H_{pm}(\omega_z) = 0 \quad (2.16)$$

$$H_{pm}(\omega_c) = \left(1 - \frac{\delta_p}{2}\right) \quad (2.18)$$

$$H_{pm}(\pi) = -\frac{\delta_s}{2} \quad (2.20)$$

$$H_{pm}(\omega_s) = \frac{\delta_s}{2} \quad (2.22)$$

Step 3: The filter design parameters k_p , k_t , k_s , ω_z , ω_0 and cutoff frequency ω_c , stopband edge frequency ω_s are computed using equations reproduced below.

$$\omega_0 = \frac{\omega_p}{2} \quad (2.15)$$

$$k_p = \frac{1}{2 \sin \omega_0} \quad (2.12)$$

$$k_t = \frac{1}{(\omega_s - \omega_c)} \cos^{-1} \left[\frac{\frac{\delta_s}{2}}{1 + \frac{\delta_p}{2}} \right] - \cos^{-1} \left[\frac{1 - \frac{\delta_p}{2}}{1 + \frac{\delta_p}{2}} \right] \quad (2.24)$$

$$\omega_z = \omega_p + \frac{\pi}{2k_t} = 2\omega_0 + \frac{\pi}{2k_t} \quad (2.17)$$

$$k_s = \frac{1}{\sin \omega_z} \quad (2.21)$$

$$\omega_c = \omega_p + \frac{1}{k_t} \cos^{-1} \left[\frac{1 - \frac{\delta_p}{2}}{1 + \frac{\delta_p}{2}} \right] \quad (2.19)$$

$$\omega_s = \omega_p + \frac{1}{k_t} \cos^{-1} \left[\frac{\frac{\delta_s}{2}}{1 + \frac{\delta_p}{2}} \right] \quad (2.23)$$

Step 4: The impulse response coefficients of the filter are obtained by substituting values of $\omega_0, k_p, k_t, \omega_z, k_s, \omega_p, \delta_p$ and δ_s in (2.28) to (2.31).

Results: The magnitude and impulse response of the filter designed is as shown in Fig. 2.3.

The filter design parameters computed are $k_t = 49.796$, $k_p = 0.57735$, $k_s = 1.1767$, $\omega_z = 0.6773 \pi$ with cutoff edge $\omega_c = 0.6668 \pi$ and stopband edge $\omega_s = 0.6767 \pi$.

The frequency domain specifications of the designed filter, obtained by measuring its magnitude response using SP toolbox are, passband edge $\omega_p = 0.6667 \pi$, $\omega_c = 0.6668 \pi$, $\omega_s = 0.6767 \pi$, transition bandwidth $(\omega_s - \omega_c) = 0.01 \pi$, passband ripple $\delta_p = 0.087 \text{dB}$ and stopband attenuation $\delta_s = 32.2 \text{dB}$ are obtained for a filter order of 701. It is found that obtained filter specifications do not match with the desired specifications i.e. stopband attenuation achieved is poor and does not improve appreciably with increase in filter order.

A6.1.2 Filter Synthesis and Design for Class II FIR Lowpass Filter with Monotonic Response without Slope Equalization

Design Example: Consider the design of a proposed Class II lowpass, linear phase, and sharp transition FIR filter to meet the following specifications: passband edge ω_c is 0.6667π transition bandwidth $(\omega_s - \omega_c)$ is 0.01π , maximum passband ripple δ_p is $\pm 0.1\text{dB}$ (0.2dB) and minimum stopband attenuation δ_s is 40dB.

Step 1: The desired filter specifications namely ω_c , $(\omega_s - \omega_c)$, δ_p and δ_s are given as in design example.

Step 2: The desired frequency response of the FIR filter is modeled using trigonometric functions are reproduced below for convenience

$$H_{pm}(\omega) = 1 - k_p \sin \omega, \quad 0 \leq \omega \leq \omega_c \quad (2.32)$$

$$H_{pm}(\omega) = (1 - \delta_p) [1 - \text{sinc}_t(\omega - \omega_c)] , \quad \omega_c \leq \omega \leq \omega_z \quad (2.33)$$

$$H_{pm}(\omega) = \frac{-k_s \delta_s}{2} \sin(\omega - \omega_z) , \quad \omega_z \leq \omega \leq \pi \quad (2.34)$$

$$H_{pm}(0) = 1$$

$$H_{pm}(\omega_c) = 1 - \delta_p \quad (2.37)$$

$$H_{pm}(\pi) = -\frac{\delta_s}{2} \quad (2.39)$$

$$H_{pm}(\omega_s) = \frac{\delta_s}{2} \quad (2.41)$$

$$H_{pm}(\omega_z) = 0 \quad (2.35)$$

Step 3: The filter design parameter k_p , k_t , k_s , ω_z and stopband edge frequency ω_s are obtained using equations reproduced below

$$k_p = \frac{\delta_p}{\sin \omega_c} \quad (2.38)$$

$$k_s = \frac{1}{\sin \omega_z} \quad (2.40)$$

$$\omega_z = \omega_c + \frac{\pi}{2k_t} \quad (2.36)$$

$$\omega_s = \omega_c + \frac{\sin^{-1} \left[1 - \frac{\delta_s}{2(1-\delta_p)} \right]}{k_t} \quad (2.42)$$

$$k_t = \frac{\sin^{-1} \left[1 - \frac{\delta_s}{2(1-\delta_p)} \right]}{(\omega_s - \omega_c)} \quad (2.43)$$

Step 4: The impulse response coefficients of the filter are obtained by substituting values of ω_c , k_p , k_t , ω_z , k_s , δ_p and δ_s in (2.47) to (2.50).

Results: The magnitude and impulse response of the filter designed for the above design is as shown in Fig.2.5. The filter design parameters computed are $k_t = 46.814$, $k_p = 0.0011547$, $k_s = 1.1782$, $\omega_z = 0.6773 \pi$ and stopband edge $\omega_s = 0.6767 \pi$.

The frequency domain specifications obtained by measurements of the magnitude response using SP toolbox are cutoff edge $\omega_c = 0.6667 \pi$, stopband edge $\omega_s = 0.6766 \pi$, transition bandwidth $(\omega_s - \omega_c) = 0.010 \pi$, passband ripple $\delta_p = 0.204 \text{dB}$ and stopband

attenuation $\delta_s = 46.3\text{dB}$ are obtained with a filter order of 701. Good stopband attenuation is achieved but filter has highest passband ripple compared to all proposed filter designs.

A6.1.3 Filter Synthesis and Design for Class III FIR Lowpass Filter with Equiripple Passband Response

Design Example: Consider the design of a proposed Class III lowpass, linear phase, sharp transition FIR filter to meet the following specifications: passband edge ω_p is 0.6667π , Transition bandwidth $(\omega_s - \omega_c)$ is 0.01π , maximum passband ripple δ_p is $\pm 0.1\text{dB}$ (0.2dB) and minimum stopband attenuation δ_s is 40 dB.

Without Slope Equalization

Step 1: The desired filter specifications namely ω_p , $(\omega_s - \omega_c)$, δ_p and δ_s are given.

Step 2: The desired frequency response of the FIR filter is modeled using trigonometric functions reproduced below for convenience

$$H_{pm}(\omega) = 1 + \frac{\delta_p}{2} \cos k_p \omega \quad 0 \leq \omega \leq \omega_p \quad (2.51)$$

$$H_{pm}(\omega) = A \cos k_t (\omega - \omega_0) \quad \omega_p \leq \omega \leq \omega_z \quad (2.52)$$

$$H_{pm}(\omega) = -\frac{\delta_s}{2} \sin k_s (\omega - \omega_z) \quad \omega_z \leq \omega \leq \pi \quad (2.53)$$

$$H_{pm}(0) = 1 + \frac{\delta_p}{2} \quad (2.57)$$

$$H_{pm}(\omega_p) = 1 \quad (2.58)$$

$$H_{pm}(\omega_c) = 1 - \frac{\delta_p}{2} \quad (2.62)$$

$$H_{pm}(\omega_s) = \frac{\delta_s}{2} \quad (2.64)$$

$$H_{pm}(\omega_z) = 0 \quad (2.67)$$

$$H_{pm}(\omega_0) = A \quad (2.61)$$

$$H_{pm}(\pi) = -\frac{\delta_s}{2} \quad (2.69)$$

Step 3: The filter design parameters $k_p, k_t, \omega_z, \omega_0$ and k_s are computed using equations reproduced below

$$k_p = \frac{2\pi(k_r + 1/4)}{\omega_p} \quad (2.56)$$

A is chosen greater than unity.

$$k_t = \frac{1}{(\omega_s - \omega_c)} \left[\cos^{-1} \left(\frac{\delta_s}{2A} \right) - \cos^{-1} \left(\frac{1 - \delta_p/2}{A} \right) \right] \quad (2.66)$$

$$\omega_0 = \omega_p - \left(\frac{1}{k_t} \right) \cos^{-1} \left(\frac{1}{A} \right) \quad (2.60)$$

$$\omega_z = \omega_0 + \frac{\pi}{2k_t} \quad (2.68)$$

$$k_s = \frac{\pi(4L + 1)}{2(\pi - \omega_z)} \quad (2.70)$$

where L is a nonnegative integer and $(L+1/4)$ number of ripples in the stopband in $[\omega_z, \pi]$.

$$\omega_s = \omega_0 + \frac{1}{k_t} \cos^{-1} \left(\frac{\delta_s}{2A} \right) \quad (2.65)$$

$$\omega_c = \omega_0 + \frac{1}{k_t} \cos^{-1} \left(\frac{1 - \frac{\delta_p}{2}}{A} \right) \quad (2.63)$$

Step 4: The impulse response coefficients are obtained by substituting values of $k_p, k_t, \omega_z, k_s, \omega_p, \delta_p, \delta_s$ and A in (2.74) to (2.78).

Results: The magnitude and impulse response of the filter designed for the above design is as shown in Fig. 2.7. In this design, $A = 1.000001$, $k_r = 8$ and $L = 108$ are chosen. The filter design parameters computed are $k_t = 48.833$, $k_p = 24.75$, $k_s = 670.1$, $\omega_z = 0.67688\pi$, $\omega_0 = 0.66665\pi$, cutoff edge $\omega_c = 0.66686\pi$ and stopband edge $\omega_s = 0.67686\pi$.

The frequency domain specifications obtained by measurements of the magnitude response using Signal Processing toolbox are passband width $\omega_p = 0.6667\pi$, $\omega_c = 0.6767\pi$, transition bandwidth $(\omega_s - \omega_c) = 0.01\pi$, passband ripple $\delta_p = 0.078\text{dB}$ and stopband attenuation $\delta_s = 35\text{dB}$ are obtained with a filter order of 701. It is found that obtained specifications match closely with the desired specifications except for lower stopband attenuation with the desired value of 40dB achieved with higher filter order.

With slope equalization

The filter design parameters k_p, k_t and k_s are computed using equations reproduced below

$$k_t = \frac{1}{(\omega_s - \omega_c)} \left[\cos^{-1} \left(\frac{\delta_s}{2A} \right) - \cos^{-1} \left(\frac{1 - \frac{\delta_p}{2}}{A} \right) \right] \quad (2.66)$$

$$k_p = \frac{2k_t(\sqrt{A^2 - 1})}{\delta_p} \quad (2.87)$$

$$k_s = \frac{2A k_t}{\delta_s} \quad (2.95)$$

The expressions for frequency parameters $k_p, \omega_z, \omega_0, \omega_s$ and ω_c are identical to those of filter design without slope equalization.

The magnitude and impulse response of the filter designed for the above design is as shown in Fig.2.8. In this design, $A=1.000001$, $k_t = 8$ and $L=108$ are chosen. The filter design parameters computed are $k_t = 47.5$, $k_p = 134.38$, $k_s = 9502.688$, $\omega_z = 0.67716\pi$, $\omega_{01} = 0.6667\pi$, stopband edge $\omega_s = 0.677146\pi$ and cutoff edge $\omega_c = 0.666869\pi$.

The frequency domain specifications obtained by measurements of the magnitude response using SP toolbox are passband edge $\omega_p = 0.6667\pi$, $\omega_c = 0.66686\pi$, $\omega_s = 0.677\pi$, transition bandwidth $(\omega_s - \omega_c) = 0.01\pi$, maximum passband ripple $\delta_p = 0.068$ dB and minimum stopband attenuation $\delta_s = 35.82$ dB are obtained with a filter order of 701. It is found that obtained specifications match closely with the desired specifications with stopband attenuation lesser than the desired value of 40 dB, which can be achieved with higher order. With slope equalization, passband loss is reduced and stopband attenuation improves compared to filter design without slope equalization for the same filter order because of reduction of Gibb's phenomenon.

A6.1.4 Filter Synthesis and Design of Class IV FIR Lowpass Filter with Equiripple Passband and Linear Transition Region with Slope Equalization

Design Example: Consider the design of a proposed Class IV lowpass, linear phase, sharp transition FIR filter to meet the following specifications: Passband edge ω_p : 0.6667π ,

Transition bandwidth $(\omega_s - \omega_c)$ is 0.01π , Maximum passband ripple δ_p : $\pm 0.1\text{dB}$ and

Minimum stopband attenuation δ_s is 40 dB.

Step 1: The desired filter specifications namely ω_p , $(\omega_s - \omega_c)$, δ_p and δ_s are given.

Step 2: The desired frequency response of the FIR filter is reproduced below.

$$H_{pm}(\omega) = 1 + \frac{\delta_p}{2} \cos k_p \omega, \quad 0 \leq \omega \leq \omega_p \quad (2.96)$$

$$H_{pm}(\omega) = 1 - \frac{(\omega - \omega_p)}{(\omega_z - \omega_p)}, \quad \omega_p \leq \omega \leq \omega_z \quad (2.97)$$

$$H_{pm}(\omega) = -\frac{\delta_s}{2} \sin k_p(\omega - \omega_z), \quad \omega_z \leq \omega \leq \pi \quad (2.98)$$

$$H_{pm}(0) = 1 + \frac{\delta_p}{2}$$

$$H_{pm}(\omega_p) = 1$$

$$H_{pm}(\omega_c) = 1 - \frac{\delta_p}{2}$$

$$H_{pm}(\omega_s) = \frac{\delta_s}{2} = \frac{\delta_p}{2}$$

$$H_{pm}(\omega_z) = 0$$

Step 3: The filter design parameters k_p and ω_z along with ω_c and ω_s computed using equations reproduced below

$$\omega_c = \omega_p + \frac{1}{k_p} \quad (2.105)$$

$$\omega_s = \omega_p + \frac{2}{k_p \delta_p} - \frac{1}{k_p} \quad (2.107)$$

$$\omega_z = \omega_p + \frac{2}{k_p \delta_p} \quad (2.109)$$

$$k_p = \frac{2(1-\delta_p)}{\delta_p(\omega_s - \omega_c)} \quad (2.112)$$

$$\delta_s = \delta_p \quad (2.111)$$

Step 4: The impulse response coefficients of the filter are obtained by substituting values of k_p, ω_z, ω_p , and $\delta_p = \delta_s$ in (2.116) to (2.118).

Results: The magnitude and impulse response of the filter designed for the above design is as shown in Fig.2.12. The filter design parameters computed are $k_p = 63598.3, \omega_z = 0.6767\pi$ with cutoff edge $\omega_c = 0.6667\pi$ and stopband edge $\omega_s = 0.6767\pi$. The frequency domain specifications obtained by measurements of the magnitude response using SP toolbox are passband edge $\omega_p = 0.6667\pi, \omega_c = 0.6667\pi, \omega_s = 0.6767\pi$, transition bandwidth $(\omega_s - \omega_c) = 0.01\pi$, passband ripple $\delta_p = 0.129\text{dB}$ and stopband attenuation $\delta_s = 40.3\text{dB}$ are obtained with a filter order of 701. It is found that obtained specifications match closely with the desired specifications.

A6.1.5 Filter Synthesis and Design of Class V FIR Lowpass Filter with Equiripple Passband, Linear Transition and Variable Ripple Density with Slope Equalization

Design Example: Consider the design of a proposed Class IV lowpass, linear phase, sharp transition FIR filter to meet the following specifications: passband edge ω_p is 0.6667π , transition bandwidth $(\omega_s - \omega_c)$ is 0.01π , maximum passband ripple δ_p is $\pm 0.1\text{dB}$ and minimum stopband attenuation δ_s is 40 dB .

Step 1: The desired filter specifications namely $\omega_p, (\omega_s - \omega_c), \delta_p$ and δ_s are given.

Step 2: The desired frequency response of the FIR filter is reproduced below.

$$H_{pm}(\omega) = 1 + \frac{\delta_p}{2} \cos k_{p0}\omega, \quad 0 \leq \omega \leq \omega_{p0} \quad (2.119)$$

$$H_{pm}(\omega) = 1 + \frac{\delta_p}{2} \cos k_p(\omega - \omega_{p0}), \quad \omega_{p0} \leq \omega \leq \omega_p \quad (2.120)$$

$$H_{pm}(\omega) = 1 - \frac{(\omega - \omega_p)}{(\omega_z - \omega_p)}, \quad \omega_p \leq \omega \leq \omega_z \quad (2.121)$$

$$H_{pm}(\omega) = -\frac{\delta_s}{2} \sin k_p(\omega - \omega_z) \quad \omega_z \leq \omega \leq \omega_{s0} \quad (2.122)$$

$$H_{pm}(\omega) = -\frac{\delta_s}{2} \cos k_{p0}(\omega - \omega_{s0}) \quad \omega_{s0} \leq \omega \leq \pi \quad (2.123)$$

$$H_{pm}(0) = 1 + \frac{\delta_p}{2} \quad \text{and} \quad H_{pm}(\omega_p) = 1$$

$$H_{pm}(\omega_c) = 1 - \frac{\delta_p}{2} \quad \text{and} \quad H_{pm}(\omega_z) = 0$$

$$H_{pm}(\omega_s) = \frac{\delta_s}{2} \quad \text{and} \quad H_{pm}(\omega_{s0}) = -\frac{\delta_s}{2}$$

Step 3: The filter design parameters $k_p, k_{p0}, \omega_z, \omega_{p0}, \omega_{s0}$ along with ω_c and ω_s are computed using equations reproduced below

$$(\omega_{s0} - \omega_z) = \left(m + \frac{1}{4}\right) \frac{2\pi}{k_p} \quad (2.124)$$

$$\omega_{p0} = \omega_p - \left(m + \frac{1}{4}\right) \frac{2\pi}{k_p} \quad (2.128)$$

$$k_{p0} = \frac{2\pi n}{\omega_{p0}} \quad (2.129)$$

$$\delta_s = \delta_p \quad (2.136)$$

$$\omega_c = \omega_p + \frac{1}{k_p} \quad (2.137)$$

$$\omega_z = \omega_p + \frac{2}{k_p \delta_p} \quad (2.138)$$

$$\omega_s = \omega_p + \frac{2}{k_p \delta_p} - \frac{1}{k_p} \quad (2.140)$$

$$k_p = \frac{2 \left[\frac{1}{\delta_p} - 1 \right]}{(\omega_s - \omega_c)} \quad (2.141)$$

Step 4: The impulse response coefficients of the filter are obtained by substituting values of $k_p, k_{p0}, \omega_z, \omega_{p0}, \omega_p, \omega_{s0}, \delta_p (= \delta_s)$ in (2.144) to (2.147). The magnitude and impulse response of the filter designed for the above design is as shown in Fig.2.17. In this design, $m=100$ and $n=4$ are chosen. The filter design parameters computed are $k_p=63598.315$, $k_{p0}=12.057$, $\omega_{p0}=0.6635 \pi$, $\omega_z=0.6767 \pi$, $\omega_{s0}=0.67983 \pi$ with cutoff edge $\omega_c=0.0007 \pi$ and stopband edge $\omega_s=0.6667 \pi$. The frequency domain specifications obtained by measurements of the magnitude response using SP toolbox are passband edge $\omega_p = 0.6667 \pi$, $\omega_s = 0.6767 \pi$, transition bandwidth $(\omega_s - \omega_c) = 0.01 \pi$, passband ripple $\delta_p = 0.13\text{dB}$ and stopband attenuation $\delta_s = 40.19\text{dB}$ are obtained for a filter order of 701. It is found that obtained specifications match closely with the desired specifications.

A6.1.6 Filter Synthesis and Design of FIR Bandpass I filter

Design Example: Consider the design of a proposed Bandpass I, linear phase, sharp transition FIR filter to meet the following specifications: Band center frequency ω_b is 0.4444π , half passband edge ω_p is 0.3333π , transition bandwidth $(\omega_s - \omega_c)$ is 0.01π , maximum passband ripple δ_p is $\pm 0.1\text{dB}$ and minimum stopband attenuation δ_s is 40dB .

Step 1: The desired filter specifications namely ω_b , ω_p , $(\omega_s - \omega_c)$, δ_p and δ_s are given.

Step 2: The desired frequency response of the FIR filter in the three regions are modeled using trigonometric functions as reproduced below

$$H_{pm}(\omega) = A_0 \left(1 + \frac{\delta_p}{2} \cos k_{pb} (\omega - \omega_b) \right), \quad \omega_b - \omega_p \leq \omega \leq \omega_b + \omega_p \quad (3.1)$$

$$H_{pm}(\omega) = A_0 \left[1 - \frac{(\omega - (\omega_b + \omega_p))}{(\omega_z - \omega_p)} \right], \quad \omega_b + \omega_p \leq \omega \leq \omega_b + \omega_z \quad (3.2)$$

$$\text{and } H_{pm}(\omega) = A_0 \left[1 - \frac{((\omega_b - \omega_p) - \omega)}{(\omega_z - \omega_p)} \right], \quad \omega_b - \omega_z \leq \omega \leq \omega_b - \omega_p \quad (3.3)$$

$$H_{pm}(\omega) = -\frac{\delta_s}{2} A_0 \sin k_{pb} (\omega - (\omega_b + \omega_z)), \quad \omega_b + \omega_z \leq \omega \leq \pi \quad (3.4)$$

$$H_{pm}(\omega) = -\frac{\delta_s}{2} A_0 \sin k_{pb} ((\omega_b - \omega_z) - \omega) \quad 0 \leq \omega \leq \omega_b - \omega_z \quad (3.5)$$

$$\omega_c = \omega_z - \left(1 - \frac{\delta_p}{2} \right) (\omega_z - \omega_p) \quad (3.7)$$

$$\omega_s = \omega_z - \frac{(\delta_s/2)(\omega_z - \omega_p)}{A_0} \quad (3.9)$$

$$(\omega_s - \omega_c) = (\omega_z - \omega_p) \left[\left(1 - \frac{\delta_p}{2} \right) - \frac{(\delta_s/2)}{A_0} \right] \quad (3.10)$$

$$k_{pb} = \frac{2}{\delta_p (\omega_s - \omega_c)} \left[\frac{(\delta_s/2)}{A_0} - \left(1 - \frac{\delta_p}{2} \right) \right] \quad (3.16)$$

$$\omega_z = \omega_p + \frac{2}{\delta_p k_{pb}} \quad (3.17)$$

And finally $A_0 = 1$

Step 3: The impulse response coefficients of the filter are obtained by substituting values of $A_0, k_{pb}, \omega_z, \omega_p, \omega_b, \delta_p$ and δ_s in (3.21) to (3.23).

Results: The magnitude and impulse response of the filter designed for the above design is as shown in Fig.3.2. The filter design parameters computed are $k_{pb} = 65043.73 \pi$, $\omega_z = 0.34338 \pi$, cutoff edge $\omega_c = 0.3333 \pi$ and stopband edge $\omega_s = 0.3433 \pi$.

The frequency domain specifications obtained by measurements of the magnitude response using SP toolbox are half passband width $\omega_p = 0.3333 \pi$, cutoff edges $\omega_{c1} = 0.3333 \pi$, $\omega_{c2} = 0.6666 \pi$, center frequency $\omega_b = 0.4444 \pi$, stopband edges $\omega_{s1} = 0.344 \pi$ and $\omega_{s2} = 0.6777 \pi$, transition band $(\omega_s - \omega_c) = 0.011 \pi$, passband ripple $\delta_p = 0.1435 \text{dB}$ and stopband attenuation $\delta_s = 39.4 \text{dB}$ for a filter order of 701. It is found that obtained specifications match closely with the desired specifications.

A6.1.7 Filter Synthesis and Design of FIR Bandpass II filter

Consider the same design example of Bandpass I filter.

Step 1: The desired filter specifications i.e. center frequency ω_b , passband edge frequencies $(\omega_b \pm \omega_p)$, transition region width $(\omega_s - \omega_c)$, passband ripple δ_p and stopband ripple δ_s are given.

Step 2: The desired frequency response of the FIR filter are modeled using trigonometric functions as reproduced below

$$H_{pm}(\omega) = \frac{\delta_s}{2} \cos k_{p0} \left((\omega_b - \omega_{s0}) - \omega \right), \quad 0 \leq \omega \leq (\omega_b - \omega_{s0}) \quad (3.24)$$

$$H_{pm}(\omega) = \frac{\delta_s}{2} \cos k_p \left(\omega - (\omega_b - \omega_{s0}) \right), \quad (\omega_b - \omega_{s0}) \leq \omega \leq (\omega_b - \omega_z) \quad (3.25)$$

$$H_{pm}(\omega) = \frac{\left[\omega - (\omega_b - \omega_z) \right]}{\left[(\omega_z - \omega_p) \right]}, \quad (\omega_b - \omega_z) \leq \omega \leq (\omega_b - \omega_p) \quad (3.26)$$

$$H_{pm}(\omega) = 1 + \frac{\delta_p}{2} \sin k_p \left[\omega - (\omega_b - \omega_p) \right], \quad (\omega_b - \omega_p) \leq \omega \leq \omega_b - \omega_{p0} \quad (3.27)$$

$$H_{pm}(\omega) = 1 + \frac{\delta_p}{2} \cos k_{p0} \left[\omega - (\omega_b - \omega_{p0}) \right], \quad (\omega_b - \omega_{p0}) \leq \omega \leq \omega_b \quad (3.28)$$

$$H_{pm}(\omega) = 1 + \frac{\delta_p}{2} \cos k_{p0} \left[(\omega - \omega_b) \right], \quad \omega_b \leq \omega \leq \omega_b + \omega_{p0} \quad (3.29)$$

$$H_{pm}(\omega) = 1 + \frac{\delta_p}{2} \cos k_p \left[\omega - (\omega_b + \omega_{p0}) \right], \quad \omega_b + \omega_{p0} \leq \omega \leq \omega_b + \omega_p \quad (3.30)$$

$$H_{pm}(\omega) = 1 - \frac{\left[\omega - (\omega_b + \omega_p) \right]}{\left[(\omega_z - \omega_p) \right]}, \quad (\omega_b + \omega_p) \leq \omega \leq \omega_b + \omega_z \quad (3.31)$$

$$H_{pm}(\omega) = -\frac{\delta_s}{2} \text{sinc}_p \left[\omega - (\omega_b + \omega_z) \right], \quad \omega_b + \omega_z \leq \omega \leq \omega_b + \omega_{s0} \quad (3.32)$$

$$H_{pm}(\omega) = \frac{\delta_s}{2} \text{cosk}_{p0} \left[\omega - (\omega_b + \omega_{s0}) \right], \quad \omega_b + \omega_{s0} \leq \omega \leq \pi \quad (3.33)$$

$$\omega_{s0} = \omega_z + \frac{2\pi(p+3/4)}{k_p}$$

$$\omega_{p0} = \omega_p - \frac{2\pi}{k_p} (m+1/4) \quad (3.36)$$

$$k_{p0} = \frac{2\pi(n/2 - m)}{\omega_{p0}} \quad (3.38)$$

p, n, m are to be chosen and n must be even.

$$\omega_z = \omega_p + \frac{2}{k_p \delta_p} \quad (3.42)$$

$$\omega_c = \omega_p + \frac{1}{k_p} \quad (3.50)$$

$$\omega_z = \omega_s + \frac{1}{k_p} = \omega_p + \frac{2}{k_p \delta_p} \quad (3.52)$$

$$\omega_s = \omega_p - \frac{1}{k_p} + \frac{2}{k_p \delta_p} \quad (3.53)$$

$$(\omega_s - \omega_c) = \frac{2}{k_p} \left(\frac{1}{\delta_p} - 1 \right) \quad (3.54)$$

$$k_p = \frac{2 \left(\frac{1}{\delta_p} - 1 \right)}{(\omega_s - \omega_c)} \quad (3.55)$$

Step 3: The impulse response coefficients of the filter are obtained by substituting values of

$A_0, k_p, k_{p0}, \omega_z, \omega_{p0}, \omega_p, \omega_{s0}, \omega_b, \delta_p$ and δ_s in (3.59) to (3.61).

Results: The magnitude and impulse response of the filter designed for the above design is as shown in Fig.3.4. Computed filter design parameters are $k_p = 63598.315$, $k_{p0} = 27.0057$, $\omega_{p0} = 0.33326257 \pi$, $\omega_z = 0.343343 \pi$, $\omega_{s0} = 0.3434298 \pi$ with cutoff edge $\omega_c = 0.33333 \pi$ and stopband edge $\omega_s = 0.34333 \pi$. The frequency domain specifications obtained by measurements of the magnitude response using SP toolbox are half passband width $\omega_p = 0.3333 \pi$, passband edges $\omega_{cl} = 0.3333 \pi$ and $\omega_c = 0.6666 \pi$, center frequency $\omega_b = 0.4444 \pi$, stopband edge $\omega_s = 0.344 \pi$ and $\omega_s = 0.6777 \pi$, transition bandwidth $(\omega_s - \omega_c) = 0.011 \pi$, maximum passband ripple $\delta_p = 0.1414 \text{dB}$ and minimum stopband attenuation $\delta_s = 40.2 \text{dB}$ for a filter order of 701. It is found that obtained specifications match closely with the desired specifications.

A6.1.8 Filter Synthesis and Design of FIR Multiband Filter

Design Example: Consider the design of a proposed Multiband, linear phase, sharp transition FIR filter to meet the following specifications:

Number of passbands : Nine

Band center frequencies ω_{bn} : As per Zwicker's model in appendix A 5.1

Half passband widths ω_{pn} : As per Zwicker's model in appendix A 5.1

Transition bandwidth of each band $(\omega_{sn} - \omega_{cn})$: 35 Hz (0.0063 normalized)

Maximum passband ripple for each band δ_p : $\pm 0.1 \text{dB}$

Minimum stopband attenuation δ_s : 40dB

Sampling frequency : 11025 Hz

Step 1: The desired filter specifications i.e. band center frequency ω_{bn} , passband edge frequencies ($\omega_{bn} \pm \omega_{pn}$), transition bandwidth ($\omega_{sn} - \omega_{cn}$), passband ripple δ_p , stopband attenuation δ_s and $\omega_{s,n-1}$ and $\omega_{s,n+1}$ center frequencies of stopbands preceding and succeeding passband BP_n are given for each of the bands.

Step 2: The desired frequency response of the FIR filter are modeled using trigonometric functions for each band as reproduced below

$$H_{pm}(\omega) = \frac{\delta_s}{2} \cos k_{p2}(\omega - \omega_{s,n-1}), \quad \omega_{s,n-1} \leq \omega \leq \omega_{s2,n-1} \quad (5.1)$$

$$H_{pm}(\omega) = \frac{\delta_s}{2} \cos k_p(\omega - \omega_{s2,n-1}), \quad \omega_{s2,n-1} \leq \omega \leq \omega_{bn} - \omega_{zn} \quad (5.2)$$

$$H_{pm}(\omega) = \frac{1}{(\omega_{zn} - \omega_{pn})} \left[\omega - (\omega_{bn} - \omega_{zn}) \right], \quad (\omega_{bn} - \omega_{zn}) \leq \omega \leq \omega_{bn} - \omega_{pn} \quad (5.3)$$

$$H_{pm}(\omega) = 1 + \frac{\delta_p}{2} \text{sink}_p \left[\omega - (\omega_{bn} - \omega_{pn}) \right], \quad (\omega_{bn} - \omega_{pn}) \leq \omega \leq \omega_{bn} - \omega_{n2} \quad (5.4)$$

$$H_{pm}(\omega) = 1 + \frac{\delta_p}{2} \text{cosk}_{p1} \left[\omega - (\omega_{bn} - \omega_{n2}) \right], \quad (\omega_{bn} - \omega_{n2}) \leq \omega \leq \omega_{bn} + \omega_{n2} \quad (5.5)$$

$$H_{pm}(\omega) = 1 + \frac{\delta_p}{2} \text{cosk}_p \left[\omega - (\omega_{bn} + \omega_{n2}) \right], \quad (\omega_{bn} + \omega_{n2}) \leq \omega \leq \omega_{bn} + \omega_{pn} \quad (5.6)$$

$$H_{pm}(\omega) = 1 - \frac{1}{(\omega_{zn} - \omega_{pn})} \left[\omega - (\omega_{bn} + \omega_{pn}) \right], \quad (\omega_{bn} + \omega_{pn}) \leq \omega \leq \omega_{bn} + \omega_{zn} \quad (5.7)$$

$$H_{pm}(\omega) = -\frac{\delta_s}{2} \text{sink}_p \left[\omega - (\omega_{bn} + \omega_{zn}) \right], \quad (\omega_{bn} + \omega_{zn}) \leq \omega \leq \omega_{s2,n+1} \quad (5.8)$$

$$H_{pm}(\omega) = \frac{\delta_s}{2} \text{sink}_{p3} \left[\omega - \omega_{s2,n+1} \right], \quad \omega_{s2,n+1} \leq \omega \leq \omega_{s,n+1} \quad (5.9)$$

Step 3: The filter design parameters $k_p, k_{p1}, k_{p2}, k_{p3}, \omega_{zn}, \omega_{n2}, \omega_{s2, n-1}, \omega_{s2, n+1}$ along with ω_{sn} and ω_{cn} for various bands of the multiband filter are computed using equations reproduced below

$$k_p = \frac{2 \left[1 - \left(\frac{\delta_s + \delta_p}{2} \right) \right]}{\delta_p (\omega_{sn} - \omega_{cn})} \quad (5.25)$$

Note that equalization of slopes leads to $\delta_s = \delta_p$.

$$k_p = \frac{2[1 - \delta_p]}{\delta_p (\omega_{sn} - \omega_{cn})} \quad (5.26)$$

$$\omega_{zn} = \omega_{sn} + \frac{1}{k_p} = \omega_{pn} + \frac{2}{k_p \delta_p}$$

$$\omega_{sn} = \omega_{zn} - \left(\frac{\delta_s}{2} \right) (\omega_{zn} - \omega_{pn}) \quad (5.21)$$

Note that equalization of slopes leads to $\delta_s = \delta_p$.

$$\omega_{sn} = \omega_{zn} - \left(\frac{1}{k_p} \right)$$

The value of ω_{cn} can be found directly from the specified value of $(\omega_{sn} - \omega_{cn})$ or

$$\omega_{cn} = \frac{\delta_p}{2} (\omega_{zn} - \omega_{pn}) + \omega_{pn} \quad (5.19)$$

$$\omega_{cn} = \left(\frac{1}{k_p} \right) + \omega_{pn}$$

$$(\omega_{sn} - \omega_{cn}) = \left(\frac{2}{k_p} \right) \left(\frac{1}{\delta_p} - 1 \right)$$

Choosing m an integer we obtain,

$$\omega_{n2} = \omega_{pn} - \left(m + \frac{1}{4}\right) \frac{2\pi}{k_p} \quad (5.12)$$

Choosing n an even integer,

$$k_{p1} = \left(\frac{n}{2} - m\right) \frac{2\pi}{\omega_{n2}} \quad (5.11)$$

Choosing p an integer,

$$\omega_{s2, n-1} = (\omega_{bn} - \omega_{zn}) - \left(p + \frac{3}{4}\right) \frac{2\pi}{k_p} \quad (5.14)$$

Choosing n0 an integer,

$$k_{p2} = 2\pi(n0 - p) / (\omega_{s2, n-1} - \omega_{s, n-1})$$

$$\omega_{s2, n-1} = \omega_{s, n-1} + (n0 - p) \frac{2\pi}{k_{p2}} \quad (5.14)$$

Choosing q an integer we obtain,

$$\omega_{s2, n+1} = (\omega_{bn} + \omega_{zn}) + \left(q + \frac{3}{4}\right) \frac{2\pi}{k_p} \quad (5.17)$$

Finally, choosing n2 an integer we obtain,

$$n2 = 42 + q;$$

$$k_{p3} = 2\pi(n2 - q) / [\omega_{s, n+1} - \omega_{s2, n+1}]$$

We have chosen $m = 100$, $p = 5$, $q = 5$, $n0 = p+2 = 7$, $n2 = 42+q = 47$.

Results: The magnitude and impulse response of the filter designed for the above design is as shown in Fig.5.4 and Fig.5.5. The filter design parameters computed are k_p , k_{p1} , k_{p2} , k_{p3} ,

ω_{pn} , ω_{zn} , ω_{sn} and ω_{cn} for various bands of the multiband filter.

From the frequency domain specifications obtained by measurements of the magnitude response using SP toolbox it is observed that passband width and center frequencies of the various bands are obtained as per Zwicker's model, transition bandwidth is 35 Hz for each band, maximum passband ripple δ_p is 0.14dB and minimum stopband attenuation δ_s is 42dB for each band. To meet these frequency specifications the minimum order of the FIR multiband filter required is 1025. It is found that obtained specifications match closely with the desired specifications.

A6.1.9 Filter Synthesis and Design of Lowpass FIR Filter using Modified FRM Approach

Design Example: Consider the design of a lowpass, linear phase, sharp transition FIR filters for the desired specifications: Cutoff edge is 0.8192π , stopband edge is 0.8292π , maximum passband ripple is $\pm 0.1\text{dB}$ (0.2 dB) and minimum stopband attenuation is 40dB using the proposed modified FRM approach.

Step 1: The desired filter specifications namely $\omega_c, (\omega_s - \omega_c), \delta_p$ and δ_s are given. In Fig.4.3, for the ideal response shown, $\omega_p = \omega_c$ and $\omega_s = \omega_z$.

Step 2: Suitable k and M are chosen. M is chosen to be an odd integer.

Step 3: Obtain value of θ for any given value of ϕ and using the model filter band edges equation referring to Fig.4.3

$$\theta = \phi - M(\omega_s - \omega_c)$$

i.e. $\theta = \phi - M(\omega_s - \omega_c)$

Step 4: Knowing k, M, θ and ϕ the band edges of the various subfilters of the FRM filter are obtained using equations below referring to Fig.4.3

Band edges of model filter $F_a(z^M)$ are given by $\frac{(2K+2)\pi-\theta}{M}$ and $\frac{(2K+2)\pi-\varphi}{M}$

Band edges of masking filter F_{ma} are given by $\frac{(2K+2)\pi+(\varphi+2\theta)}{M}$ and $\frac{(2K+2)\pi-\theta}{M}$

Band edges of complementary masking filter F_{mc} are given by $\frac{(2K+2)\pi-\varphi}{M}$ and

$$\frac{(2K+2)\pi+\theta}{M}$$

Bandpass filter stopband edges are given by $\frac{(2K+2)\pi-(\varphi+2\theta)}{M}$ and $\frac{(2K+2)\pi+\theta}{M}$

Bandpass filter passband edges are given by $\frac{(2K+2)\pi-\varphi}{M}$ and $\frac{(2K+2)\pi-\theta}{M}$

Gain of bandpass filter given by $A = \frac{2(\pi-\varphi)}{2\pi-(\theta+\varphi)}$

Choose $k = 3$, $M = 9$ and $\theta = 0.5367\pi$. The value of φ computed is $\varphi = 0.6267\pi$.

Three filters subfilters i.e. model, masking and bandpass are synthesized all with passband ripple ± 0.01 dB and stopband attenuation of 40dB. The specifications of subfilters band edges measured using SP toolbox are as follows : Model filter passband edge is 0.8193π , stopband edge is 0.8293π , masking filter passband edge is 0.8193π and stopband edge is 0.9485π , bandpass stopband edges are 0.6999π and 0.9485π , passband edges are 0.8193π and 0.8293π , center frequency is 0.8243π and final FRM filter passband edge is 0.8193π and stopband edge is 0.8293π with a transition width of 0.01π with passband ripple δ_p of 0.13dB and stopband attenuation δ_s of 42.2dB are obtained for an sum of subfilter order of 287. The band edges of subfilters obtained confirm to the designed value and the desired MFRM filter specifications are also obtained.

Appendix A6.2

LISTING OF PROGRAMS DEVELOPED IN MATLAB

Introduction:

MATLAB stands for MATrix LABoratory. It is a technical computing environment for scientific and engineering high performance numeric computation and visualization. It integrates numerical analysis, matrix computation, signal processing and graphics in an easy to use environment where problems and solutions are expressed in the same form as they are written mathematically without traditional programming. MATLAB allows us to express an algorithm in a few lines and to compute the solution with greater accuracy on a computer. MATLAB is an interactive system whose basic data element is a matrix that does not require dimensioning. It also features a family of application specific solutions called toolboxes which are a collection of specialized functions in a specific area. Areas in which toolboxes are available include signal processing, image processing, control system design, dynamic system simulation, system identification, neural networks and others. It can handle linear, nonlinear, continuous-time, discrete-time, multivariable and multirate systems.

Interactive Digital Signal Processing Tool SPTool: The SPTool command invokes a suite of graphical user interface tools that provides access to many of the signal, filter and spectral analysis functions in the tool box in a powerful, easy to use interactive signal display and exploration environment. Using SPTool we can import, export and manage signals, filters and spectra. From the SPTool you can activate its four integrated signal processing tools namely the Signal Browser for viewing, measuring and analyzing time-domain information of imported signals, the Filter Designer for designing and editing conventional FIR and IIR filters

of various lengths and types, with standard lowpass, highpass, bandpass and bandstop configurations, the Filter Viewer for viewing the characteristics of a designed or imported filter including its magnitude response, phase response, group delay, pole-zero plot, impulse response and step response and the Spectrum Viewer for graphical analysis of frequency-domain data using a variety of methods.

MATLAB programs are developed to model, design and implement proposed digital FIR lowpass, bandpass and multiband filters as per their design. The program computes various filter design parameters, filter coefficients and displays the magnitude and phase response from which filters specifications such as passband ripple, stopband attenuation, passband, stopband and transition width can be measured. Measurements are done using Signal Processing Toolbox. Various desired specifications of the filter can be easily varied and performance of the filter observed. Also a speech processing scheme for sensorineural hearing impaired using multiband filters is implemented.

Following are the programs developed using MATLAB

- MLP-1 MATLAB program to model and design Class I lowpass filter.
- MLP-2 MATLAB program to model and design Class II lowpass filter.
- MLP-3 MATLAB program to model and design Class III lowpass filter without slope equalization.
- MLP-4 MATLAB program to model and design Class III lowpass filter with slope equalization.
- MLP-5 MATLAB program to model and design Class IV lowpass filter.
- MLP-6 MATLAB program to model and design Class V lowpass filter.
- MBP-1 MATLAB program to model and design Bandpass I filter.

MBP-2	MATLAB program to model and design Bandpass II filter.
MCS	MATLAB program to model and design Cascade filter.
MMF	MATLAB program to model and design Modified FRM filter.
MFRM	MATLAB program to model and design FRM filter.
MML	MATLAB program to model and design Multiband filter.
MSP	MATLAB program to implement speech processing scheme.

References

1. T. Lunner, S. Arlinger and J. Heligren, "8-channel digital filter bank for hearing aid use: Preliminary results in monaural, diotic and dichotic models," *Scandinavian Audiology Journal*, suppl.36, pp.75-81,1993.
2. B.C.J. Moore, "An introduction to the psychology of hearing," Academic, 1997.
3. Zwicker E. "Subdivision of audio frequency range into critical bands," *Frequenzgruppen*, *Journal of the Acoustical Society of America*, vol.33, pp. 248, 1961.
4. M.C.Martin, "Critical bands in sensorineural hearing loss," *Scandinavian Audiology Journal*,vol. 3, pp.133-140,1974.
5. Studebaker G.A, Pavlovic C.V and Sherbecoe R.L. "A frequency importance function for continuous discourse," *Journal of the Acoustical Society of America*, vol. 81, pp.1130-1138, 1987.
6. D.S. Chaudari and P.C. Pandey, "Dichotic presentation of speech signals with critical band filtering for improving speech perception," *Proc. of International Conference on Acoustic, Speech and Signal Processing*, Seattle, Washington., U.S.A., June, 1998, vol. I, pp.3601-3604, June 1998.
7. Yong Ching Lim, "Frequency response masking approach for the synthesis of sharp linear phase digital filters," *IEEE Trans. Circuits Syst.*,vol.cas-33, No. 4, pp. 357-364, April 1986.
8. Johnny R. Johnson, "Introduction to Digital Signal Processing," Prentice Hall of India Private Limited, 1996.
9. Alan V. Oppenheim, A.S. Willsky and S. Hamid Nawab, "Signals and Systems,"2nd edn., Prentice Hall of India, New Delhi.

10. J.H. McClellan, T.W. Parks and L.R. Rabiner, "A computer program for designing optimum FIR linear phase digital filters," IEEE Trans. Audio Electroacoust., vol.-21, pp. 506-526, December 1973.
11. Ronald N. Bracewell, "The Fourier Transform and its Applications," Third ed. 2003, Tata McGraw-Hill Publishing Co. Ltd., India.
12. S.K. Mitra, "Digital Signal Processing: A Computer Based Approach," McGraw-Hill International Edition, 2001.
13. Zhongqi Jing and Adly T. Fam, "A new structure for narrow transition band, lowpass digital filter design," IEEE Trans. Acoust., Speech and Signal Processing, vol.ASSP-32, No. 2, pp. 362-370, April 1984.
14. Tapio Saramaki, Yrjo Neuvo and Sanjith K. Mitra, "Design of computationally efficient interpolated FIR filter," IEEE Trans. Circuits Syst.,vol.35, No.1,pp.70-88, January 1988.
15. G.Rajan, Y.Neuvo and S.K. Mitra, "On the design of sharp cutoff wideband FIR filters with reduced arithmetic complexity," IEEE Trans. Circuits Syst.,vol.35, No. 11, pp. 1447-1454,Nov.1988.
16. Tapio Sarmaki and Andly T. Fam, "Subfilter Approach for Designing Efficient FIR Filters," International Symposium on Circuits and Systems, pp.2903-2915, ISCAS, 1999.
17. P.P. Vaidyanathan, "Optimal Design of Linear Phase FIR Digital Filters with Very Flat Passbands and Equiripple Stopbands," IEEE Trans. Circuits Syst.,vol.32, No. 9, pp. 904-918, Sep. 1985.
18. Pavel Zahradnik and Miroslav Vleek, "Analytical design method for optimal

- equiripple comb FIR filter,” IEEE Circuits and Systems II Briefs, Vol. 52, No. 2, Feb. 2005
19. Lawrence R. Rabiner, James Kaiser and Ronald Schafer, “Some considerations in the design of multiband finite impulse response digital filters,” IEEE Trans. ASSP, pp 462-472, Dec.1974.
 20. Vinay K. Ingle and John G. Proakis, “Digital Signal Processing Using MATLAB,” BookWare Companion Series.
 21. Delores M. Etter, “Engineering Problem Solving with MATLAB,” 2ed., Prentice-Hall, International, Inc.
 22. Joseph Rodrigues and K. R. Pai, “New Approach to the Synthesis of Sharp Transition FIR Digital Filter,” Proceedings of the IEEE International Symposium on Industrial Electronics, Croatia, ISIE 2005.
 23. Joseph Rodrigues and K. R. Pai, “New approach to the synthesis of sharp transition FIR digital filter,” ECTI-EEC Transactions 2005 (In Print).
 24. Joseph Rodrigues and K. R. Pai, “A new model to the Synthesis of Sharp Transition FIR Digital Filter,” Proceedings of the International Conference on Information Sciences and Systems, John Hopkin’s University, USA, CISS 2005.
 25. Yrjo Neuvo, Ganesh Rajan and Sanjit K. Mishra, “Design of narrow-band FIR bandpass filters with reduced arithmetic complexity,” IEEE Trans. Circuits Syst., vol. cas -34, No. 4,pp. 409-419, April 1987.
 26. Fred Mintzer and Bede Liu, “Practical Design Rules for Optimum FIR Bandpass Digital Filters,” IEEE Trans.ASSP-27, pp 204-206, April 1979.
 27. Joseph Rodrigues and K.R. Pai, “Modified Linear Phase Frequency Response Masking

- FIR Filter,” Proceedings of the Fourth International Symposium on Image and Signal Processing and Analysis, IEEE and EURASIP, Croatia, pp. 434-439, ISPA 2005.
28. Joseph Rodrigues and K. R. Pai, “Computationally efficient sharp transition FIR filter,” Proceedings of the IASTED International Conference on Automation, Control and Information Technology , Russia, ACIT-SIP 2005.
 29. Andreas Antoniou, “Digital Filters Analysis, Design and Applications,” McGraw-Hill, Inc.
 30. Ronghuan Yang, Bede Liu and Yong Ching Lim, “A new structure of sharp transition FIR filters using frequency Response masking,” IEEE Trans. Circuits Syst., vol.35, No. 8, pp. 955-965, Aug.1988.
 31. Y.C Lim and Yong Lian “Frequency response masking approach for digital filter design: Complexity reduction via masking filter factorization,” IEEE Trans. Circuits Syst. -II, vol.41, No. 8, pp.518-525, August 1994.
 32. Y.C. Lim and Yong Lian, “The optimum design of one and two dimensional FIR filters using the Frequency Response Masking technique,” IEEE Trans. Circuits Syst., Analog and Digital Signal Processing, vol. 40, No. 2, pp. 88-95, Feb 1993.
 33. Hakan Johnson and Lars Wanhammr, “High speed recursive digital filters based on the frequency response masking approach,” IEEE Trans. Circuits Syst., vol.47, No. 1, pp. 48-60, Jan 2000.
 34. W.K.Chen, Editor, “The Circuits and Filters Handbook,” CRC Press, pp.2578-2601, 1995.
 35. Yrjo Neuvo, Ganesh Rajan and Sanjit K. Mishra, “Design of narrow-band FIR bandpass filters with reduced arithmetic complexity,” IEEE Trans. Circuits Syst., vol.

- cas -34, No. 4, pp. 409-419, April 1987.
36. Wu-Sheng Lu and Takao Hinamoto, "Optimal design of IIR Frequency-Response-Masking Filters using second-order-cone programming," IEEE Transactions on Circuits and Syst. I: Fundamental theory and applications, Vol. 50. No.11 Nov. 2003.
 37. T. Saramaki, Y.C.Lim and R. Yang, "The synthesis of half-band filter using frequency-response masking technique," IEEE Trans. Circuits Syst-II., vol.42, No. 1, pp. 58-60, Jan.1995.
 38. Y.C.Lim, "A digital filter bank for digital audio systems," IEEE Trans. Circuits Syst., vol.cas-33, No. 8, pp. 848-849, August 1986.
 39. Joseph Rodrigues and K. R. Pai, "High speed computationally efficient digital filter based on frequency response masking approach," Proceedings of the AICTE sponsored National Conference on Control, Communication and Information Systems, Goa, Jan 2004.
 40. Lucy J. Gudino, "Design of FIR filters based on Frequency Response Masking approach for signal processing applications," M.Tech. Dissertation, April 2003, Vishweshwaraiah Technological University, Karnataka.
 41. O'Shaughnessy, D., "Speech Communication: Human and Machine," Addison-Wesley, Reading, Massachusetts, 1987.
 42. Robert A. Goldenberg, Editor "Hearing Aids: A manual for clinicians," Lippincott-Raven Publishers, Philadelphia, 1996.
 43. P Bonding, "Frequency selectivity and speech discrimination in sensorineural hearing Loss," Scandinavian Audiology Journal, vol. 8 pp.205-215, 1979.
 44. Dubno J.R. and D.D. Dirks, "Auditory filter characteristics and consonant recognition

- for hearing impaired listeners,” *Journal of Acoustical Society of America*, 85, pp.1666-1675, 1989.
45. Glasberg B. R. and Moore B.C.J. “Auditory filter shapes in subjects with unilateral and bilateral cochlear impairments,” *Journal of Acoustical Society of America*, Vol.79, pp.1020 – 1033, 1986.
46. Flanagan J. L., “*Speech Analysis Synthesis and Perception*,” Springer-Verlag, New York, 1972.
47. French N.R and Steinberg J.C., “Factors governing the intelligibility of speech sounds,” *Journal of Acoustical Society of America*, vol.19, pp. 90-119, 1947.
48. Leek M.R. and Summers V., “Reduced frequency selectivity and preservation of spectral contrast in noise,” *Journal of Acoustical Society of America*, vol.100, pp.1796-1806, 1996.
49. Patterson,R.D., “Auditory filter shapes derived with noise stimuli,” *Journal of Acoustical Society of America*,vol.59(3), pp.640-654, 1976.
50. P.E.Lyregaard, “Frequency selectivity and speech intelligibility in noise,” *Scandinavian Audiology Journal*, suppl.15, pp.113-122, 1982.
51. D. S. Chaudhary and P. C. Pandey, “Critical band splitting of speech signal for reducing the effect of spectral masking in bilateral sensorineural hearing impairment,” *Fifth International Symposium on Signal Processing and its Applications*, Brisbane, Australia , ISSPA Aug. 1999.
52. Rabiner, L.R. and Schafer R.W., “*Digital Processing of the speech signals*,” Prentice Hall ,Englewood Cliffs,NJ,1978.
53. Alan V. Oppenheim, Ronald W. Schafer and John R. Buck, “*Discrete-Time Signal*

- Processing,” Prentice Hall Signal Processing Series, 2 ed.
54. D. S. Chaudhary and P. C. Pandey, “Critical filter-based speech signal processing for persons with bilateral sensorineural hearing impairment,” Journal of the Institution of Engineers (India) –CP, Vol.82, May 2001.
 55. A.N. Cheeran , P. C. Pandey and D. S. Jangmashetti, “Design of comb filters based on auditory filter bandwidth for binaural dichotic presentation for persons with sensorineural hearing impairment,” Proc. 14th International Conference on Digital Signal Processing, DSP 2002, Santorni, Greece, July, 2002.
 56. James M. Kates, “A time domain digital cochlear model,” Fifth International Symposium on Signal Processing and its Applications Brisbane, Australia, Aug. 1999.
 57. Apurva Mishra and Allyn E. Hubbard, “A cochlear filter implemented with a field programmable gate array,” IEEE Transactions on Signal Processing Vol.39, No. 12 Dec.1991 , IEEE Transactions on Circuits and Systems-II: Analog and Digital Signal Processing, Vol. 49, No. 1, Jan. 2002.
 58. *Joseph Rodrigues and Lucy Gudio.* “Speech processing scheme for reduction of spectral masking in sensorineural hearing impaired,” Proceedings of the National Conference on Control, Communication and Information Systems , Ponda, Goa, Jan 2004.
 59. *Joseph Rodrigues, K.R.Pai and K. Rajalakshmi,* “Speech processing scheme for hearing aid use,” Proceedings of the Eight conference of Indian Chapter of the Acoustical Society of America, Chennai, India, Sept. 2002.
 60. MATLAB Reference Guide: High-Performance Numeric Computation and Visualization Software. The Math Works, Inc., South Natick, MA, 1984-1994.
 61. Marc E. Herniter, “Programming in MATLAB,” Brooks/Cole, Thomson Learning, 1999.

62. Tapio Saramaki and Yrjo Neuvo, "Digital filters with equiripple magnitude and group delay," IEEE Trans. Acoustics, Speech and Signal Processing, Vol. ASSP-32, No.6, pp. 1194-1200, Dec.1984.
63. Tapio Saramaki, "A class of linear phase FIR filters for decimation, interpolation and narrow-band filtering," IEEE Trans. Acoustics, Speech and Signal Processing, Vol. ASSP-32, No.5, pp. 1023-1036, Oct.1984.
64. Clive D. Summerfield and Richard F. Lyon, "ASIC implementation of the Lyon cochlea model," International Symposium on Circuits and Systems, pp.673-676, ISCAS, Sep.1999.
65. Siegfried G. Knorr, "A hearing aid for subjects with extreme high frequency losses," IEEE Trans. Acoustics, Speech and Signal Processing, Vol. ASSP-24, No.6, pp. 473-480, Dec.1976.
66. R.E. Crochiere and P. Penfield, "On the efficient design of bandpass digital filter structures," Correspondence, IEEE Trans. Acoustics, Speech and Signal Processing, pp.380-381, Aug.1975.
67. Ivan W. Selesnick, Markus Lang and C. Sidney Burrus, "A modified algorithm for constrained least square design of multiband FIR filters without specified transition bands," Correspondence, IEEE Trans. on Signal Processing, vol. 46, No. 2, pp. 497-501, Feb 1998.
68. Her-Chang Chao, Chih Shin Lin and Bin Chang Chieu, "Minimax design of FIR digital all-pass filters," IEEE Trans. Circuits and Systems-II, Analog and Digital Signal Processing, vol. 47, No.6, pp.576-579, June 2000.
69. P.M. Lin, "On frequency transformation for non-symmetric bandpass filters," IEEE

- Trans. Circuits Syst., vol. CAS-34, No. 12, pp.1599-1601, Dec.1987.
70. Irwin Pollack, "On the effect of frequency and amplitude distortion on the intelligibility of speech in noise," *Journal of Acoustical Society of America*, Vol.24, No.5, pp.538-540, 1952.
 71. James P. Egan and Francis M. Wiener, "On the intelligibility of bands of speech in noise," *Journal of Acoustical Society of America*, Vol.18, No.2, pp.435-441, 1946.
 72. James M. Kates, "Speech enhancement based on a sinusoidal model," *Journal of speech and hearing research*, Vol.37, pp.449-465, 1994.
 73. John D. Griffiths, "Optimum linear filter for speech transmission," *Journal of Acoustical Society of America*, Vol.43, No.1, pp.61-66, July 1967.
 74. James M. Kates, "Feedback cancellation in hearing aids: Results from a computer simulation," *IEEE Trans. on Signal Processing*, vol. 39, No. 3, pp.553-562, Mar. 1998.
 75. Ellen M. Danaher and J.M. Pickett, "Some masking effects produced by low frequency vowel formants in persons with sensorineural hearing loss," *Journal of speech and hearing research*, Vol.18, pp.261-271, 1975.
 76. James Jerger, Raymond Carhart and Donald Dirks, "Binaural hearing aids and speech intelligibility," *Journal of speech and hearing research*, Vol.4, pp.137-148, 1961.
 77. Edgar Villchur, "Signal Processing to improve speech intelligibility in perceptive deafness," *Journal of Acoustical Society of America*, Vol.53, pp.1646-1657, June 1973.
 78. P. Bonding, "Clinical critical band estimation," *Scandinavian Audiology Journal*, suppl.7, pp.115-123, 1978.
 79. B.C.J. Moore, "Frequency selectivity and temporal resolution in normal and hearing impaired listeners," *British Journal of Audiology*, No.19, pp.189-201, 1985.

80. Robert C. Bilger, "Consonant confusions in patients with sensorineural hearing loss,"
Journal of speech and hearing research, Vol. 19, pp. 718-748, 1976.
81. Krederjohn and James Grotelueschen, "The enhancement of speech intelligibility in
high noise level by high pass filtering followed by rapid amplitude compression,"
IEEE Trans. Acoustics, Speech and Signal Processing, Vol. ASSP-24, No. 4, pp. 277-282,
August. 1976.

List of Publications

Paper Published in International Journal Transactions

1. "New approach to the synthesis of sharp transition FIR digital filter," ECTI Transactions on Electrical Eng., Electronics and Communications (In Print).

Papers Published in International Conference Proceedings

1. "A new model to the synthesis of sharp transition FIR digital filter," Proceedings of the International Conference on Information Sciences and Systems, John Hopkin's University, CISS 2005, USA.
2. "New approach to the synthesis of sharp transition FIR digital filter," Proceedings of the IEEE International Symposium on Industrial Electronics, ISIE 2005, Croatia.
3. "New approach to the synthesis of sharp transition FIR digital filter," Proceedings of the Electrical Eng., Electronics and Communications International Conference, ECTI-CON 2005, Thailand.
4. "Computationally efficient sharp transition FIR filter," Proceedings of the IASTED International Conference on Automation, Control and Information Technology 2005, ACIT-SIP 2005, Russia.
5. "Modified linear phase Frequency Response Masking FIR filter," Proceedings of the IEEE and EURASIP Fourth International Symposium on Image and Signal Processing and Analysis, ISPA 2005, Zagreb, Croatia.

Note: IEEE Conference proceedings can be downloaded at IEEE digital library site www.ieee.org

Papers Published in National Conference Proceedings

1. "Speech processing scheme for hearing aid use," Proceedings of the eighth Conference of Indian Chapter of the Acoustical Society of America, Chennai, India, 2002.
2. "Speech processing scheme for reduction of spectral masking in sensorineural hearing impaired," Proceedings of the National Conference on Control, Communication and Information Systems, Goa, 2004.
3. "High speed computationally efficient digital filter based on Frequency Response Masking approach," Proceedings of the National Conference on Control, Communication and Information Systems, Goa, 2004.
4. "FIR filter for speech processing applications," National Conference on Vision and Image Processing, Shimoga, 2005.